Dissertation zur Erlangung des Doktorgrades

der Fakultät für Chemie und Pharmazie

der Ludwig-Maximilians-Universität München

Investigation of the Kinetics and Intermediates of Pyridyl and Pyrimidyl Substrates during the Soai Reaction

and

Asymmetric Alkylation of Photoswitchable Systems or by β-Amino Alcohol mediated Catalysis

von

Gloria Betzenbichler

aus

Ebersberg, Deutschland

2024

Erklärung

Diese Dissertation wurde im Sinne von § 7 der Promotionsordnung vom 28. November 2011 von Herrn Prof. Dr. Oliver Trapp betreut.

<u>Eidesstattliche Versicherung</u>

Diese Dissertation wurde eigenständig und ohne unerlaubte Hilfe erarbeitet.

München, den 11.04.2024

....

(Gloria Betzenbichler)

Dissertation eingereicht am: 11.04.2024

1. Gutachter: Prof. Dr. Oliver Trapp

2. Gutachter: Prof. Dr. Paul Knochel

Mündliche Prüfung am: 27.05.2024

Danksagung

Zuallererst geht ein großer Dank an meinen Doktorvater Prof. Dr. Oliver Trapp, der mir die Möglichkeit gegeben hat, meine Promotion in seiner Gruppe und im interessanten Feld der Asymmetrischen Katalyse zu arbeiten. Diese Zeit war eine sehr wertvolle für mich, in der ich wachsen durfte, sowohl persönlich als auch fachlich. Ich danke Dir, lieber Oliver für deine Unterstützung, Deinen Input und Deine aufbauenden Worte, wenn ich selbst meine Arbeit manchmal nicht genügend wertschätzen konnte.

Bei Prof. Dr. Paul Knochel möchte ich mich bedanken, dass er sich bereit erklärt hat das Zweitgutachten für meine Dissertation zu übernehmen.

Ich möchte meinen ehemaligen Praktikanten Jürgen, Patrick, Domi, Albert und Gerrit für ihren Einsatz und Ihren Ehrgeiz danken, den sie während ihrer Forschungspraktika gezeigt haben. Vor allem freut es mich, dass Ihr, Jürgen und Patrick, so viel Freude an unserer Arbeit und an der Gruppe gefunden habt, dass auch Ihr denselben Weg eingeschlagen habt.

Carrie ich danke Dir für Deine immerwährend gute Laune, den kurzen Plausch zwischendrin und Deine Fürsorge, wenn Du mir z.B. mal wieder aus heiterem Himmel Obst vorbeigebracht hast. Nach jedem Gespräch mit Dir hatte ich auch an noch so einem schweren Tag wieder ein Lächeln auf den Lippen.

Vielen Dank auch an Dich, Brigitte. Du bist unser Heinzelmännchen, das in jeder Situation eine Lösung oder die richtige Adresse parat hat. Du warst meine bayerische Insel, bei der mir immer warm ums Herz wurde, wenn ich Dich schon von weitem im Dialekt hab reden hören. Ein weiterer Dank geht an Heike und Claudia, die organisatorisch immer alles im Griff hatten. Zu Euch konnte man immer kommen und hat ein offenes Ohr gefunden.

Dann möchte ich mich ganz herzlich bei allen früheren und gegenwärtigen Kollegen des AK Trapp bedanken, es hat Spaß gemacht mit Euch zu arbeiten. Meinen Laborkollegen Lena und Simone möchte ich einen besonderen Dank aussprechen. Ich danke Euch für ein super Arbeitsklima im Labor, gute Musik, die mal wieder Schwung in einen nicht enden wollenden Tag gebracht hat und immer wieder kleine, nette Gespräche zwischendurch.

Allen voran geht ein großer Dank an Euch, Patrick und Luca. Die Zusammenarbeit mit Euch auf unseren Themen hat mir von Anfang an sehr viel Spaß gemacht und ich bin Euch auch dankbar, dass Ihr Euch die Zeit genommen habt, meine Arbeit zu korrigieren. Und natürlich ein großes Dankeschön an Dich, liebe Sabrina. Wir haben damals zusammen angefangen, Du mit der Masterarbeit, ich mit meiner Promotion, keiner wusste genau wohin und was tun. Wir haben uns eingespielt und ich bin froh, dass ich die ganze Zeit über eine so tolle Boxpartnerin hatte. Wir haben uns manchmal so sehr verquatscht,

dass die Arbeit zur Nebensache wurde, wir haben gegrübelt und gefachsimpelt und vor allem hatten wir Spaß und haben geblödelt. Egal ob ernster Arbeitsalltag, scheinbar unlösbare Probleme, ein kurzes Sektchen in der Sonne oder ein schräger Tanz im Labor, Du warst für alles zu haben und dafür möchte ich mich herzlich bei Dir bedanken.

Andi, ich bin Dir unendlich dankbar für Deine Geduld, Deine Motivation und Deine Liebe. Du hast den größten Teil meines Studiums und meine Promotion miterlebt und immer mehr an mich geglaubt als ich es selbst tat.

Der größte Dank gilt meiner Familie, meinen Eltern und meinem Bruder, sowie meiner Oma. Ihr wart mir immer vor allem eine emotionale Stütze. Ich danke Euch für Eure Liebe und manchmal auch strenge Erziehung, die mir alles mitgegeben hat, was ich für meinen weiteren Lebensweg brauche.

Publications:

P. Möhler[+], G. Betzenbichler[+], L. Huber, A.F. Siegle, O. Trapp, *in preparation*.

      Mechanistic Analysis and Kinetic Profiling of Soai's Asymmetric Autocatalysis for Pyridyl and Pyrimidyl Substrates

Review Articles:

G. Betzenbichler, L. Huber, S. Kräh, M-L. K. Morkos, A. F. Siegle, O. Trapp, *Chirality* **2022**, *34*, 732-759.

      Chiral stationary phases and applications in gas chromatography

For their constant love and support, I dedicate this PhD thesis

to my parents Anna and Karl, to my brother Roman,

to my grandmother Matija,

and to the memory of my beloved grandparents.

Summary

The present work focused in general on asymmetric alkylation reactions. The first part of the thesis involved the investigation of the self-amplifying autocatalytic *Soai* reaction of pyridyl and pyrimidyl substrates. In addition to the unsubstituted systems, TMS-ethynyl and adamantyl-ethynyl compounds were used. The systems were analysed with regard to their kinetic reaction behaviour and intermediate structures occurring during the reaction.

Initially, both aldehydes and alcohols of the **TMSPyr**, **AdPyr** and **AdPym** systems were synthesized. The flow-injection analysis high-performance liquid chromatography (FIA-HPLC) method was used to create kinetic profiles of the respective systems. In order to qualitatively determine the influence of the aldehyde and the catalytically used product alcohol, the initial concentrations of both were varied independently of each other. It was noticed that a slower reaction was observed at low initial concentrations of both the aldehyde and the alcohol. In addition, the selectivity of product formation was poorer, particularly with more of the undesirable benzylic alcohol side product being formed. The higher the initial concentrations, the faster the reaction proceeded and the more selectively the desired product enantiomer was formed. Furthermore, it was observed that the pyridyl systems proceeded much slower than the pyrimidyl systems, which can be explained due to the additional electron-withdrawing effect by the second nitrogen enhancing the electrophilicity at the carbonyl carbon. In addition, taking into account previously investigated systems, it was found that the introduced alkynyl residues also have an influence on the reaction rate. The reaction proceeded more slowly with increasing size of the alkynyl rest, which means that the residue should not be chosen increasingly large for an efficient reaction process. From the kinetics obtained by HPLC measurements and taking the side reaction into account the mass balance was closed and the reaction orders of aldehyde and alcohol could then be calculated for each system. These resulted in a reaction order of 2 for the aldehyde and 1 for the alcohol for all three systems.

In order to determine intermediates occurring during the reaction, *in situ* high-resolution mass spectroscopic measurements were carried out on the Orbitrap-MS. The advantage here was that pulsed injections of a continuous reaction also detected transient species that may only be formed in traces. In general, similar intermediates were detected for the **AdPyr** and **AdPym** system. For the **AdPyr** system, a new intermediate was also observed in which an aldehyde molecule coordinates to the zinc alkoxide hemiacetal, further supporting the mechanism proposed by *Trapp et al.*[41a] By monitoring the formation of the assuming catalytic active hemiacetal over time, it was also possible to show that its formation proceeds slowly. At the maximum of the hemiacetal concentration, however, the linear increase of the dominant alcohol enantiomer starts. In addition, the profile of

hemiacetal formation matches the calorimetry profiles published by *Blackmond et al.*,[33] which was also attributed to the formation of the catalytically active species until the reaction starts at the maximum heat development.

The second part dealt with the combination of a photoswitch molecule with the alkylation reaction of different benzaldehyde moieties in one system in order to achieve a deflection in the formation of stereoisomers through dynamically controllable light-induced changes in the core structure. As backbone compound the dithienyl system **8** known among others from *Feringa et al*. performing autoamplification through UV light irradiation and gelling with a dopant was used.[65] As benzaldehyde moieties a benzaldehyde with the carbonyl standing in *ortho*-position to the core substrate as well as different fluoro-benzaldehydes enhancing the electron-withdrawing effect of the dithienyl were synthesized. Therefore, MIDA boronic acid esters of the aldehyde moiety were produced, which enabled clean conversions with good yields in the subsequent *Suzuki* cross-coupling reaction to the dithienyl system. In addition, the synthesized structures were irradiated with UV light (λ = 365 nm) in CDCl$_3$ and the electronic changes analysed by ^{1}H NMR. All aldehyde photoswitches except **10c** and **12** could be completely ring-closed within 30 min, which could also be determined by a colour change in the solution. The *meta*-aldehyde *para*-fluoro compound **10c** and the backbone-aldehyde substrate **12** were not completely ring-closed even after 60 min. The results therefore suggest that the substitution pattern of the fluorobenzaldehyde bound to the diarylethene appears to strongly influence the electrocyclic ring closure reaction. The electron-withdrawing aldehyde groups bound directly to the diarylethene have an even stronger influence on the electronic structure of the photoswitch as the least ring-closed isomer was formed here after UV light irradiation.

In addition, the diastereomer distribution during alkylation was influenced by the axial chirality of the open photoswitch molecule itself. By twisting away from planarity, a chiral axis is created, comparable to that of DNA. This effect suppresses the formation of the *meso*-stereoisomer as this orientation to the same side of the molecule is sterically unfavourable. When the molecule is exposed to light before alkylation, this diastereomer ratio is changed and more *meso*-product is formed as the molecule is more planar due to the ring closure. Interestingly, however, the alkylation weighs more heavily so that no ring-closed product can be obtained even with exposure during the reaction.

During the ring closing of mono-alkylated photoswitch **15**, it was further shown that the stereoinformation of the alkyl substituent has a significant influence on the stereoselectivity of the ring closing reaction. The influence of the stereochemistry was thus successfully effected from the photoswitch core to the introduction of the alkyl substituent and also *vice versa* from the alkyl substituent on the photswitch core.

The third part focused on the preparation of ß-amino alcohol ligands based on amino acid derivatives to test them in the asymmetric alkylation reaction of benzaldehyde. For this purpose, the amino alcohols were either methylated or benzylated at the amine or silylated at the alcohol functional group in moderate to good yields. With the methyl and benzyl residues, steric properties were incorporated that were expected to show different selectivities in the same reaction. In addition, in the case of diphenyl-2-pyrrolidine methanol, different electronic effects were tested by electron-withdrawing and electron-donating residues on the aryl ring. Numerous examples of ß-amino alcohols with different structures are known from the literature, which were mainly used in alkylation reactions of aldehydes with Et_2Zn and in some cases achieved good to very good results in terms of their stereoselectivity. In addition to the Et_2Zn alkylation reagent, Me_2Zn and iPr$_2$Zn were also used in this work. The yield and enantiomeric excesses were determined using chiral HPLC and with the aid of calibration lines for quantification.

For the alkylation of benzaldehyde to the corresponding alkylated alcohol, the reactions were carried out in toluene at room temperature. Initial concentrations of 30 and 100 mM were used for the benzaldehyde, whereby the ligand was used with 5 mol%. For the reaction with 100 mM benzaldehyde, aliquots were taken after 6 h and 24 h. For the reactions with 30 mM benzaldehyde, the reaction time was extended to 60 h (Figure 54).

In general, only low conversions were observed in the reactions with Me_2Zn. However, the unsubstituted **(S)-17a** and **(S)-18a** and methylated **(S)-17b** prolinol-derivatives gave good enantioselectivities in the reactions that took place. Et_2Zn showed better selectivities and yields compared to iPr$_2$Zn. For the reactions with silylated ligands as well as with iPr$_2$Zn as alkylating reagent in general, better results were achieved at lower benzaldehyde concentrations.

Furthermore, with the exception of **(S)-18a**, a trend towards better enantioselectivities was obtained with Me_2Zn and *N*-methylated, as well as iPr$_2$Zn and *N*-benzylated prolinols than when methylated species were alkylated with iPr$_2$Zn and *vice versa*. Furthermore, the non-electron withdrawing ligands showed selectivity on the side of the (*R*)-enantiomer after 6 h whereas the (*S*)-enantiomer was present with good *ee* after 24 h.

Table of Contents

List of Abbreviations

Ad	adamantly
$AlCl_3$	aliminium trichloride
APCI	atmospheric-pressure chemical ionization
aq.	Aqueous
Ar	aryl
Bn	benzyl
°C	celsius centigrade
calc.	calculated
cm	centimetre
CuI	copper iodide
d	doublet
DAIB	(2*S*)-(−)-*exo*-(Dimethylamino)isoborneol
DCM	dichlormethane
dd	doublet of doublet
DFT	density-functional theory
DMSO	dimethyl sulfoxide
DNA	deoxyribonucleic acid
dt	doublet of triplet
ee	enantiomeric excess
EI	electron impact ionization
eq.	equation
equiv.	equivalents
ESI	electcrospray ionization
Et	ethyl
EtOAc	ethyl acetate
Et_2Zn	diethylzinc
FG	functional group
FIA	flow-injection analysis
GC	gas chromatography
h	hour(s)
HCl	hydrogen chloride
HPLC	high-performance liquid chromatography

i.d.	inside diameter
*i*Pr	isopropyl
*i*Pr$_2$Zn	diisopropylzinc
IR	infra-red
J	coupling constant
LDA	Lithium diisopropylamide
lg	logarithm
m	multiplet
m	meta
M	molar
Me	methyl
MeOD-*d$_4$*	deuterated methanol
Me$_2$Zn	dimethylzinc
min	minute(s)
mL	milliliter
mm	millimeter
mM	millimolar
mmol	millimol
MS	mass spectrometry
*n*BuLi	*n*-buthyl lithium
NLE	nonlinear effect
nm	nanometer
NMR	nuclear magnetic resonance
o	ortho
p	para
Ph	phenyl
ppm	parts per million
Pym	pyrimidyl
Pyr	pyridyl
q	quartet
R	residue
RNA	ribonucleic acid
r.t.	room temperature
s	singulet

sec	second(s)
SMS	square-macrocycle-square
SPhos	2-dicyclohexylphosphino-2',6'-dimethoxybiphenyl
t	triplet
*t*Bu	*tert*-butyl
THF	tetrahudrofuran
$TiCl_4$	titanium tetrachloride
TMEDA	*N,N,N',N'*-tetramethylethane-1,2-diamine
TMS	trimethyl silyl
UV	ultraviolet
v_0	initial velocity
λ	wavelength

CHAPTER 1

Introduction

1   Introduction

Probably the greatest mystery of human history is the formation of the earth with all its steps of development as we know it today. Although scientists gain more and more knowledge about on planet ongoing processes and their conditions as of the big bang, it is not yet possible to explain the history of the earth's origin without gaps. Amongst all question marks, there is one question, probably the largest unanswered so far, which could give at the same time invaluable information about the whole life on earth and occupies numerous scientists world-wide since many years: The origin of homochirality.[1] This means that biomolecular building blocks occur in their chirality in only one form. Most biological and biochemical reactions are based on the essential amino acids, which apart from glycine, are naturally present in L-configuration. The question now is how selective chirality could arise from originally achiral molecules. The importance of unilateral chirality is also reflected in the large field of pharmacology. Since our organisms insist on biochemical processes based on only one enantiomer of biomolecules, it is also important for drug development to have the possibility to synthesize enantiomerically pure substances because the mode of action of the two provided enantiomers can differ significantly. While one enantiomer may produce the desired effect, the other may not, or may even produce an entirely different, undesired effect. Past experience has shown that using the wrong enantiomer can even have dire consequences.

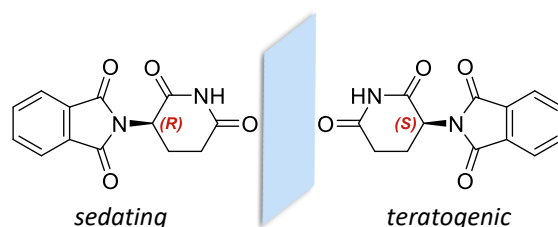*sedating*   *teratogenic*

Figure 1: The sleep-inducing (*R*)- (left) and teratogenic (*S*)-enantiomer (right) of thalidomide.

With reference to Figure 1, (*R*)-thalidomide is a pharmaceutical that has sedative and sleep-inducing effects. It was sold in the past as a racemate and used, among other things, to treat nausea during pregnancy. In the late 1950s, it became world-famous due to the Contergan® scandal.[2] Indeed, the (*S*)-enantiomer is now known for its teratogenic/fruit-damaging effects and led to an accumulation of malformations of body parts of unborn children whose extremities were severely underdeveloped or completely absent.[3] This example shows the importance of enantiomerically pure synthesis, especially in patients drug supply by the biochemical and pharmaceutical chemistry.

However, in the case of thalidomide, enantioselective synthesis could not have prevented the consequences, as it undergoes racemization very quickly and has a half-life of approx. 5.5 h in solution at 35 °C, just below body temperature.[4]

Over the last decades there have been numerous controversial theories and discoveries about the triggering impulse for the deflection from the racemic state and its amplification, both on a practical[1, 5] and theoretical[6] level. Nevertheless, the chemical pathway how originally smallest organic achiral molecules could become chiral, even enantioselective compounds, and the ability of nature to maintain this effect could not be clarified completely until today.

1.1   Asymmetric Amplification

Basically, an asymmetric reaction is based on the fact that the formation of one enantiomer is favoured by a trigger. The overall aim is to achieve 100% formation of only one enantiomer in the best case, which results in optical purity of the substance. In this context, circularly polarized light and chiral inorganic crystals were mentioned as triggers for alignment at the time of the early earth, but these did not cause complete enantioselectivity of a compound.[1, 7] Over time, chiral auxiliaries that transfer their stereoinformation to the system during the reaction have proven their worth. They undergo reversible aggregation processes with other reactants by combining two or more species *via* mostly non-covalent bonds, mainly hydrogen bonds.[8], [8b, 8c] Such processes of self-assembly and recognition are particularly well known in nature. The most famous example of such pairing behaviour is the formation of the DNA double helix where the complementary nucleobase pairs link *via* hydrogen bonds.

In order to achieve an enantiomeric excess (*ee*) when using a chiral auxiliary, a non-linear effect must occur. If a higher product *ee* is obtained than originally used by the auxiliary, this is referred to as a positive non-linear effect (+NLE). Conversely, a reaction whose product has a lower *ee* than the originally used auxiliary has a negative nonlinear effect (-NLE) (Figure 2).[7, 9]
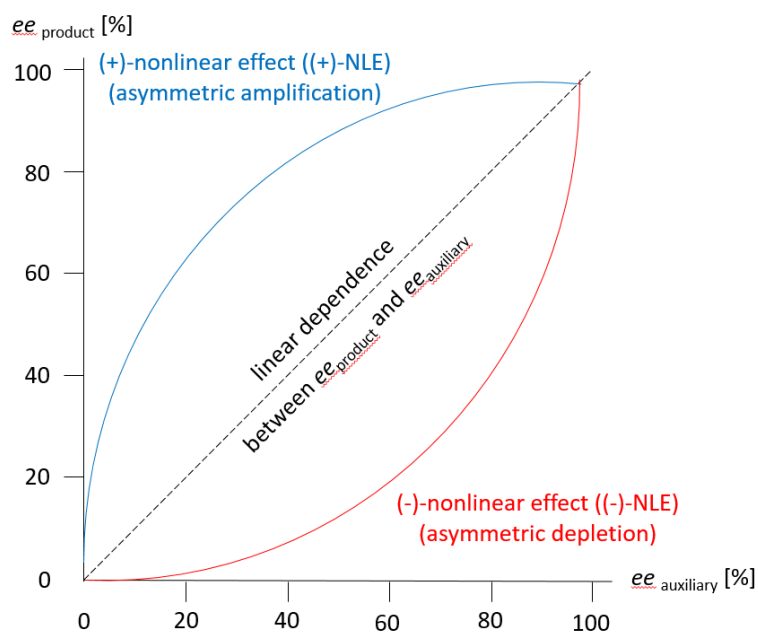
Figure 2: The relation between $ee_{product}$ and $ee_{catalyst}$ in the (+)-NLE, linear and (-)-NLE scenario.

A first plausible theory for this assumption was proposed by *Frank et al.* in 1953.[10] He explained the formation of dimers arising from either two identically configured (homochiral) or two differently configured (heterochiral) monomeric building blocks. These homochiral and heterochiral dimers are in turn diastereomeric to each other and therefore differ in their intrinsic properties, such as solubility, formation rate, transition states and other physical properties. The product enantiomers are able to catalyze the formation of the same enantiomer and simultaneously inhibit the formation of its mirror image. Thus, statistically occurring short-term enantiomeric excesses can cause stereo-amplifying effects leading to an enantiomeric excess during product formation.[10-11] In the following years, a number of reactions involving a nonlinear effect (NLE) were reported.

One of the first observations in this context was published by *Horeau* in 1969, whose work revealed strong deviations from the enantiomeric excess and experimentally determined specific rotation values of chiral derivatives of succinic acid in chloroform.[12] Later on, *Wynberg* and *Feringa* also observed differences in product formation in the oxidative coupling of chiral molecules and camphor depending on whether enantiomerically pure substrates or their racemic mixtures were used in chemical reactions.[13] Both observations could be attributed to aggregate formation through intermolecular interactions. The combination of the enantiomers to form homo- and/or heterochiral associates and the dynamic equilibria that arise in this way influence the course of the reaction and thus its yield as well as stereoselective product distribution.

Also *Kagan* has made a name for himself with his observations in studies with non-enantiomerically pure auxiliaries, which resulted in higher enantiomeric excesses than were to be expected with a linear reaction behaviour.[14] In his opinion, this could only be explained by the formation of diastereomeric aggregates, which formed spontaneously and which would not be possible by using an enantiomerically pure auxiliary.

In 1986, he described the nonlinear behaviour of an enantiomerically enriched catalyst and its impact to the products formed in asymmetric reactions. Such nonlinear effects could be observed, among others, in a diethyl tartrate-catalysed *Sharpless* epoxidation and proline-catalysed aldol-cyclization.[9b, 14] His explanation for this observation was the formation of an active diastereomeric species through self-aggregation, which resulted from the removal of the racemic diethyl tartrate from the catalytic cycle caused by the higher stability and thus lower reactivity of the heterochiral species. This explanation was proven by X-ray structure analysis and kinetic investigations.[15]

Only two years later, in 1988, *Oguni et al.* examined the nucleophilic addition of diethylzinc to benzaldehyde using ß-amino alcohols as auxiliary showing an asymmetric effect in the form of a strong positive nonlinear effect in the product formation of the secondary alcohol.[16] One of the best known examples with high *ee* is the alkylation reaction of aldehydes, especially benzaldehyde, using (2*S*)-(−)-*exo*-(Dimethylamino)isoborneol ((-)-DAIB) and diethylzinc examined by *Noyori et al*.[17] This reaction led to the publication of a plausible mechanism for the elucidation of the occurring (+)-NLE. It showed the formation of dimers from the chiral catalyst and the zinc organyl, whereby the heterochiral dimer is more stable than the homochiral dimer, which consequently decomposes in solution.[9c]

According to his observations, using a mixture of the enantiomers with low *ee*, formation of catalytically active zinc alkoxides by the chiral ß-amino alcohol and the organozinc reagent is responsible for the asymmetric formation at the alkylation reaction (Figure 3).
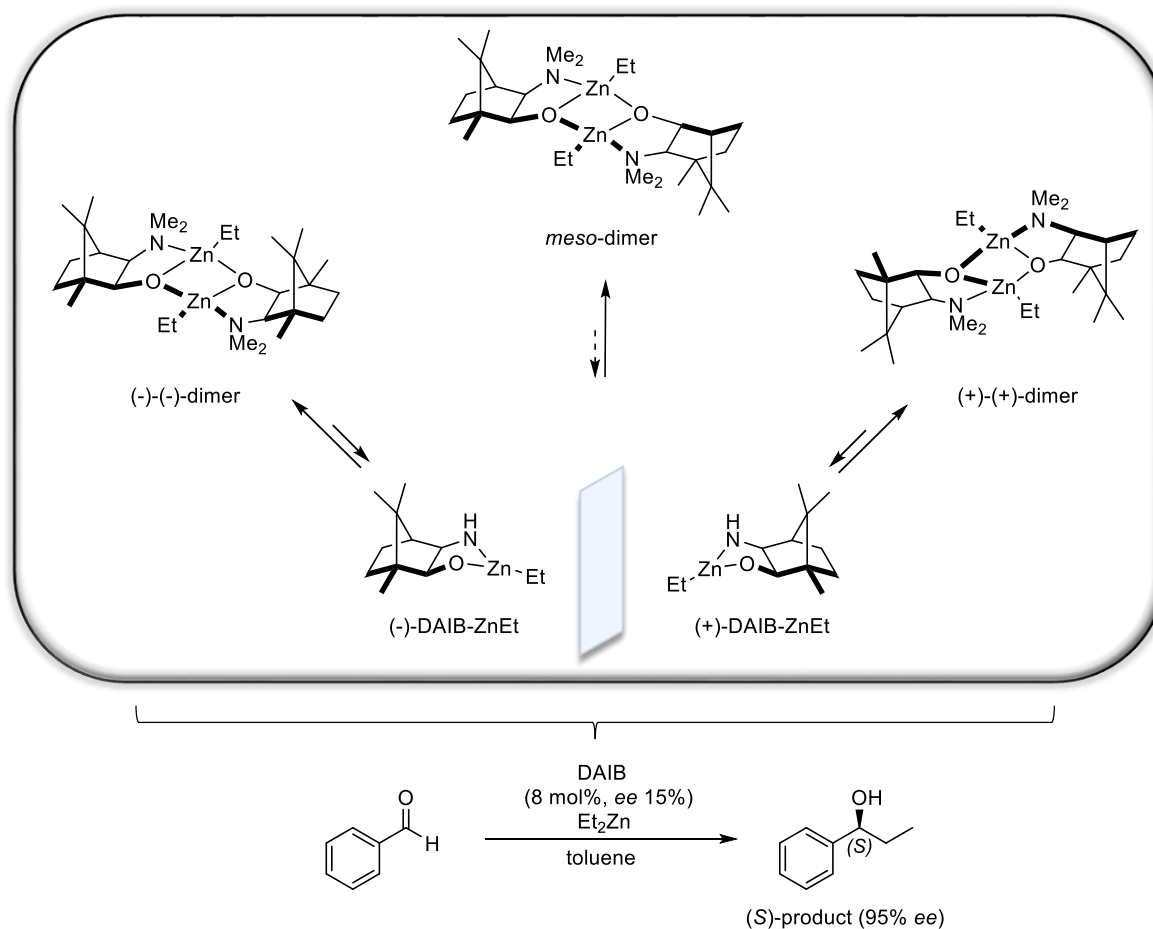
Figure 3: Asymmetric alkylation of benzaldehyde with diethylzinc as alkylating agent and enantioenriched DAIB as auxiliary showing a (+)-NLE on the product-alcohol distribution. The NLE is induced by the formation of catalyst dimers, the *meso*-form is more stable than the two homochiral complexes.[17]

1.2   Self-Amplifying Autocatalysis

Up to this point in asymmetric catalysis, the structure of the chiral catalyst was always unequal to the reactants participating in the reaction. If the step towards self-amplifying autocatalysis is now to be taken, the catalyst used must correspond to the product in terms of both structure and configuration.[18]

The first and only known reaction combining self-amplifying autocatalysis with a (+)-NLE to date, without the addition of required ligands or catalysts, is the *Soai* reaction.[19] *Kenso Soai* and coworkers discovered the reaction in 1995 which represents the alkylation of pyrimidine-5-carbaldehyde with diisopropylzinc forming the corresponding secondary chiral alcohols (Figure 4).[20]
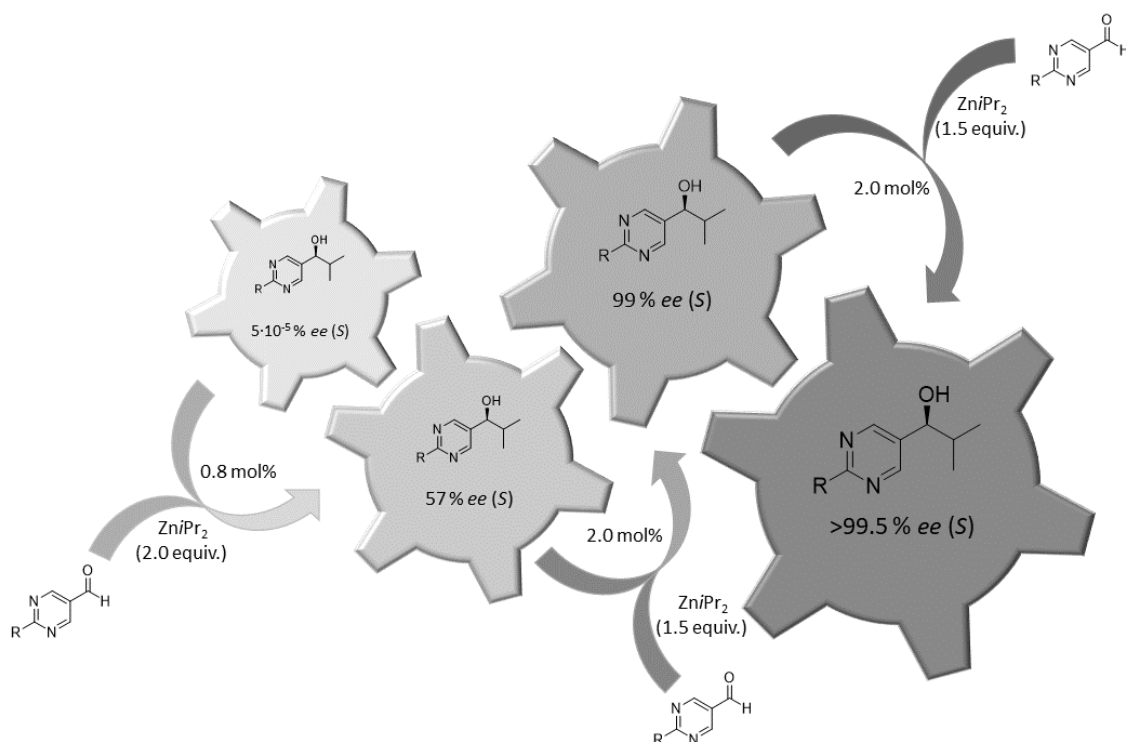
Figure 4: Self-amplifying autocatalysis of pyrimidine-5-carbaldehyde with diisopropylzinc and the addition of catalytic amounts of the newly formed product-alcohol in very low *ee* leading to almost enantiopure product within four reaction cycles.[21]

With the addition of the product with a very low enantiomeric excess (*ee*) of 2% in the first step a total *ee* of 88% within four reaction cycles was obtained.[20] The limit of this reaction is a product *ee* of 95%, even when the chiral alcohol used has an *ee* of 99%. To further develop and improve this result, some modifications were made to the pyrimidine ring, most notably the substitution at the 2-position. These results were published by *Kenso Soai*'s group in 1999, presenting a substrate consisting of a pyrimidine ring substituted at the 2-position with a *tert*-butylethynyl group and carrying an aldehyde group at the 5-position (*t*BuPym-CHO) as usual. The product alcohol was used with an *ee* of over 99.5% and resulted in asymmetric product formation with over 99% yield and an *ee* of 99.5% that was reused for the next reaction cycle. The alcohol thus obtained, performed the amplification without loss in *ee* or yield even after ten cycles.[19b, 20-21] Moreover, in further studies of the self-amplifying system, a nearly enantiomerically pure product alcohol of over 99.5% *ee* was obtained within three synthesis cycles with an alcohol of 0.00005% *ee* being employed.[21] For the first time, a reaction was found that exhibited the behaviour of perfect asymmetric autocatalysis (Figure 4).

Moreover, this powerful reaction can be initiated by a variety of other chiral molecules or chiral crystals of achiral compounds.[22] The formation of a non-racemic product can also be achieved by irradiation with circularly polarized light.[20] Even without the use of a chiral catalyst, spontaneous symmetry breaking occurs and a non-racemic product is obtained.[23] Since its discovery, the *Soai* reaction and its mechanism have provided a good reference point for further research activities and the understanding of the handedness that evolved on our planet many billions of years ago. This is based on the fact that the most widely held notion of the reinforcement and maintenance of homochirality is that the increase in enantiomeric excess is a self-amplifying process that occurs over time through self-involvement.[1]

As a consequence, the goal has also been the investigation of the reaction conditions and the mechanism, as well as possible substrates required for such asymmetric self-amplifying autocatalysis processes. Until today, the desire for a better understanding of the processes involved in such systems at the molecular level has motivated numerous research groups to conduct research in the field of asymmetric, self-amplifying reactions for many years. Amplifying systems have been identified in many fields of chemistry, but only one real self-amplifying autocatalysis has been found so far.

CHAPTER 2

Investigation of the Kinetics and
Intermediates of Pyridyl and Pyrimidyl
Soai Substrates

2.1   State of Knowledge

Initially, investigations were carried out to prove *Frank*'s theoretical model from 1953 for autocatalysis over numerous reaction cycles, which ultimately leads to homochirality. In first instance, this model is based on the ability of each enantiomer to replicate itself and secondly to suppress the formation of its mirror image. The presence of a sigmoidal kinetic reaction profile was often used as proof of the existence of asymmetric autocatalysis. However, this alone was not sufficient. In the further course of research, experiments were started with alkyl metal reagents. These are capable of building complex chiral structures, which in turn can transfer their chiral information to the reaction system, leading to nonlinear effects through self-amplification or an inhibition mechanism and thus to asymmetric enantioselective amplification. Numerous experiments and different reactions with alkylzinc reagents were able to produce both positive and negative NLEs with the aid of added chiral ligands, but no system was found that underwent autocatalysis according to *Frank*'s ideas, which can lead to homochirality. More than 40 years later, in 1995, *Kenso Soai* described an alkylation reaction of pyrimidine-5-carbaldehyde with diisopropylzinc resulting in a nearly enantiopure secondary alcohol due to the product's self-amplified autocatalysis with initially low enantiomeric excess. It is unique in its combination of self-amplification and asymmetric autocatalysis and therefore meets both requirements of *Frank*'s model on the origin of homochirality.[19b, 20]

2.1.1   Influence of Reaction Parameters and Substrates

For self-amplifying autocatalysis to take place, the individual parameters must interact with each other. There are several parameters that can favour or inhibit a successful process. To date, numerous attempts have been made, both at the theoretical level and experimentally to understand the peculiarity of their behaviour. This includes the influence of various reaction parameters on the reaction as well as the variability of the substrate scope.

After the discovery of the specificity of the reaction, systematic studies were carried out on suitable *Soai* starting substrates. In addition to pyrimidines, pyridine as well as quinoline derivatives are also suitable as basic building blocks.[24] All these formal γ-amino aldehyde molecules are transferred to chiral γ-amino alcohols after alkylation. Their related species, the β-amino alcohols are known to be good catalysts for asymmetric alkylation of aldehydes.[25] Changes in reactivity were also observed when the aromatic compound was substituted, as it improves the solubility in toluene and thus the

reaction can proceed better. In addition to the pyrimidine-5-carbaldehyde bearing an alkynyl *t*Bu at 2-position, which is the best performing and original starting compound, substrates with TMS and adamantyl residues substituted at the 2-position in particular show the best results due to the electron-withdrawing effect of the triple bond and the bulkiness of the associated residues.[19b, 23b, 26]

Furthermore, the solvent also plays an important role in the outcome of the *Soai* reaction. For example, diethyl ether and tetrahydrofuran as strongly coordinating solvents caused side reactions such as the reduction of the aldehyde to the primary alcohol. A precipitate was also formed, which in the case of diethyl ether had a higher *ee* than the reaction solution.[27] Even though numerous other solvents were tested for use in the *Soai* reaction, only toluene was satisfactory and became the standard solvent in such reactions.[19b]

As a last key parameter, the alkylating agent naturally also plays a decisive role and the reaction is strongly limited to the use of zinc organyls only.[28] In this reaction setup, the outstanding performance of diisopropyl zinc should be emphasized being the only alkylating reagent for which the desired amplification could be observed. This fact could be attributed to the steric hindrance of the isopropyl groups with the aid of DFT calculations.[28b]

The choice of the alcohol used catalytically to transfer the chiral information is also key for the outcome of the *Soai* reaction. If the product alcohol is used in approximately 20 mol% enantiomeric purity, the product is obtained with an enantiomeric excess of over 99%. If the catalyst is used with a lower enantiomeric purity, enantiomeric excesses of up to 96% can still be achieved. Between 0.2 and 20 mol% catalyst, no noticeable influence on the formation of the product alcohol (84-96% *ee*) can be observed. The use of more than 20 mol% catalyst shows much worse amplifications, whereas amounts below 0.01 mol%, although with high or low enantiomeric excesses, show a scattering of the product *ee*.[24]

In addition to the product-alcohol, other sources can also induce amplification in the *Soai* reaction. For example, circular-polarized light, amino acids[29] or isotope-labelled compounds[30] can also induce a deflection of the asymmetric reaction by creating a small deviation in the *ee* to the racemate, which is sufficient to influence the self-amplifying autocatalysis towards high yields with good *ee*'s. Even when carrying out the reaction with pyrimidine-5-carbaldehyde and diisopropylzinc without an additional trigger, *Soai et al.* were able to achieve enantioselective amplification.[23c]

In addition to the reaction substrates and the solvent, the reaction conditions can also influence the outcome of the reaction. Temperature in particular has a major influence. Between - 20 °C and +25 °C, the *Soai* reaction shows no loss of amplification. Above and below this temperature range, the reaction continues, even with full conversion. However, the enantioselectivity drops significantly. It is worth mentioning that *Blackmond* and *Brown* were able to demonstrate an inverse temperature dependence in the reaction rate in 2010.[31]

2.1.2   Mechanistic Investigations of the *Soai* Reaction

Due to its ability to spontaneously break symmetry and the even better asymmetric amplification through the use of a chiral additive, the *Soai* reaction is the only known self-amplifying autocatalysis that represents a good model for the development of homochirality.[32] Since its discovery in 1995, almost 30 years ago, it has fascinated numerous research groups who have set themselves the task of understanding and elucidating its mechanism. Scientists are also driven by the possibility of applying the knowledge gained to other systems.

The extended *Kagan* ML$_2$ Model by *Blackmond* and *Brown*

Blackmond and *Brown* proposed a first comprehensive mechanism based on an extended *Kagan* ML$_2$ model[9b, 14] in combination with *Noyori*'s reservoir model[16b] using spectroscopic, kinetic and computational data.[33] Both models from *Kagan* and *Noyori* describe the formation of dimers or higher homologues, which are responsible for the non-linear effect that occurs. The formation of monomers and dimers is in equilibrium, which is summarized by the equilibrium constants K_{homo} for homochiral and K_{hetero} for heterochiral dimers in the equilibrium constant K_{dimer}. However, the two models differ significantly in one aspect: while *Kagan* completely ignores the monomers and identifies the dimeric or higher order species as catalytic species, *Noyori* describes the monomers that are in equilibrium with catalytically inactive higher homologues in a secondary cycle and serve as a reservoir for the active catalytic cycle. In any case, the concentration and enantiomeric excess are influenced by the equilibrium between monomers and dimers, as its shift to one side results in nonlinearity. The similarity to *Noyori*'s asymmetric alkylation of aldehydes initially suggested the monomer model for the *Soai* reaction as well. However, some indications during the mechanistic investigations pointed to higher order species as catalysts.

Soai himself postulated the formation of a pyrimidyl-zinc alkoxide as the catalytically active species, which dimerizes to form homo- (*R,R* or *S,S*) and heterochiral aggregates which can interconvert.[33-34] Thereby, the equilibrium constant for the formation of the heterochiral dimer K_{hetero} is twice the constant of the homochiral dimer (K_{hetero}/K_{homo}=2).[35] An imbalance of the enantiomers present thus explains the nonlinear effect as soon as more of the more stable heterochiral dimer is formed. With kinetic investigations using reaction calorimetry, which tracks the heat generated and released during the reaction, *Blackmond* and *Brown* determined the reaction rate by time-dependent tracking of the heat flow. These measurements clearly indicated an autocatalytic reaction was taking place showing a heat development at the beginning due to the build-up of the catalytic species. After reaching the maximum, the heat development decreased again as the reaction proceeded.[36]

The observed reaction rate for the enantiomerically pure catalyst was almost twice as high as for the racemic catalyst. This led *Blackmond* and *Brown* to consider homochiral dimers as catalytic species, while the heterochiral dimers are inactive.[23b] The dimeric structures were elucidated by NMR spectroscopy adding *i*Pr$_2$Zn to the catalytically used alcohol in various enantiomeric excesses. In addition to homo- and heterochiral dimers with a central [ZnO]$_2$-unit in toluene,[34] a 12-membered macrocycle was presented.[33]

Through further kinetic investigations by *Blackmond et al.* using experiments with different stoichiometric ratios and initial concentrations, a statement could be made about the reaction order of the three reaction partners used.[31] The resulting reaction rate provided for an independence of the zinc organyl concentration, which is included in the equation in zero order. The alcohol, which is present in combination with the zinc organyl as zinc alcoholate is assigned a reaction order of 1, whereas a reaction order of 1.6 was determined for the aldehyde.[31]

Studies at low temperatures by *Ercolani et al.*, which showed higher selectivity at lower temperatures, extended the dimer model to include tetrameric complexes. The faster reaction at low temperatures was explained by the formation of reactive oligomer structures, which become unstable with increasing temperature, whereby the induction phase and reaction speed decrease. These tetrameric complexes were studied at low temperatures by *Gridnev et al.* using DFT calculations and NMR spectroscopy.[28b, 31, 34]

In 2012, *Blackmond*, *Brown* and coworkers reported the observation of a hemiacetal intermediate in kinetic measurements by NMR spectroscopy during the *Soai* reaction of 2-(adamantylacetylene-1-yl)pyrimdine-5-carbaldehyde (**AdPym-CHO**), which is presumably formed by addition of a zinkalkoxide to the aldehyde. It was observed that the formation of the hemiacetal increased with initial aldehyde concentration, but above all with decreasing temperature.[37] However, after quantum chemical DFT calculations and kinetic analyses with assumed data and activation parameters of hemiacetal formation, which do not agree with experimentally measured data,[38] *Gridnev et al.* assigned the hemiacetal intermediate the role of an unimportant secondary species as a non-direct precursor of the product alcohol.[39] Apart from *Hawbaker* and *Blackmond*'s discovery of hydroxyethers that inhibit the reaction process,[32] no importance was attached to hemiacetal structures over the years. Instead, this view supported the development of a mechanism that proceeds *via* a tetrameric alkoxide catalyst.[40]

In addition to many discoveries of intermediates and speculations about the mechanism, there has been much discussion in the past about the active catalytic species that enables self-amplifying autocatalysis. It was not until 2020 that two different groups of researchers, *Denmark et al.* and *Trapp et al.*, independently published a reaction mechanism *via* which the *Soai* reaction is supposed to take place.
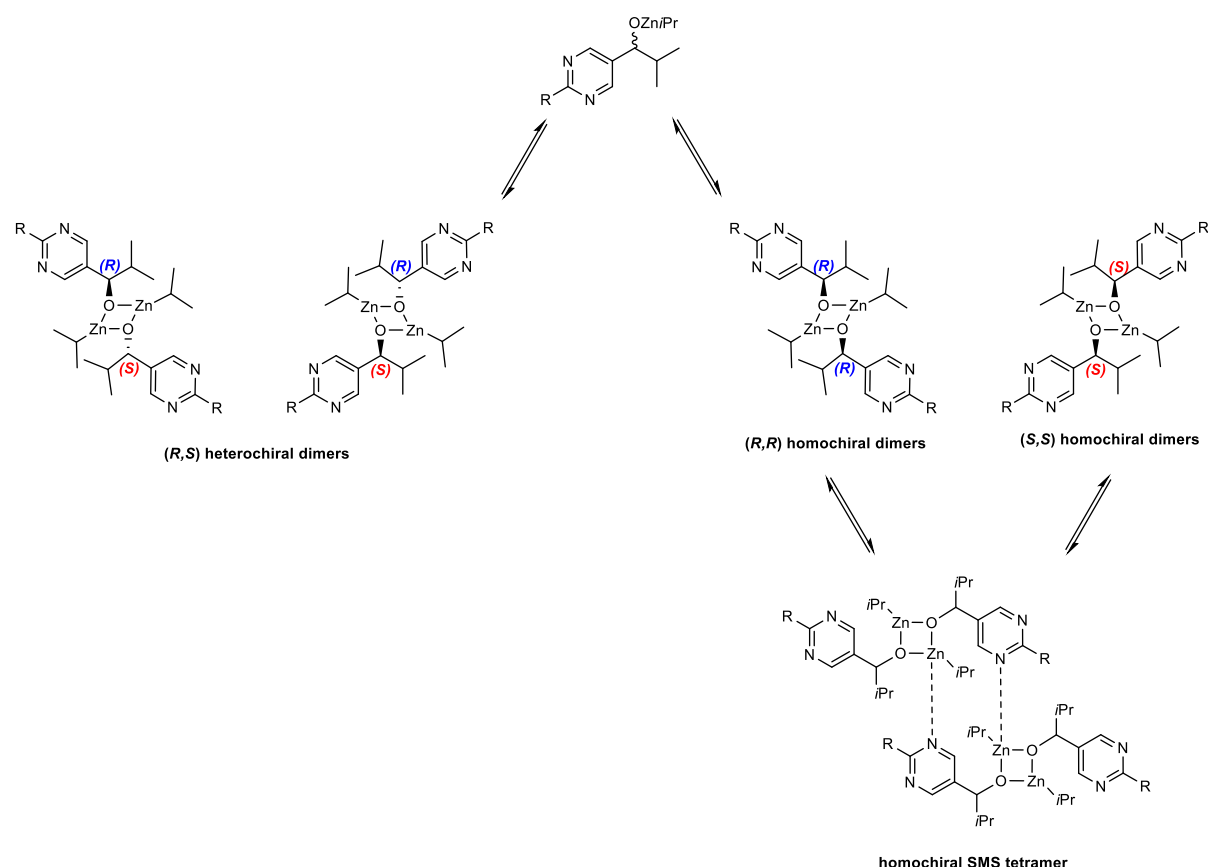
Figure 5: Dimeric and tetrameric hetero- and homochiral aggregates of a pyrimidyl alkoxide.[41]

Mechanistic Proposal by *Denmark*

In his work, *Denmark* investigated the role of the nitrogen atoms on the aryl ring of the aldehyde substrate and observed a self-amplifying autocatalytic behaviour in the reaction of TMS-ethynyl and *t*Bu-ethynyl 5-substituted 3-carbaldehydes with diisopropylzinc and non-racemic product alcohol as ligand. This demonstrated that only one nitrogen atom in the aromatic ring is sufficient for the self-amplifying character of this reaction,[42] whereas alkylation with diethylzinc did not show the desired catalysed alkylation reaction in the above-mentioned systems. The substrates also showed similar behaviour to the already known pyrimidines with regard to the inverse temperature dependence of the reaction rate.[42a]

In addition, *Denmark* investigated the structure of zinc alkoxides in solution using ^{1}H NMR measurements. He was able to identify differences between phenyl and pyridyl alkoxides, which are present as cubic tetramers or tetrameric aggregates. He assigned catalytic activity to these tetrameric aggregates, described as SMS (square-macrocycle-square) tetramers, in his "cube-escape" mechanism.

The catalytic cycle is then initiated by the aggregation of four identically configured zinc alkoxides. Only these homochiral species, in contrast to the inactive zinc alkoxides configured from two (*R*) and two (*S*) enantiomers, can bind the substrate in the further course of the process.[42a, 43] The aldehyde can then be activated by coordination at two unoccupied alkoxyzinc sites of the tetramer and alkylated in the next step by an *i*Pr₂Zn molecule (Figure 6).[43] For the reaction, reaction orders for the reactants were also determined using *in situ* React IR measurements. A first order dependence was determined for the alcohol and a zeroth order dependence for both the aldehyde and the *i*Pr₂Zn concentration.
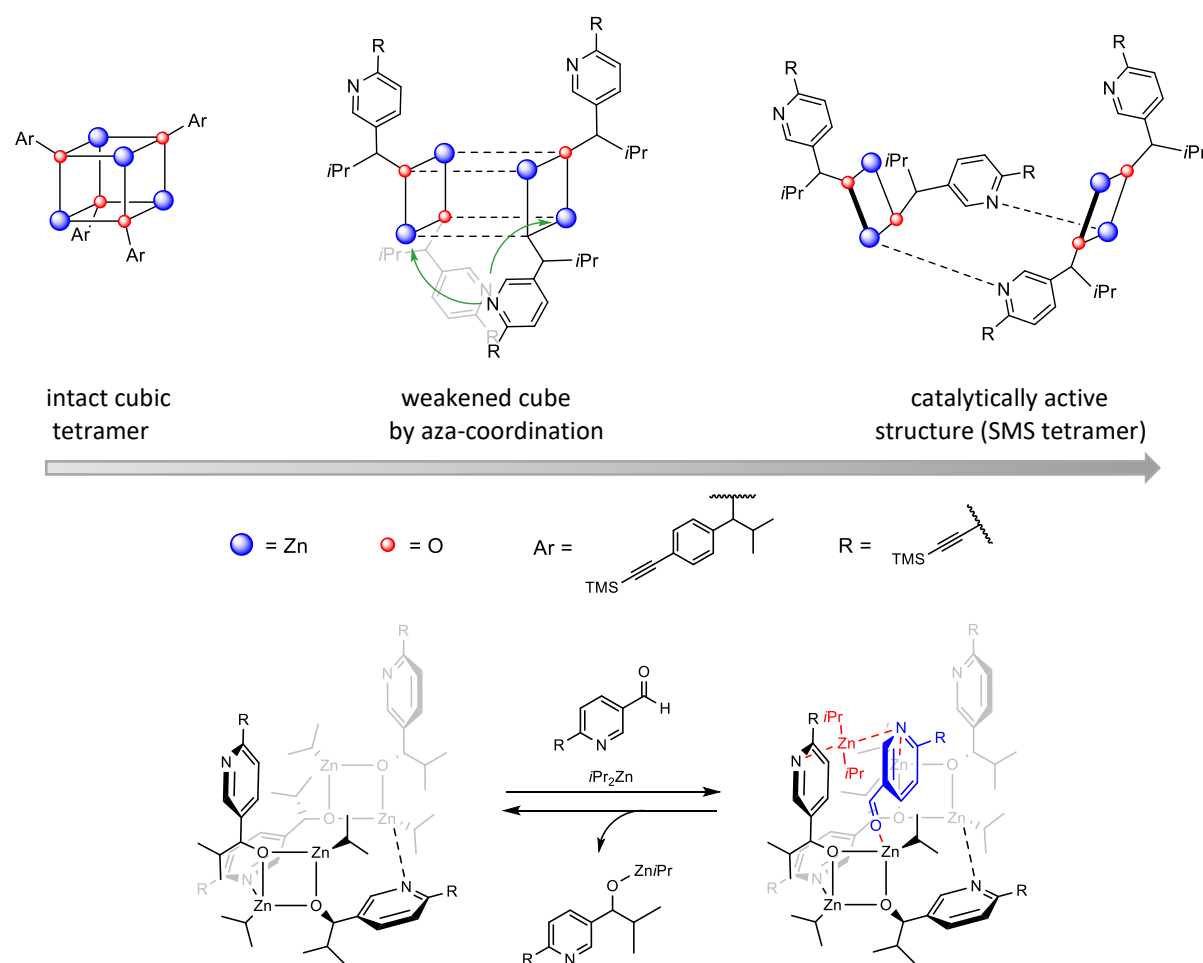
Figure 6: Autocatalytic model of the *Soai* reaction of a **TMSPyr** system *via* a SMS tetramer as catalytically active species by *Denmark et al.*[42a]

Mechanistic Proposal by *Trapp*

In contrast, the high-resolution mass spectroscopic and kinetic investigations of a *tert*-butyl ethinyl pyrimidine system (***t*BuPym**) by *Trapp et al.* indicated the formation of a transient hemiacetal zinc alkoxide as the catalytically active species. This assumption was supported by doping experiments in which a freshly initiated *Soai* reaction was added to an already running reaction. In addition, the formation of the hemiacetal zinc alkoxide species assumed to be the active catalyst was monitored in comparison with aldehyde and alcohol concentration. The parabolic course of the hemiacetal zinc alkoxide, which slowly builds up during the so-called induction phase, while the formation of the product alcohol still progresses very slowly, was remarkable. It reaches its maximum in the linear, self-amplifying increase of the product alcohol. From the kinetic data, a reaction order of 1.9 was determined for the aldehyde and a 1st order dependence in alcohol concentration. The inverse temperature dependence of the reaction kinetics can be explained by the very dynamic formation and decomposition of the hemiacetal. The formation of the diastereomeric zinc hemiacetals can reinforce an initial imbalance of the enantiomers of the product alcohol (Figure 7).[41a] Considering the autocatalytic (*R*)-cycle of the mechanism, the initial step is the formation of the zinc alkoxide **(*R*)-X₁** from the aldehyde and a diisoproylzinc. This is in equilibrium with the corresponding homo- **(*R*,*R*)-X₂** and heterochiral **(*R*,*S*)-X₂** dimers. Due to their different stabilities and formation rates, the dimers are responsible for the orientation towards the dominant enantiomer in the course of the cycle. If one of the alcohol enantiomers is present in excess, statistically more homochiral dimers are formed. By incorporating the same alcohol enantiomer into heterochiral dimers, it is removed from the equilibrium and shifted further to its side.[44] Combined with an aldehyde molecule, the zinc alcoholates **(*R*)-X₁** can form the hemiacetal zinc alkoxide structure **(*R*,*S*)-X₃**, with the equilibrium being on the side of the alcoholates. The transient hemiacetal **(*R*,*S*)-X₃** represents the catalytically active species, which is necessary for the autocatalytic amplification of the respective enantiomer. Its formation is slow, whereas the alkylation reaction proceeds rapidly as soon as the hemiacetal has been formed in sufficient quantities.
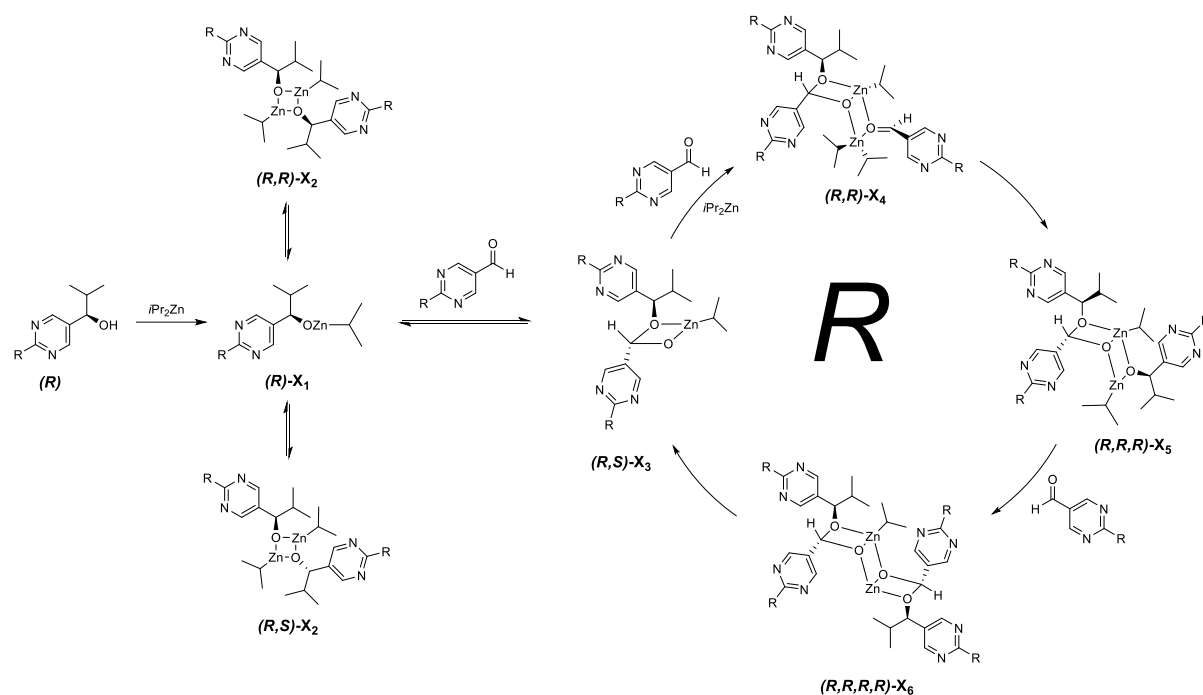
Figure 7: (*R*)-cycle of the proposed mechanism of the *Soai* reaction with the formation of the transient catalytically active Zn-hemiacetal catalyst by *Trapp et al*.[41a]

In the next step, another aldehyde molecule including a diisoproylzinc coordinates to the hemiacetal (**(*R,R*)-X₄**) which enables the alkyl transfer to another aldehyde (**(*R,R,R*)-X₅**). For this step, structurally related intermediates were identified in mass spectroscopic analyses, which further confirm the sequence of the postulated mechanism.[11a, 38] With the introduction of a further aldehyde molecule, a dimeric form of the catalytically active hemiacetal (**(*R,R,R,R*)-X₆**) is formed. Dissociation of the dimer produces two monomeric catalytically active hemiacetals.

Comparison of the two Mechanistic Proposals

At first glance, the differences, particularly in the determination of the reaction order, can be attributed to the different structures of the systems investigated. While *Denmark* obtained his results for the reaction order from studies on unsubstituted pyridine-3-carbaldehyde (**HPyr-CHO**) with catalytically added TMS-ethynyl substituted alcohol, which is a reaction in the non-autocatalytic sense, *Trapp*'s data is based on experiments with a *tert*-butyl pyrimidine system (**tBuPym**). However, the same reaction behaviour with regard to the inverse temperature dependence of the reaction rate and the same curve behaviour for all investigated systems depending on the concentration used indicate that the mechanism must proceed at least in a very similar way for both pyridines and pyrimidines - regardless of the rest. In addition, the structure of *Denmark*'s catalytically active tetramer was established during studies with the isolated zinc alkoxide without the addition of the aldehyde. The structures of the intermediates and the zinc hemiacetal in *Trapp*'s publication were established during *in situ* measurements of the ongoing reaction. Nevertheless, it is not yet possible to make a more precise statement about the behaviour of pyridines in comparison to pyrimidines. The similar behaviour of all systems with regard to the reaction profile also does not allow any conclusions to be drawn about the course of the reaction mechanism without further investigations.

2.2   Objectives

In previous work, some *Soai* substrates, whether pyridines or pyrimidines, with different residues have already been studied by different methods. In addition to the classical **tBuPym-CHO/tBuPym-OH** system, the unsubstituted and methyl-substituted heterocycles as well as trimethylsilyl (TMS) and adamantyl (Ad) acetylene pyridines and pyrimidines were also examined intensively.[20, 24, 42a, 43, 45] *Denmark et al.* observed zinc alkoxides in NMR studies,[37, 42a] as well as *Blackmond et al.* acetal intermediates during the investigation of the *Soai* reaction with adamantly pyrimidine by 2D spectroscopy. Furthermore, React IR [42a, 43] and reaction calorimetry [33, 35] have been used to gain more insights and information about the mechanism and important processes during the *Soai* reaction. Now, the still remaining and overarching problem is that all these measurement data and pieces of the puzzle are not comparable with each other, because they were obtained with different measurement methods and under varying conditions. Thus, it is not possible to make a clear statement about the general mechanism, since it could be, of course, that all these systems, especially pyridine and pyrimidine, follow a different mechanism.
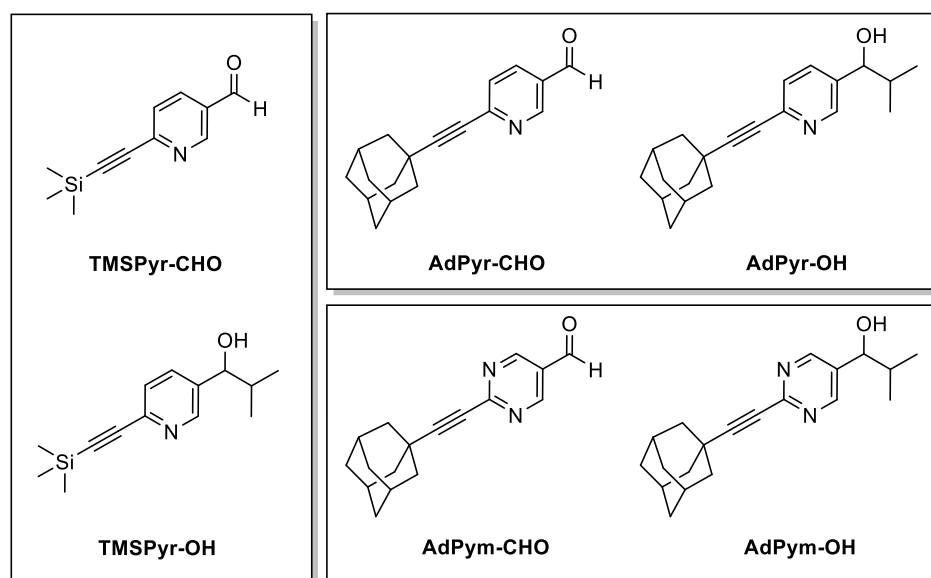

Figure 8: Overview of the three autocatalytic systems to be examined: the two pyridyl systems **TMSPyr-OH/TMSPyr-CHO** and **AdPyr-OH/AdPyr-CHO** as well as the pyrimidyl based system **AdPym-OH/AdPym-CHO**.

The aim of this work was to experimentally investigate the *Soai* systems **TMSPyr-CHO/TMSPyr-OH** as well as **AdPym-CHO/AdPym-OH** and **AdPyr-CHO/AdPyr-OH** (Figure 8) with respect to their kinetics and to identify occurring intermediates. The main focus should be on the representation of each individual reaction partner, so that a quantitative statement can be made about both the aldehyde and the reaction products at any time in the course of the reaction. For the kinetic elucidation the flow-injection analysis (FIA) *via* HPLC should be used. The separation of all reaction participants can be performed and monitored *via* this analytical method in real time due to constant injection intervals. For the investigation of the reaction intermediates, pulsed injection of samples into an APCI-Orbitrap-MS should be performed. Here, it is also possible to follow the appearance of different molecules in time.
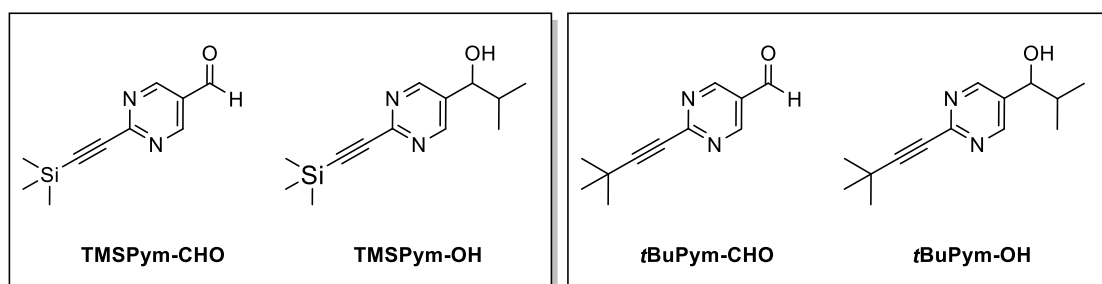
Figure 9: Pyrimidine systems **TMSPym**[46] (left) and **tBuPym**[41a] (right) previously measured in the same way by the *Trapp* group.

Afterwards, the obtained measurement data and results should be compared with each other and with systems such as **TMSPym-CHO/TMSPym-OH**[46] and **tBuPym-CHO/tBuPym-OH**[41a] (Figure 9) previously investigated in the same way. As a consequence, a clearer statement about the reaction mechanism, as well as the catalytic species of the *Soai* reaction are expected to be possible. Finally, the question can be clarified whether the pyridines and pyrimidines follow the same mechanism.

2.3   Synthesis of the Reactants

To test the *Soai* reaction with different substrates, the reactants, pyridine and pyrimidine aldehydes with different residues as well as their product alcohols had to be synthesized first.

Synthesis of the Adamantyl Residue

Unlike the TMS-acetylene residue, which was commercially available, the adamantyl-acetylene had to be prepared first. The procedure which is based on a protocol by *Negishi* for the conversion of ketones to terminal acetylenes, was adapted from *Busch* and coworkers (Scheme 1).[47]
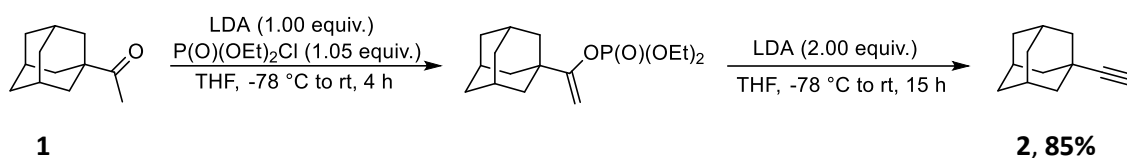
Scheme 1: Synthetic pathway towards adamantyl acetylene **2** starting from adamantyl 1-ketone **1** with LDA and diethyl chlorophosphate.[26]

First, adamantyl-1-methyl ketone **1** was treated with Lithium diisopropyl amide (LDA) and diethyl chlorophosphate to give the intermediate enol phosphate. In order to initiate a β-elimination of the phosphate, the reaction mixture was treated with LDA after 3 h. The desired adamantyl-acetylene **2** was obtained in 85% yield.[48]

Synthesis of 6-substituted Pyridine *Soai* Substrates

The synthetic procedure towards the 6-substituted pyridine-3-carbaldehydes and the corresponding alcohols was adapted from *Denmark* and coworkers.[42a]
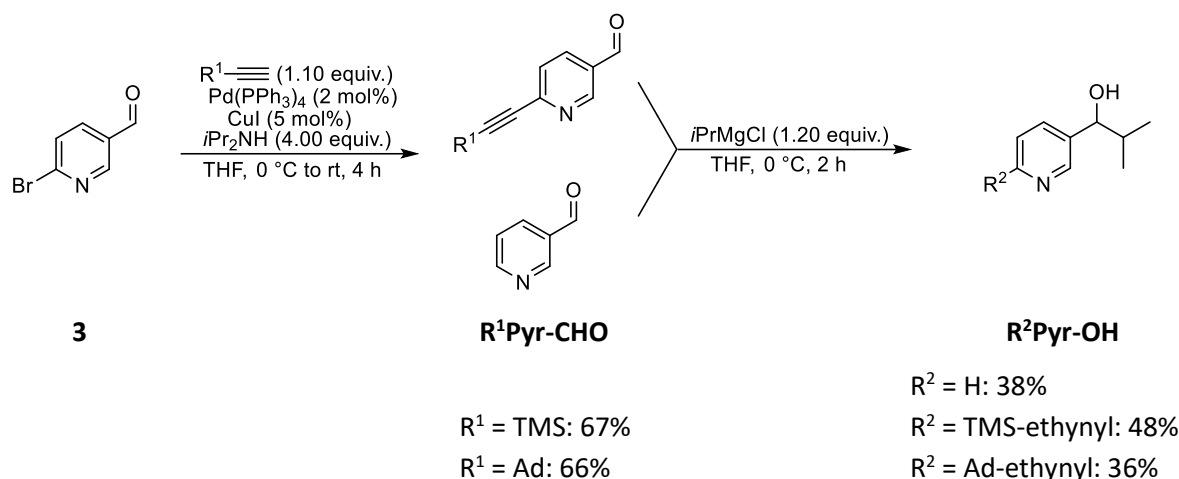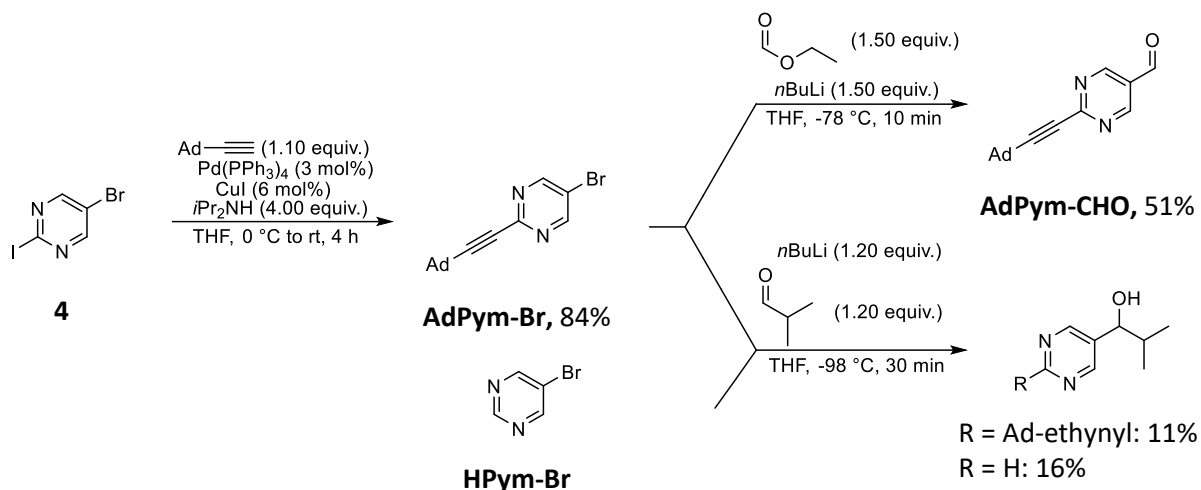

Scheme 2: Synthetic procedure towards the substituted pyridine-3-carbaldehyde **TMSPyr-CHO** and **AdPyr-CHO** *via* a *Sonogashira* cross-coupling reaction as well as the synthesis of the corresponding alcohols **TMSPyr-OH** and **AdPyr-OH**.[42a]

In order to improve the solubility of the substrates in toluene and to achieve better selectivities, acetylene residues were introduced at the 2-position.[19b, 23b, 26] The *Sonogashira* cross-coupling reaction was chosen as an efficient method to form a carbon-carbon bond between terminal alkynes and aryl halides.[49] Therefore, 6-bromonicotinaldehyde **3** was treated with Pd(PPh$_3$)$_4$, CuI as co-catalyst, and *i*Pr$_2$NH in THF and reacted with the acetylene substituent at 0 °C. After purification, the aldehydes **TMSPyr-CHO** and **AdPyr-CHO** could be isolated in good yields of 67% and 66%. A *Grignard* reaction using isopropylmagnesium chloride was performed to obtain the desired secondary alcohols **TMSPyr-OH** and **AdPyr-OH** in moderate yields of 48% and 36%, respectively (Scheme 2). The poor yields can be explained by the fact that the reduction product, benzyl alcohol, was obtained as a by-product during this type of reaction. The alcohol enantiomers were separated from each other using preparative HPLC so that they could later be used enantiomerically pure in the study of reaction kinetics.

Synthesis of 2-substituted Pyrimidine *Soai* Substrates

Pyrimidine-based substrates carrying a trimethylsilyl (TMS) or adamantly (Ad) residue at the 2-position of the heteroaryl ring were also prepared for the kinetic analyses.

Scheme 3: Synthetic procedure towards the substituted pyrimidine-5-carbaldehyde **AdPym-CHO** *via* a *Sonogashira* cross-coupling reaction as well as the synthesis of the corresponding alcohol **AdPym-OH**.[42a]

The commercially available 5-bromo-2-iodopyrimidine **4** was used as the basic building block. For this purpose, the acetylene residue was introduced at the 2-position *via* a *Sonogashira* cross-coupling reaction using Pd(PPh$_3$)$_4$, CuI and *i*Pr$_2$NH in THF. The bromo-acetylene compound **AdPym-Br** was received in 84% yield. The required functional groups, thus an aldehyde **AdPym-CHO** or an alcohol **AdPym-OH** were then obtained *via* bromine-lithium exchange using *n*BuLi at low temperatures plus either ethyl formate or isobutyraldehyde as electrophiles (Scheme 3).[26, 43] The unsubstituted **HPym-OH** was obtained in the same way in 16% yield.

It is worth mentioning that earlier attempts by the *Trapp* group to prepare the **AdPym** aldehyde according to *Denmark*'s prescription, in which the acetylene bromide was first mixed with *n*BuLi at - 97 °C and then treated with ethyl formate provided the aldehyde **AdPym-CHO** in moderate yields.[43] Therefore, a synthesis under *Barbier* conditions was employed, in which the organometallic species is generated *in situ* in the presence of the carbonyl compound.[43] For this purpose, the **AdPym-Br** was cooled to -78 °C and first the ethyl formate and then the *n*BuLi were added.

With this procedure, competing side reactions such as the undesired addition of *n*BuLi to the ethyl formate can be suppressed and the desired halogen-lithium exchange at the pyrimidyl bromide takes place much faster.[50] With the help of the improved synthesis, the **AdPym-CHO** could be obtained in 51%.

AdPym-Br was also used as the starting material in the preparation of **AdPym-OH** and was carried out by means of halogen-lithium exchange at -98 °C and subsequently converted to the alcohol by adding isobutyraldehyde. **AdPym-OH** was obtained only in low yield of 11%. The low yields can be attributed to side reactions and the low stability of the lithium intermediate, as can be observed in formylation.

Synthesis of Diisopropyl zinc

The preparation of diisopropyl zinc was carried out in accordance with a modified prescription of *Knochel* et al.[51]
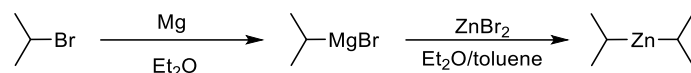
Scheme 4: Synthesis of diisopropyl zinc in toluene using a freshly prepared diisopropylmagnesium bromide *Grignard* and $ZnBr_2$.[51]

For this purpose, zinc bromide was dried under high vacuum and dissolved in diethyl ether. In addition, an isopropyl magnesium bromide *Grignard* solution was prepared from 2-bromopropane and magnesium in diethyl ether. The *Grignard* was added to the zinc bromide to obtain a highly reactive diisopropyl zinc solution (Scheme 4). Although the *Soai* reaction can also take place in ether, the usual solvent is toluene,[24, 27a] as this prevents coordinating effects that could influence the amplifying effect.[34] For this reason, toluene was added to the solution and the diethyl ether was distilled off in several cycles under high vacuum at up to 65 °C until no more diethyl ether was detectable in the ^{1}H NMR (Figure 10). However, the prepared highly concentrated diisopropylzinc solution was not stable for long despite storage in the dark and at 4 °C. After certain time, a solid precipitated and silver-gray discoloration was observed, leading to a decrease in reactivity. For this reason, most of the reactions performed were carried out with commercially available iPr$_2$Zn in toluene (1 M).
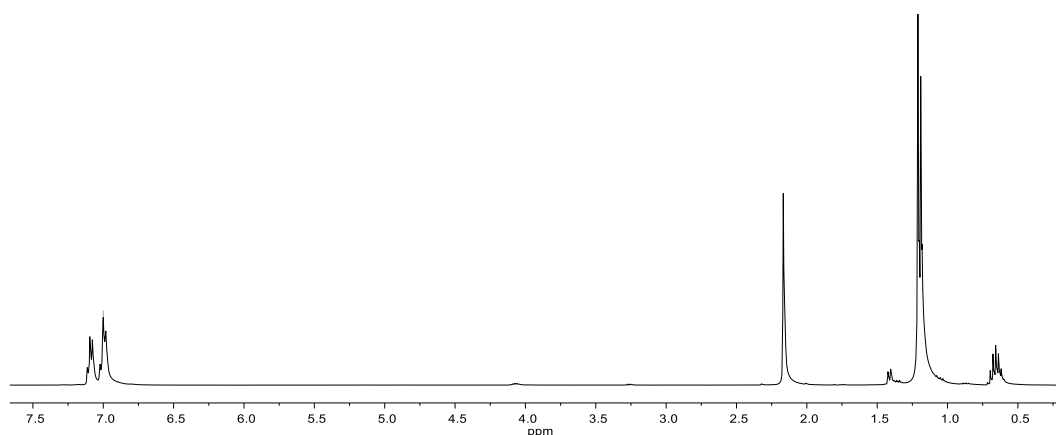

Figure 10: ^{1}H NMR of the synthesized iPr$_2$Zn in toluene free of diethyl ether. The spectrum was recorded in toluene-d_8.

2.4   Kinetic Investigations on the *Soai* Reaction

2.4.1   The Method of Flow-Injection Analysis High-Performance Liquid Chromatography
(FIA-HPLC)

The flow-injection analysis (FIA) method can be used for time-dependent concentration determination in high-performance liquid chromatography (HPLC). It is characterized by the fact that injections are taken from the same sample at constant time intervals and imaged within one chromatographic measurement.

The usage of FIA has several advantages. First of all, a high data density can be produced in a short time. Secondly, if all reaction partners are UV active, which they are in the *Soai* reaction, real-time tracking of an ongoing *Soai* reaction can be implemented by injection at constant time intervals if all components are well separated. This method enables profiling of the aldehyde as well as both product alcohols in particular and occurring by-products such as the reduction product, the corresponding benzyl alcohol. For the quantitative evaluation, a method had to be found in which the UV active solvent toluene, the aldehyde and all products are visible baseline separated. In addition, however, the signals should be as close to each other as possible so that the injection interval is as small as possible and thus a larger amount of data can be obtained. The usual solvent mixture *n*-hexane/*i*PrOH for separation on the HPLC is unsuitable in this case because the *i*PrOH forms hemiacetals with the aldehyde used as reactant,[41a] which is reflected as a plateau in the chromatogram and makes a quantitative determination in the downstream impossible. For this reason, THF is used as an alternative to *i*PrOH, as it does not react with the aldehyde used to form the hemiacetal and at the same time improves or enables solubility of all reaction partners. A constant concentration of 40 mM was used for the *i*Pr$_2$Zn since it has already been proven in previous work that the reaction order of *i*Pr$_2$Zn is 0 and the reaction is thus not dependent on the concentration of the alkylating reagent.[41a]

With the help of calibration lines, the absolute concentrations of the reactants in the course of the reaction can be calculated *via* the integrated peak areas at any time of the reaction. For the graphs, the concentrations of the aldehyde and the alcohol were calculated for each individual injection by means of a calibration line and plotted against time. In order to keep the mass balance of the reaction closed, both the products of interest for the kinetics, the two product alcohols and the reactant aldehyde, had to be integrated subsequently.

To close the mass balance, the concentration of the reduction product (RP), the benzyl alcohol as the only by-product, was then calculated from the mass difference between the reactants and the products for every single injection step (at time *t*) (**equation 1**).

$$[RP]_t = ([CHO]_{insert} + [OH]_{insert}) - ([CHO]_t + [(R)\text{-}OH]_t + [(S)\text{-}OH_t]) \qquad \textbf{(1)}$$

To gain more insights into the dependencies of the different reactants, both the alcohol and aldehyde concentrations were varied independently. For this purpose, the reactions were monitored in real-time and the reaction orders of aldehyde and alcohol were determined from the experimental data. At the end, the systems of the different derivatives, both pyrimidine and pyridine, could be compared with each other. In addition, the behaviour and data obtained could be compared with previously published work, as there are controversial views on the actual mechanism. The reaction order was also calculated differently with a zero order for aldehyde concentrations of pyridine systems by *Denmark*[42a] and a reaction order of 1.6 by *Blackmond*[31] and 1.9 by *Trapp*[41a] in pyrimidine systems on the other side. With these counterparts, it is important to find out whether the mechanisms of pyridine and pyrimidine are different or whether one of the postulates is incorrect.

For the time-resolved investigation of the different systems of the *Soai* reaction using FIA-HPLC analysis the aldehyde and alcohol stock solution in desired concentrations related to the total reaction volume of 1 mL were placed in a GC vial under inert gas atmosphere. The reaction was initiated by the addition of diisopropylzinc and after a short vortexing period, the measurement was started. The first injection took place 30 sec after initiation of the reaction.

By double logarithmic plotting of initial velocity (v_0) *versus* concentration ([compound]), a reaction order for both the aldehyde as well as the alcohol could be determined for each system.

2.4.2   Kinetic Analysis of the HPyr and HPym System

The pyridine system was separated on a Chiralpak® IG-3 column (150 mm, i.d. 4.60 mm, particle size: 3 µm; λ=250 nm) with *n*-hexane/THF = 65:35. In addition to the expected signals for the aldehyde, the alcohol enantiomers and the benzyl alcohol as a reduction product, further peaks of by-products were identified. However, a complete separation of all components could not be achieved. In a measurement with 20 injections and an injection interval of 6 min, the slow consumption of the aldehyde and the formation of the alcohol were detected. However, no significant reaction progress could be detected within 2 h (Figure 11). This indicates that the reactions proceeded very slowly and therefore the method of FIA-HPLC might not be the best monitoring method.
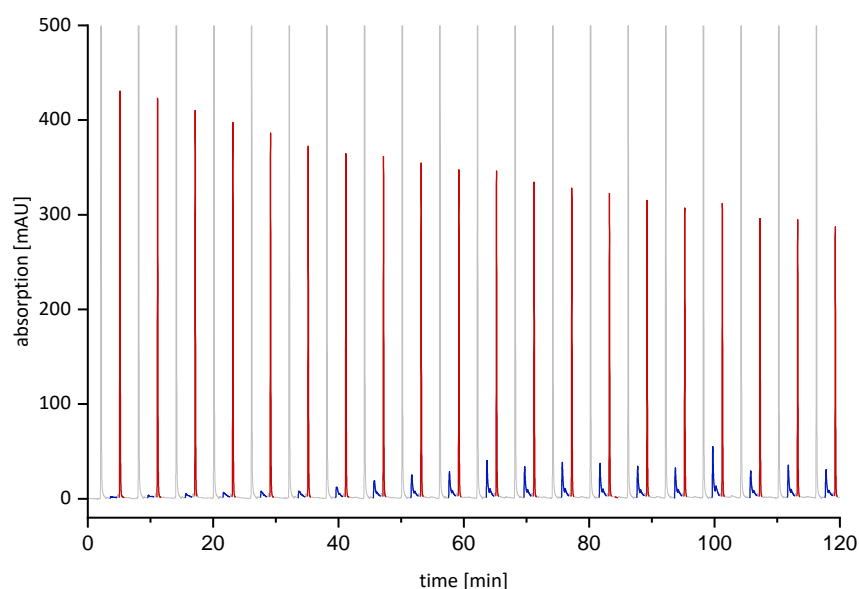
Figure 11: HPLC chromatogram of the *Soai* reaction of **HPyr-CHO** (30 mM) with **HPyr-OH** (1.5 mM) and *i*Pr$_2$Zn (40 mM). The aldehyde is shown in red, the major alcohol in blue and the solvent toluene in gray on a Chiralpak® IG-3 column (150 mm, i.d. 4.60 mm, particle size: 3 µm; λ = 250 nm) with *n*-hexane/THF = 65:35, 1.0 mL.

Due to the difficulties during the multiplexing HPLC measurements an alternative procedure to monitor the reaction progress was carried out. In this case, the reaction was performed in a *Schlenk* tube instead of a GC vial. An aliquot was taken every 15 min, quenched and prepared for HPLC measurements. However, despite a reaction time of 5.5 h, it was not possible to generate a sufficient amount of data for a comprehensive kinetic evaluation. One reason for this was the formation of additional by-products, which did not allow a quantitative determination of the concentrations. On the other hand, the reaction was not fast enough for an efficient autocatalysis to be detected.

The pyrimidine system was separated on a Chiralpak® IA column (250 mm, i.d. 4.60 mm, particle size: 5 µm; λ = 250 nm) with *n*-hexane/THF = 65:35 as running medium (Figure 12). The separation of all required reaction components was achieved in an interval of 6.5 min. However, the aldehyde peak appeared at the end of a plateau extending over an interval of 2 min. This made it impossible to quantify the aldehyde. In addition, the poor solubility of the pyrimidine in toluene made it difficult to carry out a concentration study, as a concentration of 10 mM could not even be achieved. While the slow consumption of the aldehyde could be observed, it was also clear that the minor alcohol enantiomer was formed here, while the amount of product alcohol used hardly increased or did not increase at all over the reaction time of 2 h. There could neither be seen an amplification of the product alcohol enantiomer. To determine if the aldehyde was consumed over a prolonged reaction time, the *Soai* reaction was carried out in a *Schlenk* tube over 66 h. Within this time, the aldehyde was almost completely consumed and one of the alcohol enantiomers was amplified to an enantiomeric excess of 95%, which is in good agreement with the literature.[19a] Nevertheless, some by-products were formed, too.
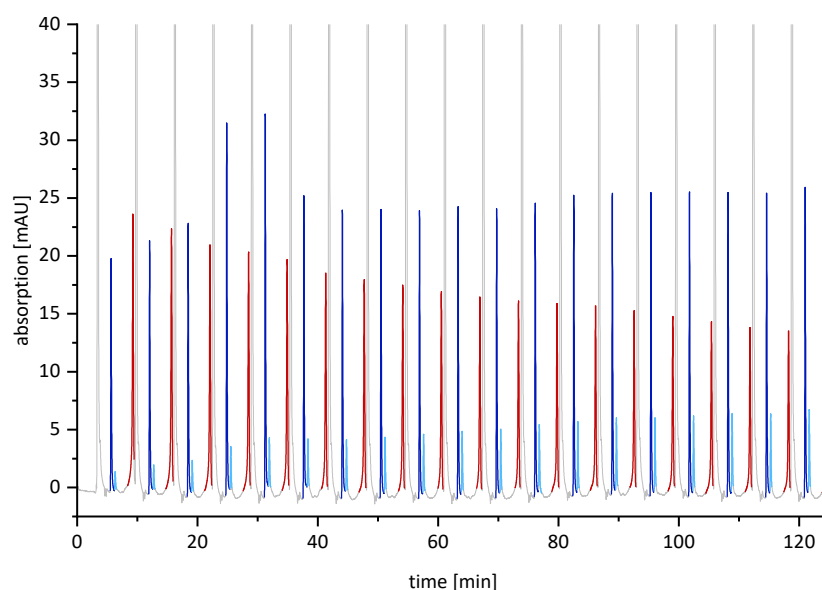
Figure 12: HPLC chromatogram of the *Soai* reaction of **HPym-CHO** (< 10 mM) with **HPym-OH** (1.5 mM) and *i*Pr$_2$Zn (40 mM). The aldehyde is shown in red, the major alcohol in dark blue, the minor alcohol in light blue and the solvent toluene in gray on a Chiralpak® IA column (250 mm, i.d. 4.60 mm, particle size: 5 μm; λ = 250 nm) with *n*-hexane/THF = 65:35, 1.0 mL.

NMR Hemiacetal Studies

Brown and *Blackmond* found hemiacetal structures appearing during the *Soai* reaction by NMR spectroscopy considering an inactive role in the mechanism.[37] The *Trapp* group set up a reaction mechanism all around a zinc alkoxide hemiacetal as a catalytically active species.[41a] For this reason, the willingness to expand hemiacetal structures was further investigated in an NMR study. For this purpose, the respective aldehyde (6 mg) was dissolved in MeOD-d_4 (6 mL) and measured at room temperature at different times. Since the formation of hemiacetals is reversible, the process was followed until the equilibrium was adjusted.

For both substrates, **HPyr** and **HPym**, a new singlet signal in the typical region of a hemiacetal (δ ~ 5.5 – 5.6 ppm)[52] was observed after 10 min. While the aldehyde signal lost intensity, shifts in the aromatic region were also observed due to the changing electronic situation of the molecule. For the **HPyr** system, hemiacetal formation was completed after 2 h (Figure 13), whereas the equilibrium between aldehyde and hemiacetal was reached within 5 h for the **HPym** system(Figure 14).
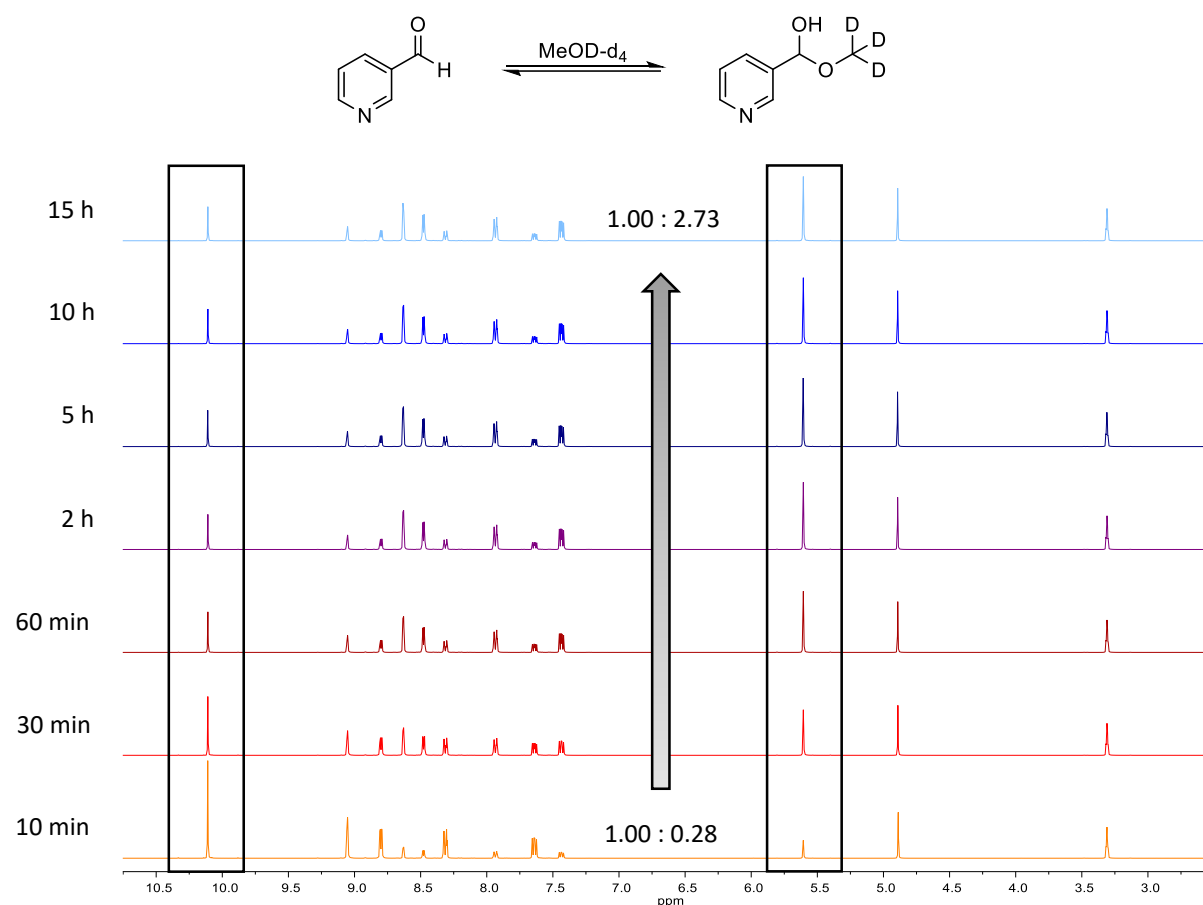

Figure 13: ^{1}H NMR spectra of the hemiacetal formation of **HPyr** with MeOD-d_4.
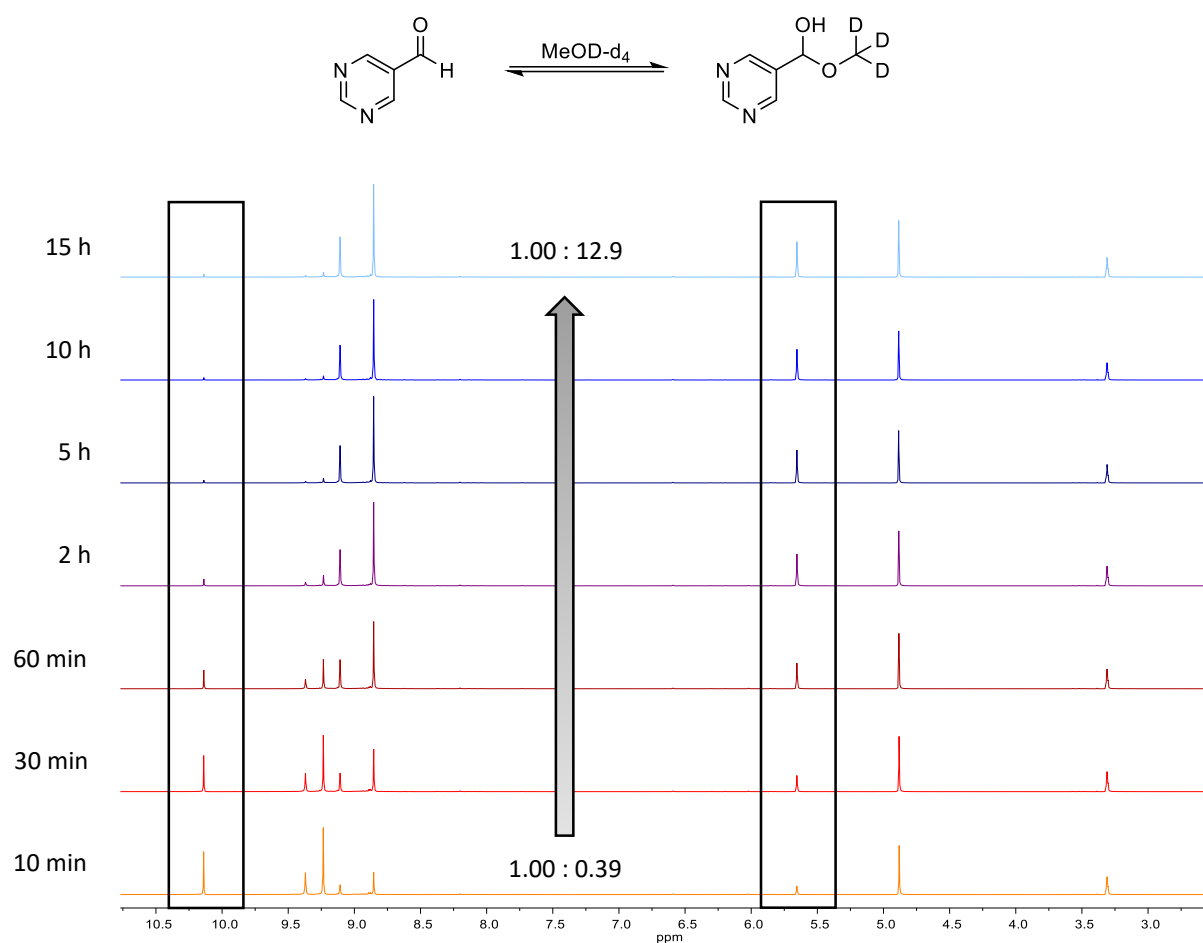
Figure 14: ^{1}H NMR spectra of the hemiacetal formation of **HPym** with MeOD-d$_4$.

The extent of the hemiacetal formation was determined by the signal integral ratio of the remaining aldehyde proton and the emerged hemiacetal proton of the ^{1}H NMR spectra. The results are shown in table 1.

Table 1: Amount of formed hemiacetal in MeOD-d$_4$ after the equilibrium was adjusted. The yield was determined from ^{1}H NMR integrals.

Aldehyde	Hemiacetal	Yield [%]
		9[53]
		73
		95

After 5 h, the **HPym** equilibrium is almost completely on the side of the hemiacetal at 95%. In contrast, the **HPyr** equilibrium has stabilized at 73% of the hemiacetal after 2 h. In comparison, benzaldehyde only forms 9% of the hemiacetal.[53] This suggests that each nitrogen atom with its electron-withdrawing effect favours the formation of the hemiacetal and thus shifts the equilibrium to its side. This trend should also be noticeable in the course of the *Soai* reaction, since according to *Trapp*'s mechanism,[41a] the ability to form a hemiacetal as a catalytically active species is decisive for the outcome of the autocatalysis.

Furthermore, NMR measurements were carried out on the formation of the hemiacetal in toluene-d_8 in order to simulate the reaction conditions. For this purpose, 1-phenylethanol was used in catalytic amounts, which represents the secondary product alcohol. The newly formed hemiacetals then have two stereocenters, which are reflected in four different stereoisomers, two pairs of enantiomers, which in turn are diasteromeric to each other (Scheme 5). If these are formed, the diastereomers can be observed in the NMR. In both reactions, however, no hemiacetal signals could be detected in the NMR either after 1.5 h or after 3 days.
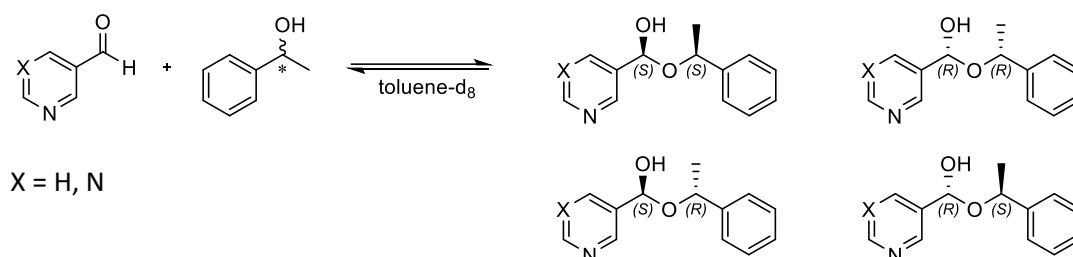
Scheme 5: Stereoisomers of the formed hemiacetal of the **HPyr-CHO** and **HPym-CHO** with 1-phenylethanol.

It is interesting to note that according to a previous study, the **HPym-CHO** gave 13% hemiacetal with 2-methyl-1-phenyl-1-propanol.[53] The difference in alkyl rest between the two systems suggests that the isopropyl rest may play a major role in the formation of the hemiacetal intermediates. The *Soai* reaction itself also shows the desired self-amplifying effect only with diisopropylzinc as diorganozinc reagent.

2.4.3   Kinetic Analysis of the TMSPyr-CHO/TMSPyr-OH System

For the **TMSPyr-CHO**/**TMSPyr-OH** system, all components were separated with *n*-hexane/THF = 80:20 and a flow rate of 1.2 mL/min on a Chiralpak® ID column at a detection wavelength of 250 nm. Under these conditions, one injection every 2.3 min was possible.

For the calibration lines aldehyde concentrations between 2.5 and 35 mM and for the alcohol concentrations between 1 and 20 mM were measured at 250 nm. The resulting integrated area of respective concentrations were plotted against the calculated concentrations. Using the equation of the trend line, the concentration at any time of the measurement can then be calculated (Figure 15).
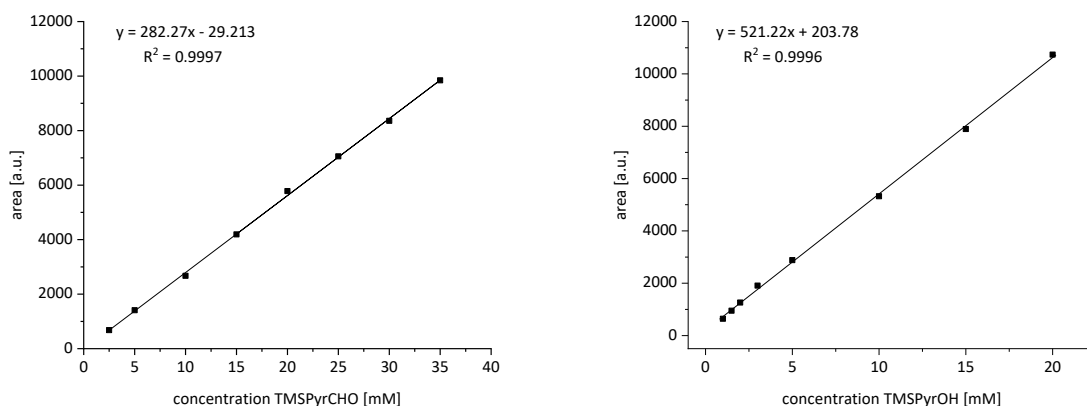
Figure 15: Calibration lines of **TMSPyr-CHO** and **TMSPyr-OH**. Measurement conditions: Chiralpak ID® (250 mm, i.d. 4.6 mm, particle size: 5 µm), *n*-hexane/THF 80:20, 1.2 mL/min, room temperature, λ = 250 nm.
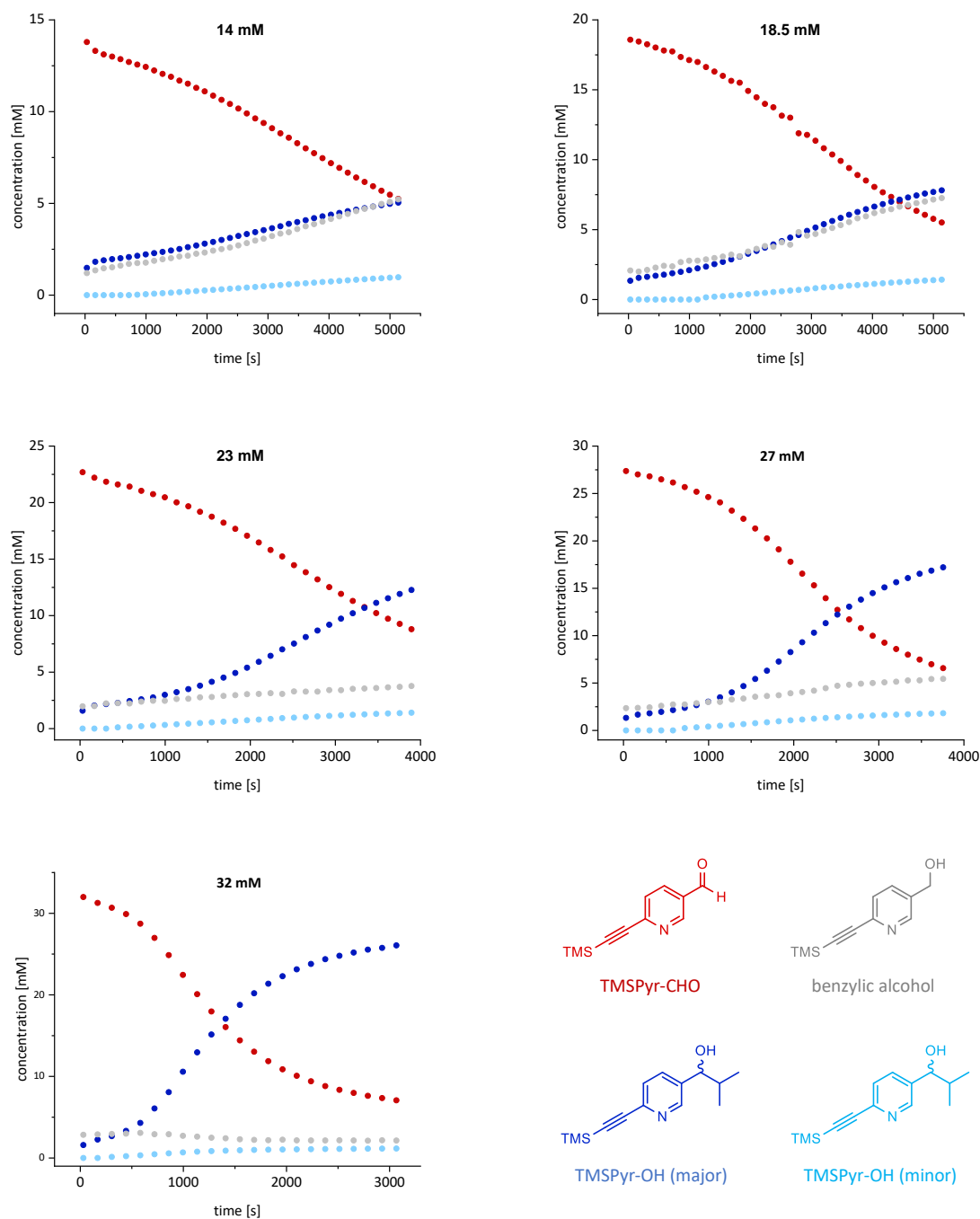
Variation of the Aldehyde Concentration

Figure 16: Kinetic curves after variation of the initial **TMSPyr-CHO** aldehyde concentration (red curve) from 14-32 mM using **TMSPyr-OH** (1.5 mM) and *i*Pr$_2$Zn (40 mM). The minor alcohol is represented in light blue and the major alcohol in dark blue. The grey curve shows the formation of the benzylic alcohol species.

For the **TMSPyr-CHO/TMSPyr-OH** system, aldehyde concentrations between 14 and 32 mM were used at a constant alcohol concentration of 1.5 mM (Figure 16).

For the lowest concentration of 14 mM used, the reaction proceeds very slowly and the concentration of aldehyde and alcohol is only balanced after 85 min. From an aldehyde concentration of 23 mM and higher, the sigmoidal course typical for an autocatalytic reaction was clearly recognized. Starting with the induction phase, in which the zinc alkoxide hemiacetal is formed and the concentration of the aldehyde and the alcohol enantiomer used remained more or less constant after the addition of iPr$_2$Zn. After the induction phase, an almost linear increase in alcohol formation was detected (dark blue curve), which starts suddenly while the aldehyde is rapidly consumed (red curve). Especially at an applied aldehyde concentration of 32 mM, the sudden onset of the autocatalytic phase was well observed by abrupt occurrence of the linear increase of the dominant alcohol enantiomer. In this case, the formation of the dominant alcohol slowly runs into saturation after about 30 min. After about 50 min the concentration of the formed dominant alcohol enantiomer remains constant.

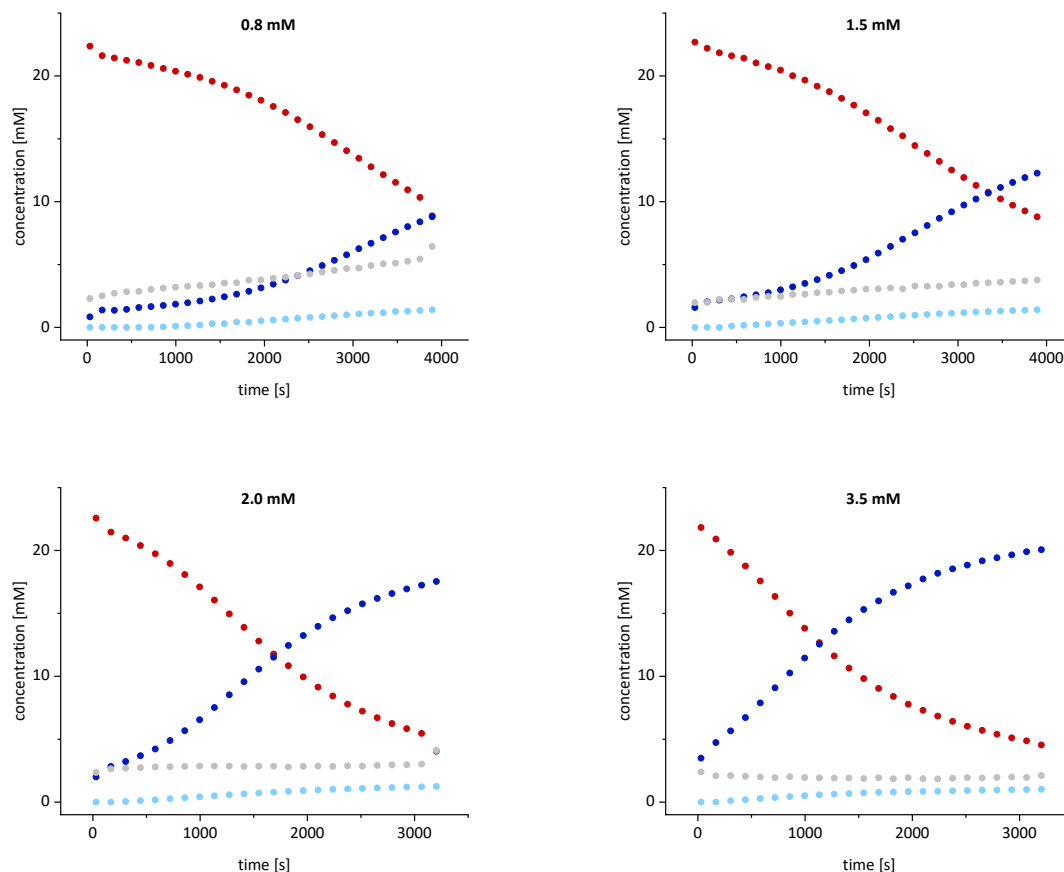**Variation of the Alcohol Concentration**

Figure 17: Kinetic curves after variation of the initial alcohol concentration from 1.0 - 3.5 mM of the initially added product enantiomer **TMSPyr-OH** (dark blue curve), an **TMSPyr-CHO** (red curve) aldehyde concentration (22 mM) and *i*Pr₂Zn (40 mM). The minor alcohol is represented in light blue and the formation of the by-product in grey.

Subsequently, the alcohol concentration of the **TMSPyr-CHO/TMSPyr-OH** system varied between 1.0 mM and 3.5 mM in the same way, using a constant aldehyde concentration of 22 mM (Figure 17). Here, a catalyst loading of 1.0 mM showed the same behaviour as before, namely that the reaction proceeded so slowly that after approximately 65 min the aldehyde and alcohol concentrations were just equalized. Even with 1.5 mM alcohol enantiomer used, the sigmoidal course of the reaction could be predicted, although the reaction was still proceeding very slow. From an alcohol concentration of 2.0 mM, the desired reaction profile was detected, with alcohol formation running into saturation from approximately 50 min onwards.

Thus, a dependence between the concentration used and the reaction time could also be established for the alcohol. The more concentrated the alcohol was used at the same aldehyde concentration, the faster the reaction proceeded. At 3.5 mM catalyst loading, the reaction was even faster with the induction phase almost imperceptible on the curve.
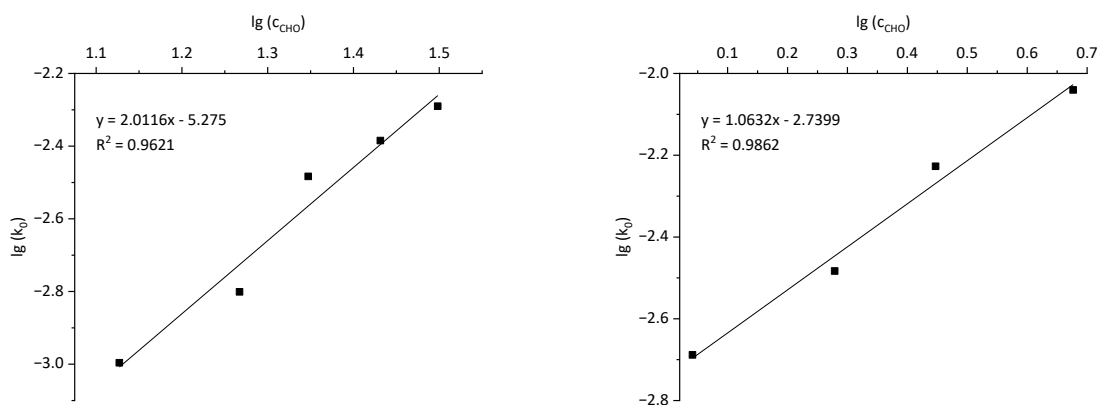

Figure 18: Determination of the reaction order for aldehyde **TMSPyr-CHO** (left) and **TMSPyr-OH** (right) by linear regression analysis of $\lg(k_0)$ against $\lg$ [aldehyde] and $\lg$ [alcohol], respectively.

By double logarithmic plotting of the initial velocity (v_0) *versus* the concentration of aldehyde and alcohol, respectively, the reaction order of 2.0 for the aldehyde and 1.1 for the alcohol was determined (Figure 18).

2.4.4   Kinetic Analysis of the AdPyr-CHO/AdPyr-OH system

For the **AdPyr-CHO/AdPyr-OH** system, all components were separated with *n*-hexane/THF = 75:25 and a flow rate of 1.0 mL/min on a Chiralpak® ID column at a detection wavelength of 250 nm. Under these conditions, one injection every 4.3 min was possible.

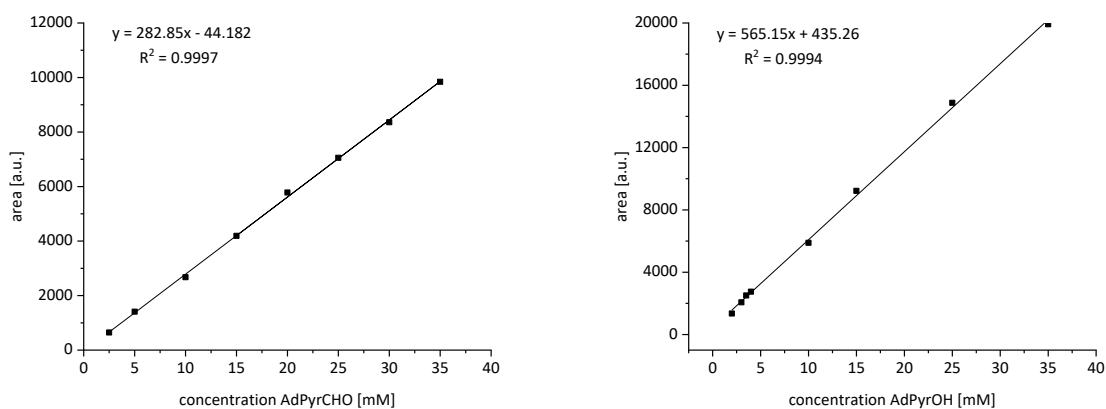Again, aldehyde concentrations between 5 and 70 mM and for the alcohol concentrations between 2 and 35 mM were measured at 250 nm for the calibration lines (Figure 19).

Figure 19: Calibration lines of AdPyr-CHO and AdPyr-OH. Measurement conditions: Chiralpak ID® (250 mm, i.d. 4.6 mm, particle size: 5 µm), *n*-hexane/THF 75:25, 1.0 mL/min, room temperature, λ = 250 nm.

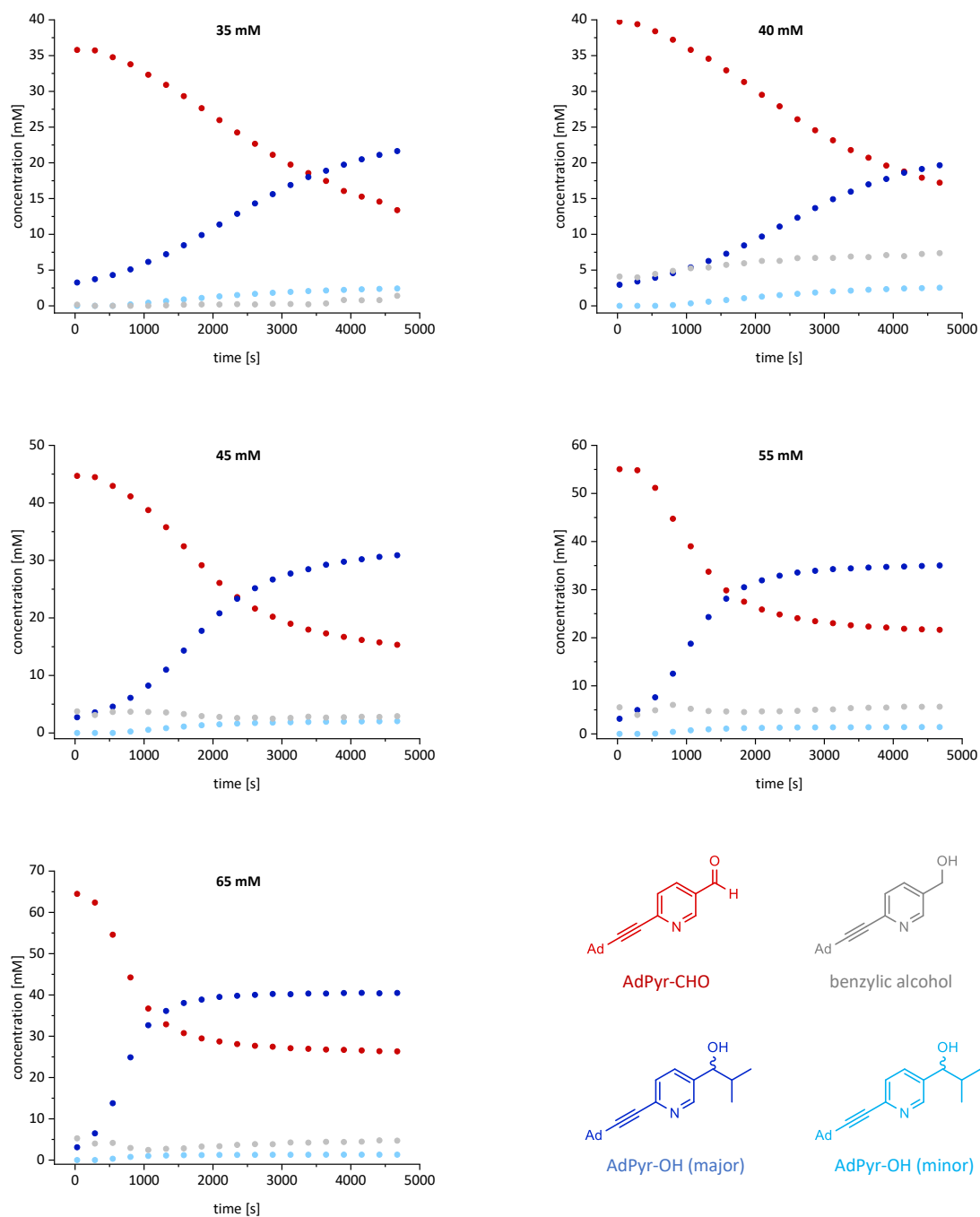**Variation of the Aldehyde Concentration**

Figure 20: Kinetic curves after variation of the initial **AdPyr-CHO** aldehyde concentration (red curve) from 35-65 mM using **AdPyr-OH** (3.0 mM) and iPr$_2$Zn (40 mM). The minor alcohol is represented in light blue and the major alcohol in dark blue. The grey curve shows the formation of the benzylic alcohol species.

For the kinetic profile of **AdPyr-CHO**, reactions were performed with aldehyde concentrations between 35 and 65 mM and a constant alcohol concentration of 3.0 mM (Figure 20). In order to achieve similarly fast reactions in this system as in the **TMSPyr** system, it was necessary to use higher concentrations of both aldehyde and alcohol, since the **AdPyr** system obviously performed slower compared to the **TMSPyr**. In order to obtain a similar rapid convergence of aldehyde consumption and alcohol formation as in the **TMSPyr** system with 32 mM aldehyde and 1.5 mM alcohol concentration (Figure 18), an aldehyde concentration of 55 mM at twice the alcohol concentration (3 mM) was required for the **AdPyr** system. Here, the sigmoidal character of the curve of alcohol formation was already depicted at the lowest used concentration of 35 mM and from a concentration of 40 mM, however, this could already be seen clearly. Especially at the aldehyde concentrations of 55 (25 min) and 65 mM (16 min), it was noticeable that the formation of the dominant alcohol enantiomer ran into saturation very quickly.

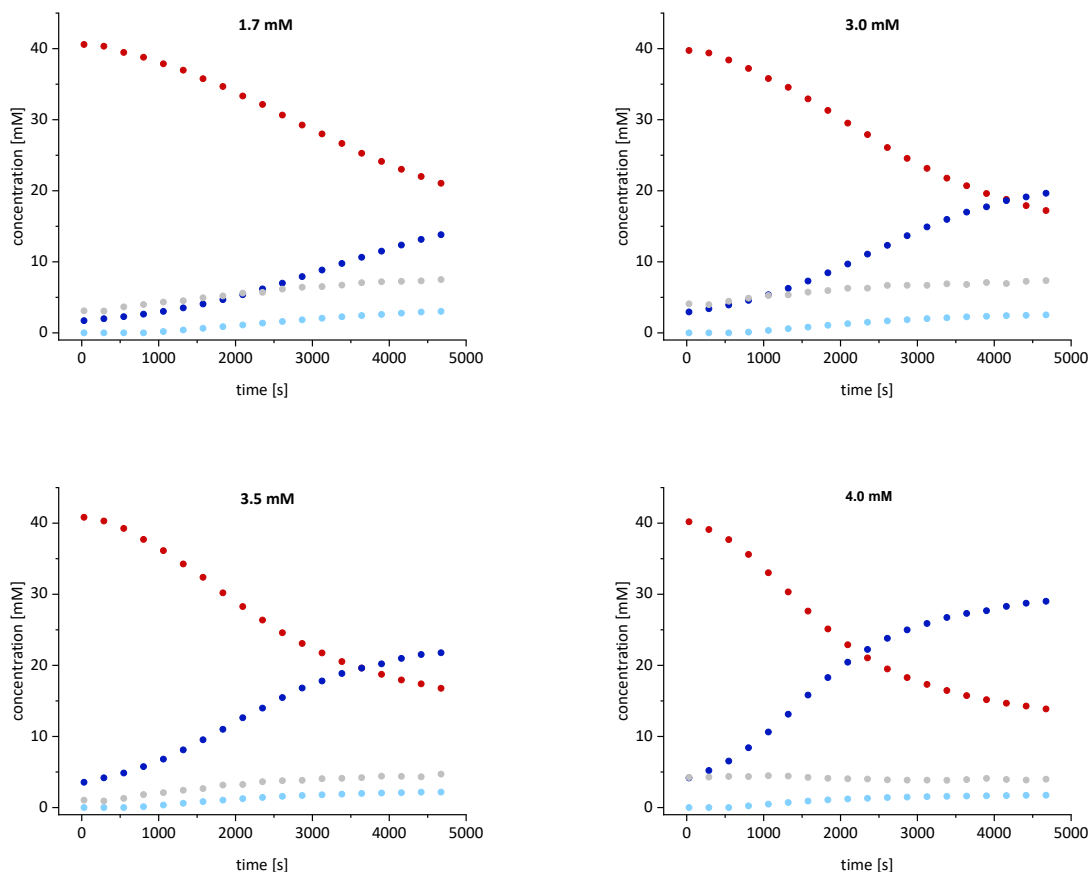**Variation of the Alcohol Concentration**

Figure 21: Kinetic curves after variation of the initial alcohol concentration from 2.0 - 4.0 mM of the initially added product enantiomer **AdPyr-OH** (dark blue curve), an **AdPyr-CHO** (red curve) aldehyde concentration (40 mM) and iPr$_2$Zn (40 mM). The minor alcohol is represented in light blue and the formation of the benzylic alcohol by-product in grey.

For the investigation of the alcohol dependence of the reaction, a constant aldehyde concentration of 40 mM was used for the **AdPyr** system and the alcohol concentration was varied between 2.0 and 6.7 mM (Figure 21). Again, for the change in alcohol concentration, the lower the alcohol concentration the slower reaction rate was observed. Thus, 2.0 mM alcohol was not sufficient to achieve parity of alcohol used and alcohol enantiomer formed after about 80 min. However, already from 3.0 mM alcohol concentration, the clear sigmoidal curve of alcohol formation was detected. Compared to the variation of the aldehyde concentration, however, less steep formation curves were obtained for the alcohol, where saturation occurred only slowly.
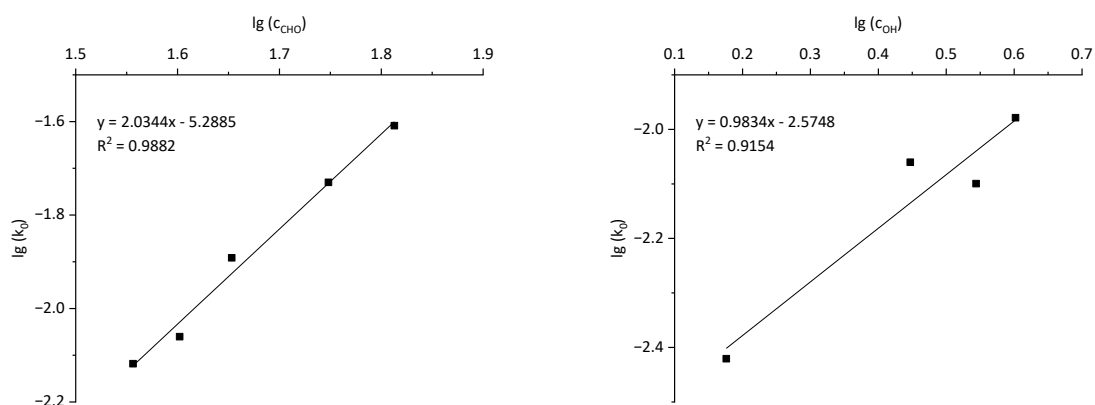
Figure 22: Determination of the reaction order for aldehyde **AdPyr-CHO** (left) and **AdPyr-OH** (right) by linear regression analysis of lg(k_0) against lg [aldehyde] and lg [alcohol], respectively.

By double logarithmic plotting of the initial velocity (v_0) *versus* the concentration of aldehyde and alcohol, respectively, the reaction order of 2.0 for the aldehyde and 1.0 for the alcohol was determined (Figure 22).

2.4.5   Kinetic Analysis of the AdPym-CHO/AdPym-OH System

For the **AdPym-CHO**/**AdPym-OH** system, all components were separated with *n*-hexane/THF = 75:25 and a flow rate of 1.0 mL/min on a Chiralpak® IC column at a detection wavelength of 250 nm for the alcohols and 280 nm for the aldehyde. Under these conditions, one injection every 3.6 min was possible.

For the calibration lines aldehyde concentrations between 5 and 50 mM were measured at 280 nm and alcohol concentrations between 1.5 and 50 mM were measured at 250 nm (Figure 23).
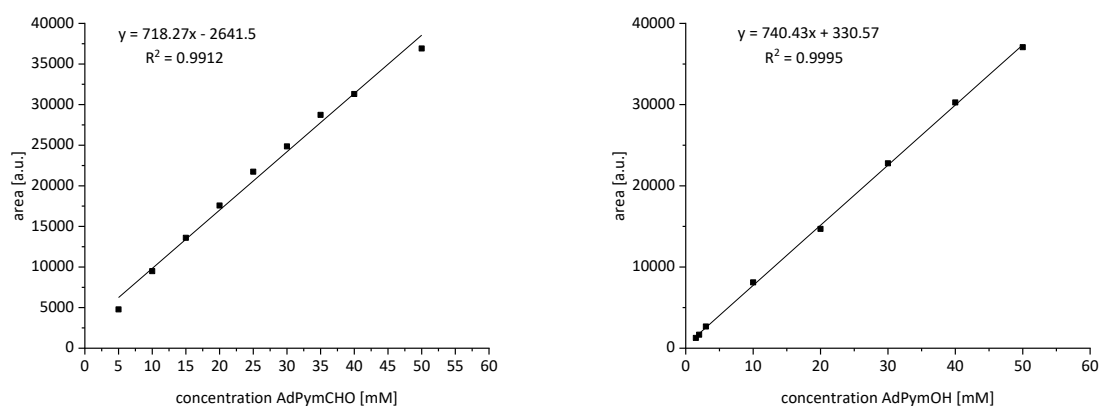
Figure 23: Calibration lines of **AdPym-CHO** and **AdPym-OH**. Measurement conditions: Chiralpak® IC column (250 mm, i.d. 20 mm, particle size: 5 µm), *n*-hexane/THF 75:25, 1.0 mL/min, room temperature, λ = 280 nm for the aldehyde (left), λ = 250 nm for the alcohol (right).

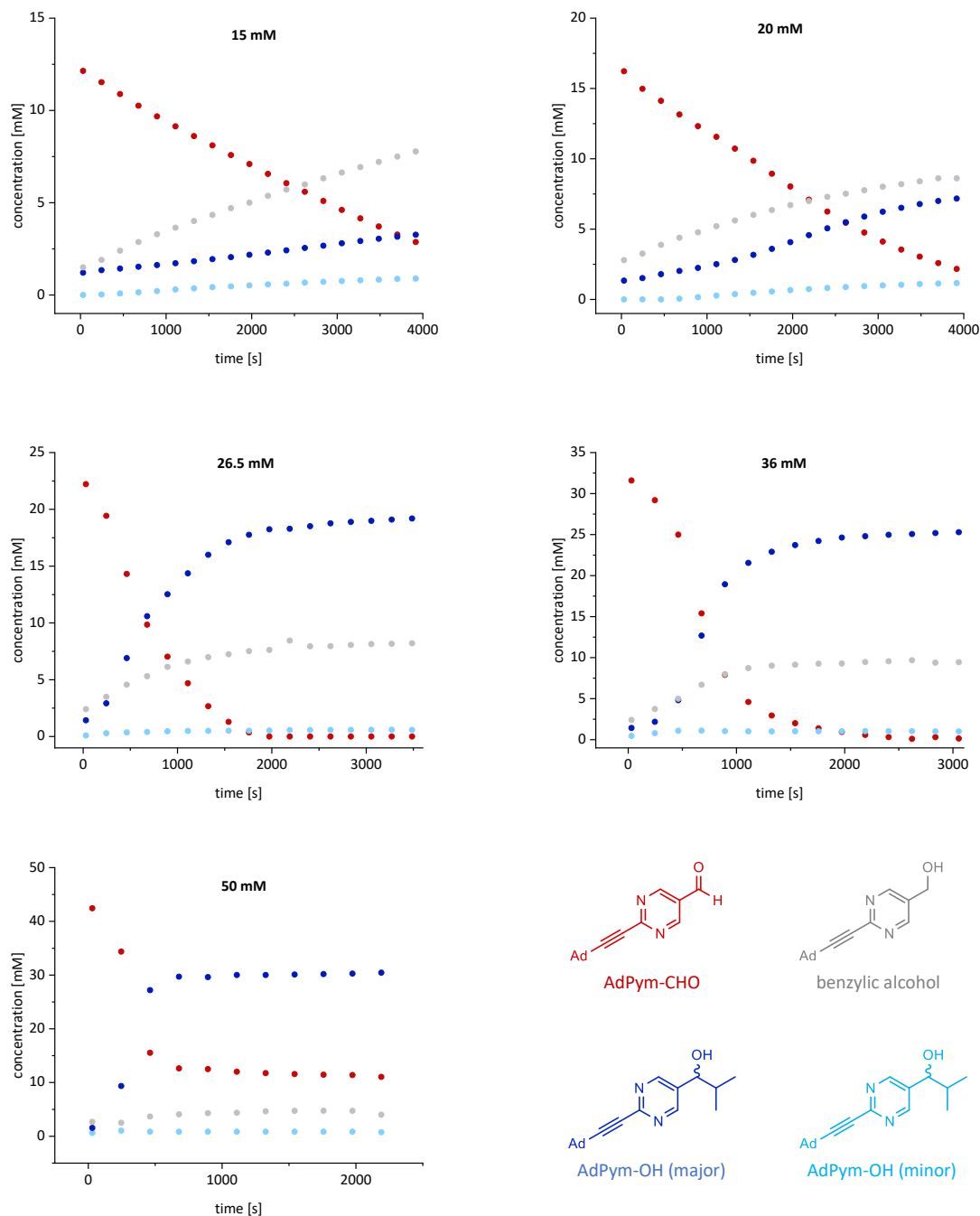**Variation of the Aldehyde Concentration**

Figure 24: Kinetic curves after variation of the initial **AdPym-CHO** aldehyde concentration (red curve) from 15-50 mM using **AdPym-OH** (1.3 mM) and *i*Pr$_2$Zn (40 mM). The minor alcohol is represented in light blue and the major alcohol in dark blue. The grey curve shows the formation of the benzylic alcohol as by-product.

For the **AdPym-CHO/AdPym-OH** system, aldehyde concentrations from 15 to 50 mM with a constant alcohol concentration of 1.3 mM were used for the kinetic profiling of the reaction (Figure 24). At an aldehyde concentration of 15 mM, the reaction performed very slow and the amount of aldehyde used and alcohol formed could first be balanced after 65 min. Between 20 and 26.5 mM aldehyde concentration, an increase by large extent in the reaction rate was observed, with the balance of the concentrations of aldehyde and alcohol shifting from 42 min to 12 min, indicating a clear acceleration in the curve. This showed a short induction phase before a sudden linear increase in alcohol formation was detected, which already ran into saturation from about 25 min. In comparison, for the **AdPyr** system, not even the highest measured concentrations (**AdPyr-CHO**: 65 mM, **AdPyr-OH**: 3.0 mM) were sufficient to achieve such a reaction rate. The rate of the reaction continues to increase above 36 mM up to 50 mM, but not as rapidly until an equalization of the concentrations of aldehyde used and alcohol formed was reached with 50 mM at about 6 min.

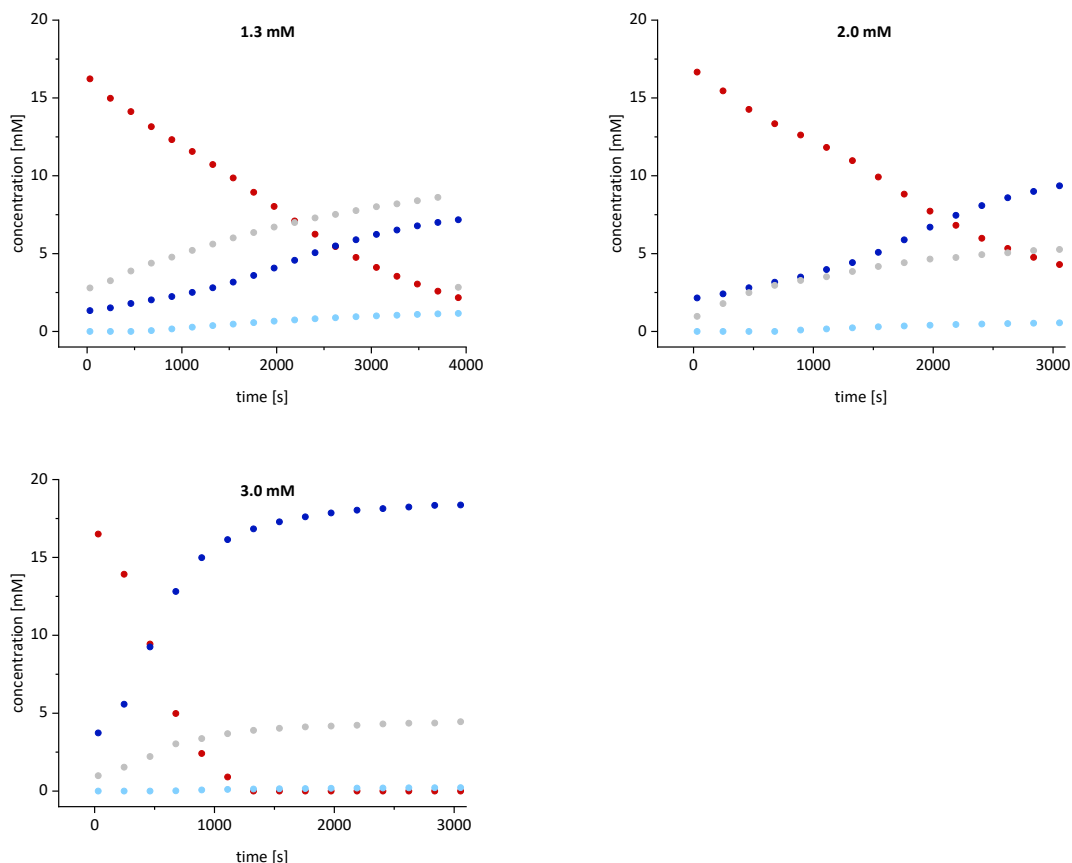**Variation of Alcohol Concentration**

Figure 25: Kinetic curves after variation of the initial alcohol concentration from 1.3 - 3.0 mM of the initially added product enantiomer **AdPym-OH** (dark blue curve), an **AdPym-CHO** (red curve) aldehyde concentration (20 mM) and *i*Pr$_2$Zn (40 mM). The minor alcohol is represented in light blue and the formation of the benzylic alcohol species in grey.

For the investigation of the alcohol dependence of the reaction, a constant aldehyde concentration of 20 mM was used for the **AdPym** system and the alcohol concentration was varied between 1.3 and 3.0 mM (Figure 25).

For 1.3 mM alcohol used, an equalization of the concentrations was observed after approximately 43 min. With 2.1 mM alcohol, the concentrations were equalized about 10 min earlier, after 36 min. Here, the sigmoidal shape of the alcohol curve could also be predicted. A rapid increase in the reaction rate was observed at 3.2 mM alcohol concentration, where the equalization of the alcohol used and the alcohol enantiomer formed took place after approximately 8 min and saturation of the alcohol concentration was observed after 25 min.
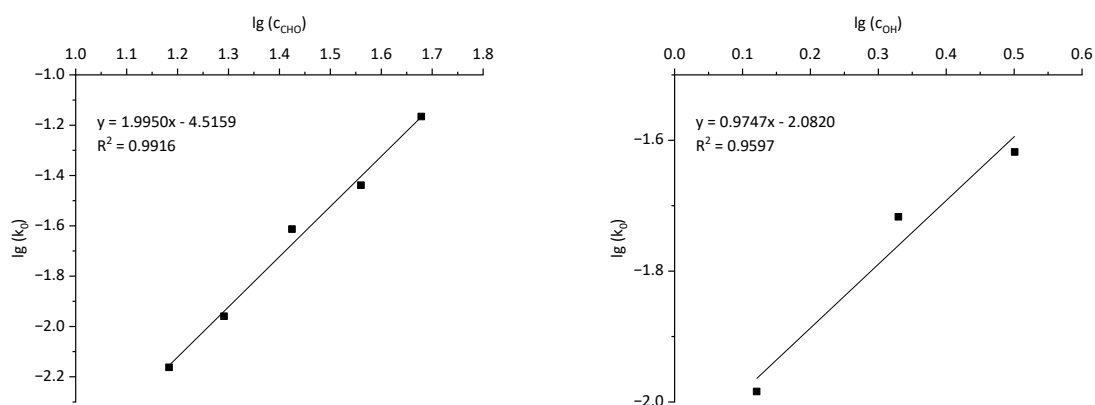
Figure 26: Determination of the reaction order for aldehyde **AdPym-CHO** (left) and **AdPym-OH** (right) by linear regression analysis of lg(k_0) against lg [aldehyde] and lg [alcohol], respectively.

By double logarithmic plotting of the initial velocity (v_0) *versus* the concentration of aldehyde and alcohol, respectively, the reaction order of 2.0 for the aldehyde and 1.0 for the alcohol was determined (Figure 26).

2.4.6   Concentration Dependency

In the course of the experiments, it was observed that the change in aldehyde concentration caused a significant change in the reaction rate. The higher the aldehyde concentration, the faster the reaction proceeds. This means that the aldehyde is consumed increasingly faster and especially the dominant enantiomer of the alcohol is formed more quickly (Figure 27). The same trend can also be detected for the concentration of the major alcohol. In addition, it was observed that the slower the reaction, the lower the selectivity between minor and major alcohol. Moreover, it can be observed that the lower the concentration is, whether aldehyde or alcohol, the more prominent is the side reaction, the formation of the benzylic alcohol species. This can clearly be recognized in Figure 25 where the chromatograms and concentration plots of the **TMSPyr** system with 14 (left) and 32 mM (right) aldehyde concentration using 1.5 mM alcohol concentration and 40 mM iPr$_2$Zn are shown. These examples show that only a fast reaction at higher concentrations, regardless of whether aldehyde or alcohol, allows a clean reaction without side reactions and a high selectivity of the product enantiomer.

For the **AdPyr-CHO/AdPyr-OH** system, higher overall concentrations had to be used to achieve similarly fast reactions compared to the **TMSPyr** system.
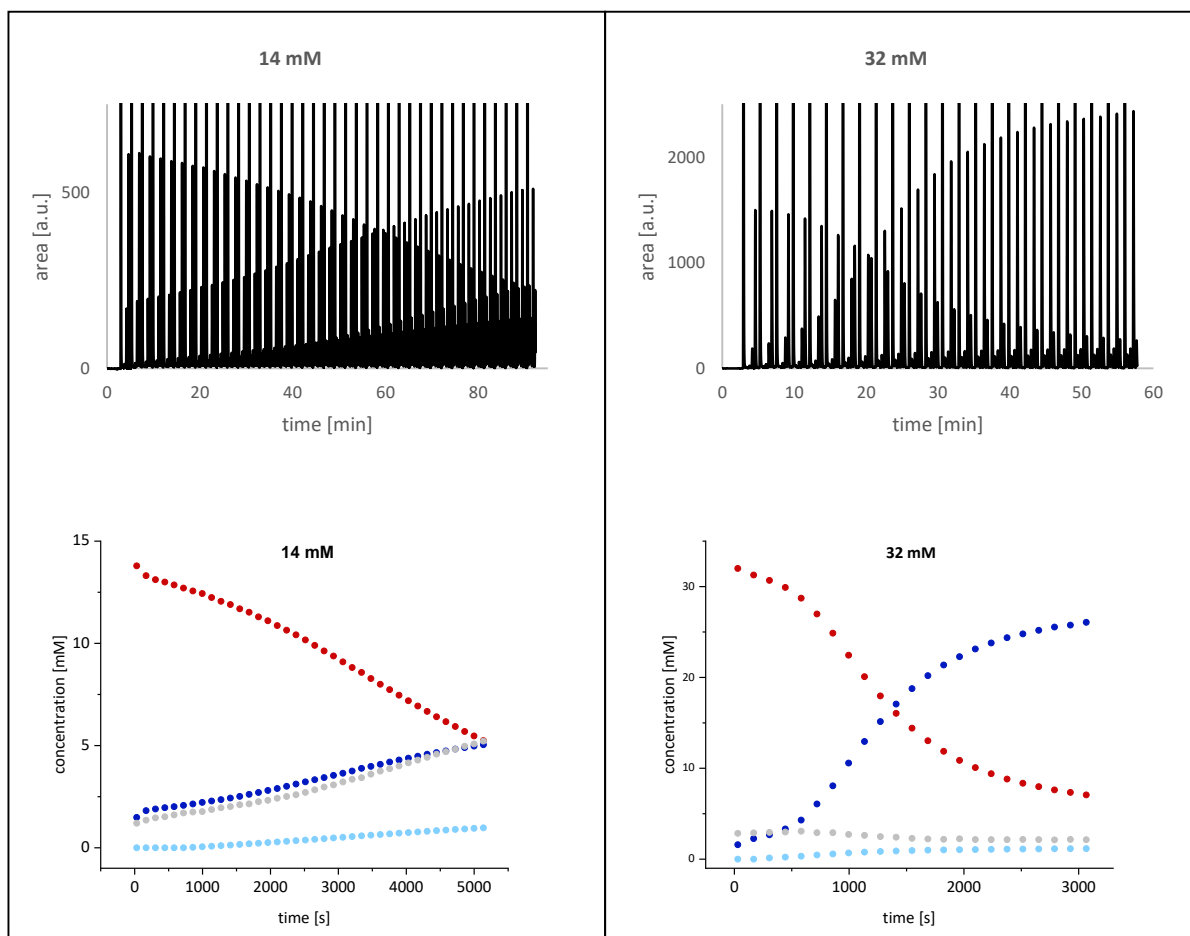
Figure 27: HPLC chromatogram of the **TMSPyr** system with varying aldehyde concentrations of 14 mM (left) and 32 mM (right) with an inserted alcohol concentration of 1.5 mM using 40 mM iPr$_2$Zn at λ = 250 nm. Chromatograms of the measured area are shown on the top and the corresponding concentration graphs after quantification on the bottom.

Reaction Orders

When calculating the reaction orders for the **TMSPyr**, **AdPyr** and **AdPym** systems, a reaction order of 2 for the aldehyde and 1 for the alcohol was obtained, respectively (see Table 2). This is also in good accordance to the previously examined systems **tBuPym**[41a] and **TMSPym**[46] and suggests that the mechanism of all five systems takes place in the same way, as the influence of aldehyde and alcohol is the same in all.

In previous studies, a reaction order between 0 and 1.9 was determined for the aldehyde by different groups.[31, 41a, 42a] Interestingly, however, when considering the side reaction in the latest studies, the reduction of the aldehyde to the primary alcohol, a reaction order of 2 is always obtained, regardless of which system is considered. The inclusion of the side reaction is important for the calculation of any kinetic step, as well as the reaction order, as only through this step the mass balance of the entire system can be closed. If the formation of the by-product is not taken into account in the calculations, only a part of the system is calculated, which, however, cannot fully correspond to reality. At low concentrations of aldehyde or alcohol, the side reaction can even run almost as fast as the alkylation itself. The higher the concentrations used and therefore the faster the reaction takes place, the more negligible the side reaction is.

These values are in good agreement with the reaction orders previously calculated for the **tBuPym**-system.[41a] Small deviations from the previously published results may be due to not taking the side reaction into account, but this is necessary for the complete mass balance. In addition, they also match the observed effects during the kinetic measurements, as the variation of the aldehyde concentration has the greatest influence on the course of the reaction rate. This means that the aldehyde is very important for the progress of the reaction as two aldehydes are involved in the reaction during the reaction mechanism.

Table 2: Calculated reaction orders for the aldehyde and the alcohol from experimental data for the **TMSPyr**, **AdPyr** and **AdPym** systems.

molecule system	reaction order CHO	reaction order OH
TMSPyr	2.0116	1.0632
AdPyr	2.0344	1.019
AdPym	1.995	0.9747

Considering all this, the herein described methods offer significant advantages compared to already published methods[33, 35, 42a, 43] for studies of reaction kinetics. In particular, the low concentrations allow to observe mainly the induction phase and the onset of the autocatalytic reaction. In addition, following the concentration change of each of the aldehydes and both product alcohols independently, being well separated from each other, allows a quantitative study of each individual reactant at any time.

Moreover, the inclusion of the side reaction, the formation of the benzylic alcohol, is of great importance, since its formation strongly depends on the concentrations used and hence on the reaction rate and allows a complete view of all processes within one system, which is important for the evaluation of reaction orders. Furthermore, this insight is essential for future simulations because it closes the mass balance of the reaction, and each reaction product can be considered. Finally, the performance of these methods offers the possibility to compare both pyrimidyl and pyridyl systems, as well as TMS, Ad and *t*Bu systems, since the results were obtained under the same conditions using identical measurement methods.

2.4.7   Structural Dependency

Comparing the three systems with each other, one can see that the pyrimidines react much faster and are therefore a more efficient autocatalytic system than the pyridines. The pyrimidine heterocycle is more electron deficient compared to the pyridine, increasing the electrophilicity of the aldehyde, so that the hemiacetal formation and in consequence the alkylation with iPr$_2$Zn is favoured. This explains why pyrimidine systems generally show a faster reaction with higher conversions. This is also in good accordance compared to the **TMSPym**[46] and *t*BuPym system[41a] previously investigated by the *Trapp* group.

In comparison to the unsubstituted *Soai* aldehydes, the introduction of an alkynyl residue allowed a better solubility in toluene and thus improved the reactivity. However, there are major differences when comparing the alkynyl residues. Taking the previously examined systems into account,[41a, 46] it can be seen that the TMS residue shows the better performance than the adamantyl residue, regardless of whether it has a pyrimidine or pyridine ring. This is due to the fact that although an alkynyl residue increases solubility, sterical demand of the substituent also plays a major role. The reaction mechanism suggests that increasingly large residues are not favourable for use in the *Soai* reaction due to steric hindrance as seen by the comparison of TMS and adamantyl. If the concentration is increased in this case, the probability of reactants meeting and a reaction becoming unavoidable also increases. This is the reason why almost twice as high concentrations (55 and 3 mM) are required for the **AdPyr** system to achieve the same reaction rate as for the **TMSPyr** system at 32 and 1.5 mM.

Comparing the two pyrimidine systems **AdPym** and **TMSPym** [46] with the *t*BuPym[41a] at approximately 26 mM aldehyde and 1.5 mM alcohol concentration, the latter ranks first as the fastest system for the enantioselective autocatalysis of the *Soai* reaction with an equalization time of the aldehyde and alcohol concentration at 7.8 min. The **TMSPym** is in second place with an equalization time of 9.8 min and the **AdPym** is in third place with 11.2 min. This results in a descending order in autocatalytic reactivity of *t*BuPym > **TMSPym** > **AdPym** > **TMSPyr** > **AdPyr** where all the influences explained above can be seen again at a glance.

In summary, it should be noted that the electronics in the system have a greater impact on the reaction rate than steric influences (see **AdPym** *vs.* **TMSPyr**). However, for both systems it is necessary that a sufficiently good solubility is achieved by the alkynyl residue, but that the size of the residue is as small as possible, otherwise steric hindrance slows down the reaction rate (see *t*BuPym > **TMSPym** > **AdPym**).
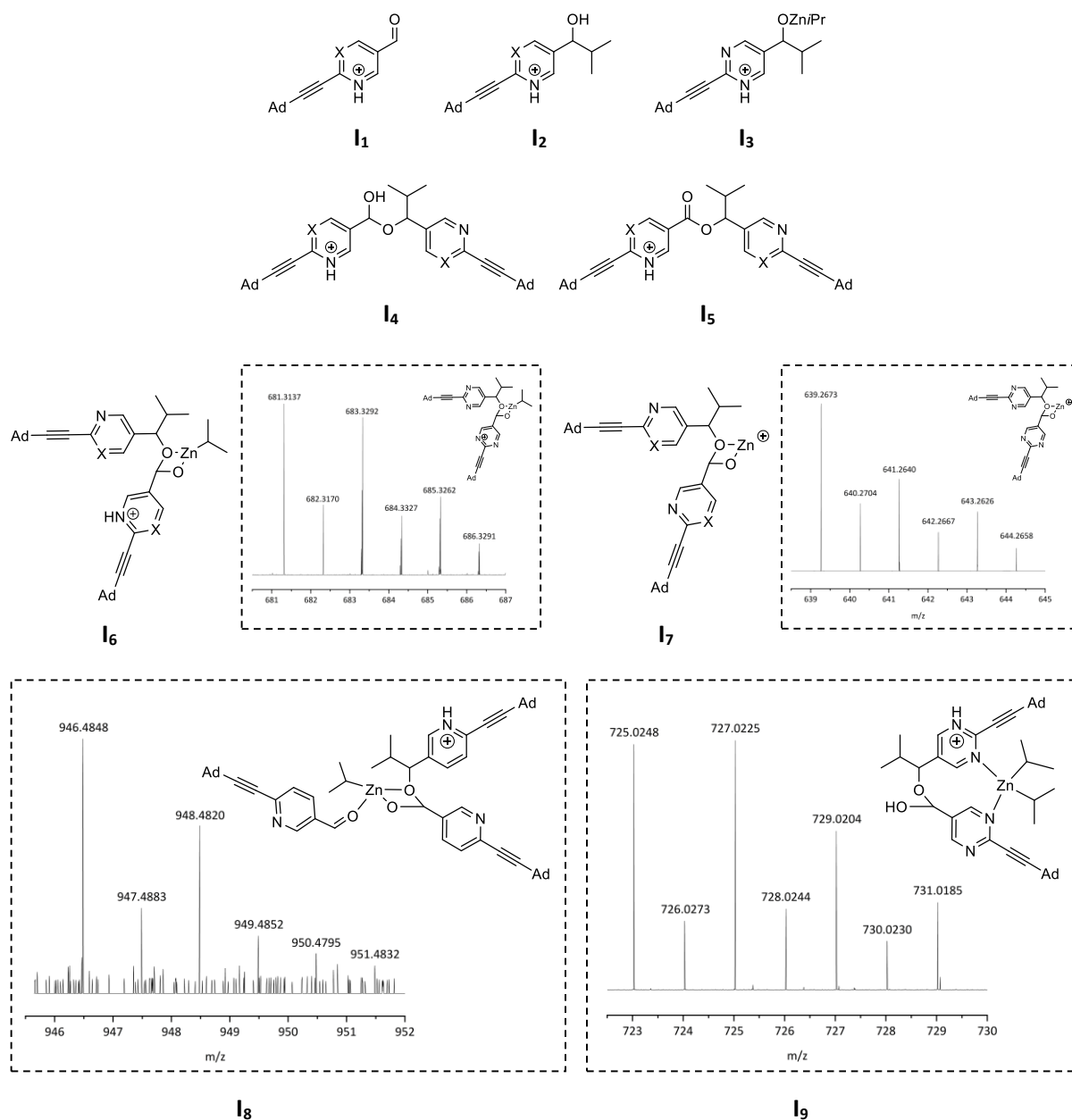
2.5   *In Situ* Mass Spectrometry

For a better understanding of the ongoing processes during the *Soai* reaction and the elucidation of the mechanism, it is not only necessary to follow the kinetics of the individual reaction partners, but above all to understand which individual intermediates are responsible for the observed trends. Of particular interest is the nature of the catalytically active species, as there is a discrepancy in the postulated mechanisms and the transient catalytic species responsible for the autocatalysis.

For this reason, the intermediates of the **AdPym** and **AdPyr** systems were observed by *in situ* high-resolution mass spectrometry performing pulsed injection of samples into an APCI-Oribtrap-MS and the course of the hemiacetals with respect to aldehyde and alcohol was followed. The reaction was prepared as for the HPLC measurements on a 1 mL scale in a GC vial and initiated by adding iPr$_2$Zn. The reaction solution was injected into the mass spectrometer through a 6-port valve system using a syringe pump and analysed using an APCI ion source at 150 °C. By switching the valve every 30 or 60 seconds and rinsing the measuring unit with dry toluene between two injections, it was enabled that the ion source was not overloaded during the measurements. This made it possible to detect even trace amounts of newly formed species due to the increased sensitivity during the reaction.

The measurements identified a number of known and new intermediates (Figure 28). Zinc compounds could be identified by means of their characteristic isotope pattern, whose 6 signals in the mass chromatogram result from the stable zinc isotopes (^{64}Zn, ^{66}Zn, ^{67}Zn, ^{68}Zn and ^{70}Zn) as well as accumulating hydrogen, nitrogen and carbon atoms.[53]

The aldehyde used **I$_1$** and the catalytically used and formed alcohol **I$_2$** was detected in protonated form in both the pyridine and the pyrimidine system. The aldehyde dimer of both systems was also found in relatively high intensity. The monomeric zinc alkoxide **AdPym**-OiPr-ZniPr **I$_3$**, which is described as the starting compound of numerous intermediates, even the catalytically active species, was also observed for both systems. In particular, dimeric [Zn-O]$_2$-structures have been described several times in the literature. Tetramer structures, which have been repeatedly discussed as catalytic species since 2007, as well as other previously observed higher aggregates of zinc alkoxide, could not be detected under the given reaction conditions. The hemiacetal form consisting of the aldehyde and the product alcohol was imaged in protonated form **I$_4$** as well as without hydroxy group. The ester intermediate **I$_5$** described by *Rotunno* is to be formed by hydride transfer of a zinc hemiacetal to the inserted aldehyde, whereby a primary zinc alkoxide is also formed.[54]

Figure 28: Identified compounds during *in situ* mass spectrometric analysis using APCI-Orbitrap-MS.

For both systems, **AdPyr** and **AdPyr**, the hemiacetal zinc alkoxide formed by an aldehyde and a zinc alkoxide **I6** was observed as well as its analog with a missing isopropyl group at the zinc atom **I7**. Such zinc hemiacetal intermediates were also found by the *Trapp* group for the autocatalytic **tBuPym**[41a] and the **TMSPyr** and **TMSPym**[46] systems in earlier investigations.

Based on these intermediates, an autocatalytic cycle was derived that proceeds *via* the transient zinc alkoxide hemiacetal from type I_6 as the catalytically active structure (Figure 29). In this work, further, two intermediates were observed that confirm the proposed hemiacetal catalysed pathway.

In particular, the newly observed intermediate I_8 for the **AdPyr** system, which consists of the hemiacetal I_6 bound to both a reactant aldehyde, once again supports the reaction mechanism previously proposed by *Trapp* and coworkers (Figure 27).[41a] This proceeds *via* the transiently formed zinc alkoxide hemiacetal, which acts as a catalytically active species (**A**). In the next step, this can coordinatively bind an aldehyde and diisopropylzinc molecule (**B**), which initiates the alkylation step towards equally orientated zinc alkoxide and zinc hemiacetal (**C**). A further aldehyde molecule can then be coordinated (**D**).

The reason why this intermediate could only be found for the pyridyl system, and only in low concentrations, is the different reactivity of the pyridyl and pyrimidyl systems. As the pyrimidyl system is much more reactive than the pyridyl system, the intermediates formed also react more quickly, which makes enrichment and therefore identification more difficult. In addition, the free hemiacetal I_4 was detected for the **AdPym** system, where one diisopropylzinc molecule is coordinated to one nitrogen atom of each pyrimidine ring I_9. Above that, further typical zinc isotope patterns were observed for both systems, **AdPym** and **AdPyr**, suggesting the same intermediates with two heterocycles and two zinc atoms. However, these could not be identified so far.
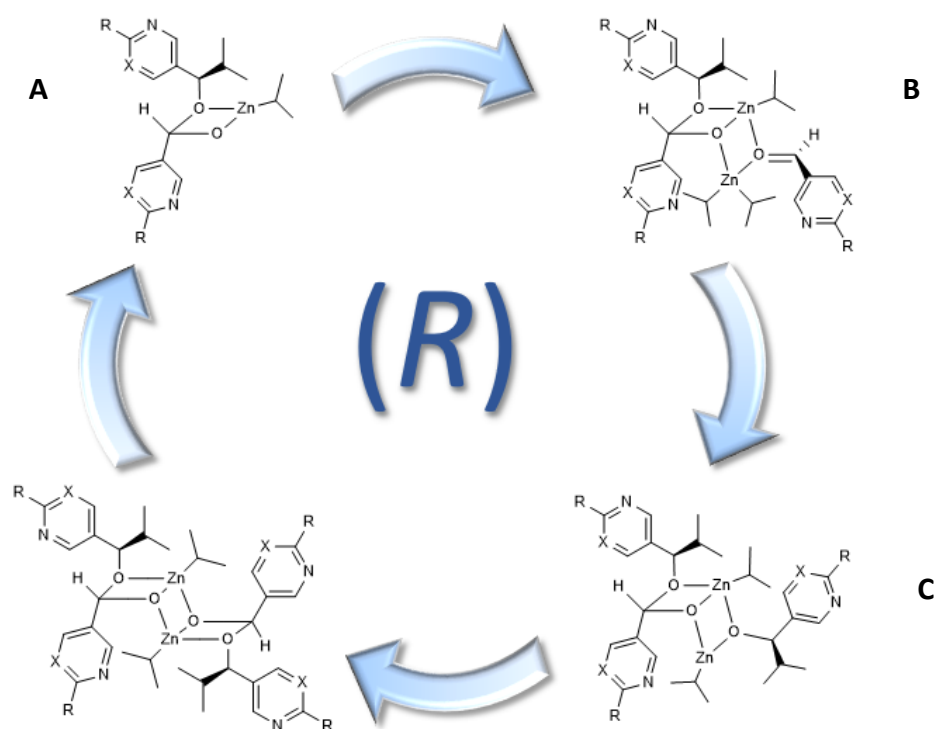
Figure 29: Catalytic mechanism of the *Soai* reaction proposed by *Trapp et al. via* a transient zinc alkoxide hemiacetal.[41a]

Together with the previously described structures,[41a, 46] the detected intermediates in this work are in good agreement with the mechanism established by *Trapp et al*. for the self-amplifying autocatalysis of the *Soai* reaction.[41a]

In addition to identifying the occurring reaction intermediates, the *in situ* mass spectrometry measurements were used to follow the time-resolved course of aldehyde and alcohol as well as of the zinc alkoxide hemiacetal I_7 in comparison to aldehyde and alcohol (Figure 30). The same curve can be observed for the consumption of the aldehyde (red) and the formation of the product alcohol (blue) as received during the kinetic measurements described in chapter 2.4. Both systems show a parabolic curve for the formation of the zinc hemiacetal I_7. For the **AdPym** system (Figure 28 right), a broader scattering can be observed.
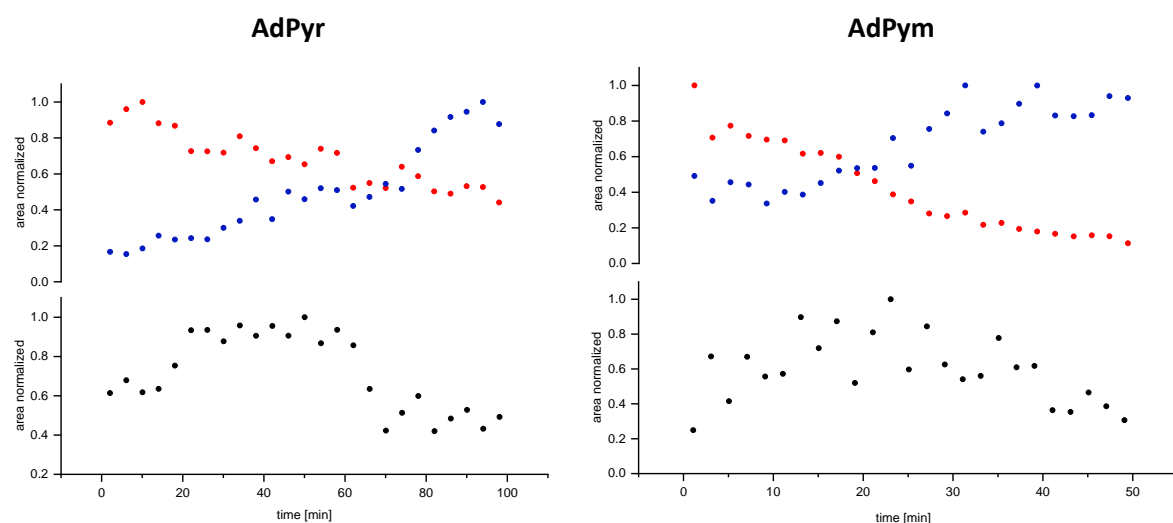
Figure 30: Normalized peak areas of the aldehyde (red) and the alcohol (blue; top) and the zinc hemiacetal I_6 (black; bottom) plotted against time. Reaction conditions **AdPyr**: 40.0 mM **AdPyr-CHO**, 3.0 mM **AdPyr-OH** (*ee* > 99%) and 40 mM *i*Pr$_2$Zn in toluene at r.t. Reaction conditions **AdPym**: 30 mM **AdPym-CHO**, 1.5 mM **AdPyr-OH** (*ee* > 99%) and 40 mM *i*Pr$_2$Zn in toluene at r.t.

However, it is particularly noticeable that the hemiacetal is enriched at the beginning of the reaction, in the induction phase, where the aldehyde is only consumed and the alcohol is formed very slowly at the same time. The linear increase in the alcohol concentration begins at the maximum of the hemiacetal formation. From this point onwards, when the amplification of the product alcohol begins, the formation of the hemiacetal also decreases again or is consumed more quickly due to the faster reaction. This is a further indication that the zinc hemiacetal is closely correlated with the self-amplification of the autocatalysis, as the linear formation of the product alcohol only begins when the hemiacetal is sufficiently formed. Both the intermediates found and the formation of the hemiacetal I_6 are consistent with the previously investigated systems *t*BuPym,[41a] **TMSPym** and **TMSPyr**.[46]

In 2001, *Blackmond* and *Brown* published the first kinetic studies using microcalorimetry to analyze the overall progress of the reaction by measuring the heat generated during the reaction. The reaction investigated showed typical behaviour of an autocatalytic process in which heat is initially generated by the formation of the catalyst (Figure 31). After reaching the maximum and the ongoing conversion of the substrates, the heat flow decreases again.[33] Interestingly, the measurement of the heat development in this reaction shows the same course as the formation of the zinc hemiacetal I_6 during the *in situ* mass spectroscopy measurements, which is described by *Trapp et al.* as a catalytic species.[41a]
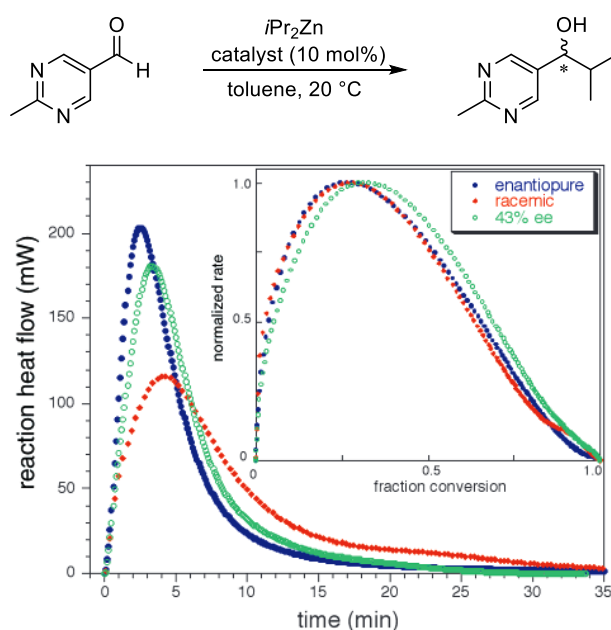
Figure 31: Time-resolved reaction heat flow for the *Soai* reaction of 2-methylpyrimidine-5-carbaldehyde with diisopropylzinc using different enantiomeric excesses of the catalyst.
Inset: normalized reaction rate as a function of fraction conversion of the aldehyde.[33]

Since consistent results and observations could now be obtained for five different systems under the same measurement conditions using the same measurement methods, it seems obvious that the self-amplifying autocatalytic mechanism for pyridine- and pyrimidine-based systems work in the same way. In addition, based on the observations and results, the assumption of the zinc alkoxide hemiacetal being the catalytically active species could be substantiated.

2.6   Summary and Outlook

This topic included the investigation of various pyridine- and pyrimidine-based *Soai* substrates with regard to their kinetic reaction behaviour and intermediate structures occurring during the reaction (Figure 32). Initially, both aldehydes and alcohols of the **TMYPyr**, **AdPyr** and **AdPym** systems were synthesized. The flow-injection analysis high-performance liquid chromatography (FIA-HPLC) method was used to create kinetic profiles of the respective systems. The methods and injection intervals were adapted for each system so that all reaction components could be analysed separately on a baseline basis without any overlap. An *n*-hexane/THF mixture was selected as the solvent mixture for elution in order to avoid the formation of a hemiacetal between aldehyde and *i*PrOH. All reaction partners could be quantified at any time with the aid of calibration lines.

In order to qualitatively determine the influence of the aldehyde and the catalytically used product alcohol, the initial concentrations of both were varied independently of each other. It was noticed that a slower reaction was observed at low initial concentrations of both the aldehyde and the alcohol. In addition, the selectivity of product formation was poorer, particularly in that more of the undesirable by-product, the benzylic alcohol was formed. The higher the initial concentrations, the faster the reaction proceeded and the more selectively the desired product enantiomer was formed. Furthermore, it was observed that the pyridyl systems proceeded much slower than the pyrimidyl ones, which is due to the additional electron-withdrawing effect by the second nitrogen, which increases the electrophilicity at the carbonyl carbon. In addition, taking into account previously investigated systems,[41a, 46] it was found that the introduced alkynyl residues also have an influence on the reaction rate. The reaction proceeded more slowly with increasing size of the alkynyl rest, which means that the residue should not be chosen increasingly large for an efficient reaction process. From the kinetics obtained by HPLC measurements and taking the side reaction into account the mass balance was closed and the reaction orders of aldehyde and alcohol could then be calculated for each system. These resulted in a reaction order of 2 for the aldehyde and 1 for the alcohol for all three systems.

In order to determine intermediates occurring during the reaction, *in situ* high-resolution mass spectroscopic measurements were carried out on the Orbitrap-MS. The advantage here was that pulsed injections of a continuous reaction also detected transient species that may only be formed in traces. In general, similar intermediates were detected for the **AdPyr** and **AdPym** system. For the **AdPyr** system, a new intermediate was also observed in which an aldehyde molecule coordinates to the zinc hemiacetal, further supporting the mechanism proposed by *Trapp et al*.[41a]

By monitoring the formation of the hemiacetal over time, it was also possible to show that its formation proceeds slowly. At the maximum of the hemiacetal concentration, however, the linear increase of the dominant alcohol enantiomer starts. In addition, the profile of hemiacetal formation matches the calorimetry profiles published by *Blackmond et al.*, which was also attributed to the formation of the catalytic species until the reaction starts at the maximum heat development.[33]
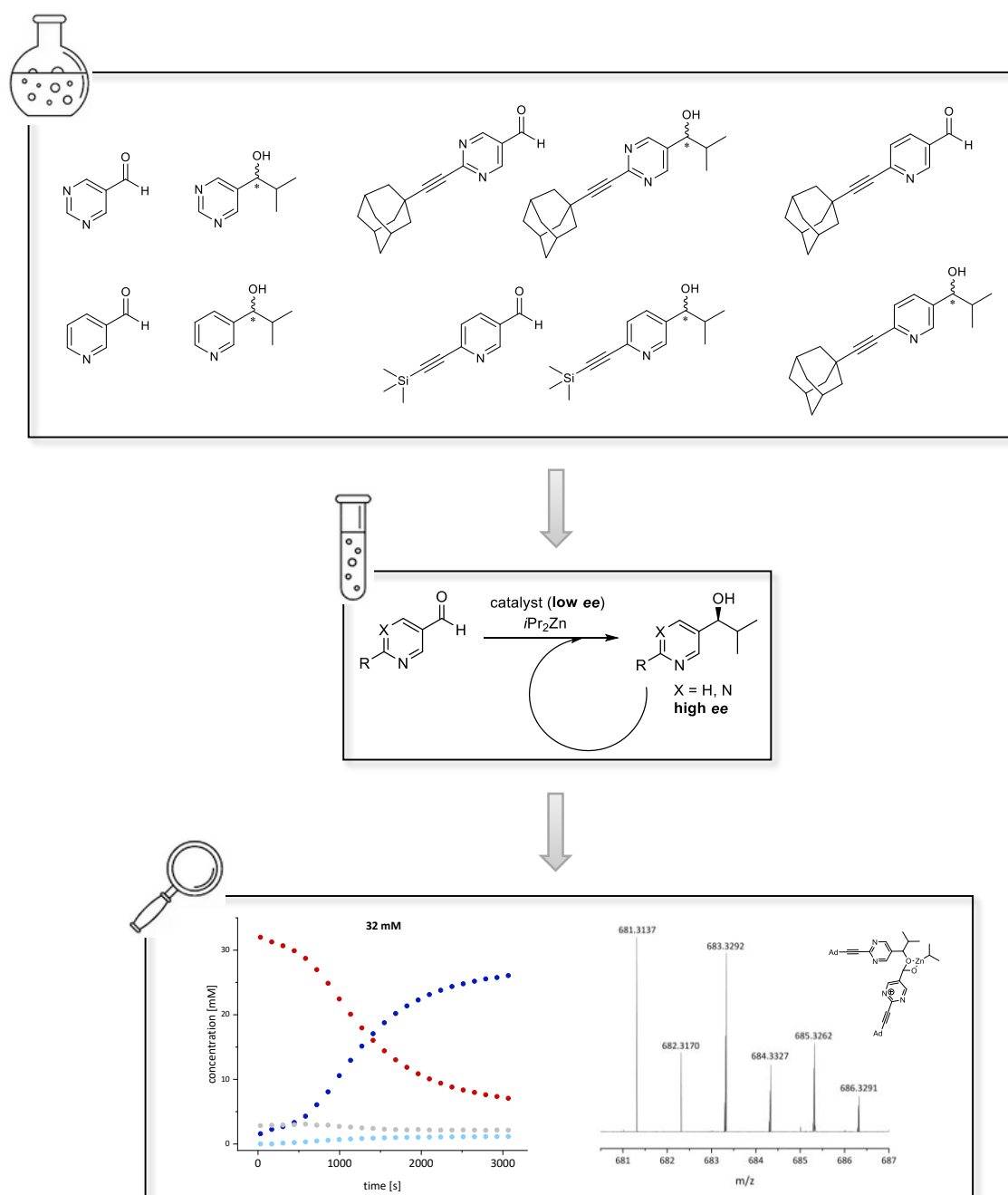

Figure 32: Overview over the mechanistic studies of pyridyl and pyrimidyl substrates in the *Soai* reaction using *in situ* mass spectrometry and FIA-HPLC measurements.

In future, the data obtained will be used to carry out computer-aided simulations. In these simulations, the individual reaction sub-steps are represented by a differential equation and its rate constant k is determined by means of iterative optimization with reference to the experimental data. With the knowledge gained in this way, all systems (**tBuPym**, **TMSPym**, **TMSPyr**, **AdPym** and **AdPyr**) can then be compared with each other and a qualitative statement can be made about the individual reaction steps.

CHAPTER 3

Asymmetric Alkylation of

Photoswitchable Systems

3.1   State of Knowledge

Ever since *Bernard Feringa*, together with *Jean-Pierre Sauvage* and *Fraser Stoddart*, was awarded the Nobel Prize in 2016 for 'the design and synthesis of molecular machines', photoswitchable molecules have been brought back to the attention. Especially the animation of his unidirectional molecular motor, known as the nanocar, remained in many minds of many scientists.[55] Such molecules can become future-relevant, artificial molecular machines in various fields such as medicine, robotics and the internet.[56] As an example, they react to external stimuli and perform a mechanical reaction similar to muscles. In addition, photoswitchable molecules were found in the human body. A prominent example is the membrane-bound photoreceptor rhodopsin.[57] The operating principle is that an 11-*cis*-retinal molecule inside the opsin protein can undergo rapid isomerization through light irradiation and becomes the all-*trans*-retinal (Figure 33). This change in shape in the retina causes an interaction with the outer opsin protein and in turn triggers a signalling cascade. The chemical signals that are released in the process can be sent to the brain as visual stimuli.[58] This then controls the release of melatonin, for example.

11-*cis*-retinal   all-*trans*-retinal
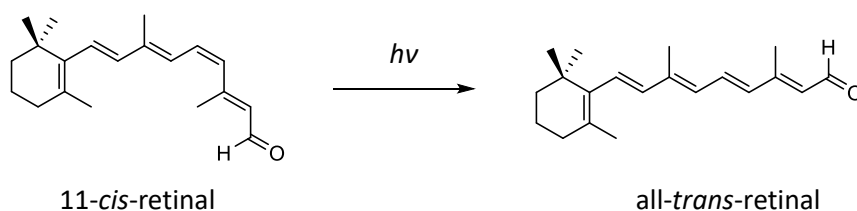
Figure 33: Isomerization of the 11-*cis*-retinal in the membrane-bound photoreceptor rhodopsin through light irradiation to the all-*trans*-retinal.

Reversible control of the conformation and activity of biomolecules is a major area of research,[59] as the study and manipulation of complex processes in living cells[60] provides an opportunity to investigate the evolution of mechanisms or progressive disease patterns.[61] Light, in particular, appears to be a suitable external control element for chemical and biological processes, as it is usually non-invasive at a variety of wavelengths and offers high spatial and temporal resolution. Moreover, it exhibits orthogonality to most elements of living systems and does not cause contamination of the sample.[59b] Another great advantage is that the wavelength and intensity of the light can be precisely regulated, which is exploited, for example, in the labelling of small molecules[62] and proteins (such as

GFP)[63] by a fluorophore. Most importantly, these light-regulated processes are usually completely reversible, and the chromophores can each switch between two or more isomeric forms at different wavelengths, hence the commonly used term "photoswitch".[59c] Many synthetic photoswitches have now been developed that undergo a reversible change in their structure when irradiated with light. One group of these is that of diarylethenes. Due to the structural presence of a part of hexatriene, a reversible photochemically induced cyclisation can take place. According to theoretical studies, the thermal stability of the two isomers is due to the low aromatic stabilisation energy of the acrylic groups, which are introduced on both sides *via* the bridging *Z*-alkene (Figure 34).[64]
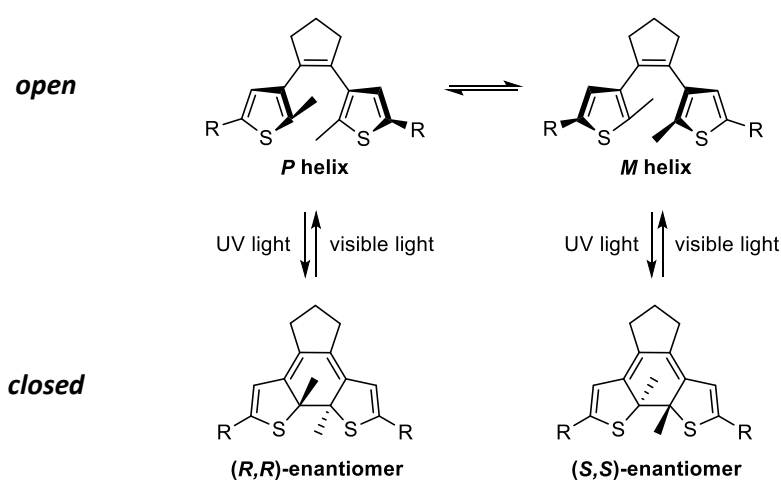
Figure 34: Helical *P* and *M* conformations of the open diarylethene and their corresponding ring-closed (*R,R*) and (*S,S*) isomers after UV light irradiation.[65]

Diarylethenes are able to switch between open and closed form. While UV light is required for ring closure, visible light is sufficient for ring opening. In open form, there are two axial chiral conformations, the *P* (clockwise) and *M* (anti-clockwise) helix.[66] Ring closure with UV light creates two stereocenters, which theoretically result in four stereoisomers. However, due to the conrotatory ring closure following the *Woodward-Hofmann* rules, in which the stereocenters can only adopt the same conformation, the ring closure results in only two stereoisomers, (*R,R*) and (*S,S*).[67] In the past, diarylethenes have been successfully used in photoswitchable molecular wires and bioactive compounds such as photoswitchable antibacterial agents, as well as in data processing systems.[68] Ring analogues of diarylethenes have also been used as structural motifs for molecular motors that perform unidirectional rotation/movement in response to light.[55]

The ligand-based autoamplification of molecular chirality was complemented by the initiation and induction of supramolecular chirality by utilization of non-covalent interactions of macromolecular systems.[69] For example, *Meijer et al.* investigated the formation and induction of supramolecular chirality in dynamic macromolecular aggregates by doping an achiral molecule with a small amount of an chiral analogue resulting in a supramolecular aggregation of chiral, columnar stacks.[70] The principle in which a small amount of a chiral molecule is used as a dopant (sergeant) and determines the overall chirality of an achiral material (soldier) is called the sergeant-soldier principle.[71] A number of articles based on the underlying principle have been published in the course of time.

Ben Feringa and coworkers published an amide-modified diarylethene photoswitch that gels in a supramolecular assembly due to hydrogen bonds between the molecules resulting in a helical structure after irradiation with UV light in 2014.[65] The addition of a small amount of one closed enantiomer to a suspension of the prochiral ring-open substance in toluene and subsequent heating produces a supramolecular gel that has a preferred orientation, which is determined by the dopant. Upon subsequent irradiation of the supramolecular gel with UV light, the ring closes and the one-sided orientation is fixed. In the case of non-doped gels, a 1:1 mixture of (*S,S*) and (*R,R*) enantiomers was obtained after UV light irradiation. By inducing supramolecular aggregates with targeted chirality, the autoamplification of molecular chirality could be achieved. However, the extent of amplification did not exceed 40% *ee* due to kinetic inhibition[65] and thus shows a less effective self-amplifying autocatalysis of the enantiomeric excess compared to the *Soai* reaction.

Another example utilizing the photoswitch system was provided by *Hecht et al.* The group used a dithienyl backbone in which a thiophene ring was replaced by a *Diels-Alder* adduct. This combination allowed the *exo*-selectivity of the thermal *Diels-Alder* reaction with a diastereomer ratio of 90:10 to be achieved by photocyclisation.[72]

These examples show that diarylethene photoswitches are capable of transferring and processing stereochemical information.

3.2   Objectives

From data storage to promising future utilization in medical robotics, photoswitch molecules are an interesting building block for many applications, especially due to their clean conversion into isomers and their stability. Above all, however, their reusability and the lack of need for costly separation of the catalysts used make this class of substances interesting materials in trigger-induced processes. In particular, the occurrence in living organisms and in biochemical processes demonstrates the relevance of the versatile photoswitches.

Another possibility is to utilize the simplicity of implementation for chemical processes in the synthesis of stereoselective reactions. It is known, for example, that circularly polarized light is sufficient as a trigger to achieve an amplification of one enantiomer in the *Soai* reaction. Ring closure reactions with a dithienylethene also produce enantiomers. The intention was to combine photoswitches with the alkylation reaction of different benzaldehyde structures in one system in order to achieve a deflection in the formation of stereoisomers through dynamically controllable light-induced changes in the core molecule. The dithienyl system, which has already shown autoamplification by gelling and doping of the substance in studies of *Feringa et al.* as an amide derivative,[65] was used as the basic structure. Benzaldehyde and fluoro-benzaldehydes should be used as reactive side chains, in which the existing electron-withdrawing effect of the dithienyl unit is further enhanced (Figure 35).
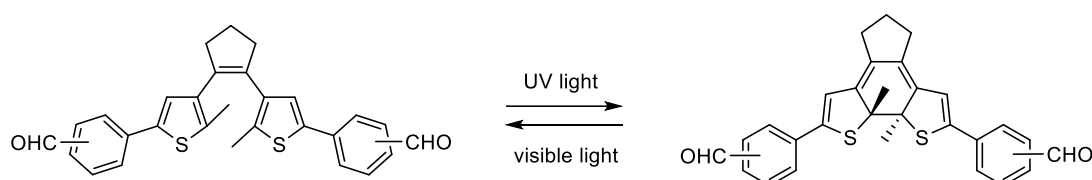
Figure 35: Exemplary dithienylethene target molecule with the dithienyl motif with benzaldehyde fluoro-benzaldehyde moieties for alkylation positions.

In addition to the synthesis of the structures, the isomerization process under the influence of UV light will be investigated using ^{1}H NMR. Furthermore, the alkylation with different alkylation reagents and their influence on the electronic situation in the molecule is intended. These compounds will also be analysed with regard to ring closure using UV light.

3.3   Synthesis of the Reactants

3.3.1   Synthesis of the Dithienylethene Core Structure

The core molecule of the desired diarylethene was adapted from *Feringa* and coworkers and consists of a cyclopentene ring linked to a thiophene derivative **6** at the 1- and 2-positions in which two chlorine substituents were introduced in α-position to the sulphur atoms. In a retrosynthetic perspective, the synthesis of dithienlyethene-based photoswitch motif **8** can be separated into three major steps (Scheme 6).[73]
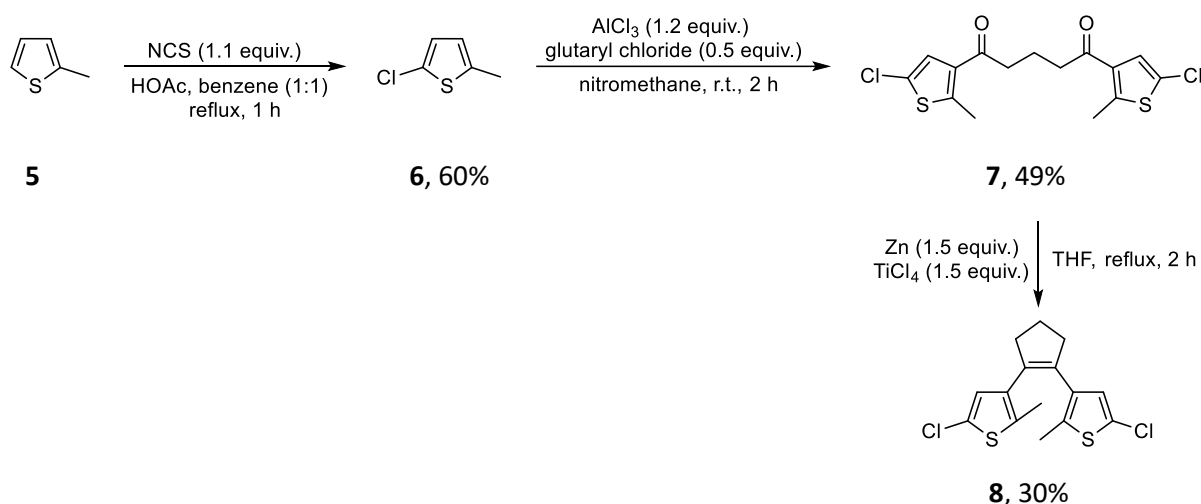
Scheme 6: Synthetic pathway towards the desired diarylethene **8** starting with the chlorination of 2-methylthiophene **4** followed by a *Friedel-Crafts*-acylation using AlCl$_3$ plus glutaryl chloride and subsequent *McMurry* reaction with Zn and TiCl$_4$.

The synthetic pathway towards the desired core structure of the photoswitch **8** started with the chlorination of the 2-position of 2-methylthiophen using *N*-chlorosuccinimide in a mixture of acetic acid and benzene (v/v = 1:1). Purification by distillation afforded **6** as a colourless liquid in 46% yield. Afterwards, the substrate was further functionalized by using a *Friedel-Crafts*-acylation. Therefore, aluminium trichloride was added in portions to an ice-cooled solution of **6** and glutaryl chloride in nitromethane. The reaction was stopped by addition of iced water and after extraction **7** was obtained as a dark brown residue in 49% yield without purification. The final step towards the dichlorodiarylethene **8** was to perform a *McMurry* reaction.

For this purpose, titanium tetrachloride was added dropwise under argon atmosphere to a dispersion of Zn dust in THF and by time, the solution turned deep blue. The ring-open precursor **7** was then added and the reaction mixture was heated to reflux, before the reaction was stopped by adding ammonium chloride. Extraction and purification *via* column chromatography gave the desired core molecule **8** in 30% yield.

3.3.2   Synthesis of MIDA Boronic Esters

In order to have the possibility of alkylating aldehydes on photoswitch molecules, the basic structure **8** had to be further functionalized in a second step. For this purpose, both chlorine substituents were replaced by benzaldehyde. A typical synthetic strategy to change a carbon-halogen bond into a carbon-carbon bond is the *Suzuki* cross-coupling reaction.[74] It represents a palladium-catalysed C-C coupling between aryl halides and organoboron compounds and was used to introduce two benzaldehyde functionalities using 2-formylphenylboronic acid to obtain compound **9a** (Scheme 7). The procedure was adapted from a reported synthesis, in which two benzaldehyde moieties were coupled to dichlorophenantroline.[75] According to the adapted procedure, the reactants were treated with sodium carbonate and Pd(PPh$_3$)$_4$ in a degassed dimethoxymethane/water mixture (v/v = 4:1). TLC revealed that besides the reactants **8** and the 2-formylphenylboronic acid a number of side products were present in the crude reaction product. Because the target molecule could not be synthesized efficiently via this route and no product was isolated after purification, another synthetic pathway had to be found.
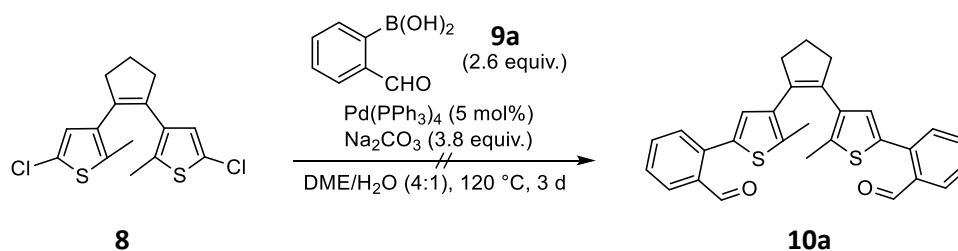

Scheme 7: *Suzuki* cross-coupling reaction of the photoswitch backbone **8** with 2-formylphenylboronic acid.

Since boronic acid is usually not compatible with many reagents and functional groups due to its high reactivity, it is usually added relatively late in the molecular structure and is often only found in smaller molecules. On the other hand, the group of sterically more demanding boronic acid esters allows the use of several often necessary reagents and conditions.[76] Nevertheless, the required harsh conditions to convert them into the free boronic acid make the handling difficult.

For this purpose, the idea was to use MIDA boronic acid esters, which are reported to lead to higher yields of the coupling product in *Suzuki* cross-coupling reactions. *N*-Methyliminodiacetic acid (MIDA)-boronate[77] offers a straight-forward solution to all these problems as it is remarkably stable and thus allows storage in the laboratory without having to prepare a boronic acid compound each time it is needed. In addition, it is highly stable towards a wide range of reagents and is non-reactive in cross-coupling under anhydrous conditions. As a quasi-protective group for boronic acids, it allows the later on needed reactive boronic acid to be released under mild hydrolysis. With a reaction time of less than 10 min at room temperature, the hydrolysis of MIDA boronates to release the boronic acid in an aqueous sodium hydroxide solution can be achieved rapidly. Furthermore, MIDA boronates can be used in chromatography due to their stability.[78] This stability is explained by the pyramidal geometry of the MIDA boronate, which prevents the inclusion of the p-orbital, which is responsible for the reactivity of boronic acids. The hydrolysis with weaker bases, such as potassium phosphate, is much slower and the release of the boronic acid occurs slower than the catalyst turnover, which may avoid unwanted side reactions of the boronic acid, such as protodeboronation.[79] Moreover, they are easily prepared from their corresponding boronic acid analogues, which are often commercially available.

Since it is known that especially electron-poor carbaldehydes can be alkylated well with zincorganyls in contrast to benzaldehyde, aldehyde-containing aryl compounds equipped with mainly electron-withdrawing substituents were chosen.[25a] In order to ensure electron deficiency fluorinated benzaldehyde derivatives were used. For comparison, a non-fluorinated benzaldehyde was also prepared to evaluate influences of electron-withdrawing functional groups to the reaction progress and yield. Moreover, two thiophene derived compounds and one furan-based substrate were selected to investigate the influence of five-membered rings and heterocycles.
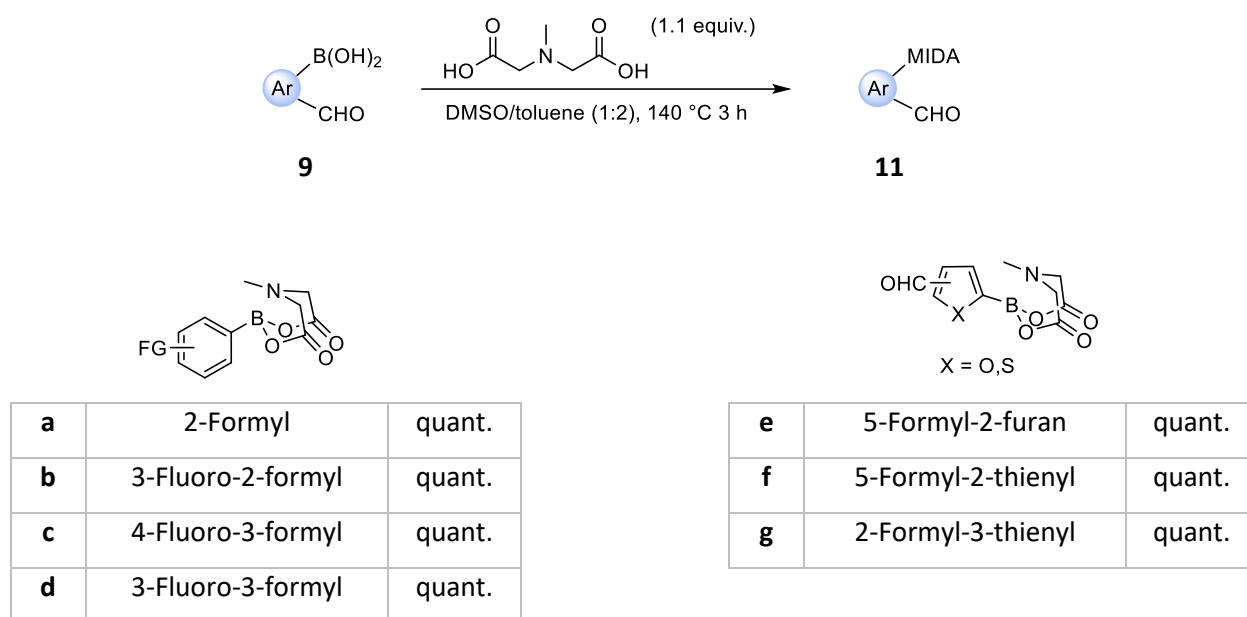
Scheme 8: Overview of the synthesized MIDA boronic esters **10** containing either a benzol (**a-d**) or a five-membered heterocycle (**e-g**).

Due to these smooth reactions with quantitative yields, MIDA boronic acid esters were used instead of boronic acid compounds for the following coupling reactions (Scheme 8). For the preparation of **11a-g**, the boronic acid **9a-g** and *N*-methyliminodiacetic (MIDA) boronic acid ester were suspended in a mixture of DMSO and toluene (v/v = 1:1) and the flask was fitted with a *Dean-Stark* trap, which was previously filled with toluene. The reaction suspension was heated to reflux for 3 h, and then cooled to room temperature. After removing the solvents under reduced pressure, the residue was lyophilized for 1-3 d. The desired MIDA boronic acid esters **11a-g** were obtained in quantitative yield and could be used without further purification in the following cross-coupling reactions.[80]

3.3.3   *Suzuki* Cross-Coupling Reaction

The typical procedure to turn a carbon-halogen and an organoboron compound into a C-C bonded substrate is the *Suzuki* cross-coupling reaction.[74] The palladium-catalysed reaction was used to couple two benzaldehyde functionalities to the previously synthesized dithienyl backbone **8**.
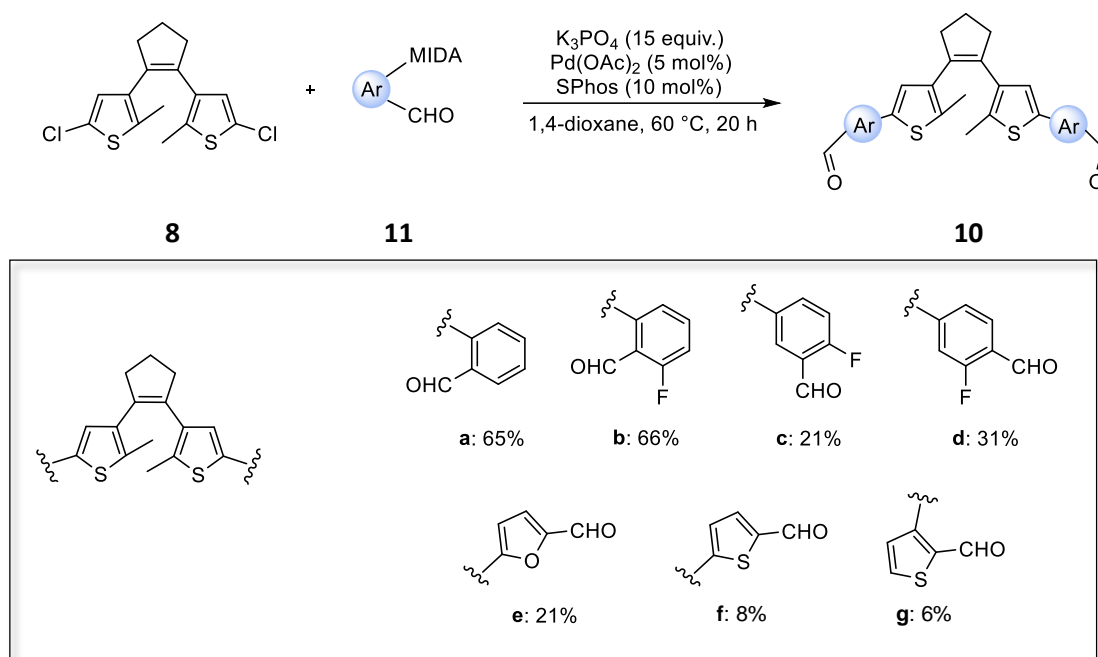
Scheme 9: *Suzuki* cross-coupling reactions of the dithienyl backbone **8** and MIDA boronic ester **11** leading to the aldehyde functionalized photoswitch **10a-g**.

For the synthesis of **10a-g**, the corresponding MIDA boronic ester **11a-g** was dissolved together with the dithienylethene **8**, SPhos and Pd(OAc)$_2$ in dry 1,4-dioxane (Scheme 10). After stirring the solution at room temperature for 10 min, a degassed potassium phosphate solution (3M) was added. The reaction mixture was stirred at room temperature for 10 min and then at 60 °C overnight. Purification by flash column chromatography gave the mono- and bis-substituted six-membered rings **10a-d** in moderate to reasonable yields. Unfortunately, in the case of the five-membered heteroarylic rings, the cross-coupling reactions only gave the desired products **10e** and **10f** in small amounts. Due to various by-products and multi-spot TLC, the products could not be isolated in sufficient purity. For this reason, the latter were not used for further investigations (Scheme 9).

In the case of the coupling product **10a** of dithienyl backbone **8** and 2-formyl MIDA boric acid ester **11a**, lilac crystals were obtained (Figure 36) which crystallise in a monoclinic unit cell (Figure 34b). In previous reports of similar molecules by *Irie* and coworkers, two different types of crystals were obtained. They showed off as mirror images of one another with *M* or *P* helicity.[81] However, the absolute configuration of the measured crystal structure could not be fixed, since the Flack parameter was not determined.
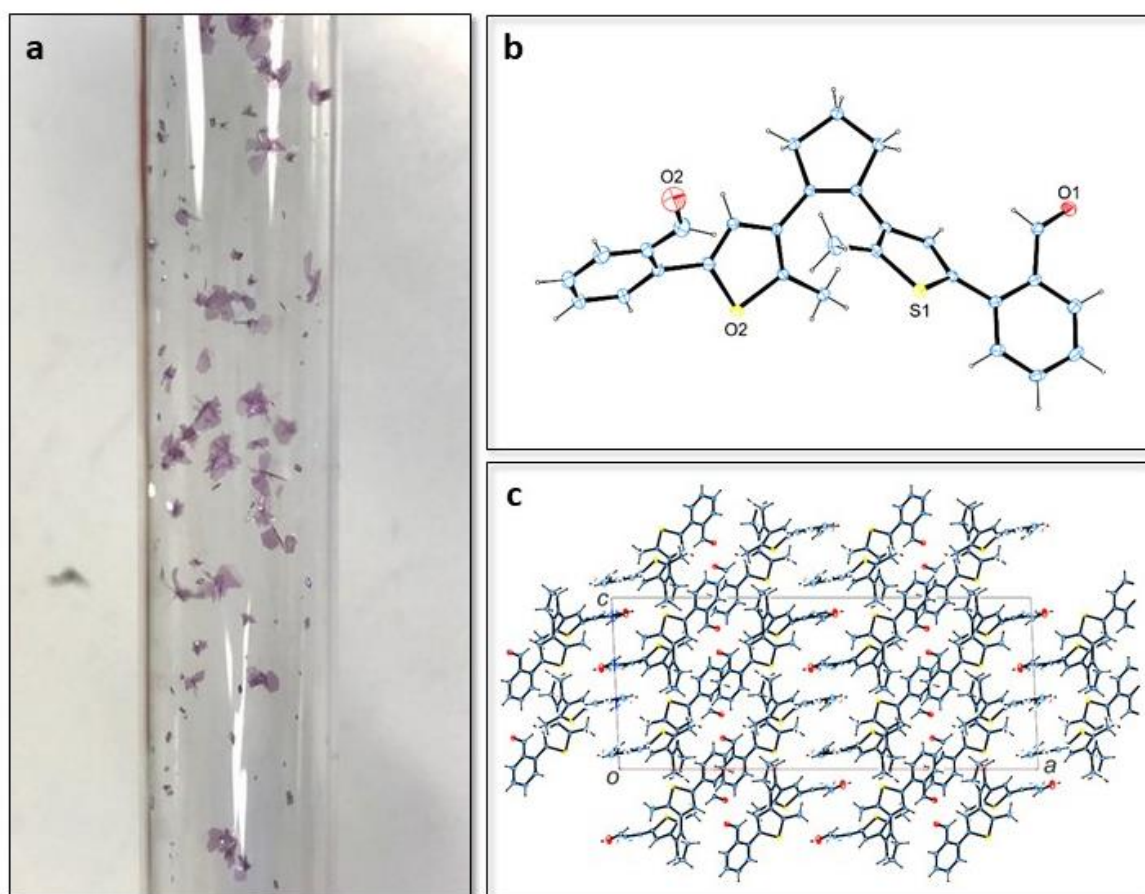
Figure 36: **a** Lilac crystals, **b** molecular crystal structure and **c** monoclinic unit cell of the photoswitch compound **10a**.

3.3.4   Direct Functionalization of the Dichlorodiarylethene

In addition to the previous described compounds, the direct functionalization of the dichlorodiarylethene **8** with an aldehyde functionality was considered. For this purpose, a literature procedure was found, which exactly describes the reaction of the backbone structure **8** into the benzaldehyde baring species **12** by halogen-metal exchange with *n*-BuLi and subsequent reaction with *N*-dimethylformamide (DMF) (Scheme 10).[82] According to this procedure, the backbone compound **8** was dissolved in THF and cooled to -78 °C. After adding *n*-BuLi and stirring at -70 °C for 2 h, DMF was added and the reaction mixture stirred at room temperature overnight. After purification, the reaction product **12** was obtained as a light blue solid in 41% yield.
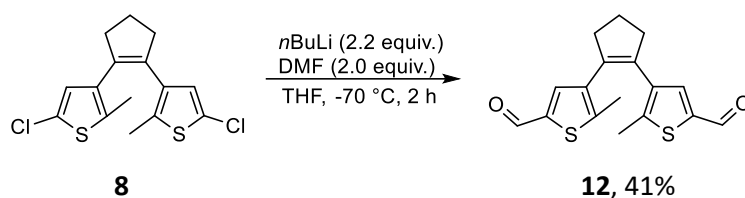
Scheme 10: Direct functionalization of the dichloroarylethene core structure **8** to afford the corresponding formylated compound **12**.

3.3.5   Investigation of Ring Closing upon Irradiation with UV Light

After successful synthesis of the functionalised diarylethene photoswitches **10**, the electrocyclic ring closing reaction induced by irradiation with UV light was studied. Therefore, a defined amount (6 mg) of the corresponding substrate **10** was dissolved in d_1-chloroform (CDCl$_3$, 0.6 mL). After recording an ^{1}H NMR spectrum, the sample was irradiated with UV light (365 nm; 13 V) for 30 and 60 min while protecting against surrounding light. Again, an ^{1}H NMR spectrum was recorded immediately after irradiation. In accordance with previous work,[83] the UV irradiation of the benzaldehyde photoswitch molecules of type **10** causes several shifts of signals in the ^{1}H NMR, in addition to the visible colour change of the sample solution by extension of the aromatic system.
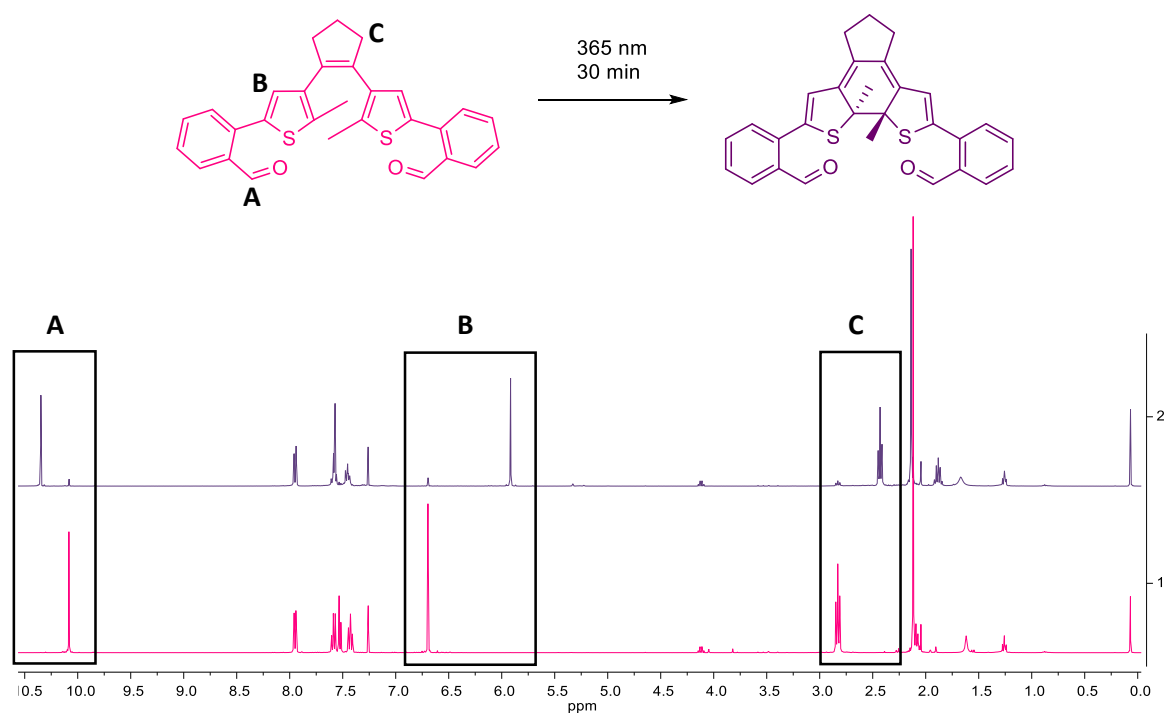
Figure 36: ^{1}H NMR spectrum of **10a** before (bottom, pink) and after (top, violet) excitation with UV light of 365 nm for 30 min in CDCl$_3$.

Besides the obvious change in colour of the compound during UV treatment from pink (before ring closure) to purple (after ring closure), a low-field shift of the aldehyde signal from 10.08 ppm to 10.35 ppm can be observed in ^{1}H NMR spectrum (**A**). Additionally, the proton belonging to the thiophene ring shows a proper high-field shift from 6.69 ppm to 5.91 ppm. This is due to the loss of aromaticity caused by ring closure, where π-electrons are shifted from the thiophene ring to the newly formed adjacent six-membered ring (**B**).

As a final observation, the electron shift of the ring closure also slightly high-fields the triplet of allylic protons of the cyclopentane ring by 0.41 ppm (**C**). Based on the ^{1}H NMR, the ring closure could be almost complete with the help of UV light irradiation within 30 min (Figure 36).

As described earlier, ring closure of dithienylethenes leads to the statistical formation of two enantiomers, (*S,S*)- and (*R,R*)-enantiomer, as another chiral centre is formed.[65] For further investigation, a sample of **10a** in *i*-hexane/*i*PrOH (v/v = 1:1, 1 mg/mL) was irradiated with UV light (365 nm) for 30 min and then analysed using HPLC. The enantiomers could be observed on a Chiralpak® IC column and a running medium mixture of *i*-hexane/*i*PrOH (95/5). However, no method could be found to visualise them completely baseline separated. In this case, the enantiomers were better separated from each other the more nonpolar the solvent mixture became. However, even a solvent mixture of *i*-hexane/*i*PrOH (98/2) was not sufficient to achieve baseline separation. Under the above conditions, the enantiomers **(*S,S*)-10a** and **(*R,R*)-10a** were eluted at 29.5 min and 30.4 min, respectively (Figure 37).
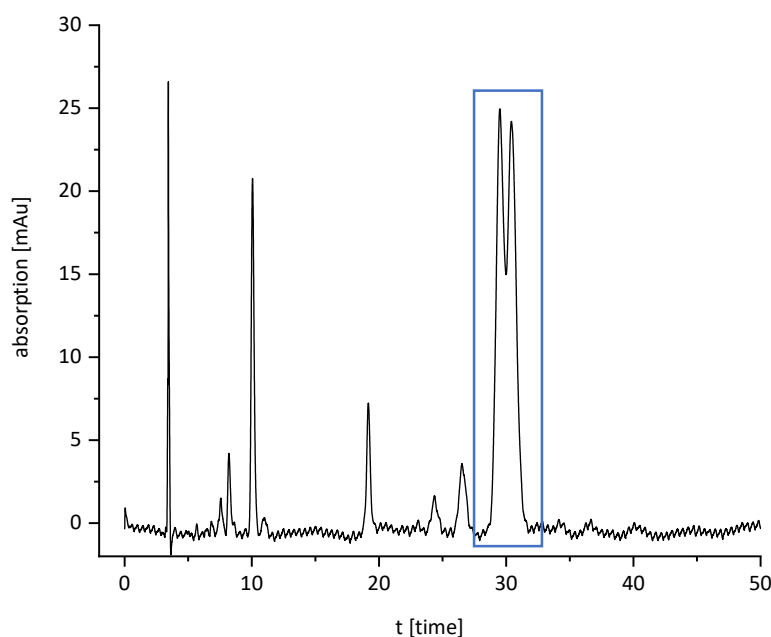
Figure 37: Chromatogram of **10a** after irradiation with UV light (365 nm) for 30 min. The chromatogram was obtained using a Chiralpak® IC column (250 mm, i.d. 20 mm, particle size: 5 μm) and *i*-hexane/*i*PrOH (95/5) as eluting solvent and at 365 nm.
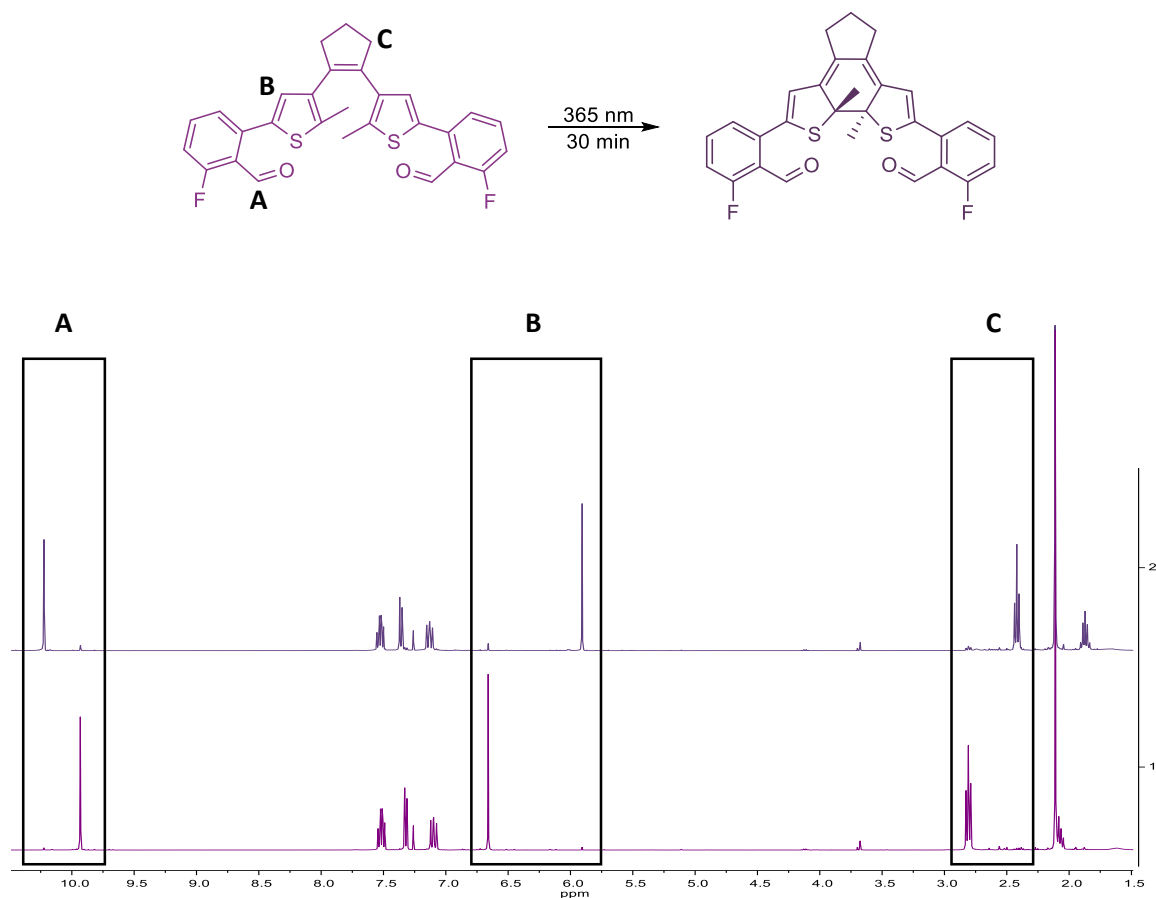
Figure 38: ^{1}H NMR spectrum of **10b** before (bottom, violet) and after (top, dark violet) excitation with UV light of 365 nm for 30 min in CDCl$_3$.

UV light exposure experiments were also performed with the *meta*-fluorinated benzaldehyde **10b**. Figure 38 shows the ^{1}H spectra of the open form before (bottom, violet) and closed form after 30 min of irradiation with UV light at 365 nm. Again, a clear shift of three signals can be seen after the exposure. First, the benzaldehyde signal **A** was shifted from 9.93 ppm to 10.22 ppm. Also the thiophene signal **B** is found at 6.66 ppm instead of 5.91 ppm after exposure to UV light. Finally, a high-field shift of the cyclopentene signal **C** by 0.39 ppm can be observed. The duration of UV light irradiation of 30 min is sufficient to achieve complete ring closure.
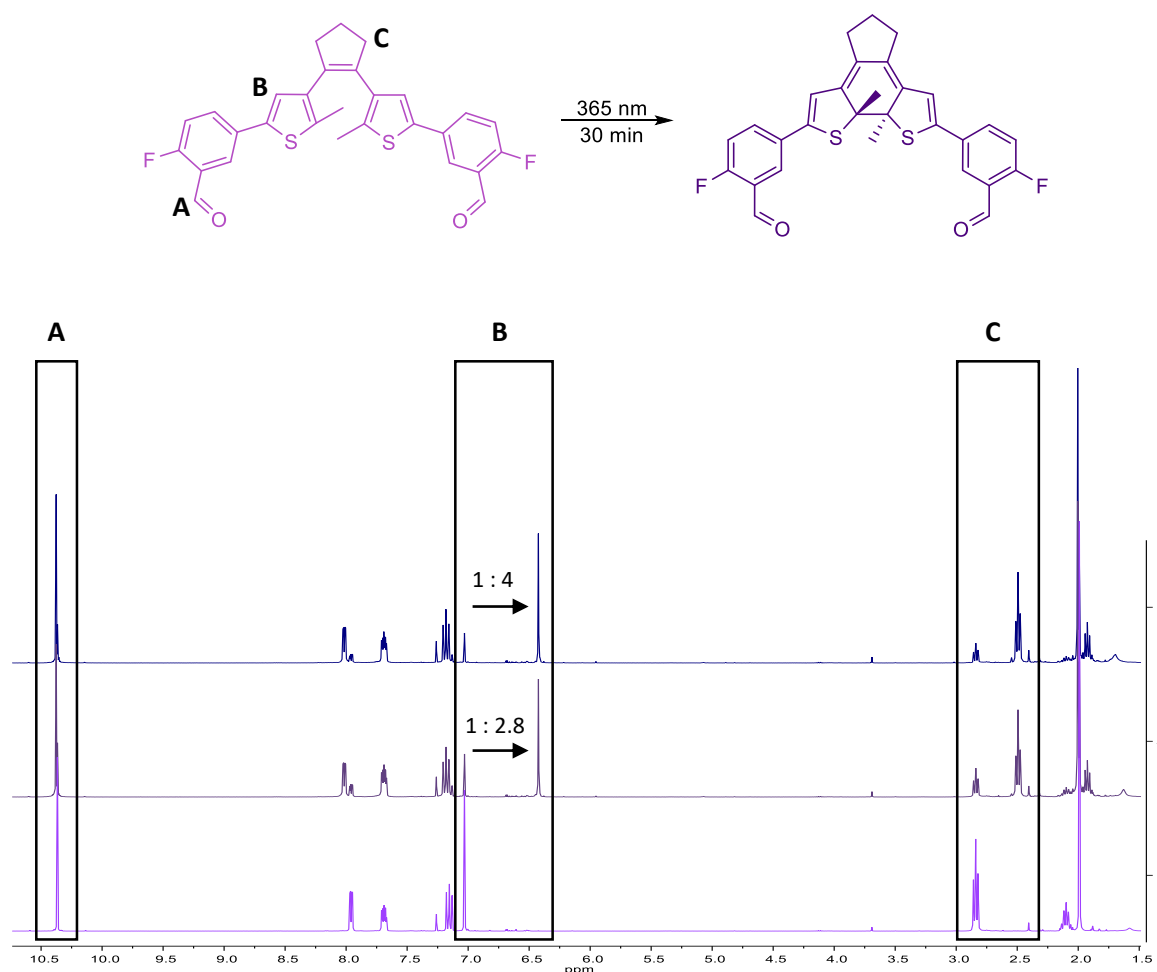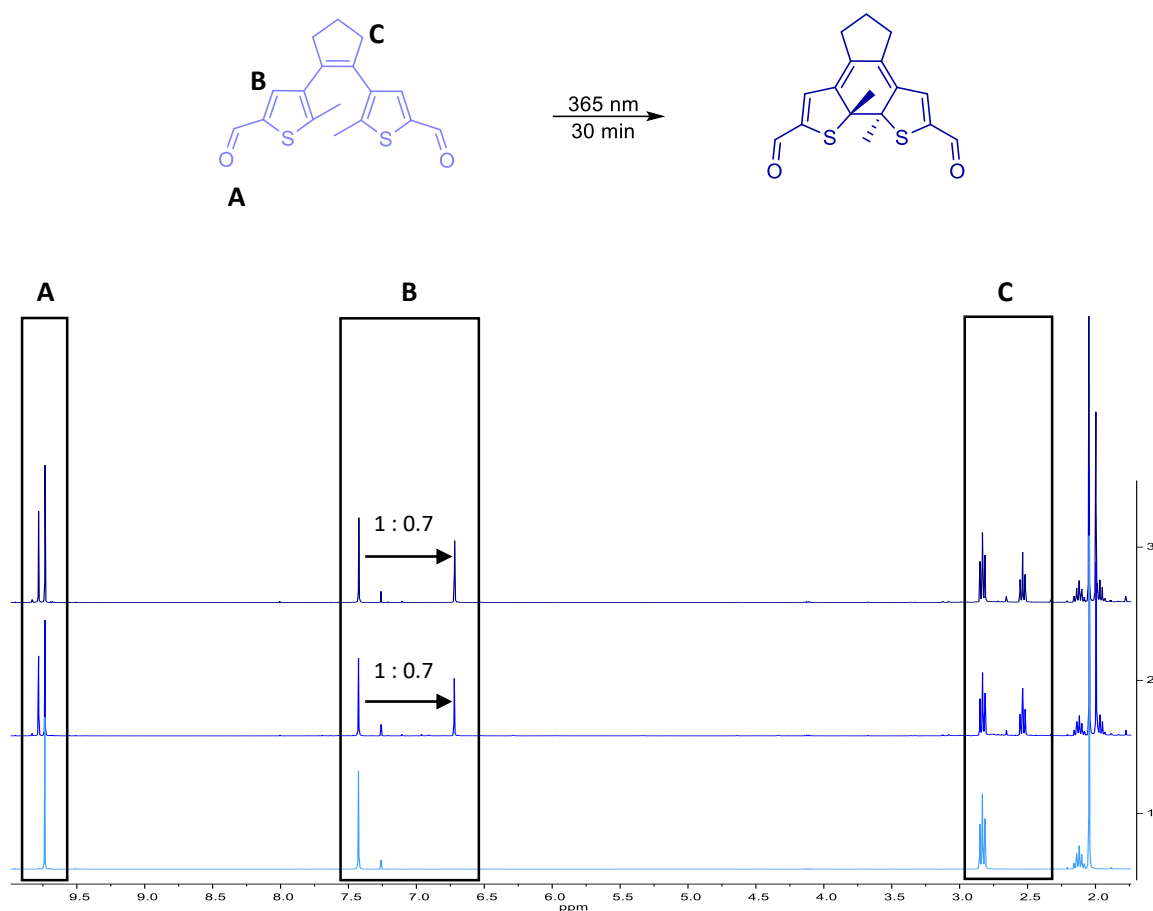
Figure 39: ^{1}H NMR spectrum of **10c** before (bottom, lilac), after 30 min (middle, purple) and 60 min (top, blue) excitation with UV light of 365 nm in CDCl₃.

The spectrum on the bottom (lilac) in Figure 39 shows the ^{1}H NMR before UV light irradiation, in the middle (purple) the spectrum after 30 min and on the top (blue) after 60 min of UV light irradiation of **10c**. The colours of the signals used in the spectra represent the true colours of the reaction solutions. By comparison of the signals of the three spectra, a high-field shift of some signals can be recognized in the two upper spectra in reference to the bottom one and assigned to the positions as denoted in the molecule above. Signal **A** related to the benzaldehyde shifts only slightly, so that it is barely visible to the naked eye and without enlargement of the area. The thiophene signal **B** from 7.03 ppm to 6.42 ppm, where it can be observed that after 30 min there is a ratio of open to closed **10c** of 1 : 2.8. Even after 60 min of irradiation with UV light, no complete closure of the ring can be registered, since the closed isomer **10c** is only present in an excess of 1 : 4. Also, the triplet signal **C**, which belongs to the CH₂-group of the cyclopentene ring, shows a shift to the high-field from 2.84 ppm to 2.49 ppm.
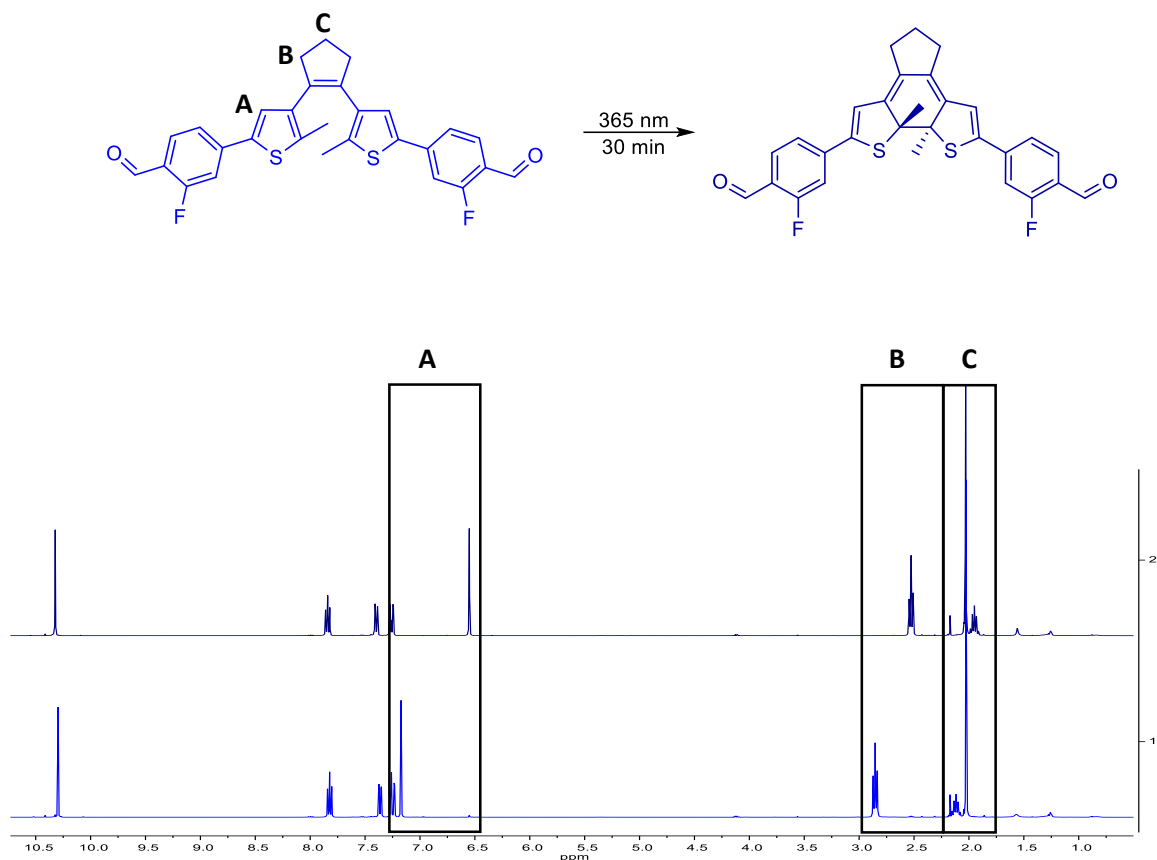
Figure 40: ^{1}H NMR spectrum of **10d** before (bottom, lighter blue) and after 30 min (top, darker blue) excitation with UV light of 365 nm in CDCl$_3$.

The bottom (light blue) spectrum of Figure 40 shows **10d** before and the top (dark blue) after UV irradiation of 30 min. Again, a high-field shift of three signals can be observed. This time the position of the benzaldehyde signal does not change. The change in signal **A** represents the H-signal of the thiophene ring and shifts from 7.17 to 6.55 ppm. The signals of the cyclopentene ring **B** and **C** shift only slightly by 0.32 and 0.17 ppm, respectively. Compared to substrate **10c** (see Figure 38 above), where the aldehyde and fluorine groups are displaced, complete ring closure occurs here within 30 min. Based on the observations made during the experiments, the fluorine in the *para*-position to the photoswitch core (**10c**) in combination with the aldehyde functional group has a much stronger electron-withdrawing effect on the backbone **8** than *vice versa* (**10b** and **10d**), so that the electrons are no longer available for the ring closure on the core molecule of the photoswitch.

Figure 41: ^{1}H NMR spectrum of **12** before (bottom, light blue), after 30 min (middle, royal blue) and 60 min (top, darker blue) excitation with UV light of 365 nm in CDCl$_3$.

Exposure of **12** changes the colour of the solution from ice blue (not exposed) to royal blue after 30 min to darker blue after 60 min. Figure 41 shows the ^{1}H spectra of each of these steps. The lowest spectrum shows compound **12** in the open state. The middle spectrum shows the ratio between the open and closed states after 30 min of exposure to UV light. It can be seen that a down-field shift of the aldehyde signal **A** occurs here for the first time, but only by 0.05 ppm. Again, the thiophene signal **B** shifts into the high-field region from 7.43 ppm to 6.72 ppm. After 60 min of UV light exposure, the same picture appears as in the middle spectrum. This means that a ring closure of substrate **12** can only be achieved to a small extent, since the ratio open to closed isomers of **12** 1 : 0.7 is not exceeded.

In summary, the observations from the UV light exposure experiments show that ring closure intensifies the colour of the sample or creates a colour change, as in the case of the directly functionalized diarylethene **8**. This is consistent with the electronic changes in ring closure, as this expands the aromatic system and then delocalizes it over the entire structure. Comparing the conversion ratios of the compounds after 30 min and 60 min of UV light irradiation, distinct differences were observed. While **10d** was completely converted to the ring-closed isomer, UV light irradiation of **10a** and **10b** gave 95% yield of the corresponding ring-closed isomer. In contrast, **10c** showed a 66% conversion to the closed isomer within 30 min of exposure to UV light and 75% after 60 min. The direct coupling of the aldehyde functionality to the backbone at substrate **12** causes such an electron pull due to the electron-withdrawing character, so that ring closure is made very difficult due to the lack of electron density. Similarly, the low conversion ratio of **10c** can be explained, since herein the *para*-position of the fluorine substituent with respect to the diarylethene unit deprives the molecule of the necessary electrons for ring closure.

3.3.6   Alkylation Experiments

After synthesizing different substrates and studying the ring closure reaction by exposure to UV light at 365 nm, alkylation reactions with the photoswitch substrates were performed. Furthermore, it was interesting to investigate whether the ring closure has an influence on the reactivity of the aldehyde functionality, since it shifts the electronic situation within the molecule, as seen in the NMR experiments.

For this purpose, both organozinc compounds (Et$_2$Zn, iPr$_2$Zn) were used, as they have also been used for alkylation reactions on aldehyde groups in the past.[17, 20] In addition, the *Grignard* reagent (iPrMgCl·LiCl, TG) was also to be tested for the alkylation step. The non-coordinating toluene was used as solvent and thus does not affect the course of the reaction, since the metals are not blocked by coordination at existing e.g. oxygen atoms. Furthermore, it promises to allow solubilisation of all substrates and has also been used in previous work for alkylation reactions of aldehydes.[20]

For the alkylation reactions, the open-ring isomer **10a** (50 mg) was dissolved in dry toluene (5 mL) and the alkylating agent was subsequently added to the reaction solution. An overview of the performed alkylation reactions with **10a** and the obtained reaction products are given in Scheme 11.

	13a	13b	13c	13d	13e
Et$_2$Zn	X	✓	✓	X	X
iPr$_2$Zn	X	X	✓	✓	X
TG	✓	X	X	✓	✓
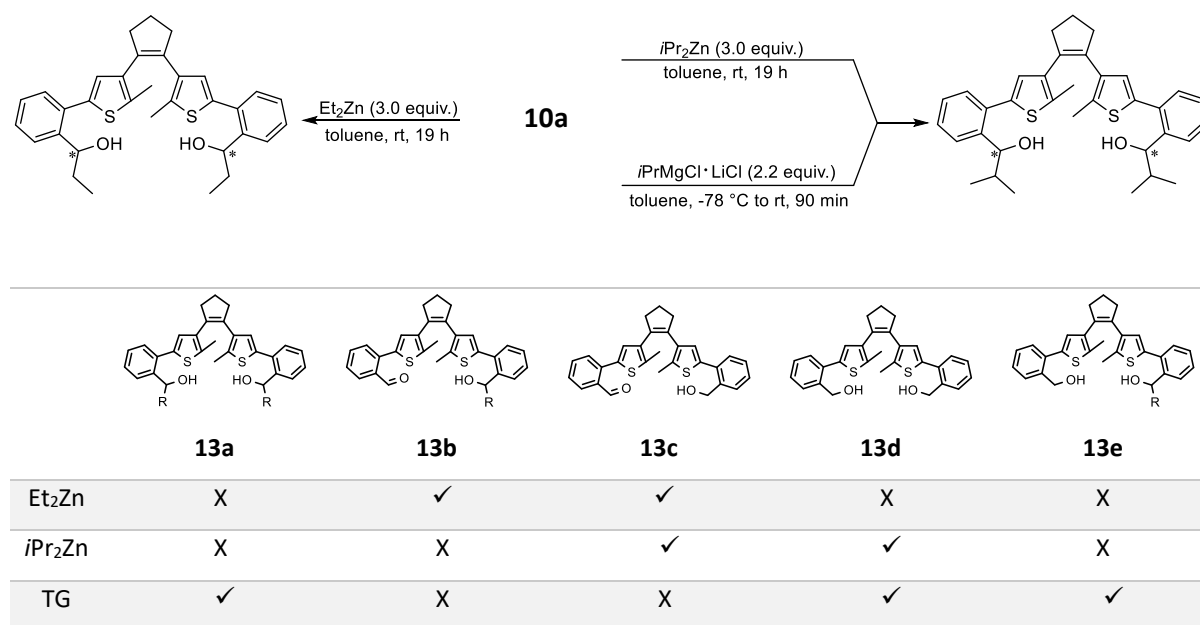
Scheme 11: Overview of the alkylation reactions of the open isomer of **10a** with Et$_2$Zn, iPr$_2$Zn and TG (iPrMgCl·LiCl).

Alkylation using Et_2Zn yielded two reaction products. The mono-alkylated **13b** and the mono-reduced form to the alcohol **13c**. An increase of the diethylzinc amount from 3.0 to 5.0 equivalents or a higher reaction temperature of 50 °C, did not provide any other product.

Reactions with iPr_2Zn gave also two reaction products. However, instead of the alkylated species, only the mono- **13c** or bis-reduced **13d** benzyl alcohols could be identified. The larger space occupied by the isopropyl group compared to the ethyl group explains the absence of the mono-alkylation of substrate **10a**. In addition, alkylation with $iPrMgCl·LiCl$ was performed as a reference of nucleophilicity, in which the reaction solution was cooled to -78 °C before addition of the *Turbo-Grignard*. After a reaction time of 90 min, no starting material, but three products could be identified. In addition to the bis-reduced molecule **13d**, two new products were formed: the mono-reduced and mono-alkylated photoswitch **13e** and the desired bis-alkylated compound **13a**. In all these reactions, there was competition between alkylation and reduction. Especially the reduction of carbonyl compounds is known as '*Grignard* reduction' as a side reaction when using *Grignard* reagents. In this process, the proton of the *Grignard* reagent, which is located in ß-position to the magnesium, is transferred to the carbonyl group. The fact that only partial, if any, alkylation occurred with the zinc organyls and that only the *Grignard* reagent was able to alkylate the reactant twice may have several reasons.

There are also differences within the series of zinc organyls, since the reactivity of the residues that bind to the zinc decreases with the series Me > Et > *i*-Pr, thus explaining why alkylation only occurred with Et_2Zn.
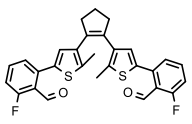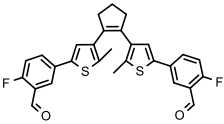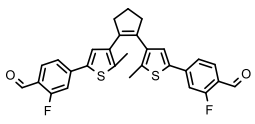
In general, organozinc compounds are much less nucleophilic. This is due to the fact that the carbon zinc bond has a covalent character because of the smaller difference in electronegativities, whereas the magnesium bond is moderately ionic.[84]

Furthermore, it is known that dialkylzinc reagents tend to be inert to simple carbonyl compounds.[17] However, this can be influenced by replacing an alkyl group with an electronegative substituent, as this increases the donor properties of the remaining alkyl group.[85] Another method to increase the moderate reactivity towards aldehydes and ketones can be the complexation of a Lewis acid such as $MgCl_2$.[86] In addition, suitable chelating ligands, e.g. ß-amino alcohols, can be added to increase the reactivity of dialkylzinc reagents towards carbonyl groups. These are known to activate the zinc reagent and make reactions previously not occurring possible in the first place.[85a, 87] Thus, either by increasing the reactivity of the zinc species or the electrophilicity of the carbonyl carbon, alkylation with organozinc compounds could be made possible.

In addition, there are also mechanistic reasons that may have caused or favoured this result. In an alkylation reaction using the *Grignard* reagent, an alcoholate is first formed by nucleophilic addition, which then reacts in a workup step to form the alcohol. In an alkylation reaction with zinc organyls, it is known that zinc aggregates are formed, which in turn can cause steric to become a problem. In this case, it explains why an alkylation reaction of **13b** takes place with Et$_2$Zn but not with *i*Pr$_2$Zn. The molecule with its size and the indicated helical structure is sterically quite challenging. In this respect, the zinc organyl with the smaller ethyl residue can still attack, whereas the isopropyl residue is already sterically hindered. The stability of the aggregates can also have an influence on the formation of the products, since the reduction as a side reaction can take place faster than the reactants are dissolved from the aggregates again in order to react further to the alkyl alcohol.

Alkylation experiments were also carried out with the fluorinated compounds **10b-d**. The introduction of fluorine changes the distribution of electron density in the molecule. This shift causes the electron density at the carbonyl-carbon to be reduced and its electrophilicity to be increased, which should favour an attack by the metal organyls. An overview of the reactions and the products obtained is shown in Table 3.

Table 3: Overview of the performed alkylation reactions with compounds **10b-d** using the same reaction conditions as with **10a**.

alkylating reagent	10b	10c	10d
Et$_2$Zn	X	X	X
*i*Pr$_2$Zn	X	X	X
*i*Pr$_2$Zn (80 °C)	alkylated/reduced	alkylated/reduced bis-reduced	X
*i*PrMgCl · LiCl	-	alkylated/reduced	bis-alkylated **(14)** alkylated/reduced **(15)**
*i*Pr$_2$Zn · MgCl$_2$ · 2 LiCl	-	alkylated/reduced	bis-alkylated **(14)** alkylated/reduced **(15)**

Similar to the alkylation experiments of **10a** with Et$_2$Zn and *i*Pr$_2$Zn, no alkylation was observed with all three substrates. In general, the fluorinated substrates seemed to be less reactive towards the zinc species as no reduction reaction occurred either. By increasing the reaction temperature to 80 °C, mono-alkylation was observed for **10b** during alkylation with *i*Pr$_2$Zn, while the other side was reduced.

For molecule **10c**, two reaction products were formed, both the mono-reduced and mono-alkylated, and the bis-reduced molecule. When *Turbo-Grignard* was used, numerous products were formed in the case of **10d**, all of which have very similar retention times and could not be separated. For **10c** and **10b**, the reaction gave the alkylated-reduced form and for **10d** even the bis-alkylated species.

Finally, the mixed salt *i*Pr$_2$Zn · MgCl$_2$ · 2 LiCl was tested to increase the reactivity of the zinc organyl and to achieve bis-alkylation for all three fluorinated substrates.[86] In fact, the expected higher reactivity was clearly shown by more undesired reaction products. However, the bis-alkylated species was only detected for **10d**. The reaction with **10c** gave a corresponding mixed species (alkylated/reduced) and in the case of **10b**, several products were formed, which could not be separated due to similar R$_f$-values. Since the *Turbo-Grignard* as well as the dialkylzinc mixed salt reagent already showed high reactivity at room temperature and produced quite a few by-products, higher reaction temperatures were not tested with these reagents. In addition, the results indicate that the reactivity of the *Turbo-Grignard* reagent and the mixed salt dialkylzinc reagent is not the limiting factor of this reaction, but rather their non-selectivity. The reason why bis-alkylation was only possible with **10d** is mainly due to steric reasons. Of all the compounds, the isopropyl residue of **10d** has the most distance to the backbone and therefore the electronic repulsion is lowest. Since the electronic situation in the molecule **10c** is comparable to that of **10d**, the reason for the bis-alkylation only for **10d** is probably that the steric does not allow alkylation. In addition, the bis-alkylation on **10b** is less favourable compared to **10d**, which also prevents double alkylation here.

Since *Oguni* and *Noyori* reported a tremendous effect on the reaction rate in the enantioselective addition of diorganozinc to aldehydes when the latter was used, the effect of nitrogen-containing ligands such as TMEDA or β-amino alcohols on the reaction should be tested.[25a] It is known from the literature that the addition of auxiliary substances, especially those with electronegative substituents, increases the reactivity of diorganozinc towards carbonyl groups. The reason for this is a change in electron density, where a stronger p-character of the orbitals makes zinc a better acceptor and at the same time increases the donor properties of the alkyl group.[25a]

The first evidence for such an assumption was provided by *Oguni* and *Omi* in 1984, when they reacted benzaldehyde with diethylzinc in the presence of a catalytic amount of (*S*)-leucinol.[25b] *Noyori* and coworkers then concluded that the efficiency of amino alcohols depends on their structure and substitution pattern and recognized that β-dialkylamino alcohols are more efficient than the corresponding *N*-monoalkyl or non-alkylated compounds. Further findings were that β-dialkylamino alcohols with sterically demanding substituents in α- and/or β-position are multifunctional applicable to increase the reaction rate.[25a] Thus, it would be interesting to use such ligands in the alkylation reactions of compounds **10b**, **10c**, and **10d** with diethylzinc or diisopropylzinc.

3.3.7   Influence of UV Light Irradiation on the Alkylation

In the following, it was investigated which influence the nature of the basic structure (open or closed form) has on the stereochemistry of the alkylation reaction with *i*PrMgCl · LiCl and thus influences the product distribution, especially in the direction of one enantiomer. In addition, it was tested what difference it makes whether the reaction solution is irradiated before or after the alkylation reaction. For this purpose, the alkylation of **10a** with *i*PrMgCl · LiCl was carried out. Firstly, a reaction solution was used, which was irradiated with UV light (365 nm) already before as well as during the entire reaction (Scheme 12).
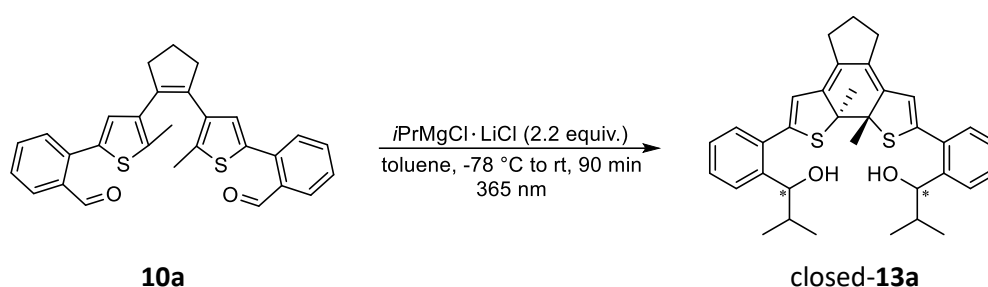
Scheme 12: Alkylation reaction of **10a** with *i*PrMgCl · LiCl with UV light irradiation (365 nm) before and during the reaction.

In this reaction, as in the alkylation reaction without irradiation, three products were obtained: the bis-alkylated compound ***i*Pr₂-13a**, the alkylated and reduced compound ***i*Pr₂-13e**, and the bis-reduced molecule **13d**. In both cases, with and without UV irradiation, a second species was observed in the ^{1}H NMR of the bis-alkylated compound ***i*Pr₂-13a**. For this observation, the signals of the *i*Pr-CH$_3$ groups are exemplified in Figure 42, where the upper spectrum shows the alkylation result without UV irradiation and the lower spectrum with UV light exposure before and during the reaction.

meso   enantiomers
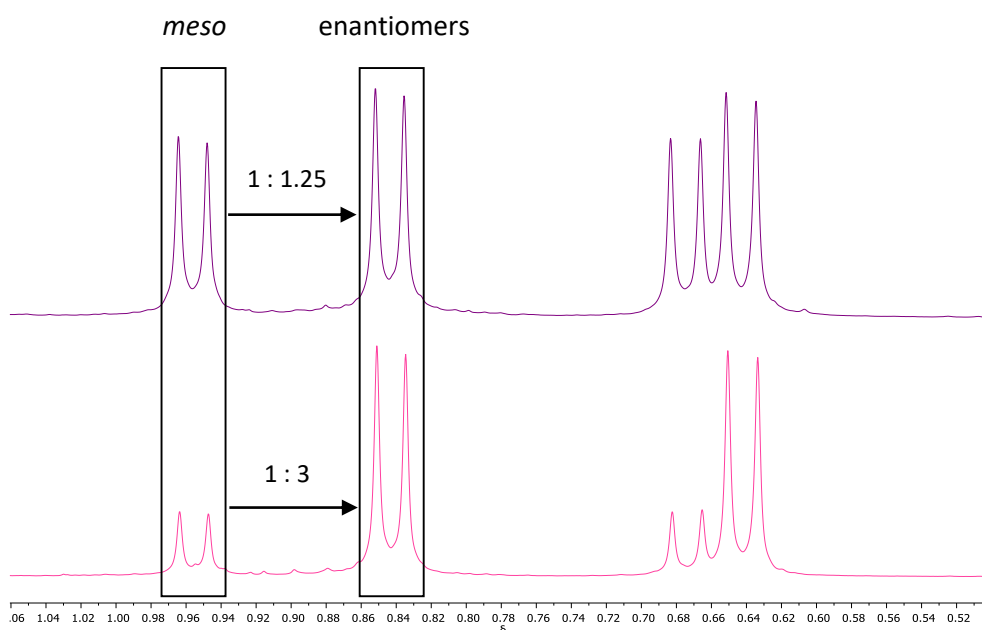
Figure 42: ^{1}H NMR (in CDCl$_3$) of the *i*Pr-CH$_3$ groups of the bis-alkylated product **13a** without exposure to UV light (bottom, pink) and irradiated before and during the alkylation reaction (top, purple).

Doublets were obtained for the *i*Pr-CH$_3$ groups, which are in different ratios to each other. The pink spectrum shows a ratio of 1 : 3, while a ratio of 1 : 1.25 can be observed for the purple spectrum. Hence, the ratio between the two species was influenced by UV light excitation as the integral ratio between the signals differs (Figure 42).

First of all, it is noticeable that the two spectra from before (pink) and after UV light exposure (purple) do not differ in their shifts, only in the intensities of the signals. This indicates that no ring-closed isomer is obtained during the alkylation reaction as the same signals are visible both before and after the exposure to UV light. In order to gain further insight into the order of the signals, the resulting isomers of **13a** were separated on chiral HPLC (Figure 43). In the following, reference is made to the outer alkyl position when describing stereocenters, while the inner stereocenters of the same configuration after the rotational ring closure are ignored. Based on the corresponding masses, the signals **I** could be assigned to the bis-alkylated isomers **13a**, which split in a ratio of 1 : 1 : 1.5. These first two peaks represent the enantiomers (*S,S*) and (*R,R*) of the ring-open form **13a**. The third peak is related to the *meso*-forms (*R,S*) and (*S,R*). The expectation for a statistical distribution of enantiomers to *meso*-compounds is 1 : 1. If now the ratio of enantiomers to *meso*-form is calculated, a relation of 1.3 : 1 is obtained. If these observations are now transferred to Figure 43, the smaller doublets in the pink spectrum can be assigned to the *meso*-form and the larger doublets to the enantiomers, since a ratio of 1.25 : 1 appears.
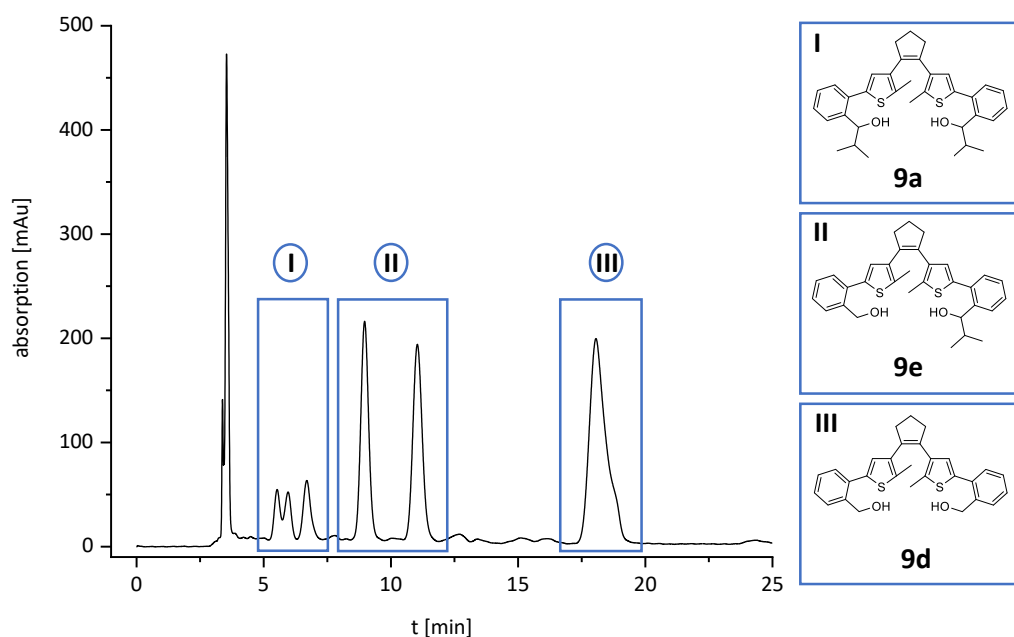
Figure 43: Chromatogram of the crude product that was obtained from the reaction of compound **10a** with *i*PrMgCl · LiCl. The chromatogram was monitored using a Chiralpak® IC column and *n*-hexane/*i*PrOH (95/5).

This unexpected observation can be attributed to a behaviour similar to that of DNA. Due to the size of the molecule and steric requirements, the structure **10a** arranges itself around an axis and adopts a helical structure, as it can be seen in the crystal structure in Figure 34. This turns an achiral molecule which has no stereocenter into a chiral structure with an axis of chirality, resulting in *M/P*-symmetry. Alkylation makes the molecule larger and, above all, the sterically demanding isopropyl groups reduce the probability of a *meso*-structure. In this case, the two alkyl groups are orientated towards each other in space. This results in steric hindrance caused by electrostatic repulsion. In comparison, the isopropyl groups in the enantiomers (*S,S*) and (*R,R*) are as far apart as possible, which favours the formation of the structure. After alkylation, the electronic situation in the molecule changes so much that the conrotatory ring closure is no longer possible. If the ring closure is carried out before alkylation, the three-dimensional structure changes in a way that the helical twist is less distinct and the molecule becomes more planar. This is also confirmed by DFT calculations of the ring-open and ring-closed isomers.[83] This change in the spatial structure means that the formation of the *meso*-product is now more favourable, which is also confirmed by NMR. Interestingly, however, the alkylation reaction dominates the ring closure, although the reaction was exposed both before and during alkylation and yet only ring-open isomers are present. In this case, no amplification of one stereoisomer could be observed by the ring closure of the photoswitch, but rather the opposite.

The peaks in **II** are related to the mono-alkylated and mono-reduced compound **10e**. These show a racemate, since a stereocenter is present at the alkyl residue, in (*R*) or (*S*) configuration. These two isomers are enantiomers to each other. The molecule which was bis-reduced on both sides **10d** without a stereocenter is detected as one peak (Figure 43, **III**).

It is also noticeable from the chromatogram that the inner stereocenters (*R,R*) and (*S,S*) are not separated after rotational ring closure under UV exposure under the given measurement conditions. This example shows that the sterochemical outcome of alkylation can be influenced by UV excitation.

After performing the alkylation reactions with the fluorinated substrates, UV experiments were also performed with the bis-alkylated compound **14** and the mixed species (alkylated/reduced) **15** of **10d**. For this purpose, the compounds were analysed by HPLC and measured before and after UV light irradiation at 365 nm for 30 min and analysed using a Chiralpak® IC column with *n*-hexane/*i*PrOH (95/5) to obtain first insights into the stereoisomers formed.

As described above, irradiation of the substrates with UV light induces ring closure of the photoswitch molecule, which proceeds in a conrotatory fashion according to the *Woodward-Hofmann* rules for systems with 6π-electrons[67] resulting in two additional stereocenters (Figure 44). However, the resulting stereocenters just give two types of absolute configuration - (*R,R*) or (*S,S*) - due to sterical hindrance and unfavourable electronic repulsion in terms of a *S,R* or *R,S* situation.
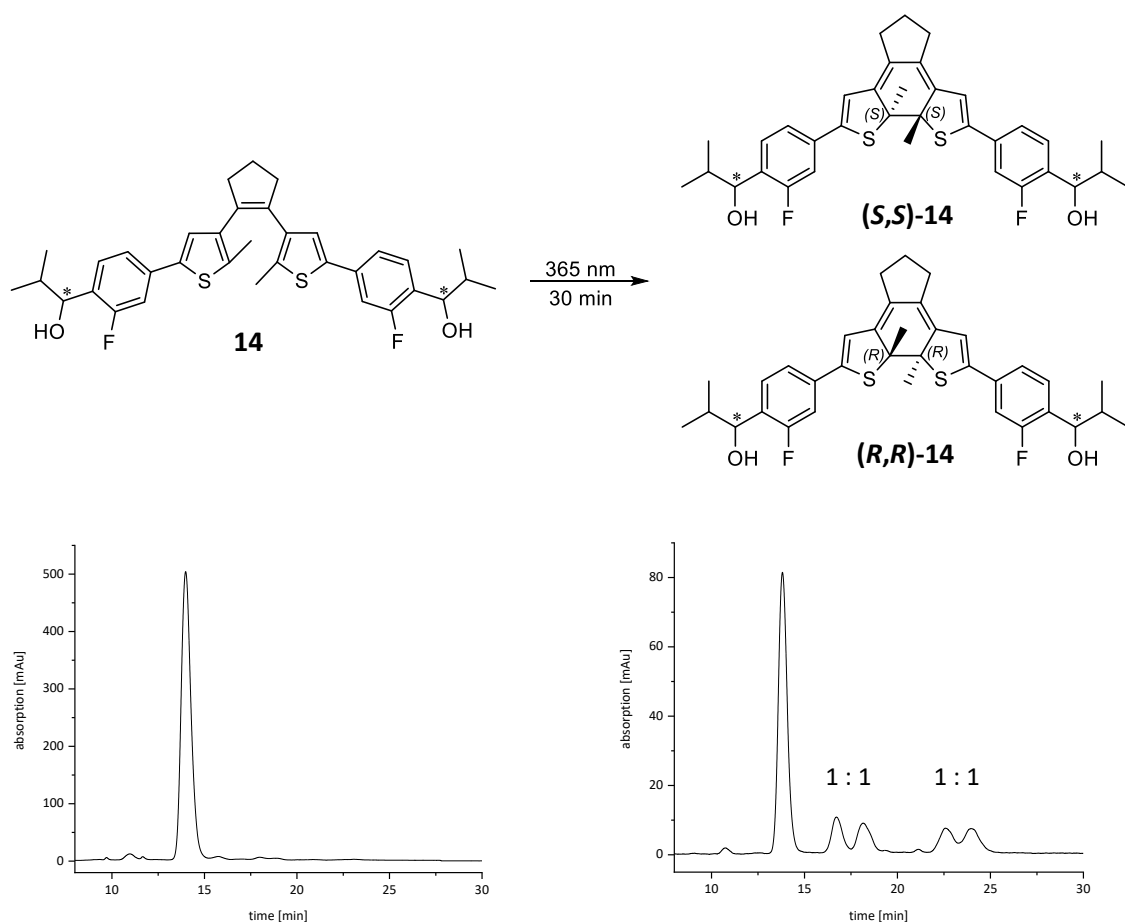
Figure 44: Through UV light irradiation of the bis-alkylatd species **14** electrocyclic ring closure gives two additional stereocenters resulting in two stereoisomers, (*R,R*) and (*S,S*) and corresponding HPLC chromatograms of the bis-alkylated **14** and after UV light irradiation (365 nm) for 30 min measured on a Chiralpak® IC column (250 mm, i.d. 20 mm, particle size: 5 μm) with *n*-hexane/*i*PrOH = (95/5).

The left side of Figure 44 shows the chromatogram of the ring-open bis-alkylated compound **14** before UV light irradiation whilst the left side demonstrates the chromatogram after exposure to UV light at 365 nm for 30 min. Due to the substituent position and the resulting change in electronic situation, the ring closure is no longer completely possible compared to the non-alkylated form **10d** (see Figure 40). After exposure, four further species can be detected on the HPLC. Figure 45 lists all possible isomers and their stereospecific relationship to each other.
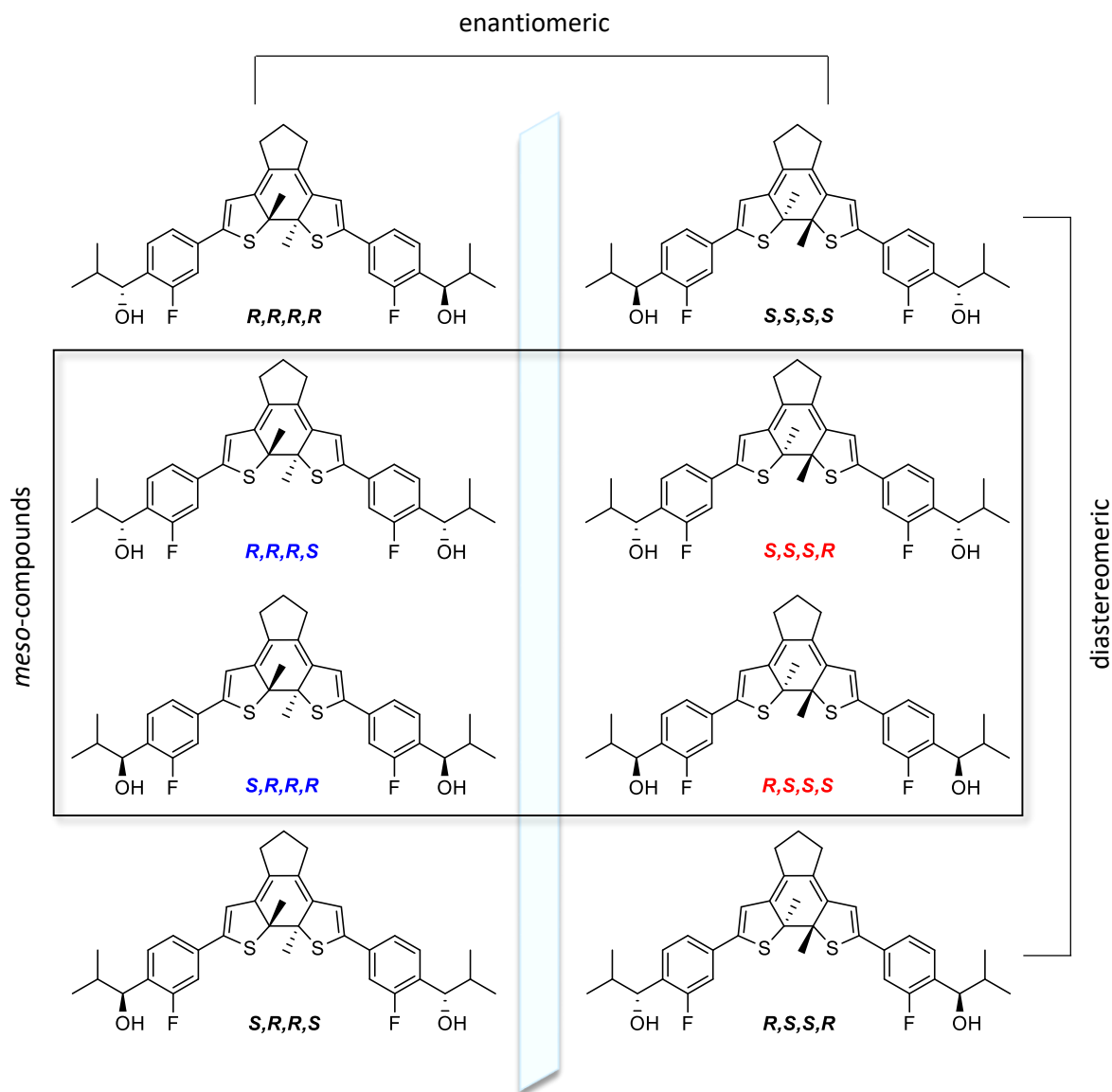
Figure 45: Overview over the eight possible stereoisomers accessible in the conrotatory ring closing reaction of **14**.

The open form of **14** has two stereocenters, resulting in four possible stereoisomers, of which two form a pair of enantiomers (*R,R* and *S,S*). The other two stereoisomers are achiral due to an internal molecular mirror plane and therefore are *meso*-compounds (*R,S* and *S,R*). The ring closure by UV light creates two new stereocenters, which theoretically lead to sixteen possible stereoisomers. However, due to the conrotatory ring closure, through which the two middle stereocenters can only adopt the same configuration, eight of a possible sixteen stereoisomers remain. The remaining isomers can be divided into two groups in which the core molecule adopts the (*R,R*) (left column) or (*S,S*) configuration (right column). The neighbouring molecule in the left and right columns form a pair of enantiomers.

The second and third molecules of a column can be converted into one another by rotating around a C_2-axis and the blue- and red-coloured stereoisomers are each *meso*-compounds and therefore the same. Consequently, these also behave in the same way chromatographically, so that the signals coincide in the chromatographic analysis. For these reasons, you would theoretically see more signals than is practically the case. For the open isomer, three signals are expected in the ratio 1 : 2 : 1 for the (*R*,*R*)-, the *meso*- and the (*S*,*S*)-isomer. In contrast, only one signal could be detected for the open form at 13.8 min (Figure 44 left chromatogram). After ring closure, six signals are expected, two of which belong to the diastereomeric enantiomer pairs from line 1 and 4, each of which splits again and can also be observed in the chromatogram. Two signals are also expected for the *pseudo-meso*-structures, but these appear to result in one large peak (Figure 44 right chromatogram).

In this case, it seems that under the chromatographically conditions applied, no resolution of the respective inner stereocenters, i.e. the enantiomer pairs of Figure 45, could be achieved. This means that after the ring closure, only diastereoisomeric compounds can be observed in the right-hand chromatogram, neglecting the main peak. The main peak is related to the ring-opened species, which was not completely converted into the ring-closed species by UV light irradiation. This assumption is mainly supported by the fact that this peak has the same retention time as the ring-opened species before UV irradiation. Therefore, the newly formed peaks after UV light irradiation in the right chromatogram each correspond to a diastereoisomeric compound from Figure 45, whereby the enantiomer pairs do not split. The diastereoisomers appear as theoretically expected in a ratio 1 : 1 : 1 : 1. By using the amylose-based Chiralpak® IF column with *n*-hexane/*i*PrOH (95/5), an indication of the presence of two peaks could be achieved (Figure 46), which supports the assumption that the enantiomers cannot be adequately resolved simultaneously with the diastereoisomers. Nevertheless, no measurement condition could be found where complete separation could be achieved for clear analysis.
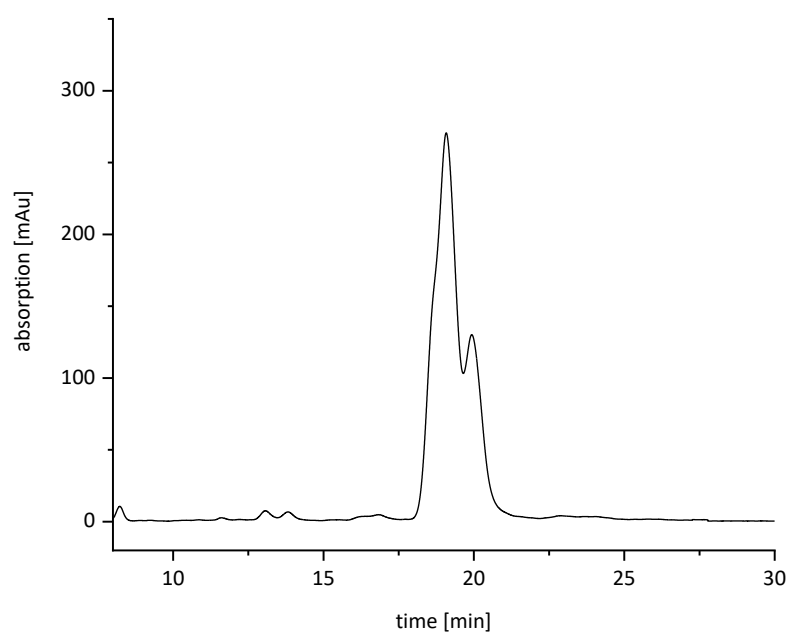
Figure 46: HPLC chromatogram of the open bis-alkylated species **14** before UV light irradiation on a Chiralpak® IF column (250 mm, i.d. 4.6 mm, particle size: 5 µm) with *n*-hexane/*i*PrOH (95/5).

The 'diastereomer theory' interpretation of the results is also confirmed by the analyses of the mixed (alkylated and reduced) species **15**. The sample was prepared and subsequently analysed by HPLC before and after irradiation with UV light (365 nm) for 30 min (Figure 47).
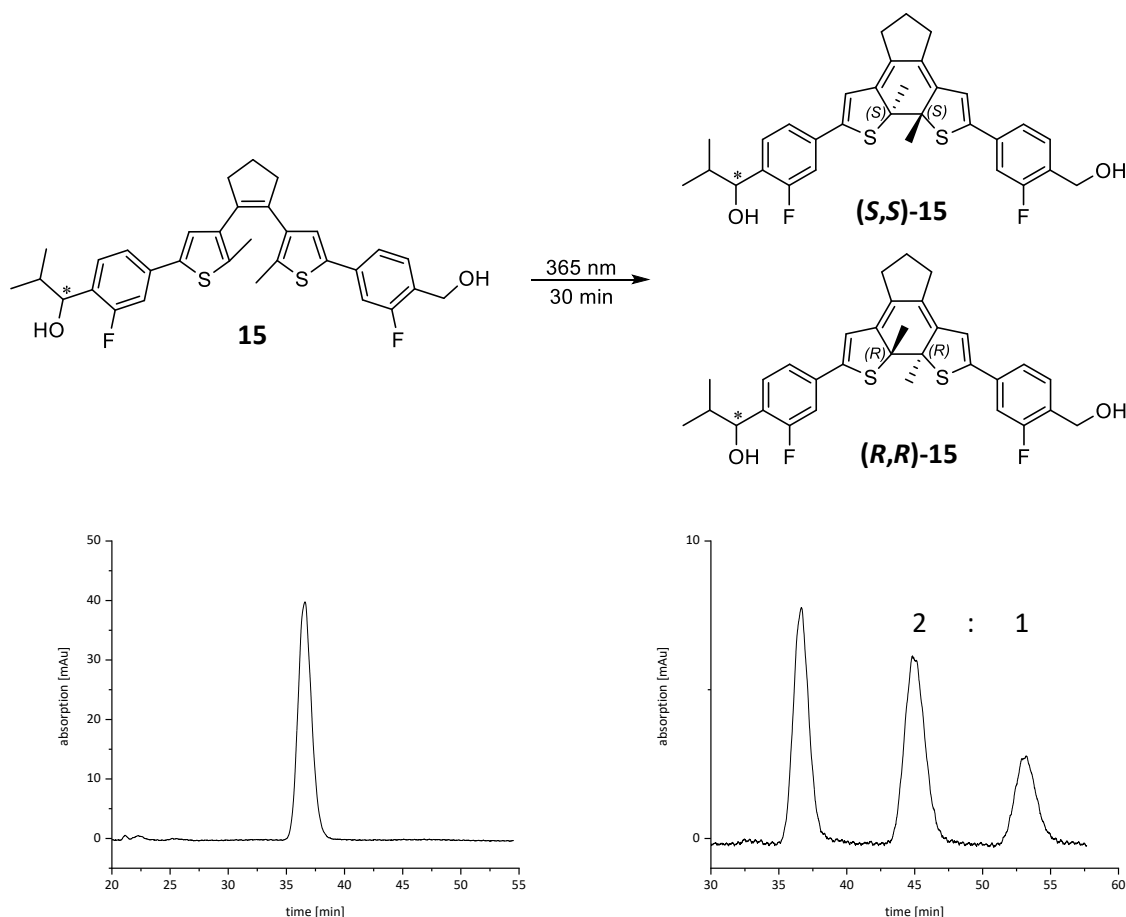

Figure 47: HPLC chromatograms of the mixed species **15** (alkylated and reduced) before (left) and after (right) UV light irradiation (365 nm) for 30 min. The samples were measured using a Chiralpak® IC column with *n*-hexane/*i*PrOH (95/5).

The chromatogram of the ring-open form of **15** can be seen on the left-hand side of Figure 47. In the open form, the molecule has one stereocenter, which leads to two stereoisomers which are enantiomeric to each other. However, even here only one peak can be observed under the given measurement conditions. After ring closure by UV light irradiation, a total of three stereocenters can be found in the molecule. Due to the conrotatory ring closure, however, only four of the theoretical eight stereoisomers are possible in the end. The four stereoisomers can be divided into two pairs of enantiomers: (*S,S,S*)-**15** and (*R,R,R*)-**15** as well as (*S,R,R*)-**15** and (*R,S,S*)-**15** (Figure 48).
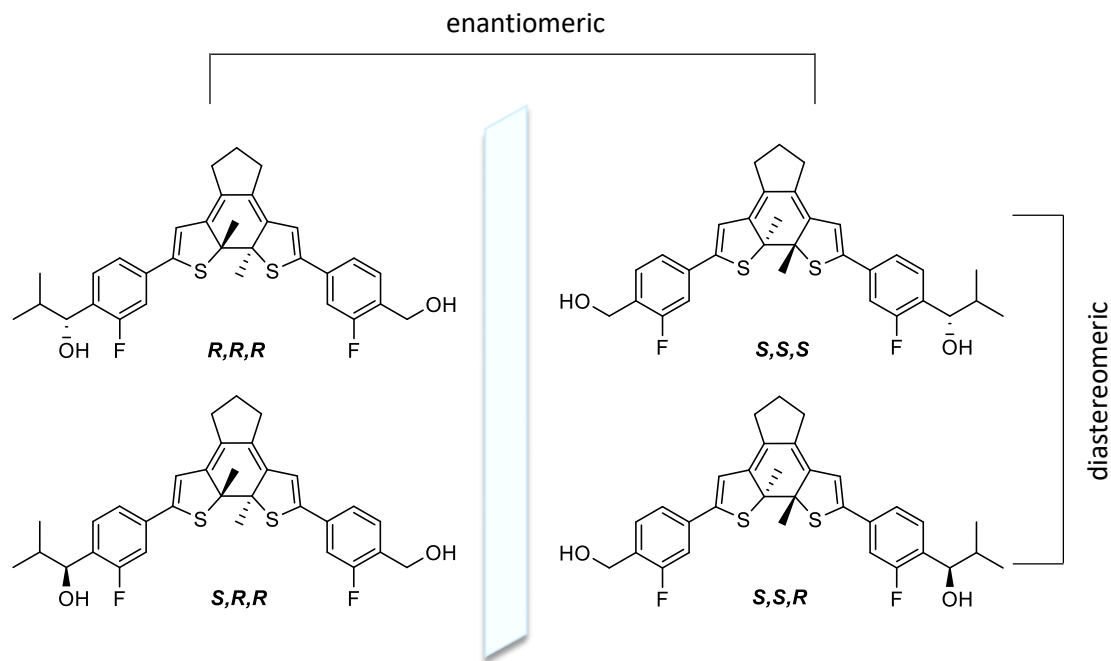
Figure 48: Overview over the four possible stereoisomers accessible in the conrotatory ring closing reaction of **15**.

According to the above explanation, a peak is to be expected for each pair of enantiomers that is diastereomeric to each other. In addition to the supposed signal of the open species, which again has the same retention time as before UV light exposure, two peaks can in fact be seen in the chromatogram. What is striking here is that the diastereomers were formed in unequal amounts this time, in a ratio of 2 : 1, which is explained by the stereoelectivity of the ring closure upon UV light irradiation. In this case, it can be assumed that the more dominant enantiomer pair at 45 min represents the (*R*,*R*,*R*)/(*S*,*S*,*S*) enantiomer pair in the upper row (Figure 48). As mentioned above, it is also more favourable here if the substituents are arranged alternately after conrotatory ring closure, which is the case for (*R*,*R*,*R*)/(*S*,*S*,*S*)-**15** for the two methyl groups and the secondary alcohol.

The observations made during measurements on the various HPLC columns Chiralpak® IC and IF also indicate that the different isomers could not be completely separated under the measurement conditions used and therefore a complete picture of all the species present cannot be obtained.

Finally, it was shown that the orientation of the stereoinformation can be transferred both from the backbone to the side chains and *vice versa*. In the case of **10a**, the ring closure of the carbonyl photoswitch changed the distribution of the isomers after alkylation, while the orientation of the methyl groups after conrotatory ring closure was influenced by the chiral secondary alcohol substituent due to previous alkylation in the case of **15**.

3.4   Summary and Outlook

In summary, the aim of this chapter was to combine a photoswitch molecule with the alkylation reaction of different benzaldehyde moieties in one system in order to achieve a deflection in the formation of stereoisomers through dynamically controllable light-induced changes in the core structure (Figure 49). As backbone compound the dithienyl system **8** known among others from *Feringa et al*. performing autoamplification through UV light irradiation and gelling with a dopant. As benzaldehyde moieties a benzaldehyde with the carbonyl standing in *ortho*-position to the core substrate as well as different fluoro-benzaldehydes enhancing the electron-withdrawing effect of the dithienyl were used. MIDA boronic acid esters were produced in quantitative yield for the coupling of the aldehyde side chain, which enabled clean conversions with good yields in the subsequent *Suzuki* cross-coupling reaction. This was necessary because the couplings with boronic acids showed no to poor conversions and made purification impossible due to a large number of by-products. In addition, the synthesized compounds were irradiated with UV light (λ = 365 nm) in CDCl$_3$ and the electronic changes analysed by ^{1}H NMR. All aldehyde photoswitches except **10c** and **12** could be completely ring-closed within 30 min, which could also be determined by a colour change in the solution. The *meta*-aldehyde *para*-fluoro compound **10c** and the backbone-aldehyde substrate **12** were not completely ring-closed even after 60 min. The results therefore suggest that the substitution pattern of the fluorobenzaldehyde bound to the diarylethene appears to strongly influence the electrocyclic ring closure reaction. The electron-withdrawing aldehyde groups bound directly to the diarylethene have an even stronger influence on the electronic structure of the photoswitch as the least ring-closed isomer was formed here after UV light irradiation.

In addition, the diastereomer distribution during alkylation was influenced by the axial chirality of the open photoswitch molecule itself. By twisting away from planarity, a chiral axis is created, comparable to that of DNA. This effect suppresses the formation of the *meso*-stereoisomer, as this orientation to the same side of the molecule is sterically unfavourable. When the molecule is exposed to light before alkylation, this diastereomer ratio is changed and more *meso*-product is formed as the molecule is more planar due to the ring closure. Interestingly, however, the alkylation weighs more heavily so that no ring-closed product can be obtained even with exposure during the reaction.

During the ring closing of mono-alkylated photoswitch **15**, it was further shown that the stereoinformation of the alkyl substituent has a significant influence on the stereoselectivity of the ring closing reaction. The influence of the stereochemistry was thus successfully effected from the photoswitch core to the introduction of the alkyl substituent and also *vice versa* from the alkyl substituent on the photswitch core.
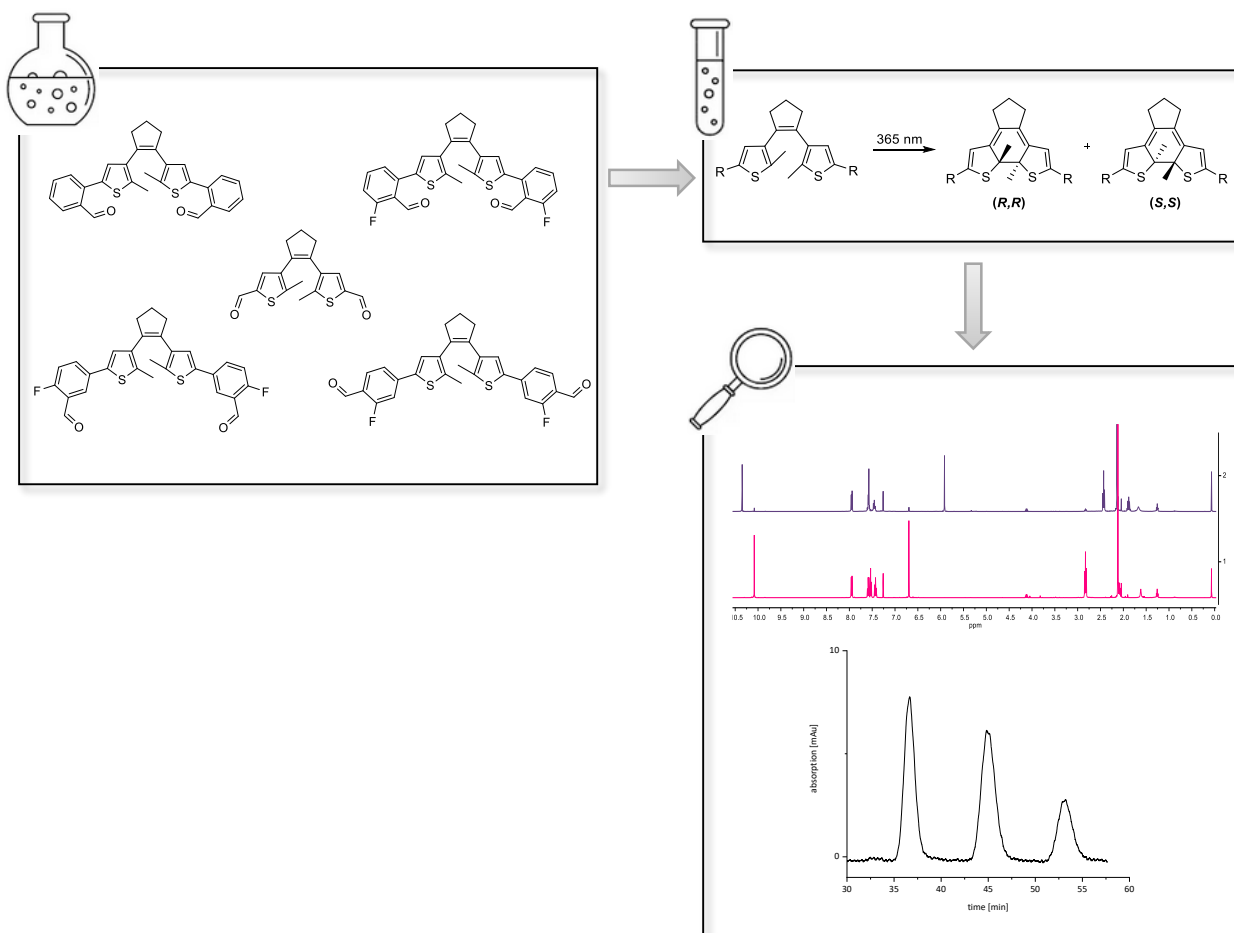

Figure 49: Overview over the synthesized phostoswitch molecules and the analytical methods ^{1}H NMR and HPLC-MS used for investigation after ring closure by UV light irradiation and its impact on alkylation reactions.

In the future, it would be possible to use ligands, such as ß-amino alcohols, in the alkylation reaction that favour or enable the addition in a similar way to the alkylation of benzaldehyde. Since the electron density shifts towards the backbone due to the UV-triggered ring closure, it would also be conceivable that the ring closing reaction is also carried out first with the fluorinated photoswitch compounds before alkylation. In addition, the mixture of enantiomers of **15** (in a ratio of 2 : 1, Figure 47), for example, can be separated in order to crystallize them so that can be investigated which enantiomer is preferentially formed and why. In addition, this mixture can also be used as a ligand for other asymmetric reactions to see if it causes a deflection. It would also be interesting to incorporate nitrogen-containing aromatic compounds with an aldehyde function instead of benzaldehyde, as it is known that these can be alkylated well without the addition of an auxiliary.

CHAPTER 4

Asymmetric Alkylation of Benzaldehyde by

ß-Amino Alcohol mediated Catalysis

4.1   State of Knowledge

The alkylation of the carbonyl group is an important tool in the field of organic synthesis, which is of great significance as a sub-step of a reaction cascade or as a single reaction leading to the target molecule, since enantiomerically pure secondary alcohols play a major role in many naturally occurring, biologically or pharmaceutically active compounds. Since the first steps by *Grignard* and his doctor father *Barbier* in the field of the alkylation of carbonyl groups using metalorganic reagents in the early 20th century, this reaction has generated a great deal of interest and over time has spawned a wave of new alkylation reagents.[88] An important step was the use of various main group and transition metals to control the chemo- and regioselectivity of the alkylation of carbonyl compounds. However, stereoselective control is more difficult to achieve, especially with conventional organolithium or organomagnesium reagents. Initially, the use of diorganozinc compounds allowed access to the desired secondary alcohols by alkylation of aldehydes.[89] However, it is not possible to convert all aldehydes to the corresponding secondary alcohols under mild conditions and in a controlled manner. In particular, the enantioselective alkyl addition to benzaldehyde poses a challenge, as it is largely not converted to the desired alcohol without further additives. *Oguni* and *Omi* found the solution to this problem in 1984 when they were able to catalyse the alkylation of benzaldehyde with diethylzinc with moderate enantioselectivities from up to 49% *ee* using easily available chiral 2-amino-1-alcohols.[25b] In this combination, it was important that non-coordinating solvents such as toluene and hexane were used instead of the solvents normally used for organometallic reactions. However, no alkylation takes place in these solvents without the addition of an amino alcohol ligand as auxiliary. By adding the chiral trigger, coordination to the metal can take place, forming a catalyst that enables stereo-controlled alkylation.[17, 25b]

However, it was *Noyori* who succeeded in achieving high enantioselectivities by using 2 mol% of (-)-DAIB with an *ee* of 14% as catalyst in the alkylation reaction of benzaldehyde with diethylzinc and obtained the product (*S*)-1-phenylpropanol with up to 98% *ee*. Such a (+)-NLE was also observed when using dimethylzinc, but to a smaller extent. This (+)-NLE is due to the fact that diastereomeric complexes are formed from the dialkylzinc and the catalyst DAIB, which in turn have different properties and stabilities.[17, 85a]

In the following years, numerous research groups have focused on investigating the reaction mechanism, which is shown in simplified form in Figure 50.
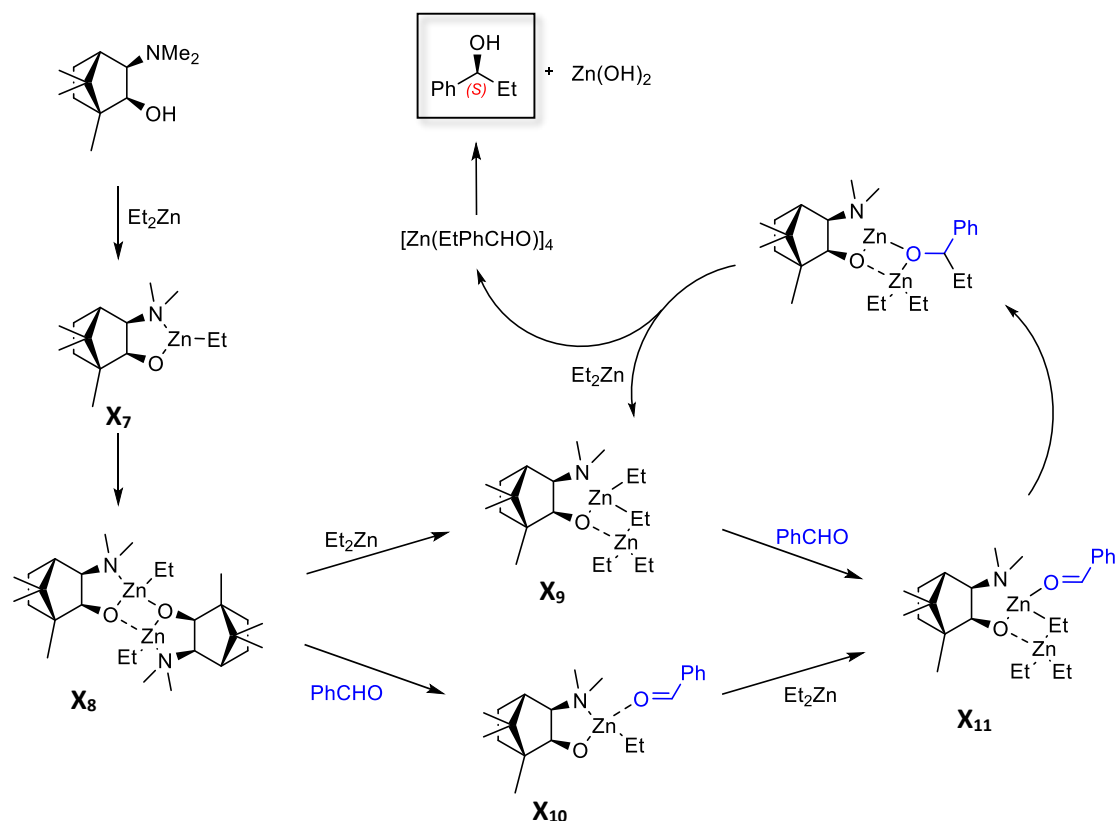
Figure 50: Schematic catalytic mechanism of the asymmetric alkylation of benzaldehyde with Et$_2$Zn using DAIB as chiral ligand by *Noyori*.[17, 90]

In the first step, the amino alcohol forms a zinc alkoxide with a zinc alkylorganyl **X₇**. This can then form homo- or heterochiral dimers **X₈**, with the heterochiral complex being thermodynamically favoured. The diastereomeric, heterochiral dimer is cleaved by the coordination of another dialkylzinc molecule **X₉** or the carbonyl **X₁₀**. These two complexes can combine and then form the basis for the desired alkyl transfer **X₁₁**, the nucleophilic attack of the bridging alkyl residue on the carbonyl group. This rate-determining step directs the stereoselectivity. After renewed coordination of either a dialkylzinc molecule or an aldehyde, the resulting complex finally decomposes to form **X₉** and **X₁₀** and a tetrameric zinc alkoxide complex which ultimately hydrolyses to the chiral product alcohol.

Over the years, the mechanism has been supported and supplemented by experimental data,[90b] quantum chemical calculations,[91] transition state modelling,[91a, 92] single-crystal structure analysis and NMR studies of individual components.[17, 90] In 2020, however, *Bellemin-Laponnaz et al.* published studies which, based on mathematical modelling, indicate that the mechanism is more complex, involving monomers, dimers and higher-order aggregates.[93]

Since the discovery of *Oguni* and *Omi* in 1984, numerous enantioselective catalysts based on ß-amino alcohols were investigated and tested in the alkylation reaction of benzaldehyde with dialkylzinc reagents. In addition to naturally occurring ß-amino alcohols, pyrrolidine carbalcohols based on the natural amino acid proline were initially produced and tested. High enantioselectivities were achieved, particularly with *N*-derivatized substrates and substrates modified in the 2-position to the alcohol.[94] This opens up a wide range of possibilities, as the other amino acids can also serve as basic building blocks as well as a large variety of natural product derivatives. Above all, the simple commercial access is a great advantage here, as well as the fact that modification is usually possible in a few simple steps using already known methods.

When testing differently modified substrates in the alkylation reaction, it was found that the different residues incorporated have a major influence on the enantioselective output of the reaction. In general, no clear trend can be observed, as even small changes in the catalyst molecule can have a major impact on enantioselectivity. For other basic building blocks, the same modification can show a completely different effect. However, there is also no clear trend in the general structure of the ligands, as both structurally rigid or sterically demanding,[95] as well as electron-donating[94a, 96] or electron-withdrawing[95a, 97] compounds have shown good performance in terms of their stereoselectivity.

4.1   Objectives

Numerous results on enantioselective alkylation, especially of benzaldehyde, using ß-amino alcohols have so far shown promising and very good enantioselectivities. The focus has often been on catalysts developed on the basis of amino acids. Mechanistic insights have also been gained to a large extent in order to better understand the effect of (+)-NLE. It is obvious that ß-amino alcohols are also suitable for autocatalytic systems in which they catalyse their own formation through the alkylation of ß-amino aldehydes with dialkylzinc reagents. So far, the *Soai* reaction is the only autocatalytic reaction in which the reaction product catalyses its own enantioselective formation in a highly selective and effective manner. It would be a major breakthrough for research to achieve the discovery of a second autocatalytic system based on the knowledge already gained about the mechanism of the individual well-performing systems.

Based on good results using β-amino alcohols as ligands for asymmetric alkylation of carbonyls with diorganozinc reagents, mainly Et$_2$Zn, the aim of this topic was to create a catalyst library of ß-amino alcohols. The basic structure is to be derived from amino acids, with L-prolinol in particular as the starting point. Starting from diphenyl-2-pyrrolidine methanol, the influence of electronic effects caused by different residues (green) on the phenyl rings will be investigated. In addition, the influence of the steric of the ligand attached to the primary alcohol (red) or amine group (blue) in particular will be studied. These synthesized ligands are then tested in the standard reaction, the alkylation of benzaldehyde, with various dialkylzinc reagents (Me$_2$Zn, Et$_2$Zn, *i*Pr$_2$Zn) in order to obtain an initial hint regarding their ligand properties (Figure 51).
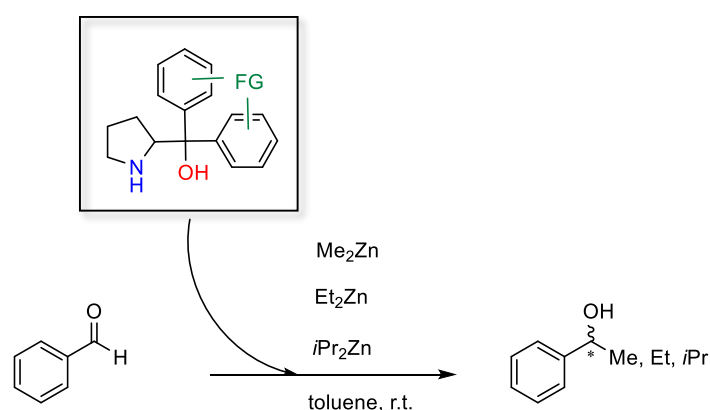
Figure 51: Schematic reaction scope towards various β-amino alcohols as ligands for testing in the asymmetric alkylation of benzaldehyde using different diorganozinc reagents.

4.3   Synthesis of β-Amino Alcohol Ligands Based on Chiral Amino Acid Scaffolds

Amino acids and their derivatives are often an important component of synthetic chemical reactions. Derived from nature, their functional groups, which are able to enter into inter- and intramolecular interactions and thus enable supramolecular structures, are often utilized. Their stereoconfiguration in particular gives rise to unique structural images that are essential for life. They are also well suited as ligands for asymmetric catalysis, which can pass on their stereoinformation to the reaction system. Derived from some amino acids, in particular proline, which has already shown good performance in asymmetric alkylation in the past, ß-amino alcohols were prepared for later use in the enantioselective asymmetric alkylation of benzaldehyde.

(*S*)-16a   (*R*)-16a   (*S*)-16b   (*S*)-16c   (*S*)-16d

(*S*)-17a   (*S*)-17b   (*S*)-17c
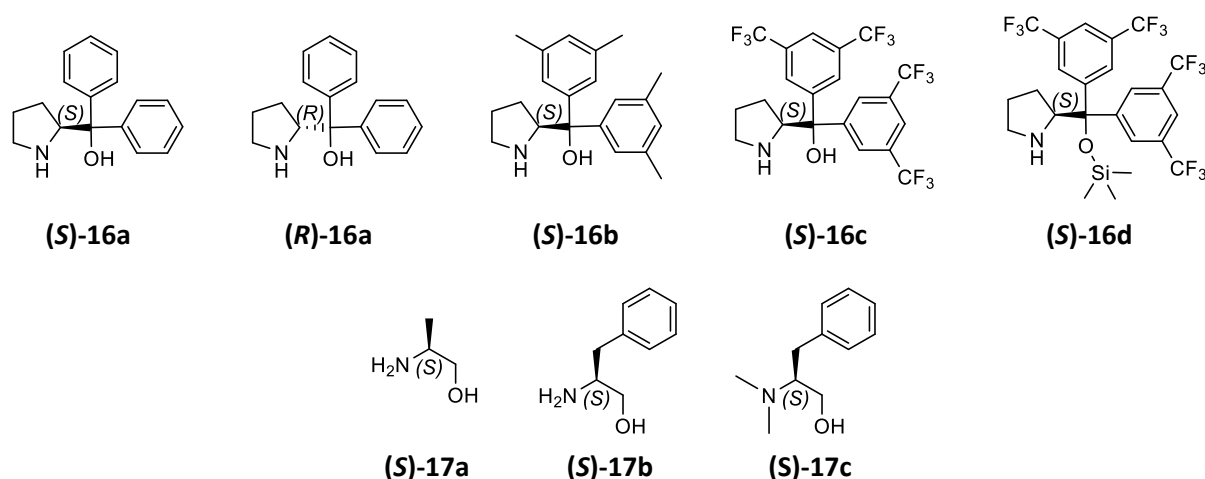
Figure 52: Overview over used ß-amino alcohols for derivatization.

The ß-amino alcohol **(S)-16a** has already been used for the asymmetric alkylation with diethylzinc and generated the (*S*)-product in 92% enantiomeric excess.[94c] The (*R*)-enantiomer **(R)-16a** also showed high enantiomeric excess in product formation, especially with fluorinated aldehydes.[98] Various commercially available ß-amino alcohols derived from amino acids were selected for derivatization on nitrogen (Figure 52).

4.3.1   Methylated Ligands

The methylation reaction was carried out in a S_N2-type reaction using methyl iodide as alkylating reagent and Na_2CO_3 as mild base quenching any formed hydrogen iodide during the reaction.[99] The three desired N-derivatized amino acids **(S)-17a-c** were obtained in moderate yields. The methyl groups on the aryl ring **(S)-17b**, with their electron-donating effect, favoured the reaction over the electron-withdrawing CF_3-groups (Scheme 13).
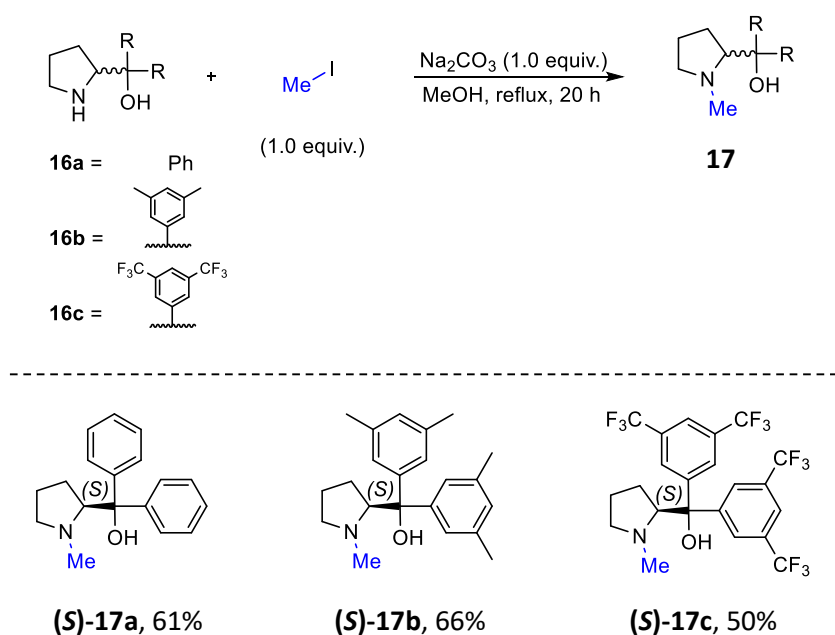
Scheme 13: Methylation reaction using methyl iodide and sodium carbonate.

4.3.2   Benzylated Ligands

Derivatization with benzyl bromide was carried out in the same way as methylation under 4.3.1. In contrast to the methyl group, the benzyl group offers greater steric demand, which should have a greater influence on the enantioselectivity during the reaction and thus provide better *ee*'s.[17] The influence on the nucleophilicity of the nitrogen atom is also influenced by the benzyl group, as this has an electron-donating effect, which has the consequence that the coordinative properties of the nitrogen atom are increased.

The non-substituted phenyl derivatives **18a** and **18c** were obtained in quantitative yield with no other side products being formed during the reaction. Again, the compound with the electron-withdrawing CF$_3$-groups at the aryl was responsible for the poorest yield (Scheme 14).
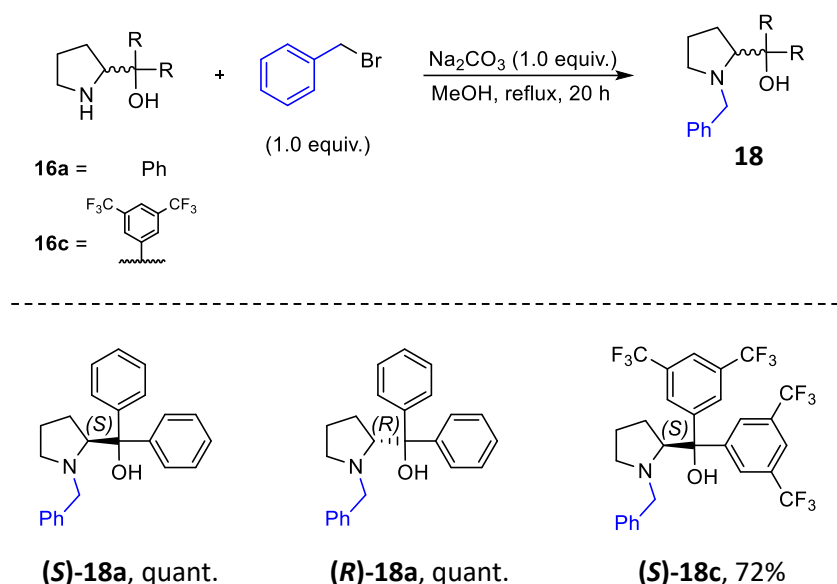
Scheme 14: Benzylation reaction using benzyl bromide in the presence of Na$_2$CO$_3$.

In addition to the structures mentioned above, (*S*)-alaninol **(S)-17a** was also prepared in a bis-benzylated form **(S)-19a** by doubling the equivalents of benzyl bromide (Scheme 15).
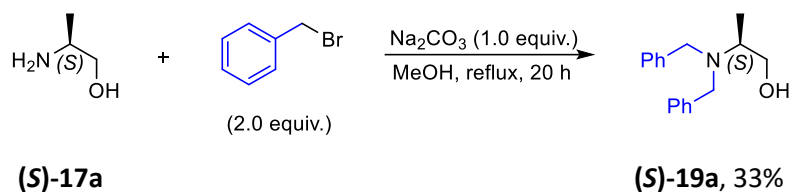
Scheme 15: Benzylation reaction of (*S*)-alaninol using benzyl bromide in the presence of Na$_2$CO$_3$.

Furthermore, the mono-benzylated ß-amino alcohol **(S)-19b** was prepared from (*S*)-phenyl alaninol **(S)-17b** adapted from a literature known procedure.[100]
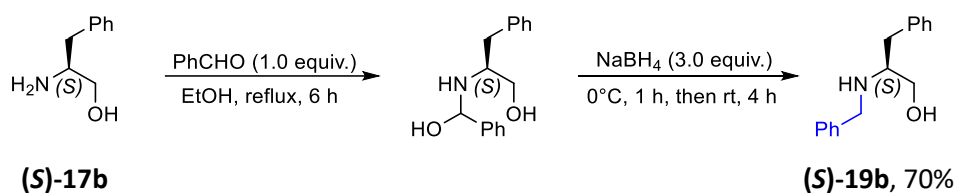
Scheme 16: Mono-benzylation of (S)-phenyl alaninol **(S)-17b** with benzaldehyde and NaBH$_4$.

In the first step, (*S*)-phenyl alaninol **(S)-17b** was reacted with benzaldehyde in ethanol. After 6 h, the formed hemiaminal was reduced with NaBH$_4$ to give the desired mono-benzylated amino alcohol **(S)-19b** in 70% yield after column chromatography (Scheme 16).

4.3.3   Silylated Ligands

According to a known procedure, the silylation of (*S*)-2-(dimethylamino)-3-phenylpropan-1-ol **(S)-17b** was performed with 1*H*-imidazole to quench emerging acid during the reaction.[101] Instead of TMS, TIPS was used as silylating agent because of its higher stability towards reaction conditions.[102] After workup, purification *via* column chromatography could not separate some side products. However, the impure product was used in the upcoming catalytic reactions (Scheme 17).

(S)-17b   **(S)-19c,** 87%
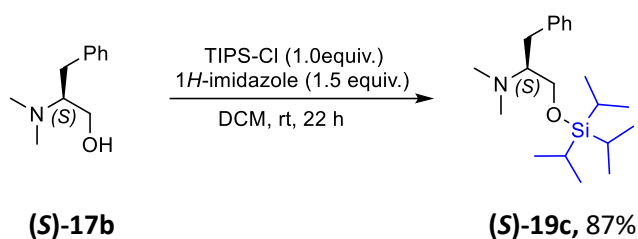
Scheme 17: Silylation of *N,N*-dimethyl phenylalaninol **(S)-17b** with TIPS-Cl and imidazole.

In general, all compounds retained their stereoinformation during the reactions carried out.

4.4   Application of the Synthesized ß-Amino Alcohol Ligands for the Asymmetric Alkylation of Benzaldehyde

The above-mentioned, synthesized ß-amino alcohol ligands were subsequently tested for asymmetric alkylation reactions of benzaldehyde using different zinc organyls (Figure 53). Therefore, benzaldehyde was chosen since it is used as standard substrate for asymmetric alkylation reactions with dialkylzinc compounds. Above all, it often shows better selectivities compared to aliphatic aldehyde substrates.[87] A benzaldehyde concentration of 100 mM was used. The range of aldehyde concentrations typically used for alkylation reactions with zinc organyls extend from ~10 to 60 mM in the self-amplifying autocatalytic *Soai* reaction[19a, 20, 41a] to higher concentrations up to 600 mM[25b] for other asymmetric alkylation reactions.

For the alkylation reactions benzaldehyde was reacted with 1.5 equiv. of the different zinc organyls, namely Me$_2$Zn, Et$_2$Zn and *i*Pr$_2$Zn, using the previously prepared enantiopure ligands with 5 mol%.

Toluene was chosen as solvent due to no coordinating properties. Coordinating solvents can be distorted because of blocked reaction sites caused by the solvent. Since alkylation reactions with diorganozinc reagents often show poorer selectivities and yields at lower reaction temperatures, the experiments were carried out at room temperature.[98, 103]
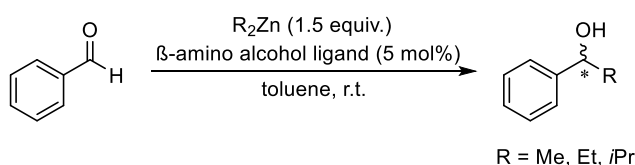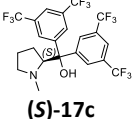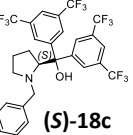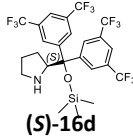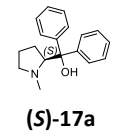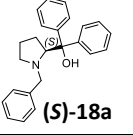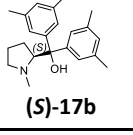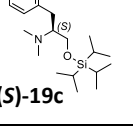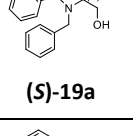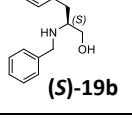

Figure 53: Alkylation reaction of benzaldehyde using ß-amino alcohols as ligand and zinc organyls (R$_2$Zn: R = Me, Et, *i*Pr) as alkylating reagent.

In practice, benzaldehyde and the ligand were dissolved in toluene and stirred for 5 min. Afterwards, the reaction was initiated with the addition of the organozinc species (1M in toluene) and the reaction mixture stirred at room temperature. For analysis, aliquots were taken after different time and quenched with HCl (1M). After a little workup and separation of the organic phase, the solvent was removed as its high absorption causes the desired signals to disappear in the noise when separated on the HPLC. The enantiomer ratio of the product was analysed by HPLC on a Chiralpak® OD-H column using *n*-hexane/*i*PrOH = 95/5 and a flow rate of 1 mL/min. The enantiomer ratios were then determined by integrating the respective enantiomer peaks and the yield was calculated based on the sum of the peak areas of the two enantiomers using calibration lines of dilution series of commercially available enantiomers. The results of the β-amino alcohol catalysed alkylation reactions are shown in Table 4.

In general, it was observed that alkylation with Me_2Zn shows the worst conversion, whereas Et_2Zn shows a better performance compared to iPr_2Zn. Above all, it is known from literature that alkylation reactions of aldehydes with Me_2Zn generate less good enantiomeric excesses compared to catalysis with Et_2Zn, which can be attributed to the lower reactivity of the methylated zinc reagent.[17, 90b, 98, 104] However, it is worth mentioning that in a few cases an *ee* of over 90% could also be achieved with Me_2Zn, too.[17, 90b, 98, 104] In 2007, *Ando et al.* reported asymmetric alkylation with Me_2Zn using a fluorine ligand, which even resulted in an enantiomeric excess of 96%.[105] Although such results have so far remained exceptions, they show that the possibility of achieving good enantioselectivities using the methylating zinc organyl exists and should be considered.

With the proline-based ligands with *N*-methyl and N-benzyl derivatization, Me_2Zn shows an unexpectedly good performance with regard to stereoselectivity. Interestingly, the prolinol derivatives with unsubstituted (**(S)-17a** and **(S)-18a**) and methyl-substituted phenyl rings (**(S)-17b**) yield the (*R*)-enantiomer in large excess after 6 h reaction time, whereas after 24 h the (*S*)-enantiomer was formed with good *ee*. The electron-withdrawing analogue **(S)-17c** achieves 68% *ee* after 24 h, whereas the benzylated **(S)-18c** shows moderate a *ee* with 42%. No significant enantiomeric excesses could be achieved for the remaining ligands. However, the yield did not exceed 7% for any reaction. Reactions with added non-prolinol ligands in particular did not show any formation of the desired product.

Table 4: Enantiomeric excesses and chemical yields of the asymmetric alkylation reaction of benzaldehyde with Me$_2$Zn, Et$_2$Zn, and iPr$_2$Zn in toluene at room temperature. Yields were determined by HPLC quantification.

catalyst	reaction time	Me$_2$Zn (100 mM)		Et$_2$Zn (100 mM)		iPr$_2$Zn (100 mM)	
		ee [%]	yield [%]	*ee* [%]	yield [%]	*ee* [%]	yield [%]
(*S*)-17c	6 h	52 (*S*)	1	64 (*S*)	7	34 (*S*)	9
	24 h	68 (*S*)	5	58 (*S*)	23	12 (*S*)	20
(*S*)-18c	6 h	-	-	33 (*S*)	12	42 (*S*)	7
	24 h	42 (*S*)	1	33 (*R*)	29	42 (*R*)	16
(*S*)-16d	6 h	-	-	48 (*S*)	4	1 (*R*)	3
	24 h	11 (*S*)	1	35 (*S*)	10	9 (*R*)	9
(*S*)-17a	6 h	73 (*R*)	1	72 (*S*)	61	2 (*S*)	24
	24 h	70 (*S*)	2	70 (*S*)	67	12 (*R*)	41
(*S*)-18a	6 h	91 (*R*)	2	20 (*S*)	18	42 (*R*)	11
	24 h	65 (*S*)	1	28 (*S*)	65	39 (*R*)	43
(*S*)-17b	6 h	54 (*R*)	3	54 (*S*)	39	27 (*R*)	11
	24 h	46 (*S*)	7	67 (*S*)	75	18 (*R*)	28
(*S*)-19c	6 h	3 (*S*)	2	4 (*R*)	3	9 (*R*)	8
	24 h	8 (*S*)	5	6 (*R*)	14	8 (*R*)	24
(*S*)-19a	6 h	-	-	68 (*R*)	6	46 (*R*)	2
	24 h	-	-	72 (*R*)	12	51 (*R*)	5
(*S*)-19b	6 h	-	-	5 (*S*)	4	23 (*R*)	4
	24 h	-	-	26 (*R*)	10	33 (*R*)	10

The alkylation of benzaldehyde with Et_2Zn represents the standard reaction for testing the performance of ligands in this context. In particular, the ligands that showed exceptionally good selectivity did so in the above reaction setup,[98, 104b, 104c] as did the most famous example with DAIB.[17] This is mainly due to the higher reactivity of Et_2Zn compared to its methyl analogue.

In general, the reactions with Et_2Zn show a higher conversion than those with Me_2Zn. Again, especially the ligands with unsubstituted phenyl groups **(S)-17a** and **(S)-18a** as well as with methylated phenyl substituents **(S)-17b** show the best conversion, whereby the *N*-methylated derivatives **(S)-17a** and **(S)-17b** already show a moderate conversion after 6 h. For the *N*-methylated prolinol ligands **(S)-17c**, **(S)-17a** and **(S)-17b** the best selectivities could be obtained with moderate *ee* values from 54 to 72%, whereby the substitution of the aromatic ligand compounds, although electron-withdrawing, electron-shifting or in between, makes no difference. However, the ligand **(S)-17a** has been used previously for the enantioselective alkylation of benzaldehyde with Et_2Zn, where a much higher enantiomeric excess of 97% *ee* was achieved.[94c] For the same ligands with *N*-benzyl residue, the reaction with the electron-withdrawing aryl **(S)-18c** resulted in slightly higher *ee*'s than for **(S)-18a**. However, it was striking that the stereoinformation for **(S)-18c** reversed during the reaction within 18 h, from 33% (*S*) after 6 h to 33% (*R*) after 24 h. The bis-*N*-benzylated ligand **(S)-19a** also showed reverse stereoselectivity, even after 6 h reaction time, and achieved with 72% *ee* the best result for asymmetric alkylation using Et_2Zn after 24 h.

Looking at the ligands **(S)-17c** and **(S)-18c**, as well as **(S)-17a** and **(S)-18a** and their selectivities, it is noticeable that the methyl residue on the amine provides mainly better selectivities with Me_2Zn and Et_2Zn than with *i*Pr_2Zn. Conversely, the *N*-benzylated ligand **(S)-18c** shows better results with *i*Pr_2Zn than with Me_2Zn. In this case, a kind of HSAB concept from acid-base chemistry seems to apply, in which soft acids react preferentially with soft bases and hard acids with hard bases.[106] This principle can be transferred here, whereby the large benzyl residue favours a reaction with the large *i*Pr residue rather than with the small ethyl rest.

The silylated ligands generally show low selectivities except of *O*-TMS prolinol **(S)-16d** alkylating with Et_2Zn. Above all, however, alkylation with *i*Pr_2Zn shows virtually no selectivity in the case of **(S)-16d**. The free amine is also responsible for the poor results, as can also be seen for the phenyl alaninol derivative **(S)-19b**, with which no alkylation reagent achieves good selectivities.

Another general observation for all reactions is the stereochemical reversal in most reactions with iPr$_2$Zn. If the enantiomers of the product alcohols are separated under the measurement conditions, the (*R*)- and then the (*S*)-enantiomer elute in the case of Me$_2$Zn and Et$_2$Zn. In the case of the iPr-product, the order is reversed and the (*S*)-enantiomer appears first.

In addition, reactions were carried out with 30 mM benzaldehyde, 5 mol% of the respective ligand and an extended reaction time of 60 h. An *ee* of 82% of the (*S*)-enantiomer was obtained for **(S)-17a** using Et$_2$Zn. For the electron-withdrawing and *N*-methylated derivative **(S)-17c**, an *ee* of 74% of the (*S*)-enantiomer was also detected within 60 h at a lower concentration. **(S)-18c** showed the same result under the reaction conditions as for 100 mM and **(S)-18a** was able to increase the enantiomeric excess at low concentration by 14% from 28 to 42% *ee*. All other ligands yielded poorer enantioselectivities with Et$_2$Zn at 30 mM benzaldehyde than at 100 mM.

With iPr$_2$Zn, the silylated species in particular were able to achieve better selectivities under the above-mentioned reaction conditions. For the TMS-derivative **(S)16-d**, 42% of the (*R*)-enantiomer was obtained after 60 h. The TIPS-derivative **(S)-19c** also showed a better performance in terms of selectivity with 42% *ee*. For the *N*-benzylated prolinols **(S)-18c** and **(S)-18a**, approximately the same *ee* could be obtained. With 38% *ee* of the (*R*)-enantiomer, **(S)-17a** gave a much better result than the reaction with 100 mM benzaldehyde.

In the reactions with low aldehyde concentration, a catalyst loading of 2 mol% was also tested, which led to improved enantioselectivities in similar systems.[25b, 85a]

4.5   Summary and Outlook

This chapter focused on the preparation of ß-amino alcohol ligands based on amino acid derivatives, especially prolinol, to test them in the asymmetric alkylation reaction of benzaldehyde. For this purpose, the amino alcohols were either methylated or benzylated at the amine or silylated at the alcohol functional group in moderate to good yields. With the methyl and benzyl residues, steric properties were incorporated that were expected to show different selectivities in the same reaction. In addition, in the case of diphenyl-2-pyrrolidine methanol, different electronic effects were tested by electron-withdrawing and electron-donating residues on the aryl ring. Numerous examples of ß-amino alcohols with different structures are known from the literature, which were mainly used in alkylation reactions of aldehydes with diethylzinc and in some cases achieved good to very good results in terms of their stereoselectivity. In addition to the Et$_2$Zn alkylation reagent, Me$_2$Zn and iPr$_2$Zn were also used in this work. The yield and enantiomeric excesses were determined using a chiral HPLC and with the aid of calibration lines for quantification (Figure 54).
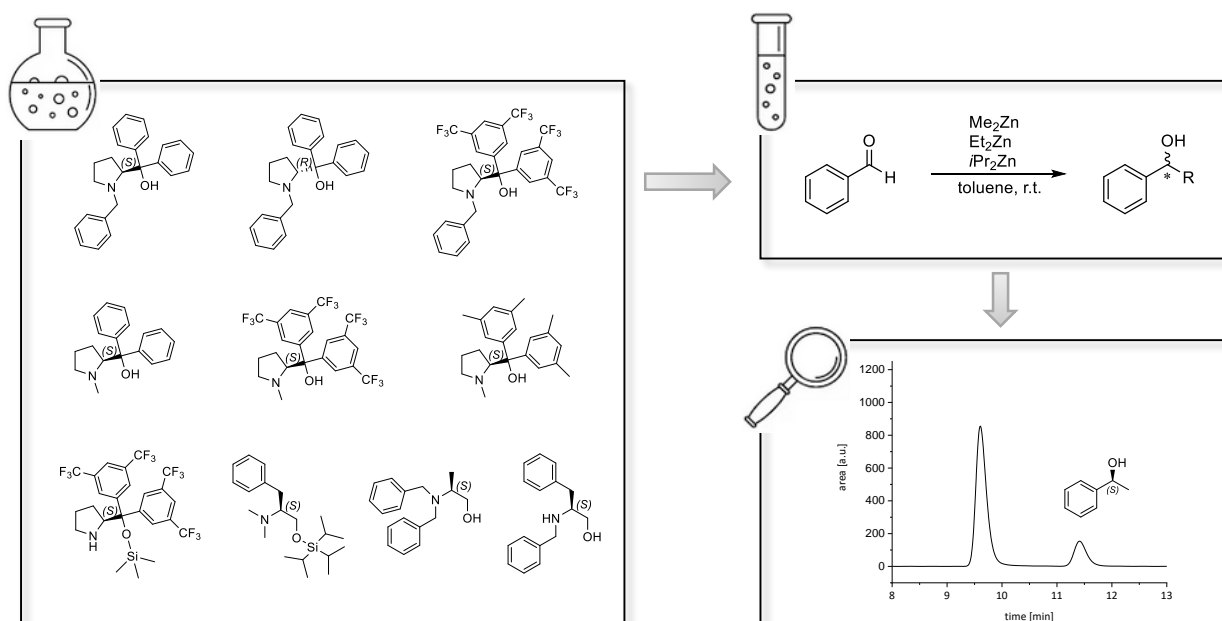
Figure 54: Overview over ß-amino alcohol ligands synthesized and tested in asymmetric alkylation reactions using Me$_2$Zn, Et$_2$Zn and iPr$_2$Zn as alkylating agent.

The main focus was on the reaction of benzaldehyde to the corresponding alkylated alcohol. The reactions were carried out at room temperature in toluene. Initial concentrations of 30 and 100 mM were used for the benzaldehyde, whereby the ligand was used at 5 mol%. For the reaction with 100 mM benzaldehyde, aliquots were taken after 6 h and 24 h. For the reactions with 30 mM benzaldehyde, the reaction time was extended to 60 h (Figure 54).

In general, only low conversions were observed in the reactions with Me_2Zn. However, the unsubstituted **(S)-17a** and **(S)-18a** and methylated **(S)-17b** prolinol-derivatives gave good enantioselectivities in the reactions that took place. Et_2Zn showed better selectivities and yields compared to iPr$_2$Zn. For the reactions with silylated ligands, as well as with iPr$_2$Zn as alkylating reagent in general, better results were achieved at lower benzaldehyde concentrations.

Furthermore, with the exception of **(S)-18a**, a trend towards better enantioselectivities was obtained with Me_2Zn and *N*-methylated, as well as iPr$_2$Zn and *N*-benzylated prolinols than when methylated species were alkylated with iPr$_2$Zn and *vice versa*. Furthermore, the non-electron withdrawing ligands showed selectivity on the side of the (*R*)-enantiomer after 6 h whereas the (*S*)-enantiomer was present with good *ee* after 24 h.

CHAPTER 5

Experimental Part

5.1   General Considerations

All reactions involving the use of moisture and/or oxygen sensitive substances were carried out in glassware, previously dried with a heat-gun under an argon atmosphere, using standard *Schlenk* techniques. Syringes were used to transfer solvents or reagents and purged three times with argon prior to use. Purified products were concentrated using a rotary evaporator and subsequently dried under high vacuum on the *Schlenk* line. All chemicals obtained from commercial sources were used without further purification.

5.2   Reagents

All chemicals obtained from commercial sources (*abcr GmbH*, *Acros Organics b.v.b.a.*, *Sigma-Aldrich Co. LLC*, *Alfa Aesar*, *Thermo Fisher Scientific* and *TCI Europe N.V.*) were used without further purification. Dry solvents were taken from the solvent purification system MB SPS-800 and used immediately.

Organomagnesium and **-zinc** compounds were titrated against iodine in THF.[107]

Organolithium reagents, such as *n*BuLi were titrated against *i*PrOH using 1,10-phenanthroline as indicator.[108]

ZnCl$_2$ (1.0 M in THF)
This solution was prepared by drying ZnCl$_2$ (34.1 g, 250 mmol) under high vacuum (1 mbar) for 24 h at 150 °C. After cooling to room temperature, dry THF (250 mL) was added and stirring was continued until the salt was completely dissolved.

iPr$_2$Zn in toluene

The reaction was performed as modified procedure from *Knochel* and coworkers.[51]

In a flame-dried *Schlenk* flask (1 L), ZnBr$_2$ (113 g, 500 mmol, 0.50 equiv.) was dried *in vacuo* for 4 h and subsequently dissolved in dry Et$_2$O (500 mL). Meanwhile, a flame-dried three-necked round bottom flask (2 L) equipped with an inlet adapter, a reflux condenser and a septum, was charged with Mg (26.7 g, 1.10 mol, 1.10 equiv.) and Et$_2$O (600 mL) was added. To this mixture, 2-bromopropane (123 g, 93.9 mL, 1.00 mol, 1.00 equiv.) was added dropwise over a period of 4 h. After the addition was completed, the reaction mixture was stirred for 30 min. The liquid phase was transferred into a flame-dried *Schlenk* flask (2 L) *via* cannula and the ZnBr$_2$ in Et$_2$O was added. The reaction mixture was stirred at room temperature overnight. The majority of the Et$_2$O was removed under reduced pressure. Afterwards, dry toluene (100 mL) was added. The resulting suspension was distilled under reduced pressure (90 °C, 0.1 mbar) into another cooled (N$_2$) *Schlenk* flask (250 mL) to yield an iPr$_2$Zn solution in toluene (3.23 M).

^{1}H-NMR (toluene-d_8, 400 MHz, ppm) δ = 1.20 (d, 12H, 4 x CH$_3$), 0.61 (m, 2H, CH).

5.3   Chromatography

Flash column chromatography was performed using silica gel (technical grade, pore size 60 Å) produced by *Sigma-Aldrich*.

Thin layer chromatography (TLC) was performed using aluminium plates coated with SiO$_2$ (*Merck* 60, F$_{254}$). Components were visualized by fluorescence quenching during irradiation with UV light (254 nm) or by staining of the TLC plate with *Seebach*'s Magic stain (containing phosphomolybdic acid, Ce(SO$_4$)$_2$, conc. H$_2$SO$_4$ and H$_2$O).

5.4   Analytical Data

NMR spectra were recorded on a *Bruker* AVIII HD400, *Varian* mercury and *Varian* Vnmrs spectrometer. Chemical shifts are reported as δ-values in ppm referenced to the residual solvent peak. NMR spectra were recorded on solutions in $CDCl_3$ (chloroform: $\delta = 7.26$ ppm for ^1H NMR and $\delta = 77.4$ ppm for ^{13}C NMR), CD_2Cl_2 (methylene chloride: $\delta = 5.32$ ppm for ^1H NMR and $\delta = 53.8$ ppm for ^{13}C NMR) and DMSO-d_6 (dimethyl sulfoxide: $\delta = 2.50$ ppm for ^1H NMR and $\delta = 39.5$ ppm for ^{13}C NMR).[109] For the characterization of the observed signal multiplicities the following abbreviations were used: s (singulet), d (doublet), t (triplet), q (quartet), dd (doublet of doublet), dt (doublet of triplet), m (multiplet).

Infrared spectra were recorded from 4000-600 cm^{-1} on a *Nicolet* 6700 FT-IR spectrometer. Samples were measured neat (Diamond ATR). The absorption bands were reported in wave numbers (cm^{-1}) and for characterization of the observed signal intensities the following abbreviations were used: vs (very strong), s (strong), m (medium) and w (weak).

High Resolution Mass Spectrometry was carried out using the flow-injection analysis (FIA/ESI) with a *Surveyor* MS pump at a flow rate of 100 μL/min with acetonitrile/water as running agent. Each 1-10 μL sample solution was injected using an inline filter. EI spectra were recorded on *Finnigan MAT 95Q* or *Finnigan MAT 90* instruments for electron impact ionization (EI).

In situ mass spectrometric studies were performed using a *Q Exactive Plus* Orbitrap mass spectrometer (*Thermo Scientific*). The instrument was operated at a resolution of m/Δm = 280 000. The reaction mixture was injected in periodic intervals using a 6-port valve which was connected to a HPLC pump and a syringe pump, resulting in Δt = 2 min for **AdPyr** and Δt = 1 min for **AdPyr**. Ionization using an APCI interface with a flow rate of 200 μl/min and a mass range between 150-1750 m/z was used.

High Performance Liquid Chromatography-Mass Spectrometry and semi-preparative HPLC measurements were performed on an *Agilent Technologies* 1200 Infinity HPLC device equipped with a photodiode array detector (DAD) and a quadrupole mass spectrometer. Ionization was performed using APCI. The columns used with chiral stationary phases were purchased from *Daicel Chemical Industries, Ltd* and the solvents with HPLC grade were purchased from *Sigma-Aldrich*.

The kinetic measurements of the *Soai* reaction were performed using the flow-injection analysis (FIA) method. The injection intervals and running conditions are described in the chapters of the respective systems. For each injection, 0.35 min flush time of the loop was subtracted from the defined injection intervals.

Preparative HPLC separations were performed on an *Agilent 1260 Infinity* HPLC. Achiral stationary phases were purchased from *Chiral Technologies*. The HPLC-grade solvents were obtained from *Sigma-Aldrich*.

The enantiomers of the racemic TMS pyridine alcohol **TMSPyr-OH** were separated using a Chiralpak® IG-3 column (250 mm, i.d. 20 mm, particle size: 5 μm) and *n*-hexane/*i*PrOH (90/10) at a flow rate of 18.9 mL/min.

The enantiomers of the racemic adamantyl pyridine alcohol **AdPyr-OH** were separated using a Chiralpak® IC column (250 mm, i.d. 20 mm, particle size: 5 μm) and *n*-hexane/*i*PrOH (75/25) at a flow rate of 18.9 mL/min.

The enantiomers of the racemic adamantyl pyrimidine alcohol **AdPym-OH** were separated using a Chiralpak® IB column (250 mm, i.d. 20 mm, particle size: 5 μm) and *n*-hexane/*i*PrOH (75/25) at a flow rate of 18.9 mL/min.

Crystallographic data were measured on a *Bruker* D8 Venture TXS system equipped with a multilayer mirror monochromator and a Mo Kα rotating anode X-ray tube (λ = 0.71073 Å). The frames were integrated with the Bruker SAINT software package.[110] Data were corrected for absorption effects using the Multi-Scan method (SADABS).[111] The structure was solved and refined using the *Bruker SHELXTL* Software Package.[112] All hydrogen atoms have been calculated in ideal geometry riding on their parent atoms. The disorder of the benzaldehyde moiety has been described by a split model using the non-disordered moiety as geometrical model. The ratio of site occupation factors for the two disordered parts refined to 0.52/0.48. The figures have been drawn at the 50% ellipsoid probability level.[113] In the case of disorder the less-occupied parts have been neglected for the figures.

## 5.5   Synthesis of the *Soai* Substrates

Ethinyl Adamantane   (2)
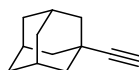
LDA solution (1.00 M in THF, 30.0mL, 30.0 mmol, 1.00 equiv.) was cooled to −78 °C. A solution of adamantyl methyl ketone **1** (4.93 g, 30.0 mmol, 1.00 equiv.) in THF (15 mL) was added dropwise. After stirring for 1 h, chloro diethyl phosphate (4.35 mL, 30.0 mmol, 1.00 equiv.) was added dropwise. The reaction mixture was allowed to warm to room temperature. After stirring for 3 h, the reaction mixture was added dropwise to a second LDA solution (1.00 M in THF, 60.0 mL, 60.0 mmol, 2.00 equiv.) at −78 °C. The solution was stirred at room temperature for 15 h. The reaction was quenched by the addition of water (100 mL). The aqueous layer was extracted with pentane (3 x 100 mL) and the combined organic phase was washed with ice-cold aqueous HCl (1M, 2 x 140 mL) and saturated NaHCO$_3$ solution (200 mL), dried over Na$_2$SO$_4$ and filtered. The solvents were removed *in vacuo* and purification of the crude product was achieved by flash column chromatography (cyclohexane/ethyl acetate = 10:1). **5** was obtained as white solid (4.01 g, 25.5 mmol, 85%).[26]

^{1}H NMR (CDCl$_3$, 400 MHz): δ [ppm] = 2.10 (s, 1H, alkenyl-CH), 1.96 (t, J = 3.2 Hz, 3H, 3 x Ad-CH), 1.89 (d, J = 2.9 Hz, 6H), 1.69 (t, J = 3.2 Hz, 6H).

^{13}C NMR (CDCl$_3$, 151 MHz): δ [ppm] = 93.2, 66.7, 42.8, 36.4, 29.5, 28.0.

HR-MS (EI, 70 eV): m/z calc. for C$_{12}$H$_{16}$: 160.1252, found: 160.1245.

6-((trimethylsilyl)ethynyl)nicotinaldehyde   (TMSPyr-CHO)
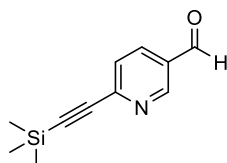
6-Bromo-pyridine-3-carboxaldehyde **3** (1.50 g, 8.06 mmol, 1.00 equiv.), Pd(PPh$_3$)$_4$ (186 mg, 161 µmol, 2 mol%) and CuI (76.8 mg, 403 µmol, 5 mol%) were dissolved in THF (20 mL). The mixture was cooled to 0 °C and *N,N*-diisopropylethylamine (5.49 mL, 32.3 mmol, 4.00 equiv.) was added. After stirring at 0 °C for 5 min, trimethylsilylacetylene (1.23 mg, 8.87 mmol, 1.10 equiv.) was added dropwise. After 1 h, the mixture was allowed to warm to room temperature stirred for another 6 h. The reaction mixture was filtered through *Celite* and rewashed with diethyl ether (160 mL). The solvents were removed under reduced pressure. Purification of the crude material was achieved by sublimation (0.015 mbar, 65-70 °C) to obtain **TMSPyr-CHO** as a white crystalline solid (1.10 g, 5.40 mmol, 67%).[42a]

^{1}H NMR (CDCl$_3$, 400 MHz): δ [ppm] = 10.10 (d, J = 0.5 Hz, 1H, CHO), 9.02 (dd, J = 2.2, 0.9 Hz, 1H, Ar), 8.12 (dd, J = 8.1, 2.1 Hz, 1H, Ar), 7.60 (dt, J = 8.1, 0.8 Hz, 1H, Ar), 0.29 (s, 9H, 3 x CH$_3$).

^{13}C NMR (CDCl$_3$, 400 MHz): δ [ppm] = 189.3, 152.2, 147.9, 135.5, 130.9, 127.6, 103.6, 100.1, 0.5.

HR-MS (EI, 70 eV): m/z calc. for C$_{11}$H$_{13}$NOSi: 203.0766; found: 188.0524.

6-((adamantan-1-yl)ethynyl)nicotinaldehyde   (AdPyr-CHO)
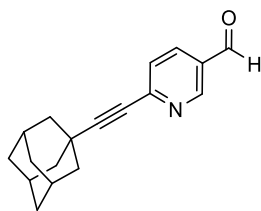
Ethinyl adamantane **2** (2.61g, 16.3 mmol, 1.10 equiv.) was dissolved in dry THF (10 mL). In a separate *Schlenk* flask, 6-Bromo-pyridine-3-carboxaldehyde **3** (2.75 g, 14.8 mmol, 1.00 equiv.), CuI (141 mg, 793 µmol, 5 mol%) and Pd(PPh$_3$)$_4$ (342 mg, 296 µmol, 2 mol%) were dissolved in dry THF (120 mL). Diisopropylamine (8.29 mL, 59.1 mmol, 4.00 equiv.) was added and the mixture was degassed by passing argon through for 20 min. The ethinyl adamantane solution was added at 0 °C. After stirring at room temperature for 24 h, the reaction mixture was filtered through *Celite*. The solvents were removed under reduced pressure and the crude material was purified *via* column chromatography (cyclohexane/ethyl acetate = 10:1) to yield compound **AdPyr-CHO** as a white solid (2.59 g, 9.76 mmol, 66%).

^{1}H NMR (CDCl$_3$, 400 MHz): δ [ppm] = 10.08 (s, 1H, CHO), 8.99 (d, J = 2.2 Hz, 1H, Ar), 8.10 (dd, J = 8.1, 2.1 Hz, 1H, Ar), 7.52 (d, J = 8.1 Hz, 1H, Ar), 2.01 (d, J = 1.3 Hz, 10H, Ad), 1.73 (d, J = 2.4 Hz, 5H, Ad).

^{13}C NMR (CDCl$_3$, 151 MHz): δ [ppm] = 197.4, 189.8, 151.9, 135.8, 129.5, 127.3, 77.3, 77.0, 76.7, 42.1, 36.2, 30.3, 27.7.

HR-MS (EI, 70 eV): m/z calc. for C$_{18}$H$_{19}$NO: 265.1467, found: 265.1462.

2-methyl-1-(pyridin-3-yl)propan-1-ol (HPyr-OH)
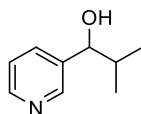
The reaction was performed according to the literature.[42a]

3-pyridinecarboxaldehyde (2.63 mL, 28.0 mmol, 1.00 equiv.) was dissolved in dry THF (240 mL) and stirred at room temperature for 10 min. isopropylmagnesium chloride (18.0 mL, 1.88 M in ether, 33.8 mmol, 1.20 equiv.) was added dropwise over 15 min and stirred at room temperature for 1 h. The reaction mixture was quenched by adding 1 M aq. HCl (42 mL) and stirred vigorously for 15 min. Potassium carbonate (10 g) was then added and stirred for another 15 min. The aqueous layer was washed with ethyl acetate (5 x 60 mL) and the combined organic phases were dried over Na_2SO_4, filtered off and concentrated under reduced pressure to obtain a pale yellow oil. The crude product was purified by column chromatography (DCM/MeOH, 10%) to give **HPyr-OH** (1.59 g, 10.5 mmol, 38%) as a pale yellow oil.

^{1}H NMR (400 MHz, DMSO-*d6*) δ [ppm] = 8.47 (d, J = 2.0 Hz, 1H, Ar), 8.43 (dd, J = 4.7, 1.7 Hz, 1H, Ar), 7.67 (dt, J = 7.9, 1.7 Hz, 1H, Ar), 7.33 (ddd, J = 7.8, 4.7, 0.9 Hz, 1H, Ar), 5.27 (d, J = 4.5 Hz, 1H, -OH), 4.30 (dd, J = 6.2, 4.5 Hz, 1H, -CH-OH), 1.83 (dq, J = 13.4, 6.7 Hz, 1H, -CH-(CH₃)₂), 0.85 (d, J = 6.7 Hz, 3H, CH₃), 0.74 (d, J = 6.8 Hz, 3H, CH₃).

^{13}C NMR (101 MHz, DMSO-*d6*) δ [ppm] = 148.1, 147.9, 140.0, 134.1, 123.1, 75.3, 34.8, 18.8, 17.8.

**HR-MS (EI, 70 eV):** m/z: calc. for $C_9H_{13}ON$: 151.0997; found: 151.0990.

2-Methyl-((2-trimethylsilylalkynyl)-5-pyrimidinyl)propanol   (TMSPyr-OH)
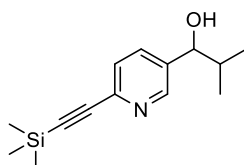
TMSPyr-CHO (1.00 g, 4.92 mmol, 1.00 equiv.) was dissolved in dry THF (50 mL). The solution was cooled in an ice bath and *i*PrMgCl solution (1.86 M in diethyl ether, 3.17 mL, 5.90 mmol, 1.20 equiv.) was added dropwise. The reaction mixture was stirred at room temperature for 2 h and quenched by the addition of saturated NH_4Cl solution (20 mL). The mixture was diluted with water (50 mL) and stirred for a further 10 min. The aqueous and organic layers were separated and the aqueous layer was extracted with ethyl acetate (3 x 50 mL). The combined organic layers were dried over Na_2SO_4, filtrated and the solvents were removed under reduced pressure. The crude product was purified *via* column chromatography (pentane/acetone, 90/10) to yield the product **TMSPyr-OH** (584 mg, 2.36 mmol, 48%) as an orange oil which solidified over time.[42a]

¹H NMR (CDCl₃, 400 MHz): δ [ppm] = 8.48 (dt, J = 2.2, 0.7 Hz, 1H, Ar), 7.66 (ddd, J= 8.0, 2.2, 0.6 Hz, 1H, Ar), 7.45 (dd, J = 8.1, 0.8 Hz, 1H, Ar), 4.48 (d, J = 6.3 Hz, 1H), 1.95 (m, 1H) 0.95 (d, J = 6.7 Hz, 3H), 0.83 (d, J = 6.8 Hz, 3H), 0.27 (s, 9H).

¹³C NMR (CDCl₃, 151 MHz): δ [ppm] = 148.1, 141.5, 138.6, 134.6, 126.9, 103.1, 95.5, 77.0, 35.3, 18.6, 17.6, -0.3.

HR-MS (EI, 70 eV): m/z calc. for $C_{14}H_{21}NOSi$: 247.1392, found: 248.1463 [M+H]⁺.

2-Methyl-(6-((adamant-1-yl)ethynyl)pyridin-3-yl)propanol   (AdPyr-OH)
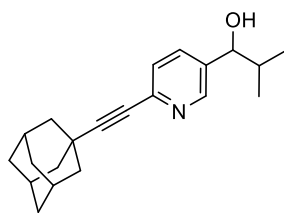
AdPyr-CHO (1.50 mg, 5.65 mmol, 1.00 equiv.) was dissolved in dry THF (50 mL). The solution was cooled to 0 °C before dropwise adding *i*PrMgCl solution (1.86 M in diethyl ether, 3.65 mL, 6.78 mmol, 1.20 equiv.). The ice bath was removed and the reaction mixture was stirred at room temperature for 2 h before quenching the reaction with saturated NH_4Cl solution (25 mL). The mixture was diluted with water (50 mL) and stirred for a further 10 min. The aqueous and organic layers were separated and the aqueous layer was extracted with ethyl acetate (3x 50 mL). The solvents were removed under reduced pressure. The obtained crude material was purified by column chromatography (cyclohexane/ethyl acetate, 2/1) to yield compound **AdPyr-OH** as orange solid (629 mg, 2.03 mmol, 36%).[42a]

¹H NMR (CDCl₃, 600 MHz): δ [ppm] = 8.45 (d, J = 2.2 Hz, 1H, Ar), 7.63 (dd, J = 8.1, 2.2 Hz, 1H, Ar), 7.37 (d, J = 8.0 Hz, 1H, Ar), 4.46 (d, J =6.4 Hz, 1H, OH), 2.04 (s, 6H), 1.99 (s, 9H), 1.97 – 1.92 (m, 1H), 0.95 (d, J =6.7 Hz, 3H, CH₃), 0.82 (d, J =6.8 Hz, 3H, CH₃).

¹³C NMR (CDCl₃, 151 MHz): δ [ppm] = 147.9, 142.5, 137.9, 134.7, 126.7, 99.2, 78.8, 77.1, 42.4, 36.4, 35.3, 30.1, 27.9, 18.7, 17.9.

HR-MS (ESI): m/z calc. for $C_{21}H_{27}NO$: 309.2093, found: 309.2086.

**5-Bromo-2-((adamantyl)ethynyl)pyrimidine   (AdPym-Br)**
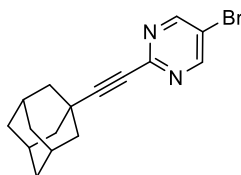
5-Bromo-2-iodo-pyrimidine **4** (4.23 g, 14.9 mmol, 1.00 equiv.), CuI (113 mg, 0.59 mmol, 4 mol%) and Pd(PPh$_3$)$_4$ (343 mg, 0.30 µmol, 2 mol%) were dissolved in dry THF (60 mL). Diisopropylamine (8.32 mL, 59.4 mmol, 4.00 equiv.) was added and the mixture was degassed by passing argon through for 25 min. The reaction mixture was cooled to 0 °C and ethinyl adamantane **2** (2.62 g, 16.3 mmol, 1.10 equiv.) was added. The reaction was stirred at room temperature for 48 h, filtered through *Celite* and the solvents were removed under reduced pressure. Purification of the crude product was achieved *via* column chromatography (cyclohexane/ethyl acetate = 50:1) to yield the product **AdPym-Br** as a yellowish solid (3.94 mg, 12.4 mmol, 84%).[26]

^{1}H NMR (CDCl$_3$, 600 MHz): δ [ppm] = 8.72 (s, 2H, Ar), 2.01 (s, 9H, Ad), 1.72 (s, 6H, Ad).

^{13}C NMR (CDCl$_3$, 151 MHz): δ [ppm] = 157.9, 151.4, 118.6, 99.3, 78.3, 42.0, 36.3, 30.2, 27.8.

HR-MS (EI, 70 eV): m/z calc. for C$_{16}$H$_{17}$N$_2$Br: 316.0575; found: 316.0563.

**2-(Ethynyl-adamantyl)-pyrimidine-5-carbaldehyde   (AdPym-CHO)**
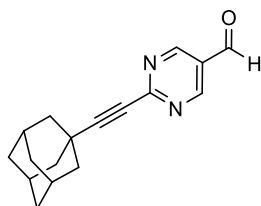
AdPym-Br (1.28 g, 4.05 mmol, 1.00 equiv.) was dried at 100 °C in high vacuum for 30 min and dissolved in dry THF (30 mL). Ethyl formate (0.49 mL, 6.07 mmol, 1.50 equiv.) was added at −78 °C and the mixture was stirred for 5 min. Afterwards, *n*BuLi (2.2 M in hexane, 2.76 mL, 6.07 mmol, 1.50 equiv.) was added dropwise over a period of 10 min and the mixture was stirred at −78 °C for further 15 min. The reaction was quenched by the dropwise addition of conc. acetic acid (0.36 mL, 6.07 mmol, 1.50 equiv.) and saturated Na_2CO_3 solution (35 mL) was added. The aqueous layer was extracted with DCM (3 x 30 mL) and the combined organic phase was dried over Na_2SO_4, filtered off and the solvents were removed under reduced pressure. Purification of the crude product *via* column chromatography (cyclohexane/ethyl acetate = 20:1) gave **AdPym-CHO** as a white solid (550 mg, 2.06 mmol, 51%).[26, 50]

^{1}H NMR (CDCl$_3$, 600 MHz): δ [ppm] = 10.12 (s, 1H, CHO), 9.10 (s, 2H, Ar), 2.07 – 2.00 (s, 9H, Ad), 1.74 (d, J = 2.9 Hz, 6H, Ad).

^{13}C NMR (CDCl$_3$, 151 MHz): δ [ppm] = 188.6, 158.6, 156.8, 126.5, 103.1, 79.7, 42.1, 36.4, 30.6, 27.9, 27.2.

HR-MS (EI, 70 eV): m/z calc. for $C_{17}H_{18}N_2O$: 266.1419, found: 266.1415.

2-Methyl-((2-adamantylalkynyl)-5-pyrimidyl)propanol   (AdPym-OH)
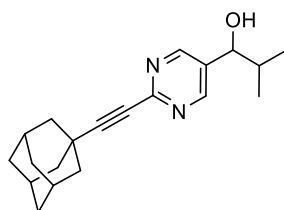
AdPym-Br (1.34 g, 4.21 mmol, 1.00 equiv.) was dissolved in dry THF (40 mL), the solution was cooled to −97 °C and *n*BuLi (2.50 M in hexane, 2.02 mL, 5.05 mmol, 1.20 equiv.) was added dropwise. After stirring at −97 °C for 10 min, isobutyraldehyde (0.46 mL, 5.05 mmol, 1.20 equiv.) was added dropwise. The reaction mixture was stirred at −97 °C for another 20 min. Afterwards, the reaction was quenched by adding HCl (2M in Et$_2$O, 2.11 mL, 4.22 mmol, 1.00 equiv.). After adding saturated Na$_2$CO$_3$ solution (15 mL), the layers were separated. The aqueous layer was extracted with ethyl acetate (3 x 25 mL). The combined organic layers were dried over Na$_2$SO$_4$, filtered off and the solvents were removed *in vacuo*. Purification of the crude material was by column chromatography (cyclohexane/ethyl acetate = 8:1) gave **AdPym-OH** as a white solid (144 mg, 0.46 mmol, 11%).[43]

^{1}H NMR (CDCl$_3$, 600 MHz): δ [ppm] = 8.62 (s, 2H, Ar), 4.51 (d, J = 6.0 Hz, 1H, OH), 2.04 − 1.93 (m, 10H, Ad), 1.71 (t, J = 3.1 Hz, 6H,), 0.94 (d, J = 6.7 Hz, 3H, CH$_3$), 0.87 (d, J = 6.8 Hz, 3H, CH$_3$).

^{13}C NMR (CDCl$_3$, 151 MHz): δ [ppm] = 155.7, 152.0, 134.3, 98.3, 78.6, 75.3, 42.1, 36.3, 35.3, 30.1, 27.8, 18.5, 17.5.

HR-MS (ESI): m/z calc. for C$_{20}$H$_{27}$N$_2$O [M+H]$^+$: 311.2118, found: 311.2123.

2-methyl-1-(pyrimidin-5-yl)propan-1-ol   (HPym-OH)
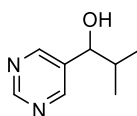
The reaction was performed according to the literature.[114]

5-bromopyrimidine (5.00 g, 31.5 mmol, 1.00 equiv.) was dissolved in dry THF (200 mL). The solution was cooled to -90 °C and *n*BuLi (23.0 mL, 1.50 M in hexane, 34.6 mmol, 1.50 equiv.) was added dropwise and stirred for 15 min. Isobutyraldehyde (2.87 mL, 31.5 mmol, 1.00 equiv.) was then added over a period of 15 min and stirred at -90 °C for another 30 min. The reaction mixture was quenched by adding 2 M aq. HCl (19 mL) and was allowed to warm to room temperature. The reaction mixture was concentrated under reduced pressure, basified using saturated aq. NaHCO$_3$ (50 mL) and water was added to dissolve the salt. The aqueous layer was washed with ethyl acetate (5 x 50 mL). The combined organic phases were dried over Na$_2$SO$_4$, filtered off and the solvent was removed *in vacuo*. The crude product was purified by column chromatography (ethyl acetate) to give **HPym-OH** (784 mg, 5.15 mmol, 16%) as a pale yellow oil.

^{1}H NMR (400 MHz, DMSO-*d$_6$*) δ [ppm]= 9.06 (s, 1H, Ar), 8.70 (s, 2H, Ar), 5.46 (d, J = 4.6 Hz, 1H, -OH), 4.38 (dd, J = 6.0, 4.5 Hz, 1H, -CH-OH), 1.89 (dq, J = 13.5, 6.7 Hz, 1H, -CH-(CH$_3$)$_2$, 0.85 (d, J = 6.7 Hz, 3H, CH$_3$), 0.78 (d, J = 6.8 Hz, 3H, CH$_3$).

^{13}C NMR (101 MHz, DMSO-*d$_6$*) δ [ppm] = 157.1, 154.6, 137.4, 73.3, 34.4, 18.5, 17.5.

HR-MS (ESI): m/z: calc. for C$_8$H$_{13}$ON$_2$ [M+H]$^+$: 153.0983; found: 153.1021.

5.5.1   General Procedure for FIA-HPLC Measurements

Under an inert gas atmosphere an HPLC vial (1.5 mL) was filled with toluene stock solutions of aldehyde (0.86 mL) and alcohol (0.1 mL) and sealed. Immediately after the addition of diisopropylzinc (1 M in toluene, 0.04 mL), the reaction mixture (total volume of 1 mL) was shaken and the FIA-HPLC measurement started. The first injection was made approximately after 30 sec after the addition of the diisopropyl zinc.

For the **TMSPyr-CHO/TMSPyr-OH** system, the following injections were made after a time interval of 2.3 min.

For the **AdPyr-CHO/AdPyr-OH**, the following injections were made after a time interval of 4.3 min.

For the **AdPym-CHO/AdPym-OH**, the following injections were made after a time interval of 3.6 min. The loop flush time was set on 0.35 min.

5.5.2   General Procedure for the *In Situ* Mass Spectrometric Orbitrap-MS Measurements

Under an inert gas atmosphere an HPLC vial (1.5 mL) was filled with toluene stock solutions of aldehyde (0.86 mL) and alcohol (0.1 mL) and sealed. Immediately after the addition of diisopropylzinc (1 M in toluene, 0.04 mL), the reaction mixture (total volume of 1 mL) was shaken and injected into the Orbitrap-MS using a syringe pump. The first injection was made approximately 1.3 min after the addition of the diisopropyl zinc. A 6-port valve was used to flush the loop with toluene between injections, resulting in $\Delta t = 2$ min for **AdPyr** and $\Delta t = 1$ min for **AdPyr**.

5.6   Synthesis of the Photoswitchable Systems

5.6.1   Typical Procedures

Typical procedure for the preparation of MIDA esters from boronic acids and methyliminodiacetic acid (MIDA, 11a-g) (TP1)

The synthesis was performed according to the literature.[80]

The boronic acid (1.00 equiv.) and *N*-Methyliminodiacetic acid (MIDA) (1.10 equiv.) were suspended in DMSO and toluene (v/v = 1/2). The flasked was equipped with a *Dean-Stark* trap which was filled with toluene. The suspension was heated to reflux and and stirred at 130 °C for 3 h. The resulting mixture was cooled to room temperature and then the solvents were evaporated. The residue was lyophilized for 2 d. The resulting solid was obtained quantitatively and used without further purification.

Typical procedure for the *Suzuki* cross-coupling reaction of the *Feringa* building block (8) and the MIDA boronates (10a-g) (TP2)

The synthesis was performed according to the literature.[115]

The MIDA ester (2.00 equiv.), the *Feringa* building block (**8**) (1.00 equiv.), SPhos (10 mol%) and palladium acetate (5 mol%) were dissolved in dry 1,4-dioxane (mL). The reaction mixture was stirred at room temperature for 10 min and an aqueous sodium phosphate solution (3.0 M in H_2O, 15.0 equiv.), which was previously degassed for 30 min., was added. The reaction mixture was stirred at room temperature for 10 min, then heated to 60 °C overnight. The resulting dark reaction mixture was cooled to room temperature and diluted with sodium hydroxide (1 M, mL) and diethyl ether. The aqueous layer was separated and extracted with diethyl ether (3x). The combined organic phases were dried over sodium sulfate, filtered off and the solvents removed under reduced pressure. The residue was purified by column chromatography (*i*Hex/EtOAc) to afford the desired product.

5.6.2   Synthesis of the *Feringa* Building Block (8)
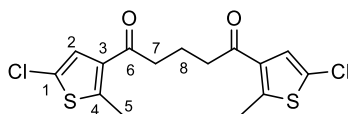
2-chloro-5-methylthiophene   (6)
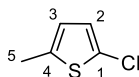
To 2-methylthiophene **5** (50.0 g, 509 mmol, 1.00 equiv.) and *N*-chlorosuccinimide (73.7 g, 560 mmol, 1.10 equiv.) were added a mixture of benzene (200 mL) and acetic acid (200 mL) and the suspension was stirred for 30 min at room temperature and then heated to reflux for 1 h. The cooled mixture was diluted with 3 M aq. NaOH (170 mL). The organic phase was washed with 3 M aq. NaOH solution (3 x 300 mL), dried over Na_2SO_4, filtered and the solvent was removed in *vacuo* to give a pale yellow liquid. Purification *via* vacuum distillation (25 mbar, 55 °C) yielded **6** as a colourless liquid (30.8 g, 232 mmol, 46%).[73]

^{1}H NMR (400 MHz, Chloroform-*d*) δ [ppm] = 6.69 (d, *J* = 3.6 Hz, 1H, H2), 6.53 – 6.50 (m, 1H, H3), 2.41 (d, *J* = 1.2 Hz, 3H, H5).

^{13}C NMR (101 MHz, Chloroform-*d*) δ [ppm] = 138.6 (C4), 126.6 (C1), 125.9 (C2), 124.5 (C3), 15.7 (C5).

FT-IR (ATR): v_{max} [cm^{-1}] = 3085 (w), 3059 (w), 2952 (w), 2920 (m), 2861 (w), 2738 (w), 1724 (w), 1547 (s), 1457 (m), 1380 (w), 1349 (w), 1338 (w), 1321 (w), 1217 (m), 1158 (m), 1060 (m), 1026 (m), 1015 (m), 1004 (m), 958 (m), 857 (w), 785 (s), 732 (w), 701 (w), 668 (m).

HR-MS (EI, 70 eV): m/z calc. for C_5H_5ClS: 131.9800; found: 131.9794.

**1,5-Bis(5-chloro-2-methylthiophen-3-yl)pentan-1,5-dion   (7)**

AlCl$_3$ (37.2 g, 279 mmol, 1.20 equiv.) was added in portions to a solution of 2-Chloro-5-methylthiophene **6** (30.8 g, 232 mmol, 1.00 equiv.) and glutaryl chloride (19.6 g, 116 mmol, 0.50 equiv.) in nitromethane (235 mL) at 0 °C under vigorous stirring. The reaction mixture was stirred at room temperature for 2 h. Iced water (100 mL) was cautiously added to the reaction mixture. The aqueous layer was extracted with Et$_2$O (3 x 150 mL). The combined organic layers were washed with water (3 x 150 mL), dried over Na$_2$SO$_4$, filtered and the solvent was removed under reduced pressure to give **7** as a brown semisolid (41.3 g, 114 mmol, 49%). The product was used without further purification.[73]

^{1}H NMR (400 MHz, Chloroform-*d*) δ [ppm] = 7.18 (s, 2H, H2), 2.86 (t, *J* = 6.9 Hz, 4H, H7), 2.66 (s, 6H, H5), 2.06 (p, *J* = 6.9 Hz, 2H, H8).

^{13}C NMR (101 MHz, Chloroform-*d*) δ [ppm] = 195.1 (C6), 147.9 (C3/4), 135.0 (C3/4), 127.0 (C2), 125.4 (C1), 40.6 (C7), 18.3 (C8), 16.2 (C5).

FT-IR (ATR): ν$_{max}$ [cm^{-1}] = 3319 (w), 3095 (m), 3079 (w), 2955 (w), 2943 (w), 2914 (w), 1707 (m), 1666 (s), 1522 (s), 1454 (s), 1402 (w), 1381 (w), 1368 (m), 1353 (w), 1334 (m), 1334 (w), 1212 (s), 1199 (w), 1165 (w), 1156 (w), 1141 (m), 1116 (w), 1067 (w), 1005 (s), 997 (w), 976 (w), 958 (m), 884 (w), 856 (s), 824 (s), 773 (s), 747 (s).

HR-MS (ESI): m/z calc. for C$_{15}$H$_{15}$O$_2$Cl$_2$S$_2$ [M+H]$^+$: 360.9886; found: 360.9887.

1,2-bis(5-chloro-2-methylthiophen-3-yl)cyclopent-1-ene   (8)
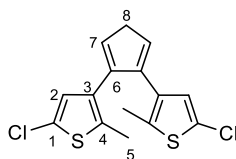
THF (dry, 330 mL) and Zn dust (11.2 g, 171 mmol, 1.50 equiv.) were placed under a nitrogen atmosphere in a three-necked round bottom flask equipped with stirring bar. $TiCl_4$ (32.5 g, 171 mmol, 1.50 equiv.) was added carefully using a dropping funnel. The solution turned deep blue and was heated to reflux for 1 h. Afterwards, the reaction mixture was immediately cooled in an ice bath and 1,5-Bis(5-chloro-2-methylthiophen-3-yl)pentane-1,5-dione **7** (41.3 g, 114 mmol, 1.00 equiv.) was added in portions. This mixture was heated to reflux for 2 h, subsequently quenched with saturated aq. NH_4Cl (120 mL) and extracted with Et_2O (3 x 150 mL). The combined organic layers were washed with water (2 x 150 mL), dried over Na_2SO_4, filtered and the solvent was removed under reduced pressure. Purification *via* flash column chromatography (SiO_2, *i*Hex) yielded **8** as an off-white solid (11.2 g, 34.0 mmol, 30%).[73]

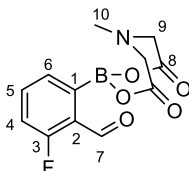**^{1}H NMR (400 MHz, Chloroform-*d*)** δ [ppm] = 6.57 (s, 1H, H2), 2.71 (t, *J* = 7.5 Hz, 2H, H7), 2.02 (p, *J* = 7.5 Hz, 2H, H8), 1.88 (s, 3H, H5).

^{13}C NMR (101 MHz, Chloroform-*d*) δ [ppm] = 134.7 (C4), 134.6 (C6), 133.4 (C3), 126.8 (C2), 125.3 (C1), 38.5 (C7), 23.0 (C8), 14.3 (C5).

HR-MS (EI, 70 eV): m/z calc. for C15H14Cl$_2$S$_2$: 327.9914; found: 327.9910.

5.6.3   Synthesis of the MIDA Boronic Esters

2-fluoro-6-(6-methyl-4,8-dioxo-1,3,6,2-dioxazaborocan-2-yl)benzaldehyde   (11b)

According to **TP1**, 3-fluoro-2-formylphenylboronic acid **9b** (1.00 g, 5.95 mmol, 1.00 equiv.) and MIDA (964 mg, 6.55 mmol, 1.10 equiv.) were suspended in DMSO (2.40 mL) and toluene (4.80 mL). The flask was fitted with a Dean Stark trap, which was filled with toluene. The beige suspension was heated to reflux and stirred at 130 °C for 3 h. The resulting brown solution was cooled to room temperature and then the solvents were evaporated. Subsequently, the liquid residue was lyophilized for 1 d. TLC indicated complete conversion. The beige reaction product **11b** (1.82 g, 6.52 mmol, quant.) was quantitatively obtained and was used without further purification.[80]

¹H NMR (800 MHz, DMSO-*d*₆) δ [ppm] = 10.42 (s, 1H, H7), 7.74 – 7.66 (m, 1H, H5), 7.52 – 7.46 (m, 1H, H6), 7.41 (ddd, *J* = 11.1 Hz, J = 8.3 Hz, J = 1.1 Hz, 1H, H4), 4.42 (d, *J* = 17.3 Hz, 2H, H9), 4.27 (d, *J* = 17.4 Hz, 2H, H9), 2.71 (s, 3H, H10).

¹³C NMR (201 MHz, DMSO-*d*₆) δ [ppm] = 192.5 (C7), 192.4 (C7) 169.4 (C8), 164.9 (C3), 163.6 (C3), 140.2 (C1), 134.6 (C5), 131.3 (C6), 128.5 (C2), 117.3 (C4), 64.2 (C9), 49.0 (C10).

FT-IR (cm⁻¹): 3067 (w), 3016 (w), 2980 (w), 2899 (w), 1742 (s), 1703 (m), 1564 (m), 1450 (m), 1413 (m), 1341 (m), 1310 (m), 1259 (m), 1233 (s), 1190 (m), 1164 (m), 1078 (m), 1046 (s), 1000 (m), 878 (m), 797 (s), 731 (m), 704 (m).

HR-MS (ESI) calc. for $C_{12}H_{15}BFN_2O_5^+$: 297.1053 [M + NH₄]⁺; found: 297.1053 [M + NH₄]⁺.

**2-fluoro-5-(6-methyl-4,8-dioxo-1,3,6,2-dioxazaborocan-2-yl)benzaldehyde   (11c)**
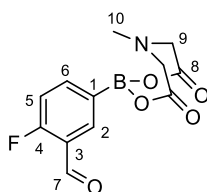
According to **TP 1**, 4-fluoro-3-formylphenylboronic acid **9c** (1.00 g, 5.95 mmol, 1.00 equiv.) and MIDA (964 mg, 6.55 mmol, 1.10 equiv.) were suspended in DMSO (2.40 mL) and toluene (4.80 mL). The flask was fitted with a Dean Stark trap, which was filled with toluene. The beige suspension was heated to reflux and stirred at 130 °C for 3 h. The resulting brown solution was cooled to room temperature and then the solvents were evaporated. Subsequently, the liquid residue was lyophilized for 1 d. TLC indicated complete conversion. The beige reaction product **11c** (1.78 g, 6.38 mmol, quant.) was quantitatively obtained and was used without further purification.[80]

^{1}H NMR (800 MHz, DMSO-d_6) δ [ppm] = 10.25 (s, 1H, H7), 7.93 (dd, *J* = 7.4 Hz, J = 2.0 Hz, 1H, H2), 7.81 (ddd, *J* = 8.0 Hz, J = 5.5 Hz, *J* = 2.0 Hz, 1H, H6), 7.39 (dd, *J* = 10.9 Hz, *J* = 8.3 Hz, 1H, H5), 4.36 (d, *J* = 17.2 Hz, 2H, H9), 4.16 (d, *J* = 17.2 Hz, 2H, H9), 2.54 (s, 3H, H10).

^{13}C NMR (201 MHz, DMSO-d_6) δ [ppm] = 188.3 (C7), 169.3 (C8), 164.8 (C4), 163.5 (C4), 141.1 (C6), 134.0 (C2), 133.4 (C1), 123.0 (C3), 116.1 (C5), 116.0 (C5), 62.1 (C9), 47.7 (C10).

FT-IR (cm^{-1}): 3018 (w), 2963 (w), 2871 (w), 2766 (w), 1773 (m), 1755 (m), 1693 (m), 1601 (m), 1490 (w), 1473 (w), 1455 (w), 1394 (w), 1336 (m), 1271 (m), 1240 (m), 1142 (m), 1107 (m), 1046 (m), 1006 (s), 893 (m), 826 (s).

HR-MS (ESI) calc. for $C_{12}H_{10}BFNO_5^-$: 278.0642 [M-H]$^-$; found: 278.0646 [M-H]$^-$.

2-fluoro-4-(6-methyl-4,8-dioxo-1,3,6,2-dioxazaborocan-2-yl)benzaldehyde   (11d)
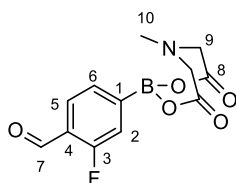

According to **TP1**, 3-fluoro-4-formylphenylboronic acid **9d** (1.00 g, 5.95 mmol, 1.00 equiv.) and MIDA (964 mg, 6.55 mmol, 1.10 equiv.) were suspended in DMSO (2.40 mL) and toluene (4.80 mL). The flask was fitted with a Dean Stark trap, which was filled with toluene. The beige suspension was heated to reflux and stirred at 130 °C for 3 h. The resulting brown solution was cooled to room temperature and then the solvents were evaporated. Subsequently, the liquid residue was lyophilized for 2 d. TLC indicated complete conversion. The beige reaction product **11d** (1.99 g, 7.13 mmol, quant.) was quantitatively obtained and was used without further purification.[80]

^{1}H NMR (800 MHz, DMSO-d_6) δ [ppm] = 10.25 (s, 1H, H7), 7.83 (t, J = 7.2 Hz, 1H, H5), 7.45 (dt, J = 7.6 Hz, J = 0.9 Hz, 1H, H6), 7.40 (dd, J = 11.3 Hz, J = 1.0 Hz, 1H, H2), 4.38 (d, J = 17.2 Hz, 2H, H9), 4.18 (d, J = 17.2 Hz, 2H, H9), 2.57 (s, 3H, H10).

^{13}C NMR (201 MHz, DMSO-d_6) δ [ppm] = 188.1 (C7), 169.2 (C8), 163.6 (C3), 162.3 (C3), 147.8 (C1), 128.9 (C5), 128.5 (C5), 124.0 (C4), 123.9 (C4), 120.3 (2), 120.2 (C2), 62.1 (C9), 47.7 (C10).

FT-IR (cm^{-1}): 3606 (w), 3526 (w), 3010 (w), 2962 (w), 1742 (m), 1680 (m), 1621 (w), 1494 (w), 1398 (m), 1264 (m), 1239 (m), 1201 (m), 1161 (m), 1041 (m), 994 (m), 948 (m), 895 (m), 818 (m).

HR-MS (ESI) calc. for $C_{12}H_{10}BFNO_5^-$: 278.0624 [M-H]$^-$; found: 278.0648 [M-H]$^-$.

## 5-(6-methyl-4,8-dioxo-1,3,6,2-dioxazaborocan-2-yl)furan-2-carbaldehyde   (11e)
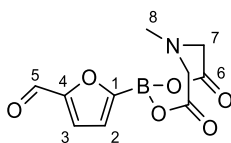
According to **TP1**, 5-formyl-2-furanylboronic acid **9e** (2.50 g, 17.9 mmol, 1.00 equiv.) and MIDA (2.89 g, 19.7 mmol, 1.10 equiv.) were suspended in DMSO (6 mL) and toluene (12.5 mL). The flask was fitted with a Dean Stark trap, which was filled with toluene. The beige suspension was heated to reflux and stirred at 130 °C for 3 h. The resulting brown solution was cooled to room temperature and then the solvents were evaporated. Subsequently, the liquid residue was lyophilized for 1 d. TLC indicated complete conversion. The brown reaction product **11e** (4.67 g, 18.6 mmol, quant.) was quantitatively obtained and was used without further purification.[80]

¹H NMR (800 MHz, DMSO-*d*₆) δ [ppm] = 9.63 (s, 1H, H5), 7.51 (d, *J* = 3.5 Hz, 1H, H3), 6.90 (d, *J* = 3.5 Hz, 1H, H2), 4.40 (d, *J* = 17.2 Hz, 2H, H7), 4.17 (d, *J* = 17.2 Hz, 2H, H7), 2.66 (s, 3H, H8).

¹³C NMR (201 MHz, DMSO-*d*₆) δ [ppm] = 178.6 (C5), 168.9 (C6), 162.6 (C1), 155.2 (C4), 122.9 (C3), 120.3 (C2), 61.8 (C7), 47.4 (C8).

FT-IR (cm⁻¹): 3141 (w), 3010 (w), 2964 (w), 1763 (m), 1669 (m), 1564 (w), 1456 (w), 1391 (w), 1335 (m), 1315 (w), 1276 (m), 1234 (m), 1186 (s), 1042 (s), 1032 (m), 954 (s), 899 (m), 825 (s), 758 (s), 696 (m).

HR-MS (ESI) calc. for $C_{10}H_9BNO_6^-$: 250.0528 [M-H]⁻; found: 250.0531 [M-H]⁻.

5-(6-methyl-4,8-dioxo-1,3,6,2-dioxazaborocan-2-yl)thiophene-2-carbaldehyde   (11f)
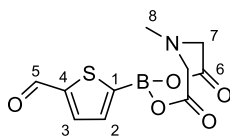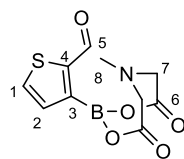

According to **TP1**, 5-formyl-2-thienylboronic acid **9f** (2.50 g, 16.0 mmol, 1.00 equiv.) and MIDA (2.58 g, 17.6 mmol, 1.10 equiv.) were suspended in DMSO (6 mL) and toluene (12.5 mL). The flask was fitted with a Dean Stark trap, which was filled with toluene. The brown suspension was heated to reflux and stirred at 130 °C for 3 h. The resulting brown solution was cooled to room temperature and then the solvents were evaporated. Subsequently, the liquid residue was lyophilized for 1 d. TLC indicated complete conversion. The brown reaction product **11f** (4.46 g, 16.7 mmol, quant.) was obtained quantitatively and used without further purification.[80]

^{1}H NMR (800 MHz, DMSO-d_6) δ [ppm] = 9.94 (s, 1H, H5), 8.04 (d, *J* = 3.6 Hz, 1H, H3), 7.43 (d, *J* = 3.6 Hz, 1H, H2), 4.41 (d, *J* = 17.2 Hz, 2H, H7), 4.19 (d, *J* = 17.2 Hz, 2H, H7), 2.65 (s, 3H, H8).

^{13}C-NMR (201 MHz, DMSO-d_6, ppm) δ [ppm] = 184.0 (C5), 168.7 (C6), 149.3 (C1), 146.4 (C4), 138.5 (C3), 134.4 (C2), 61.7 (C7), 47.6 (C8).

FT-IR (cm^{-1}): 3008 (w), 2944 (w), 1749 (m), 1657 (m), 1518 (w), 1464 (m), 1334 (w), 1275 (m), 1216 (m), 1249 (m), 1162 (m), 1143 (m), 1024 (m), 980 (m), 959 (m), 892 (m), 816 (s), 760 (m), 669 (m).

HR-MS (ESI) calc. for $C_{10}H_9BNO_5S^-$: 266.0300 [M-H]$^-$; found: 266.0303 [M-H]$^-$.

3-(6-methyl-4,8-dioxo-1,3,6,2-dioxazaborocan-2-yl)thiophene-2-carbaldehyde   (11g)

According to **TP1**, 2-formyl-3-thiopheneboronic acid **9g** (2.50 g, 16.0 mmol, 1.00 equiv.) and MIDA (2.58 g, 17.6 mmol, 1.10 equiv.) were suspended in DMSO (6 mL) and toluene (12.5 mL). The flask was fitted with a Dean Stark trap, which was filled with toluene. The brown suspension was heated to reflux and stirred at 130 °C for 3 h. The resulting brown-beige solution was cooled to room temperature and then the solvents were evaporated. Subsequently, the liquid residue was lyophilized for 4 d. TLC indicated complete conversion. The brown reaction product **11g** (4.47 g, 16.7 mmol, quant.) was quantitatively obtained and was used without further purification.[80]

^{1}H NMR (800 MHz, DMSO-d_6) δ [ppm] = 10.05 (d, *J* = 1.2 Hz, 1H, H5), 8.07 (dd, *J* = 4.9 Hz, J = 1.2 Hz, 1H, H1), 7.26 (d, *J* = 4.8 Hz, 1H, H2), 4.41 (d, *J* = 17.2 Hz, 2H, H7), 4.22 (d, *J* = 17.2 Hz, 2H, H7), 2.64 (s, 3H, H8).

^{13}C NMR (201 MHz, DMSO-d_6) δ [ppm] = 185.0 (C5), 169.0 (C6), 148.3 (C3, C4), 135.0 (C2), 134.7 (C1), 62.4 (C7), 47.7 (C8).

FT-IR (cm^{-1}): 3108 (w), 3009 (w), 2975 (w), 1742 (m), 1640 (s), 1506 (w), 1454 (m), 1413 (m), 1353 (m), 1333 (m), 1291 (m), 1228 (m), 1195 (m), 1103 (m), 1031 (s), 978 (m), 951 (m), 907 (m), 876 (m), 858 (s), 758 (s), 706 (m), 682 (m), 664 (m).

HR-MS (ESI) calc. for $C_{10}H_9BNO_5S^-$: 266.0300 [M-H]$^-$; found: 266.0304 [M-H]$^-$.

5.6.4   *Suzuki* Cross-Coupling Reaction

**2,2'-(cyclopent-1-ene-1,2-diylbis(5-methylthiophene-4,2-diyl))dibenzaldehyde   (10a)**
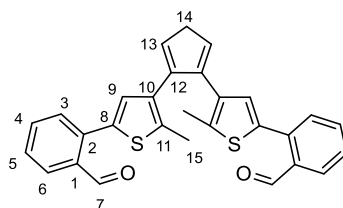
According to **TP2**, the *Feringa* building block **8** (1.01 mg, 3.08 mmol, 1.00 equiv.), MIDA benzaldehyde **11a** (1.61 mg, 6.15 mmol, 2.00 equiv.), SPhos (126 mg, 0.31 mmol, 10 mol%) and Pd(OAc)$_2$ (34.5 mg, 0.15 mmol, 5 mol%) were suspended in 1,4-dioxane (dry, 40 mL). Then, aq. 3M K$_3$PO$_4$ (7.70 mL, 23.1 mmol 7.50 equiv.) which was previously degassed with argon for 30 min prior to use. The reaction mixture was heated to 60 °C for 24 h and diluted with 1M NaOH (30 mL) and Et$_2$O (30 mL) after cooling to room temperature. The aqueous layer was washed with Et$_2$O (3 x 30 mL), the combined organic phases dried over Na$_2$SO$_4$, filtered and concentrated under reduced pressure. The crude product was purified *via* flash column chromatography (SiO$_2$; iHex/EtOAc = 40:1; R$_f$ = 1.35) to give the desired product **10a** as a pink crystalline solid (938 mg, 2.00 mmol, 65%).[115]

^{1}H NMR (400 MHz, Chloroform-*d*) δ [ppm] = 10.08 (s, 1H, H7), 7.95 (dd, *J* = 7.8 Hz, *J* = 1.4 Hz, 1H, H6), 7.59 (td, *J* = 7.5, *J* = 1.5 Hz, 1H, H4), 7.52 (dd, *J* = 7.8 Hz, *J* = 1.4 Hz, 1H, H3), 7.43 (t, *J* = 7.4 Hz, 1H, H5), 6.70 (s, 1H, H9), 2.83 (t, *J* = 7.4 Hz, 2H, H13), 2.12 (s, 3H, H15), 2.10 (m, 2H, H14).

^{13}C NMR (101 MHz, Chloroform-*d*) δ [ppm] = 192.2 (C7), 138.2 (C2), 137.1 (C10/C11), 136.7 (C10/C11), 135.2 (C12), 134.8 (C8), 134.0 (C1), 133.7 (C4), 131.2 (C9), 131.1 (C3), 128.0 (C6), 127.9 (C5), 38.3 (C13), 23.2 (C14), 14.5 (C15).

HR-MS (ESI) calc. for C$_{29}$H$_{25}$O$_2$S$_2^+$: 469.1290 [M+H]$^+$; found: 469.1295 [M+H]$^+$.

**6,6'-(cyclopent-1-ene-1,2-diylbis(5-methylthiophene-4,2-diyl))bis(2-fluorobenzaldehyde) (10b)**
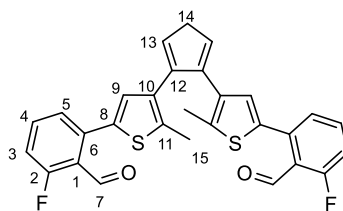
According to **TP2**, MIDA ester **11b** (1.12 g, 4.00 mmol, 2.00 equiv.), the *Feringa* building block **8** (658 mg, 2.00 mmol, 1.00 equiv.), SPhos (821 mg, 0.200 mmol, 10 mol%) and palladium acetate (22.4 mg, 0.100 mmol, 5 mol%) were dissolved in dry 1,4-dioxane (26 mL). After the resulting yellow-brown reaction mixture was stirred at room temperature for 10 min, a solution of sodium phosphate (3M, 3.18 g, 15.0 mmol, 7.50 equiv.), which was previously degassed for 30 min, was added. The reaction mixture was stirred for 10 min at room temperature, then heated to 60 °C and stirred overnight. The resulting brown reaction mixture was cooled to room temperature and was diluted with sodium hydroxide (1M, 17 mL) and diethyl ether (17 mL). The phases were separated and the aqueous phase was extracted with diethyl ether (3 x 20 mL). The combined organic phases were dried oversodium sulfate, filtered off and the solvents were removed under reduced pressure. The highly viscous purple residue was purified by column chromatography (*i*-Hex/EtOAc v/v 30:1 → 20:1, R_f = 0.42) to afford compound **10b** (664 mg, 1.31 mmol, 66%) as violet crystalline solid.[115]

^{1}H NMR (400 MHz, Chloroform-*d*) δ [ppm] = 9.93 (d, *J* = 0.7 Hz, 1H, H7), 7.52 (td, *J* = 8.1 Hz, *J* = 5.4 Hz, 1H, H4), 7.32 (dd, *J* = 7.8 Hz, *J* = 1.0 Hz, 1H, H5), 7.10 (ddt, *J* = 10.2 Hz, *J* = 8.3 Hz, *J* = 0.9 Hz, 1H, H3), 6.66 (s, 1H, H9), 2.81 (t, *J* = 7.5 Hz, 2H, H13), 2.11 (s, 3H, H15), 2.10 – 2.00 (m, 2H, H14).

^{13}C NMR (151 MHz, Chloroform-*d*) δ [ppm] = 189.4 (C7), 162.4 (C2), 160.6 (C2), 139.1 (C6), 137.7 (C10/C11), 136.8 (C10/C11), 135.2 (C12), 134.3 (C4), 134.1 (C8), 131.7 (C9), 126.6 (C5), 123.0 (C1), 122.9 (C1), 115.8 (C3), 115.7 (C3), 38.3 (C13), 23.2 (C14), 14.5 (C15).

FT-IR (cm^{-1}): 2952 (w), 2912 (w), 2844 (w), 1627 (s), 1603 (s), 1566 (m), 1484 (m), 1442 (m), 1396 (m), 1292 (m), 1191 (m), 1170 (m), 1081 (m), 872 (m), 793 (s), 755 (m), 727 (m), 675 (m).

HR-MS (EI, 70 eV): calc. for $C_{29}H_{22}O_2F_2S_2^{\cdot+}$: 504.1024 [M$^{\cdot+}$]; found: 504.1023 [M$^{\cdot+}$].

5,5'-(cyclopent-1-ene-1,2-diylbis(5-methylthiophene-4,2-diyl))bis(2-fluorobenzaldehyde)   (10c)
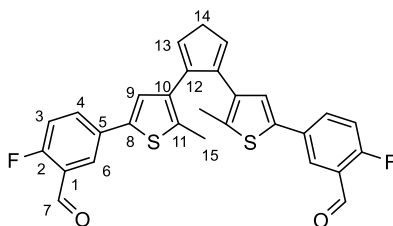
According to **TP2**, MIDA ester **11c** (1.79 g, 6.42 mmol, 2.00 equiv.), the *Feringa* building block **8** (1.06 g, 3.21 mmol, 1.00 equiv.), SPhos (132 mg, 0.321 mmol, 10 mol%) and palladium acetate (36.0 mg, 0.160 mmol, 5 mol%) were dissolved in dry 1,4-dioxane (42 mL). After the resulting yellow-brown reaction mixture was stirred at room temperature for 10 min, a solution of sodium phosphate (3M, 10.2 g, 48.1 mmol, 15.0 equiv.), which was previously degassed for 30 min, was added. The reaction mixture was stirred for 10 min at room temperature, then heated to 60 °C and stirred overnight. The resulting dark red reaction mixture was cooled to room temperature and was diluted with sodium hydroxide (1M, 30 mL) and diethyl ether (30 mL). The phases were separated and the aqueous phase was extracted with diethyl ether (3 x 30 mL). The combined organic phases were dried over sodium sulfate, filtered off and the solvents were removed under reduced pressure. The highly viscous purple residue was purified by column chromatography (*i*-Hex/EtOAc v/v 40:1, R_f = 0.22) to afford compound **10c** (419 mg, 0.830 mmol, 23%) as purple crystalline solid.[115]

^{1}H NMR (800 MHz, Chloroform-*d*) δ [ppm] = 10.37 (s, 1H, H7), 7.96 (dd, *J* = 6.4 Hz, *J* = 2.6 Hz, 1H, H6), 7.69 (ddd, *J* = 8.6 Hz, *J* = 4.9 Hz, *J* = 2.5 Hz, 1H, H4), 7.15 (dd, *J* = 9.8 Hz, *J* = 8.6 Hz, 1H, H3), 7.03 (s, 1H, H9), 2.84 (t, *J* = 7.4 Hz, 2H, H13), 2.10 (m, 2H, H14), 1.99 (s, 3H, H15).

^{13}C NMR (201 MHz, Chloroform-*d*) δ [ppm] = 187.2 (C7), 164.4 (C2), 163.2 (C2), 137.3 (C8), 137.1 (C10), 135.6 (C11), 134.9 (C12), 133.1 (C4), 131.7 (C5), 125.1 (C9), 125.0 (C6), 124.3 (C1), 117.2 (C3), 117.1 (C3), 38.6 (C13), 23.2 (C14), 14.6 (C15).

FT-IR (cm^{-1}): 3046 (w), 2912 (w), 2845 (w), 2761 (w), 1691 (m), 1602 (m), 1557 (w), 1498 (m), 1470 (m), 1439 (w), 1396 (m), 1285 (m), 1249 (m), 1217 (m), 1149 (m), 1109 (m), 1027 (w), 988 (w), 899 (m), 875 (m), 825 (s), 810 (m), 755 (m), 712 (m), 683 (m), 658 (m).

HR-MS (EI, 70 eV): calc. for $C_{29}H_{22}F_2O_2S_2$·$^+$: 504.1024 [M·$^+$]; found: 504.1021 [M·$^+$].

4,4'-(cyclopent-1-ene-1,2-diylbis(5-methylthiophene-4,2-diyl))bis(2-fluorobenzaldehyde) (10d)
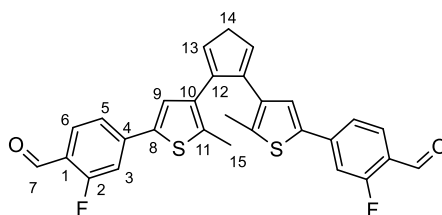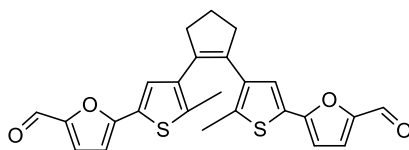

According to **TP2**, MIDA ester **11b** (1.98 g, 7.10 mmol, 2.00 equiv.), the *Feringa* building block **8** (1.17 g, 3.55 mmol, 1.00 equiv.), SPhos (146 mg, 0.355 mmol, 10 mol%) and palladium acetate (39.8 mg, 0.177 mmol, 5 mol%) were dissolved in dry 1,4-dioxane (46 mL). After the resulting yellow-brown reaction mixture was stirred at room temperature for 10 min, a solution of sodium phosphate (3M, 11.3 g, 53.2 mmol, 15.0 equiv.), which was previously degassed for 30 min, was added. The reaction mixture was stirred for 10 min at room temperature, then heated to 60 °C and stirred overnight. The resulting dark blue reaction mixture was cooled to room temperature and was diluted with sodium hydroxide (1M, 30 mL) and diethyl ether (30 mL). The phases were separated and the aqueous phase was extracted with diethyl ether (3 x 30 mL). The combined organic phases were dried over sodium sulfate, filtered off and the solvents were removed under reduced pressure. The highly viscous blue residue was purified by column chromatography (*i*-Hex/EtOAc v/v 20:1 → 10:1, R_f = 0.58) to afford compound **10d** (563 mg, 1.11 mmol, 31%) as blue crystalline solid.[115]

^{1}H NMR (600 MHz, Chloroform-*d*) δ [ppm] = 10.29 (d, *J* = 0.8 Hz, 1H, H7), 7.82 (t, *J* = 7.7 Hz, 1H, H6), 7.36 (ddd, *J* = 8.1 Hz, *J* = 1.7 Hz, *J* = 0.7 Hz, 1H, H5), 7.24 (dd, *J* = 11.7 Hz, *J* = 1.7 Hz, 1H, H3), 7.17 (s, 1H, H9), 2.85 (t, *J* = 7.4 Hz, 2H, H13), 2.14 – 2.08 (m, 2H, H14), 2.03 (s, 3H, H15).

^{13}C NMR (151 MHz, Chloroform-*d*) δ [ppm] = 186.5 (C7), 166.0 (C2), 164.3 (C2), 142.5 (C4), 138.1 (C10/C11), 137.4 (C10/C11), 137.3 (C8), 135.0 (C12), 129.4 (C6), 126.8 (C9), 122.4 (C1), 121.2 (C5), 112.4 (C3), 112.3 (C3), 38.6 (C13), 23.1 (C14), 14.8 (C15).

FT-IR (cm^{-1}): 2953 (w), 2847 (w), 2753 (w), 1688 (s), 1613 (s), 1561 (m), 1506 (m), 1493 (m), 1454 (m), 1424 (s), 1392 (m), 1351 (m), 1311 (m), 1242 (m), 1207 (m), 1177 (m), 1112 (m), 852 (s), 823 (s), 804 (s), 758 (m), 702 (m), 682 (m), 663 (m).

HR-MS (EI, 70 eV): calc. for $C_{29}H_{22}F_2O_2S_2^{\cdot+}$: 504.1024 [M$^{\cdot+}$]; found: 504.1024 [M$^{\cdot+}$].

5,5'-(cyclopent-1-ene-1,2-diylbis(5-methylthiophene-4,2-diyl))bis(furan-2-carbaldehyde)   (10e)

According to **TP2**, MIDA ester **11e** (2.21 g, 8.80 mmol, 2.20 equiv.), the *Feringa* building block **8** (1.32 g, 4.00 mmol, 1.00 equiv.), SPhos (164 mg, 400 µmol, 10 mol%) and palladium acetate (44.9 mg, 177 µmol, 5 mol%) were dissolved in dry 1,4-dioxane (58 mL). After the resulting brown reaction mixture was stirred at room temperature for 10 min, a solution of sodium phosphate (3M, 12.7 g, 60.0 mmol, 15.0 equiv.), which was previously degassed for 30 min, was added. The reaction mixture was stirred for 10 min at room temperature, then heated to 60 °C and stirred overnight. The resulting dark blue reaction mixture was cooled to room temperature and was diluted with sodium hydroxide (1M, 38 mL) and diethyl ether (38 mL). The phases were separated and the aqueous phase was extracted with diethyl ether (3 x 40 mL). The combined organic phases were dried over sodium sulfate, filtered off and the solvents were removed under reduced pressure. The highly viscous blue residue was purified by column chromatography (*i*-Hex/EtOAc v/v 30:1 → 10:1) to afford compound **10e** (378 mg, 843 µmol, 21%) as a colourless solid.[115]

^{1}H NMR (600 MHz, Chloroform-*d*) δ [ppm] = 9.57 (s, 1H), 7.40 – 7.10 (m, 3H), 6.53 (d, *J* = 3.7 Hz, 1H), 3.69 (d, *J* = 13.8 Hz, 22H), 2.82 (t, *J* = 7.5 Hz, 2H), 2.64 (s, 9H), 2.38 (t, *J* = 7.3 Hz, 6H).

^{13}C NMR (151 MHz, Chloroform-*d*) δ [ppm] = 173.5, 172.9, 155.0, 151.4, 137.9, 137.0, 134.9, 127.7, 127.3, 107.1, 77.4, 77.2, 77.0, 52.0, 51.8, 51.7, 38.8, 33.2, 29.0, 24.5, 23.1, 20.2, 14.7.

HR-MS (EI, 70 eV): calc. for $C_{25}H_{20}O_4S_2$$^{.+}$: 448.0803 [M$^{.+}$]; found: 448.0796 [M$^{.+}$].

4',4'''-(cyclopent-1-ene-1,2-diyl)bis(5'-methyl-[2,2'-bithiophene]-5-carbaldehyde)   (10f)
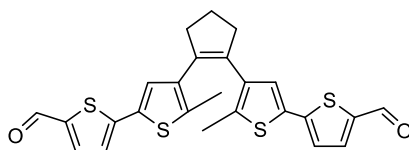
According to **TP2**, MIDA ester **11f** (2.94 g, 11.0 mmol, 2.20 equiv.), the *Feringa* building block **8** (1.65 g, 4.00 mmol, 1.00 equiv.), SPhos (205 mg, 500 µmol, 10 mol%) and palladium acetate (56.1 mg, 250 µmol, 5 mol%) were dissolved in dry 1,4-dioxane (72 mL). After the resulting yellow reaction mixture was stirred at room temperature for 10 min, a solution of sodium phosphate (3M, 15.9 g, 75.0 mmol, 15.0 equiv.), which was previously degassed for 30 min, was added. The reaction mixture was stirred for 10 min at room temperature, then heated to 60 °C and stirred overnight. The resulting dark blue reaction mixture was cooled to room temperature and was diluted with sodium hydroxide (1M, 48 mL) and diethyl ether (48 mL). The phases were separated and the aqueous phase was extracted with diethyl ether (3 x 50 mL). The combined organic phases were dried over sodium sulfate, filtered off and the solvents were removed under reduced pressure. The highly viscous blue residue was purified by column chromatography (*i*-Hex/EtOAc v/v 20:1 → 5:1) to afford compound **10f** (163 mg, 339 µmol, 8%) as a yellowish solid.[115] Due to remaining impurities and the low yield, no adequate analysis could be made.

HR-MS (EI, 70 eV): calc. for $C_{25}H_{20}O_2S_4^{.+}$: 480.0346 [M$^{.+}$]; found: 480.0389 [M$^{.+}$].

4,4'-(cyclopent-1-ene-1,2-diyl)bis(5-methyl-[2,3'-bithiophene]-2'-carbaldehyde) (10g)
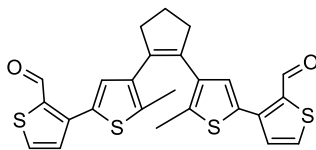
According to **TP2**, MIDA ester **11g** (2.94 g, 11.0 mmol, 2.20 equiv.), the *Feringa* building block **8** (1.65 g, 4.00 mmol, 1.00 equiv.), SPhos (205 mg, 500 µmol, 10 mol%) and palladium acetate (56.1 mg, 250 µmol, 5 mol%) were dissolved in dry 1,4-dioxane (72 mL). After the resulting yellow reaction mixture was stirred at room temperature for 10 min, a solution of sodium phosphate (3M, 15.9 g, 75.0 mmol, 15.0 equiv.), which was previously degassed for 30 min, was added. The reaction mixture was stirred for 10 min at room temperature, then heated to 60 °C and stirred overnight. The resulting dark blue reaction mixture was cooled to room temperature and was diluted with sodium hydroxide (1M, 48 mL) and diethyl ether (48 mL). The phases were separated and the aqueous phase was extracted with diethyl ether (3 x 50 mL). The combined organic phases were dried over sodium sulfate, filtered off and the solvents were removed under reduced pressure. The highly viscous blue residue was purified by column chromatography (*i*-Hex/EtOAc v/v 20:1 → 10:1). to afford compound **10g** (120 mg, 250 µmol, 6%) as a yellowish solid.[115] Due to remaining impurities and the low yield, no adequate analysis could be made.

HR-MS (EI, 70 eV): calc. for $C_{25}H_{20}O_2S_4^{\cdot+}$: 480.0346 [M$^{\cdot+}$]; found: 480.0402 [M$^{\cdot+}$].

5.7   Synthesis of the ß-Amino Alcohol Ligands

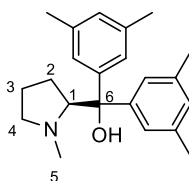**(*S*)-(1-methylpyrrolidin-2-yl)diphenylmethanol   ((*S*)-17a)**
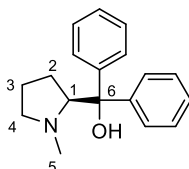
(*S*)-diphenyl(pyrrolidin-2-yl)methanol **(*S*)-16a** (1.00 g, 3.95 mmol, 1.00 equiv.) was dissolved in MeOH (15 mL). Sodium carbonate (418 mg, 3.95 mmol, 1.00 equiv.) and iodomethane (250 µL, 3.95 mmol, 1.00 equiv.) were added to the solution and refluxed for 20 h. After cooling to room temperature, the reaction was quenched with H_2O and the aqueous phase was extracted with EtOAc (3 x 30 mL). The combined organic layers were dried over Na_2SO_4, filtered off and the solvent was removed *in vacuo*. The crude product was purified *via* column chromatography (cyclohexane/EtOAc = 9:1 with 0.5% NEt_3) and the product **(*S*)-17a** was obtained as a white solid (643 mg, 2.40 mmol, 61%).

¹H NMR (800 MHz, CD₂Cl₂) δ [ppm] = 7.65 (d, *J* = 7.9 Hz, 2H, H-*ortho*-Ar), 7.53 (d, *J* = 7.9 Hz, 2H, H-*ortho*-Ar), 7.27 (td, *J* = 7.8, 2.1 Hz, 4H, H-*meta*-Ar), 7.15 (td, *J* = 7.3, 2.2 Hz, 2H, H-*para*-Ar), 3.65 (dd, *J* = 9.5, 4.8 Hz, 1H, H1), 3.11 (t, *J* = 8.0 Hz, 1H, H4), 2.46 (dt, *J* = 16.6, 7.7 Hz, 1H, H4), 1.90 (dq, *J* = 12.8, 9.0 Hz, 1H, H2), 1.83 (s, 3H, H5), 1.65 (m, 4H, H3, H3, H2).

¹³C NMR (201 MHz, CD₂Cl₂) δ [ppm] = 149.0 (C-Ar), 147.5 (C-Ar), 128.4 (C-*para*-Ar), 128.3 (C-*meta*-Ar), 126.5 (C-*para*-Ar), 126.5 (C-*para*-Ar), 125.8 (C-*ortho*-Ar), 125.8 (C-*ortho*-Ar), 77.7 (C6), 72.1 (C1), 59.5 (C4), 43.1 (C5), 30.2 (C2), 24.4 (C3).

HR-MS (EI, 70 eV): m/z calc. for $C_{18}H_{22}NO$: 268.1696, found: 268.1696.
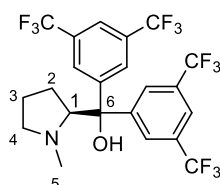
(*S*)-bis(3,5-dimethylphenyl)(1-methylpyrrolidin-2-yl)methanol   ((*S*)-17b)

(*S*)-bis(3,5-dimethylphenyl)(pyrrolidin-2-yl)methanol **(S)-16b**   (1.00 g, 3.23 mmol, 1.00 equiv.) was dissolved in MeOH (15 mL). Sodium carbonate (411 mg, 3.88 mmol, 1.20 equiv.) and iodomethane (241 μL, 3.88 mmol, 1.20 equiv.) were added to the solution and refluxed for 20 h. After cooling to room temperature, the reaction was quenched with H_2O and the aqueous phase was extracted with EtOAc (1 x 50 mL and 3 x 30 mL). The combined organic layers were dried over Na_2SO_4, filtered off and the solvent was removed *in vacuo*. The crude product was purified *via* column chromatography (cyclohexane/EtOAc = 9:1) and the product **(S)-17b** was obtained as a white solid (693 mg, 2.14 mmol, 66%).

¹H NMR (400 MHz, CD₂Cl₂) δ [ppm] = 7.24 (dt, *J* = 1.5, 0.7 Hz, 2H, H-*ortho*-Ar), 7.12 (dt, *J* = 1.5, 0.7 Hz, 2H, H-*o*-Ar), 6.78 (dtt, *J* = 3.2, 1.6, 0.8 Hz, 2H, H-*para*-Ar), 4.63 (br, 1H, HO), 3.60 (dd, *J* = 9.4, 4.7 Hz, 1H, H1), 3.08 (dddd, *J* = 8.8, 5.9, 2.8, 1.4 Hz, 1H, H4), 2.44 (ddd, *J* = 9.9, 9.0, 6.9 Hz, 1H, H4), 2.28 (d, *J* = 0.8 Hz, 12H, 4 × H₃C-*meta*-Ar), 1.84 (s, 4H, H₃C5, H2), 1.70 – 1.54 (m, 3H, H2, H3, H3).

¹³C NMR (101 MHz, CD₂Cl₂) δ [ppm] = 149.0 (C-Ar), 147.5 (C-Ar), 137.8 (4C, 4 x C-*meta*-Ar), 127.9 (2C, C-*para*-Ar), 123.6 (4C, C-*ortho*-Ar), 77.5 (C6), 72.0 (C1), 59.5 (C4), 43.2 (C5), 30.2 (C2), 24.4 (C3), 21.7 (4C, H₃C-*meta*-Ar).

HR-MS (**ESI**): m/z calc. for $C_{22}H_{30}NO$ [M+H]⁺: 324.23219, found: 324.23287.

(*S*)-bis(3,5-bis(trifluoromethyl)phenyl)(1-methylpyrrolidin-2-yl)methanol   ((*S*)-17c)

(*S*)-bis(3,5-bis(trifluoromethyl)phenyl)(pyrrolidin-2-yl)methanol   **(*S*)-16c**   (1.00   g,   1.90   mmol, 1.00 equiv.) was dissolved in MeOH (15 mL). Sodium carbonate (202 mg, 1.90 mmol, 1.00 equiv.) and Iodomethane (120 µL, 1.90 mmol, 1.00 equiv.) were added to the solution and refluxed for 20 h. After cooling to room temperature, the reaction was quenched with H_2O and the aqueous phase was extracted with EtOAc (3 x 50 mL). The combined organic layers were dried over Na_2SO_4, filtered off and the solvent was removed *in vacuo*. The crude product was purified *via* column chromatography (cyclohexane/EtOAc = 9:1) and the product **(*S*)-17c** was obtained as a white solid (510 mg, 0.95 mmol, 50%).

^{1}H NMR (599 MHz, CD$_2$Cl$_2$) δ [ppm] = 8.18 – 8.16 (m, 2H, H-*ortho*-Ar), 8.04 – 8.01 (m, 2H, H-*ortho*-Ar), 7.78 – 7.74 (m, 2H, H-*para*-Ar), 5.38 (s, 1H, HO), 3.72 (dd, *J* = 9.1, 5.5 Hz, 1H, H1), 3.17 (ddd, *J* = 9.4, 5.6, 3.8 Hz, 1H, H4), 2.55 (td, *J* = 9.3, 7.8 Hz, 1H, H4), 1.85 (m, 4H, H2, H5), 1.72 – 1.67 (m, 2H, H3, H3), 1.51 – 1.45 (m, 1H, H2).

^{13}C-NMR (151 MHz, CD$_2$Cl$_2$) δ [ppm] = 150.3 (C-Ar), 148.4 (C-Ar), 132.0 (qd, *J* = 33.2, 13.7 Hz, 4C, 4 × F$_3$C-*meta*-Ar), 126.4 – 126.1 (m, 2C, 2 x C-*ortho*-Ar), 126.1 – 126.0 (m, 2C, 2 x C-*ortho*-Ar), 124.6 (d, *J* = 1.9 Hz, 2C, 2 x C-*meta*-Ar), 122.8 (d, *J* = 1.8 Hz, 2C, 2 x C-*meta*-Ar), 121.5 (p, *J* = 3.9 Hz, C-*para*-Ar), 121.4 (p, *J* = 3.9 Hz, C-*para*-Ar), 77.0 (C6), 71.9 (C1), 59.1 (C4), 42.9 (C5), 30.2 (C2), 24.0 (C3).

HR-MS (**ESI**): m/z calc. for C$_{22}$H$_{18}$F$_{12}$NO [M+H]$^+$: 540.11913, found: 540.12137.

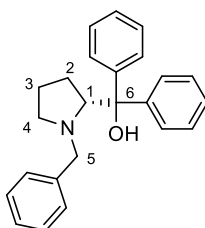**(*S*)-(1-benzylpyrrolidin-2-yl)diphenylmethanol   ((*S*)-18a)**
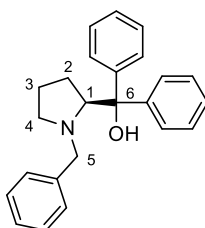
(*S*)-diphenyl(pyrrolidin-2-yl)methanol **(*S*)-16a** (1.00 g, 3.95 mmol, 1.00 equiv.) was dissolved in MeOH (15 mL). Sodium carbonate (418 mg, 3.95 mmol, 1.00 equiv.) and benzyl bromide (470 µL, 3.95 mmol, 1.00 equiv.) were added to the solution and refluxed for 20 h. After cooling to room temperature, the reaction was quenched with H_2O and the aqueous phase was extracted with EtOAc (1 x 50 mL and 3 x 30 mL). The combined organic layers were dried over Na_2SO_4, filtered off and the solvent was removed *in vacuo*. The product **(*S*)-18a** was obtained as a white solid in quantitative yield.

^{1}H NMR (400 MHz, CD$_2$Cl$_2$) δ [ppm] = 7.76 – 7.70 (m, 2H, 2 × H-*ortho*-Ar), 7.60 – 7.56 (m, 2H, 2 × H-*ortho*-Ar), 7.33 – 7.16 (m, 8H, 4 × H-*meta*-Ar, H-*para*-Ar, 2 × H-*meta*-Ph, H-*p*-Ph), 7.16 – 7.09 (m, 1H, H-*para*-Ar), 7.07 – 7.03 (m, 2H, H-*ortho*-Ph), 4.88 (br, 1H, HO), 4.01 (dd, *J* = 9.5, 4.5 Hz, 1H, H4, H1), 3.23 (d, *J* = 12.7 Hz, 1H, H5), 3.06 (d, *J* = 12.7 Hz, 1H, H5), 2.94 – 2.83 (m, 1H, H4), 2.44 – 2.27 (m, 1H, H4), 2.05 – 1.85 (m, 1H, H2), 1.74 – 1.58 (m, 3H, H3, H3, H2).

^{13}C NMR (101 MHz, CD$_2$Cl$_2$) δ [ppm] = 148.8 (C-Ar), 147.4 (C-Ar), 140.2 (C-Ph), 128.9 (C-*ortho*-Ph), 128.6 (C-*meta*-Ph), 128.4 (C-*meta*-Ar), 128.4 (C-*meta*-Ar), 127.2 (C-*para*-Ph), 126.7 (C-*para*-Ar), 126.6 (C-*para*-Ar), 126.0 (C-*ortho*-Ar), 125.9 (C-*ortho*-Ar), 78.2 (C6), 70.9 (C1), 60.9 (C5), 55.9 (C4), 30.1 (C2), 24.6 (C3).

HR-MS (EI, 70 eV): m/z calc. for C$_{24}$H$_{24}$NO: 342.1858, found: 342.1849.

(R)-(1-benzylpyrrolidin-2-yl)diphenylmethanol   ((R)-18a)

(R)-diphenyl(pyrrolidin-2-yl)methanol **(R)-16a** (1.00 g, 3.95 mmol, 1.00 equiv.) was dissolved in MeOH (15 mL). Sodium carbonate (418 mg, 3.95 mmol, 1.00 equiv.) and benzyl bromide (470 μL, 3.95 mmol, 1.00 equiv.) were added to the solution and refluxed for 20 h. After cooling to room temperature, the reaction was quenched with H_2O and the aqueous phase was extracted with EtOAc (1 x 50 mL and 3 x 30 mL). The combined organic layers were dried over Na_2SO_4, filtered off and the solvent was removed *in vacuo*. The product **(R)-18a** was obtained as a white solid in quantitative yield.

^{1}H NMR (400 MHz, CD$_2$Cl$_2$) δ [ppm] = 7.76 − 7.71 (m, 2H, 2 × H-*ortho*-Ar), 7.62 − 7.56 (m, 2H, 2 × H-*ortho*-Ar), 7.34 − 7.14 (m, 8H, 4 × H-*meta*-Ar, H-*para*-Ar, 2 × H-*meta*-Ph, H-*para*-Ph), 7.15 − 7.09 (m, 1H, H-*para*-Ar), 7.07 − 7.03 (m, 2H, H-*ortho*-Ph), 4.89 (br, 1H, HO), 4.01 (dd, *J* = 9.4, 4.5 Hz, 1H, H1), 3.23 (d, *J* = 12.7 Hz, 1H, H5), 3.06 (d, *J* = 12.7 Hz, 1H, H5), 2.95 − 2.84 (m, 1H, H4), 2.42 − 2.32 (m, 1H, H4), 2.04 − 1.91 (m, 1H, H2), 1.76 − 1.54 (m, 3H, H3, H3, H2).

^{13}C-NMR (101 MHz, CD$_2$Cl$_2$) δ [ppm] = 148.9 (C-Ar), 147.5 (C-Ar), 140.4 (C-Ph), 129.0 (C-*ortho*-Ph), 128.7 (C-*meta*-Ph), 128.6 (C-*meta*-Ar), 128.6 (C-*meta*-Ar), 127.3 (C-*para*-Ph), 126.9 (C-*para*-Ar), 126.7 (C-*para*-Ar), 126.2 (C-*ortho*-Ar), 126.1 (C-*ortho*-Ar), 78.4 (C6), 71.1 (C1), 61.1 (C5), 56.0 (C4), 30.3 (C2), 24.7 (C3).

HR-MS (EI, 70 eV): m/z calc. for $C_{24}H_{24}NO$: 342.1858, found: 342.1865.

(*S*)-(1-benzylpyrrolidin-2-yl)bis(3,5-bis(trifluoromethyl)phenyl)methanol   ((*S*)-18c)
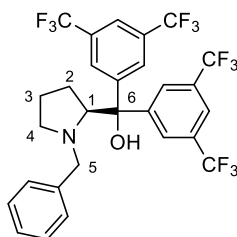
(*S*)-bis(3,5-bis(trifluoromethyl)phenyl)(pyrrolidine-2-yl)methanol **(*S*)-16c** (1.00 g, 1.90 mmol, 1.00 equiv.) was dissolved in MeOH (15 mL). Sodium carbonate (202 mg, 1.90 mmol, 1.00 equiv.) and benzyl bromide (230 µL, 1.90 mmol, 1.00 equiv.) were added to the solution and refluxed for 20 h. After cooling to room temperature, the reaction was quenched with H_2O and the aqueous phase was extracted with EtOAc (3 x 50 mL). The combined organic layers were dried over Na_2SO_4, filtered off and the solvent was removed *in vacuo*. The crude product was purified *via* column chromatography (cyclohexane/EtOAc = 9:1) and the product **(*S*)-18c** was obtained as a white solid (838 mg, 1.36 mmol, 72%).

¹H NMR (800 MHz, CD₂Cl₂) δ [ppm] = 8.22 (d, *J* = 1.6 Hz, 2H, H-*ortho*-Ar), 8.09 − 8.05 (m, 2H, H-*ortho*-Ar), 7.79 (d, *J* = 1.9 Hz, 1H, H-*para*-Ar), 7.74 (d, *J* = 1.9 Hz, 1H, H-*para*-Ar), 7.25 − 7.17 (m, 3H, 2 × H-*meta*-Ph, H-*para*-Ph), 6.98 z(dd, *J* = 7.1, 1.7 Hz, 2H, H-*ortho*-Ph), 5.46 (s, 1H, HO), 4.10 − 4.07 (m, 1H, H1), 3.23 (d, *J* = 12.9 Hz, 1H, H5), 3.12 (d, *J* = 12.9 Hz, 1H, H5), 2.99 (ddd, *J* = 10.0, 6.5, 3.6 Hz, 1H, H4), 2.52 (td, *J* = 9.6, 6.7 Hz, 1H, H4), 1.97 (dq, *J* = 13.3, 8.7 Hz, 1H, H2), 1.74 − 1.64 (m, 2H, H3), 1.56 (ddt, *J* = 13.1, 8.1, 4.9 Hz, 2H, H2).

¹³C NMR (201 MHz, CD₂Cl₂) δ [ppm] = 150.1 (C-Ar), 148.3 (C-Ar), 138.95 (C-Ph), 132.4 − 131.8 (m, 2 C, 2 × C-*meta*-Ar), 128.7 (2 C, 2 × C-*ortho*-Ph), 128.6 (2 C, 2 × C-*ortho*-Ph), 127.6 (C-*para*-Ph), 126.6 − 126.1 (m, 4C, 4 x C-*ortho*-Ar), 124.4 (d, *J* = 12.5 Hz, 2C, 2 × F₃C-*meta*-Ar), 123.0 (d, *J* = 12.6 Hz, 2C, 2 × F₃C-*meta*-Ar), 121.8 - 121.4 (m, 2 C, 2 × C-*para*-Ar), 77.7 (C6), 71.1 (C1), 60.9 (C5), 55.9 (C4), 30.2 (C2), 24.5 (C3).

**HR-MS** (ESI): m/z calc. for $C_{28}H_{22}F_{12}NO$ [M+H]⁺: 616.15043, found: 616.15351.

(*S*)-2-(dibenzylamino)propan-1-ol   ((*S*)-19a)
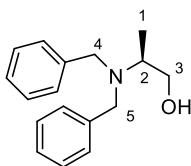
(*S*)-2-aminopropan-1-ol **(*S*)-17a** (1.00 g, 13.3 mmol, 1.00 equiv.) was dissolved in MeOH (15 mL). Sodium carbonate (1.41 g, 13.3 mmol, 1.00 equiv.) and benzyl bromide (3.16 mL, 26.6 mmol, 2.00 equiv.) were added to the solution and refluxed for 20 h. After cooling to room temperature, the reaction was quenched with H_2O and the aqueous phase was extracted with EtOAc (1 x 50 mL and 3 x 30 mL). The combined organic layers were dried over Na_2SO_4, filtered off and the solvent was removed *in vacuo*. The crude product was purified *via* column chromatography (cyclohexane/EtOAc = 9:1) and the product **(*S*)-19a** was obtained as a colourless oil (1.13 g, 4.41 mmol, 33%).

^{1}H NMR (400 MHz, CD$_2$Cl$_2$) δ [ppm] = 7.36 – 7.21 (m, 10H, H-Ph), 3.80 (d, *J* = 13.4 Hz, 2H, H4, H5), 3.44 (t, *J* = 10.5 Hz, 1H, H3), 3.37 (d, *J* = 13.4 Hz, 2H, H4, H5), 3.28 (dd, *J* = 10.7, 5.0 Hz, 1H, H3), 2.92 (dqd, *J* = 10.5, 6.7, 5.0 Hz, 1H, H2), 0.98 (d, *J* = 6.7 Hz, 3H, H1).

^{13}C NMR (101 MHz, CD$_2$Cl$_2$) δ [ppm] = 140.1 (C-Ph), 129.4 (C-Ph), 128.8 (C-Ph), 127.5 (C-Ph), 63.0 (C3), 54.7 (C2), 53.2 (2C, C4, C5), 8.8 (C1).

HR-MS (**ESI**): m/z calc. for $C_{12}H_{22}NO$ [M+H]$^+$: 256.16959, found: 256.17012.
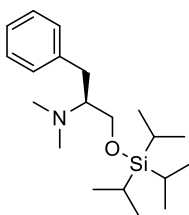
(*S*)-2-(benzylamino)-3-phenylpropan-1-ol   ((*S*)-19b)
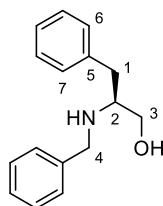
(*S*)-2-amino-3-phenylpropan-1-ol **(S)-17b** (1.00 g, 6.61 mmol, 1.00 equiv.) was dissolved in EtOH (60 mL). Benzaldehyde (670 μL, 6.61 mmol, 1.00 equiv.) was added to the solution and refluxed for 6 h. After cooling the reaction to room temperature, $NaBH_4$ (1.10 g, 29.1 mmol, 3.00 equiv.) was added stepwise over a period for 1 h at 0 °C. The reaction was then brought up to room temperature and stirred for 4 h. The reaction mixture was extracted with DCM (2 x 50 mL and 1 x 30 mL). The combined organic layer was washed with brine (3 x 30 mL), dried over Na_2SO_4, filtered off and the solvent was removed *in vacuo*. The crude product was purified *via* column chromatography (DCM/MeOH = 99:1) and the product **(S)-19b** was obtained as a white solid (1.12 g, 4.46 mmol, 70%).

¹H NMR (800 MHz, CD₂Cl₂) δ [ppm] = 7.31 – 7.27 (m, 4H), 7.24 – 7.21 (m, 4H), 7.19 – 7.17 (m, 2H, H6, H7), 3.79 – 3.74 (m, 2H, H4, H4), 3.58 (dd, *J* = 10.7, 3.9 Hz, 1H, H3), 3.28 (dd, *J* = 10.7, 5.5 Hz, 1H, H3), 2.93 (tdd, *J* = 7.0, 5.5, 3.9 Hz, 1H, H2), 2.82 (dd, *J* = 13.7, 7.0 Hz, 1H, H1), 2.74 (dd, *J* = 13.6, 6.9 Hz, 1H, H1).

¹³C NMR (201 MHz, CD₂Cl₂) δ [ppm] = 140.9 (C-Ph), 139.2 (C5), 129.6 (2C, C6, C7), 128.9 (C-Ar), 128.7 (C-Ph), 128.4 (C-Ph), 127.3 (C-Ar), 126.7 (C-Ph), 62.8 (C3), 59.9 (C2), 51.3 (C4), 38.4 (C1).

HR-MS (**ESI**): m/z calc. for $C_{16}H_{20}NO$ [M+H]⁺: 242.15394, found: 242.15404.

(*S*)-*N,N*-dimethyl-1-phenyl-3-((triisopropylsilyl)oxy)propan-2-amine   ((*S*)-19c)

(S)-2-(dibenzylamino)-3-phenylpropan-1-ol **(*S*)-17b** (1.00 g, 5.58 mmol, 1.00 equiv.) and imidazole (570 mg, 8.37 mmol, 1.50 equiv.) were dissolved in dry DCM (15 mL) under inert atmosphere. TIPS (1.19 mL, 5.58 mmol, 1.00 equiv.) was added to the solution and stirred for 22 h. The reaction was subsequently washed with H2O (15 mL), aqueous NaOH (10%, 15 mL) and H2O (15 mL). The crude product was purified *via* column chromatography (cyclohexane/EtOAc, 9:1) and the product **(*S*)-19c** was obtained as a colourless oil (1.63 g, 4.85 mmol, 87%). The exact yield could not be determined because of remaining impurities. The product was used without further purification.

HR-MS (EI, 70 eV): m/z calc. for $C_{20}H_{37}NOSi$: 335.2644, found: 335.2640.

5.7.1   General Procedure for the β-Amino Alcohol mediated Asymmetric Alkylation of Benzaldehyde
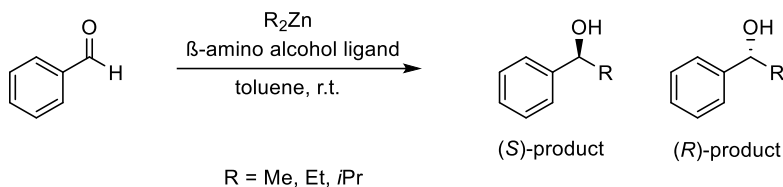
Benzaldehyde (30.0 μL, 300 μmol, 1.00 equiv.) was filled into a flame-dried *Schlenk* flask. A stock solution of the β-amino alcohol (15.0 μmol, 5 mol%) was added to the flask. Then, dry toluene was added to a total volume of 2.55 mL. The dialkylzinc (1 M in toluene, 450 μmol, 1.50 equiv.) was added. The reaction mixture was stirred at r.t. For quantitative analysis, an aliquot (0.5 mL) was taken after 6 h and 24 h and quenched with 1M HCl. After separation of the organic layer, the solvent was removed under reduced pressure. The residue was dissolved in *n*-hexane/*i*PrOH (1:1, 1 mL). For HPLC analysis on a Chiralpak® OD-H column (250 mm, i.d. 4.6 mm, particle size 5 μm, λ = 210 nm) a flow rate of 1 mL/min was used with *n*-hexane/*i*PrOH = 95:5 and an injection volume of 1 μL.

Calibration Lines for Yield Determination

Figure 55: Separation of the Enantiomers of of 1-phenylethan-1-ol.

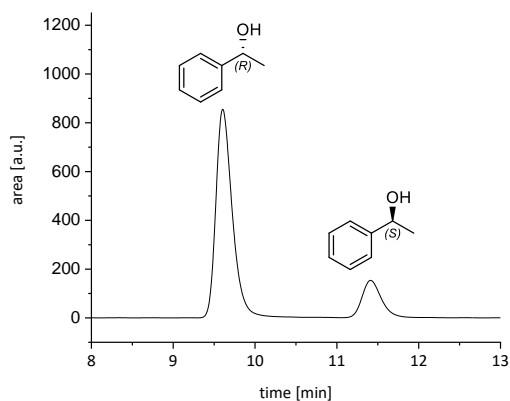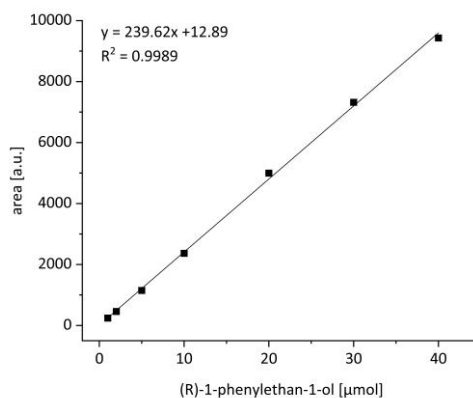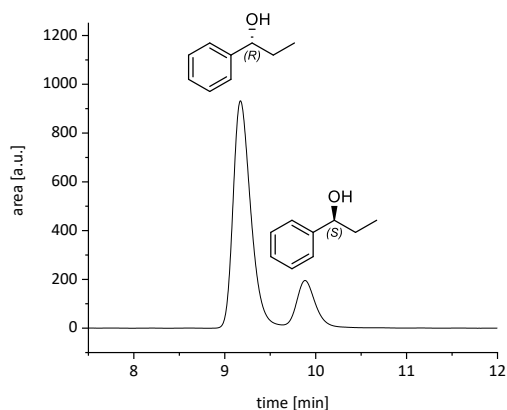Figure 56: Calibration line of dilution series 1-phenylethan-1-ol.

Figure 57: Separation of the Enantiomers of of 1-phenylpropan-1-ol.
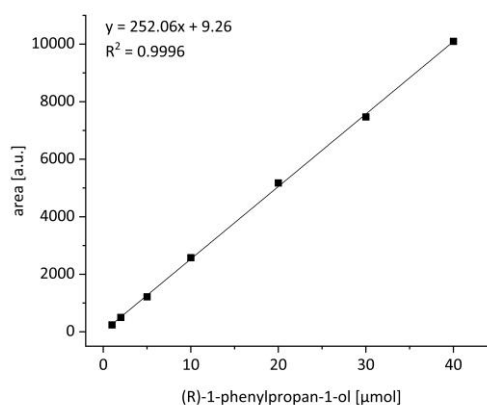
Figure 58: Calibration line of dilution series 1-phenylpropan-1-ol.
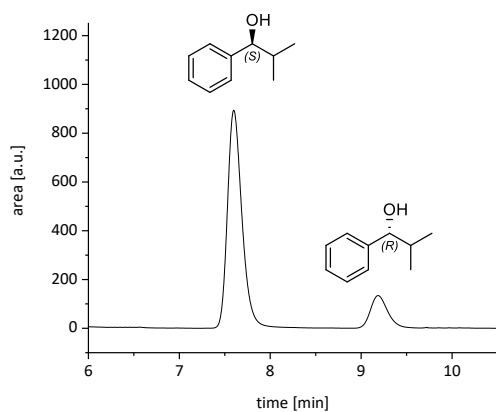
Figure 59: Separation of the Enantiomers of of 2-methyl-1-phenylpropan-1-ol.
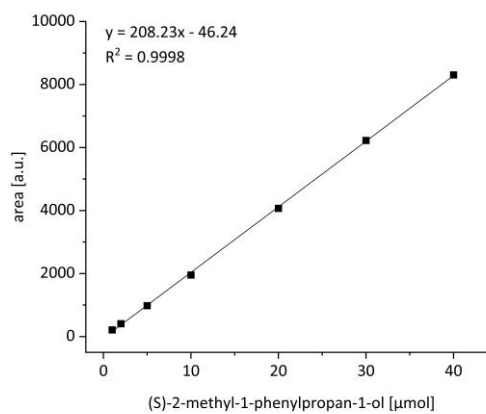
Figure 60: Calibration line of dilution series 2-methyl-1-phenylpropan-1-ol.

CHAPTER 6

Appendix

6.1   Crystallographic data
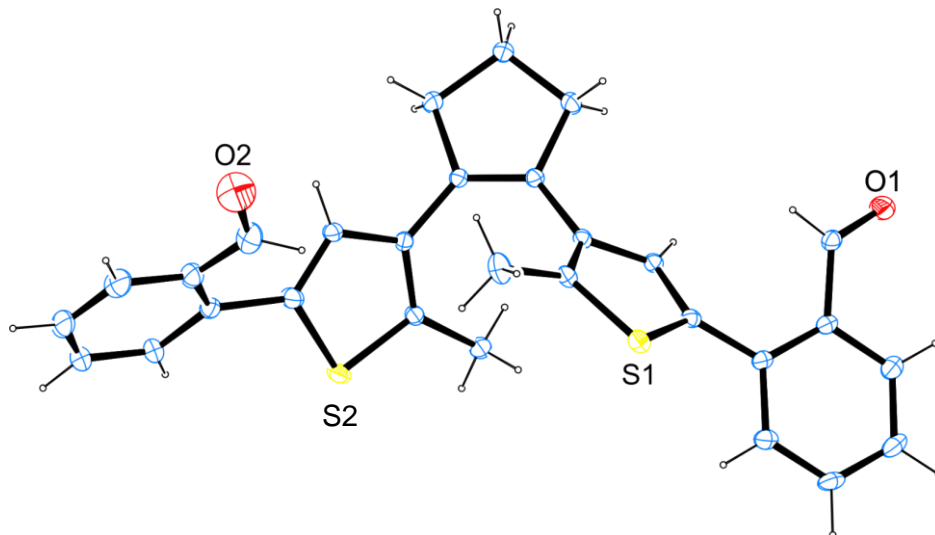
ID	$C_{29}H_{24}O_2S_2$_zv320_trapp	absorption correction	Multi-Scan
net formula	$C_{29}H_{24}O_2S_2$	transmission factor range	0.96–0.99
M_r/g mol^{-1}	468.60	refls. measured	39252
crystal size/mm	0.140 × 0.140 × 0.040	R_{int}	0.0545
T/K	173.(2)	mean $\sigma(I)/I$	0.0296
radiation	MoKα	θ range	2.343–26.368
diffractometer	'Bruker D8 Venture TXS'	observed refls.	3908
crystal system	monoclinic	x, y (weighting scheme)	0.0336, 5.3784
space group	'C 1 2/c 1'	hydrogen refinement	constr
a/Å	35.605(2)	Flack parameter	?
b/Å	8.9661(6)	refls in refinement	4752
c/Å	14.5896(10)	parameters	373
α/°	90	restraints	51
β/°	92.589(2)	$R(F_{obs})$	0.0391
γ/°	90	$R_w(F^2)$	0.0960
V/Å^3	4652.8(5)	S	1.081
Z	8	shift/error$_{max}$	0.001
calc. density/g cm^{-3}	1.338	max electron density/e Å^{-3}	0.294
μ/mm^{-1}	0.254	min electron density/e Å^{-3}	−0.286

6.2   Literature

[1]   B. L. Feringa, R. A. van Delden, *Angew. Chem. Int. Ed.* **1999**, *38*, 3418-3438.

[2]   K. Roth, *Chem. unserer Zeit* **2005**, *39*, 212-217.

[3]   T. Eriksson, S. Björkman, B. Roth, P. Höglund, *J. Pharm. Pharmacol.* **2000**, *52*, 807-817.

[4]   G. Schoetz, O. Trapp, V. Schurig, *Electrophoresis* **2001**, *22*, 3185-3190.

[5]   a) W. E. Elias, *J. Chem. Educ.* **1972**, *49*, 448; b) S. Aiba, N. Takamatsu, T. Sasai, Y. Tokunaga, T. Kawasaki, *Chem. Commun.* **2016**, *52*, 10834-10837; c) W. Langenbeck, G. Triem, *Z. Phys. Chem.* **1936**, *177*, 401-408; d) V. Pavlov, E. Klabunovskii, *Curr. Org. Chem.* **2014**, *18*, 93-114; e) L.-C. Sogutoglu, R. R. E. Steendam, H. Meekes, E. Vlieg, F. P. J. T. Rutjes, *Chem. Soc. Rev.* **2015**, *44*, 6723-6732.

[6]   a) G. Wald, *Ann. N.Y. Acad. Sci.* **1957**, *69*, 352-368; b) J. S. Siegel, *Chirality* **1998**, *10*, 24-27; c) W. H. Mills, *Chem. Ind.* **1932**, 750–759 ; d) K. Mislow, *Collect. Czech. Chem. Commun.* **2003**, *68*, 849-864.

[7]   T. Satyanarayana, S. Abraham, H. B. Kagan, *Angew. Chem. Int. Ed.* **2009**, *48*, 456-494.

[8]   a) I. M. A. L. F. Lindoy, *Self-assembly in Supramolecular Systems* **2000**, *Royal Society of Chemistry*, pp. 1-7; b) Y. Geiger, S. Bellemin-Laponnaz, *ChemCatChem* **2022**, *14*, e202200165; c) G. Storch, O. Trapp, *Nat. Chem.* **2017**, *9*, 179-187.

[9]   a) H. B. K. D. R. Fenwick, *Topics on Stereochemistry* **1999**, *John Wiley and Sons*, pp. 257-296; b) D. Guillaneux, S.-H. Zhao, O. Samuel, D. Rainford, H. B. Kagan, *J. Am. Chem. Soc.* **1994**, *116*, 9430-9439; c) C. Girard, H. B. Kagan, *Angew. Chem. Int. Ed.* **1998**, *37*, 2922-2959.

[10]   F. C. Frank, *Biochim. Biophys. Acta* **1953**, *11*, 459-463.

[11]   a) O. Trapp, *Frontiers in Chemistry* **2020**, *8*; b) Q. Sallembien, L. Bouteiller, J. Crassous, M. Raynal, *Chem. Soc. Rev.* **2022**, *51*, 3436-3476; c) M. E. Noble-Terán, T. Buhse, J.-M. Cruz, C. Coudret, J.-C. Micheau, *ChemCatChem* **2016**, *8*, 1836-1845.

[12]   A. Horeau, *Tetrahedron Lett.* **1969**, *10*, 3121-3124.

[13]   a) B. Feringa, H. Wynberg, *J. Am. Chem. Soc.* **1976**, *98*, 3372-3373; b) H. Wynberg, B. Feringa, *Tetrahedron* **1976**, *32*, 2831-2834.

[14]   C. Puchot, O. Samuel, E. Dunach, S. Zhao, C. Agami, H. B. Kagan, *J. Am. Chem. Soc.* **1986**, *108*, 2353-2357.

[15]   a) M. G. Finn, K. B. Sharpless, *J. Am. Chem. Soc.* **1991**, *113*, 113-126; b) S. S. Woodard, M. G. Finn, K. B. Sharpless, *J. Am. Chem. Soc.* **1991**, *113*, 106-113.

[16]   a) N. Oguni, Y. Matsuda, T. Kaneko, *J. Am. Chem. Soc.* **1988**, *110*, 7877-7878; b) M. Kitamura, S. Suga, H. Oka, R. Noyori, *J. Am. Chem. Soc.* **1998**, *120*, 9800-9809.

[17]   M. Kitamura, S. Okada, S. Suga, R. Noyori, *J. Am. Chem. Soc.* **1989**, *111*, 4028-4036.

[18]   T. K. K. Soai, *Top. Curr. Chem.* **2007**, *284*, 1-33.

[19]   a) T. Shibata, H. Morioka, T. Hayase, K. Choji, K. Soai, *J. Am. Chem. Soc.* **1996**, *118*, 471-472; b) T. Shibata, S. Yonekubo, K. Soai, *Angew. Chem. Int. Ed.* **1999**, *38*, 659-661.

[20]   K. Soai, T. Shibata, H. Morioka, K. Choji, *Nature* **1995**, *378*, 767-768.

[21]   I. Sato, H. Urabe, S. Ishiguro, T. Shibata, K. Soai, *Angew. Chem. Int. Ed.* **2003**, *42*, 315-317.

[22]   a) J. Podlech, T. Gehring, *Angew. Chem. Int. Ed.* **2005**, *44*, 5776-5777; b) T. Kawasaki, K. Suzuki, Y. Hakoda, K. Soai, *Angew. Chem. Int. Ed.* **2008**, *47*, 496-499; c) T. Kawasaki, Y. Harada, K. Suzuki, T. Tobita, N. Florini, G. Pályi, K. Soai, *Org. Lett.* **2008**, *10*, 4085-4088.

[23]   a) D. A. Singleton, L. K. Vo, *Org. Lett.* **2003**, *5*, 4337-4339; b) I. D. Gridnev, J. M. Serafimov, H. Quiney, J. M. Brown, *Organic & Biomolecular Chemistry* **2003**, *1*, 3811-3819; c) K. Soai, I. Sato, T. Shibata, S. Komiya, M. Hayashi, Y. Matsueda, H. Imamura, T. Hayase, H. Morioka, H. Tabira, J. Yamamoto, Y. Kowata, *Tetrahedron: Asymmetry* **2003**, *14*, 185-188; d) T. Kawasaki, K. Suzuki, M. Shimizu, K. Ishikawa, K. Soai, *Chirality* **2006**, *18*, 479-482.

[24]   T. Gehring, M. Busch, M. Schlageter, D. Weingand, *Chirality* **2010**, *22 Suppl 1*, E173-182.

[25]   a) R. Noyori, S. Suga, K. Kawai, S. Okada, M. Kitamura, N. Oguni, M. Hayashi, T. Kaneko, Y. Matsuda, *J. Organomet. Chem.* **1990**, *382*, 19-37; b) N. Oguni, T. Omi, *Tetrahedron Lett.* **1984**, *25*, 2823-2824.

[26]   M. Busch, M. Schlageter, D. Weingand, T. Gehring, *Chem. - Eur. J.* **2009**, *15*, 8251-8258.

[27]   a) F. G. Buono, H. Iwamura, D. G. Blackmond, *Angew. Chem. Int. Ed.* **2004**, *43*, 2099-2103; b) D. A. Singleton, L. K. Vo, *J. Am. Chem. Soc.* **2002**, *124*, 10010-10011.

[28]   a) K. Soai, S. Niwa, H. Hori, *J. Chem. Soc., Chem. Commun.* **1990**, 982-983; b) J. Klankermayer, I. D. Gridnev, J. M. Brown, *Chem. Commun.* **2007**, 3151-3153.

[29]   T. Shibata, J. Yamamoto, N. Matsumoto, S. Yonekubo, S. Osanai, K. Soai, *J. Am. Chem. Soc.* **1998**, *120*, 12157-12158.

[30]   T. Kawasaki, Y. Matsumura, T. Tsutsumi, K. Suzuki, M. Ito, K. Soai, *Science* **2009**, *324*, 492-495.

[31]   M. Quaranta, T. Gehring, B. Odell, J. M. Brown, D. G. Blackmond, *J. Am. Chem. Soc.* **2010**, *132*, 15104-15107.

[32]   N. A. Hawbaker, D. G. Blackmond, *ACS Central Science* **2018**, *4*, 776-780.

[33]   D. G. Blackmond, C. R. McMillan, S. Ramdeehul, A. Schorm, J. M. Brown, *J. Am. Chem. Soc.* **2001**, *123*, 10103-10104.

[34]   I. D. Gridnev, J. M. Serafimov, J. M. Brown, *Angew. Chem. Int. Ed.* **2004**, *43*, 4884-4887.

[35]   D. G. Blackmond, *Tetrahedron: Asymmetry* **2006**, *17*, 584-589.

[36]   I. G. J. M. Brown, J. Klankermayer, *Amplification of Chirality* **2008**, *Springer Berlin Heidelberg*, pp. 35-65.

[37]   T. Gehring, M. Quaranta, B. Odell, D. G. Blackmond, J. M. Brown, *Angew. Chem. Int. Ed.* **2012**, *51*, 9539-9542.

[38]   O. Trapp, *Elucidation of Soai's Asymmetric Autocatalysis* **2022**, *Royal Society of Chemistry*, pp. 239-272.

[39]   I. Gridnev, A. Vorobiev, *Bull. Chem. Soc. Jpn.* **2015**, *88*, 333-340.

[40]   M. E. Noble-Terán, J.-M. Cruz, J.-C. Micheau, T. Buhse, *ChemCatChem* **2018**, *10*, 642-648.

[41]   a) O. Trapp, S. Lamour, F. Maier, A. F. Siegle, K. Zawatzky, B. F. Straub, *Chem. - Eur. J.* **2020**, *26*, 15871-15880; b) A. Matsumoto, A. Tanaka, Y. Kaimori, N. Hara, Y. Mikata, K. Soai, *Chem. Commun.* **2021**, *57*, 11209-11212.

[42]   a) S. V. Athavale, A. Simon, K. N. Houk, S. E. Denmark, *Nat. Chem.* **2020**, *12*, 412-423; b) C. Romagnoli, B. Sieng, M. Amedjkouh, *Eur. J. Org. Chem.* **2015**, *2015*, 4087-4092.

[43]   S. V. Athavale, A. Simon, K. N. Houk, S. E. Denmark, *J. Am. Chem. Soc.* **2020**, *142*, 18387-18406.

[44]   M. H. Todd, *Chem. Soc. Rev.* **2002**, *31*, 211-222.

[45]   K. Soai, A. Matsumoto, T. Kawasaki, *Isr. J. Chem.* **2021**, *61*, 507-516.

[46]   P. Möhler, *Mechanistic and Kinetic Studies on the Soai Reaction* **2023**, *Master Thesis*, LMU München.

[47]   E. Negishi, A. O. King, W. L. Klima, W. Patterson, A. Silveira, Jr., *The Journal of Organic Chemistry* **1980**, *45*, 2526-2528.

[48]   I. M. Lyapkalo, M. A. K. Vogel, E. V. Boltukhina, J. Vavřík, *Synlett* **2009**, *2009*, 558-561.

[49]   K. Sonogashira, Y. Tohda, N. Hagihara, *Tetrahedron Lett.* **1975**, *16*, 4467-4470.

[50]   R. T. Kenny, F. Liu, *Asian Journal of Organic Chemistry* **2022**, *11*, e202100787.

[51]   E. Hupe, M. I. Calaza, P. Knochel, *Chem. - Eur. J.* **2003**, *9*, 2789-2796.

[52]   M. Anteunis, G. Swaelens, J. Gelan, *Tetrahedron* **1971**, *27*, 1917-1929.

[53]   S. Lamour, *Untersuchung relevanter Modellsysteme im präbiotischen Kontext -Mechanistische Untersuchungen zum Halbacetal-Modell der Soai-Reaktion als Konzept für die Entstehung von Homochiralität & Die Synthese von Monosacchariden unter mechanochemischen Bedingungen* **2019**, *Dissertation*, LMU München.

[54]   G. Rotunno, D. Petersen, M. Amedjkouh, *ChemSystemsChem* **2020**, *2*, e1900060.

[55]   N. Koumura, R. W. Zijlstra, R. A. van Delden, N. Harada, B. L. Feringa, *Nature* **1999**, *401*, 152-155.

[56]   N. El-Atab, R. B. Mishra, F. Al-Modaf, L. Joharji, A. A. Alsharif, H. Alamoudi, M. Diaz, N. Qaiser, M. M. Hussain, *Advanced Intelligent Systems* **2020**, *2*, 2000128.

[57]   O. P. Ernst, D. T. Lodowski, M. Elstner, P. Hegemann, L. S. Brown, H. Kandori, *Chem. Rev.* **2014**, *114*, 126-163.

[58]   K. Inuzuka, R. S. Becker, *Nature* **1968**, *219*, 383-385.

[59]   a) I. Willner, S. Rubin, *Angew. Chem. Int. Ed. Engl.* **1996**, *35*, 367-385; b) G. Mayer, A. Heckel, *Angew. Chem. Int. Ed. Engl.* **2006**, *45*, 4900-4921; c) C. Dugave, L. Demange, *Chem. Rev.* **2003**, *103*, 2475-2532.

[60]   a) T. Fehrentz, M. Schönberger, D. Trauner, *Angew. Chem. Int. Ed.* **2011**, *50*, 12156-12182; b) W. Szymański, J. M. Beierle, H. A. V. Kistemaker, W. A. Velema, B. L. Feringa, *Chem. Rev.* **2013**, *113*, 6114-6178.

[61]   A. Deiters, *ChemBioChem* **2010**, *11*, 47-53.

[62]   M. S. Gonçalves, *Chem. Rev.* **2009**, *109*, 190-212.

[63]   R. H. Newman, M. D. Fosbrink, J. Zhang, *Chem. Rev.* **2011**, *111*, 3614-3666.

[64]   S. Nakamura, M. Irie, *The Journal of Organic Chemistry* **1988**, *53*, 6136-6138.

[65]   D. J. van Dijken, J. M. Beierle, M. C. A. Stuart, W. Szymański, W. R. Browne, B. L. Feringa, *Angew. Chem. Int. Ed.* **2014**, *53*, 5073-5077.

[66]   N. Katsonis, A. Minoia, T. Kudernac, T. Mutai, H. Xu, H. Uji-i, R. Lazzaroni, S. De Feyter, B. L. Feringa, *J. Am. Chem. Soc.* **2008**, *130*, 386-387.

[67]   R. B. Woodward, R. Hoffmann, *Angew. Chem. Int. Ed. Engl.* **1969**, *8*, 781-853.

[68]   a) Z. Li, Y. Wang, M. Li, H. Zhang, H. Guo, H. Ya, J. Yin, *Organic & Biomolecular Chemistry* **2018**, *16*, 6988-6997; b) J. Zhang, H. Tian, *Advanced Optical Materials* **2018**, *6*, 1701278.

[69]   a) A. R. A. Palmans, E. W. Meijer, *Angew. Chem. Int. Ed.* **2007**, *46*, 8948-8968; b) R. Eelkema, B. L. Feringa, *Organic & Biomolecular Chemistry* **2006**, *4*, 3729-3745.

[70]   A. R. A. Palmans, J. A. J. M. Vekemans, E. E. Havinga, E. W. Meijer, *Angew. Chem. Int. Ed. Engl.* **1997**, *36*, 2648-2651.

[71]   M. M. Green, M. P. Reidy, R. D. Johnson, G. Darling, D. J. O'Leary, G. Willson, *J. Am. Chem. Soc.* **1989**, *111*, 6452-6454.

[72]   K. Broi, A. Fuhrmann, A. Dallmann, F. Berger, S. Hecht, *ChemPhotoChem* **2019**, *3*, 461-466.

[73]   Linda N. Lucas, Jaap J. D. d. Jong, Jan H. v. Esch, Richard M. Kellogg, Ben L. Feringa, *Eur. J. Org. Chem.* **2003**, *2003*, 155-166.

[74]   N. Miyaura, A. Suzuki, *Chem. Rev.* **1995**, *95*, 2457-2483.

[75]   M. H. Rønne, D. Cho, M. R. Madsen, J. B. Jakobsen, S. Eom, É. Escoudé, H. C. D. Hammershøj, D. U. Nielsen, S. U. Pedersen, M. H. Baik, T. Skrydstrup, K. Daasbjerg, *J. Am. Chem. Soc.* **2020**, *142*, 4265-4275.

[76]   a) D. S. Matteson, A. A. Kandil, R. Soundararajan, *J. Am. Chem. Soc.* **1990**, *112*, 3964-3969; b) D. S. Matteson, H.-W. Man, O. C. Ho, *J. Am. Chem. Soc.* **1996**, *118*, 4560-4566; c) J. E. A. Luithle, J. Pietruszka, *The Journal of Organic Chemistry* **2000**, *65*, 9194-9200; d) G. Hilt, P. Bolze, *Synthesis* **2005**, *2005*, 2091-2115.

[77]   T. Mancilla, R. Contreras, B. Wrackmeyer, *J. Organomet. Chem.* **1986**, *307*, 1-6.

[78]   a) E. P. Gillis, M. D. Burke, *J. Am. Chem. Soc.* **2007**, *129*, 6716-6717; b) S. J. Lee, K. C. Gray, J. S. Paek, M. D. Burke, *J. Am. Chem. Soc.* **2008**, *130*, 466-468.

[79]   D. Blakemore, *Synthetic Methods in Drug Discovery* **2016**, *Royal Society of Chemistry*, pp. 1-69.

[80]   E. P. Gillis, M. D. Burke, *J. Am. Chem. Soc.* **2008**, *130*, 14084-14085.

[81]   S. Yamamoto, K. Matsuda, M. Irie, *Angew. Chem. Int. Ed.* **2003**, *42*, 1636-1639.

[82]   L. Jiang, J. Wu, Q. Li, G. Deng, X. Zhang, Z. Li, K. Chen, K. S. Chiang, *Journal of Materials Chemistry C* **2019**, *7*, 6257-6265.

[83]   J. Yuan, Y. Bao, *Mol. Cryst. Liq. Cryst.* **2020**, *712*, 24-30.

[84]   A. D. Benischke, M. Ellwart, M. R. Becker, P. Knochel, *Synthesis* **2016**, *48*, 1101-1107.

[85]   a) M. Kitamura, S. Suga, K. Kawai, R. Noyori, *J. Am. Chem. Soc.* **1986**, *108*, 6071-6072; b) P. Knochel, R. D. Singer, *Chem. Rev.* **1993**, *93*, 2117-2188.

[86]   A. Metzger, S. Bernhardt, G. Manolikakes, P. Knochel, *Angew. Chem. Int. Ed.* **2010**, *49*, 4665-4668.

[87]   K. Soai, S. Niwa, *Chem. Rev.* **1992**, *92*, 833-856.

[88]   a) P. Barbier, *Acad. Sci., Paris, C. R.* **1899**, *128*, 110-111; b) V. Grignard, *Acad. Sci., Paris, C. R.* **1900**, *129*, 1322-1324.

[89]   R. Noyori, M. Kitamura, *Angew. Chem. Int. Ed. Engl.* **1991**, *30*, 49-69.

[90]   a) M. Yamakawa, R. Noyori, *J. Am. Chem. Soc.* **1995**, *117*, 6327-6335; b) M. Kitamura, H. Oka, R. Noyori, *Tetrahedron* **1999**, *55*, 3605-3614.

[91]   a) B. Goldfuss, K. N. Houk, *The Journal of Organic Chemistry* **1998**, *63*, 8998-9006; b) J. Vázquez, M. A. Pericàs, F. Maseras, A. Lledós, *The Journal of Organic Chemistry* **2000**, *65*, 7303-7309.

[92]   B. Goldfuss, M. Steigelmann, S. I. Khan, K. N. Houk, *J. Org. Chem.* **2000**, *65*, 77-82.

[93]   a) Y. Geiger, T. Achard, A. Maisse-François, S. Bellemin-Laponnaz, *Nature Catalysis* **2020**, *3*, 422-426; b) T. A. Y. Geiger, A. Maisse-François, S. Bellemin-Laponnaz, *Chem. Sci.* **2020**, *11*, 12453-12463.

[94]   a) K. Soai, A. Ookawa, T. Kaba, K. Ogawa, *J. Am. Chem. Soc.* **1987**, *109*, 7111-7115; b) A. Ookawa, K. Soai, *J. Chem. Soc., Perkin Trans. 1* **1987**, 1465-1471; c) K. Soai, A. Ookawa, K. Ogawa, T. Kaba, *J. Chem. Soc., Chem. Commun.* **1987**, 467-468.

[95]   a) S. Lauzon, T. Ollevier, *Chem. Commun.* **2021**, *57*, 11025-11028; b) S. Bastin, F. Agbossou-Niedercorn, J. Brocard, L. Pélinski, *Tetrahedron: Asymmetry* **2001**, *12*, 2399-2408; c) J. M. Andrés, M. A. Martínez, R. Pedrosa, A. Pérez-Encabo, *Tetrahedron: Asymmetry* **1994**, *5*, 67-72.

[96]   a) M. Asami, S. Inoue, *Chem. Lett.* **1991**, *20*, 685-688; b) P. Delair, C. Einhorn, J. Einhorn, J. L. Luche, *Tetrahedron* **1995**, *51*, 165-172; c) Y. Kawanami, T. Mitsuie, M. Miki, T. Sakamoto, K. Nishitani, *Tetrahedron* **2000**, *56*, 175-178; d) J. Beliczey, G. Giffels, U. Kragl, C. Wandrey, *Tetrahedron: Asymmetry* **1997**, *8*, 1529-1530; e) I. Sato, T. Saito, K. Soai, *Chem. Commun.* **2000**, 2471-2472.

[97]   a) T. Katagiri, Y. Fujiwara, S. Takahashi, N. Ozaki, K. Uneyama, *Chem. Commun.* **2002**, 986-987; b) M. Yus, D. J. Ramón, O. Prieto, *Tetrahedron: Asymmetry* **2003**, *14*, 1103-1114.

[98]   T. Hayase, T. Sugiyama, M. Suzuki, T. Shibata, K. Soai, *J. Fluorine Chem.* **1997**, *84*, 1-5.

[99]   Y. Nakao, H. Idei, K. S. Kanyiva, T. Hiyama, *J. Am. Chem. Soc.* **2009**, *131*, 15996-15997.

[100]   X. Li, N. Chen, J. Xu, *Synthesis* **2019**, *51*, 3336-3344.

[101]   H.-X. L. Q.-F. Li, Y.-M. Cui, P.-P. Xu, *Eur. J. Med. Chem.* **2015**, *104*, 97-105.

[102]   R. F. Cunico, L. Bedell, *The Journal of Organic Chemistry* **1980**, *45*, 4797-4798.

[103]   E. L. Penny A. Chaloner, S. A. Renuka Perera, *J. Chem. Soc., Perkin Trans. 1* **1991**, 2731-2735.

[104]   a) W. A. Nugent, *Chem. Commun.* **1999**, 1369-1370; b) L. Pu, *Acc. Chem. Res.* **2014**, *47*, 1523-1535; c) M.-C. Wang, Q.-J. Zhang, G.-W. Li, Z.-K. Liu, *Tetrahedron: Asymmetry* **2009**, *20*, 288-292.

[105]   G. Blay, I. Fernández, V. Hernández-Olmos, A. Marco-Aleixandre, J. R. Pedro, *Tetrahedron: Asymmetry* **2005**, *16*, 1953-1958.

[106]   R. G. Pearson, *J. Am. Chem. Soc.* **1963**, *85*, 3533-3539.

[107]   P. K. Arkady Krasovskiy, *Synthesis* **2006**, *5*, 890-891.

[108]   H.-S. Lin, L. A. Paquette, *Synth. Commun.* **1994**, *24*, 2503-2506.

[109]   G. R. Fulmer, A. J. M. Miller, N. H. Sherden, H. E. Gottlieb, A. Nudelman, B. M. Stoltz, J. E. Bercaw, K. I. Goldberg, *Organometallics* **2010**, *29*, 2176-2179.

[110]   Bruker, *SAINT* **2012**, *Bruker AXS, Inc.*, USA.

[111]   G. M. Sheldrick, *SADABS* **1996**, University of Göttingen, Germany.

[112]   G. M. Sheldrick, *Acta Cryst. A71* **2015**, 3-8.

[113]   L. J. Farrugia, *J. Appl. Cryst.* **2012**, *45*, 849-854.

[114]   O. Trapp, S. Lamour, F. Maier, A. F. Siegle, K. Zawatzky, B. F. Straub, *Chemistry* **2020**, *26*, 15871-15880.

[115]   D. M. Knapp, E. P. Gillis, M. D. Burke, *J. Am. Chem. Soc.* **2009**, *131*, 6961-6963.